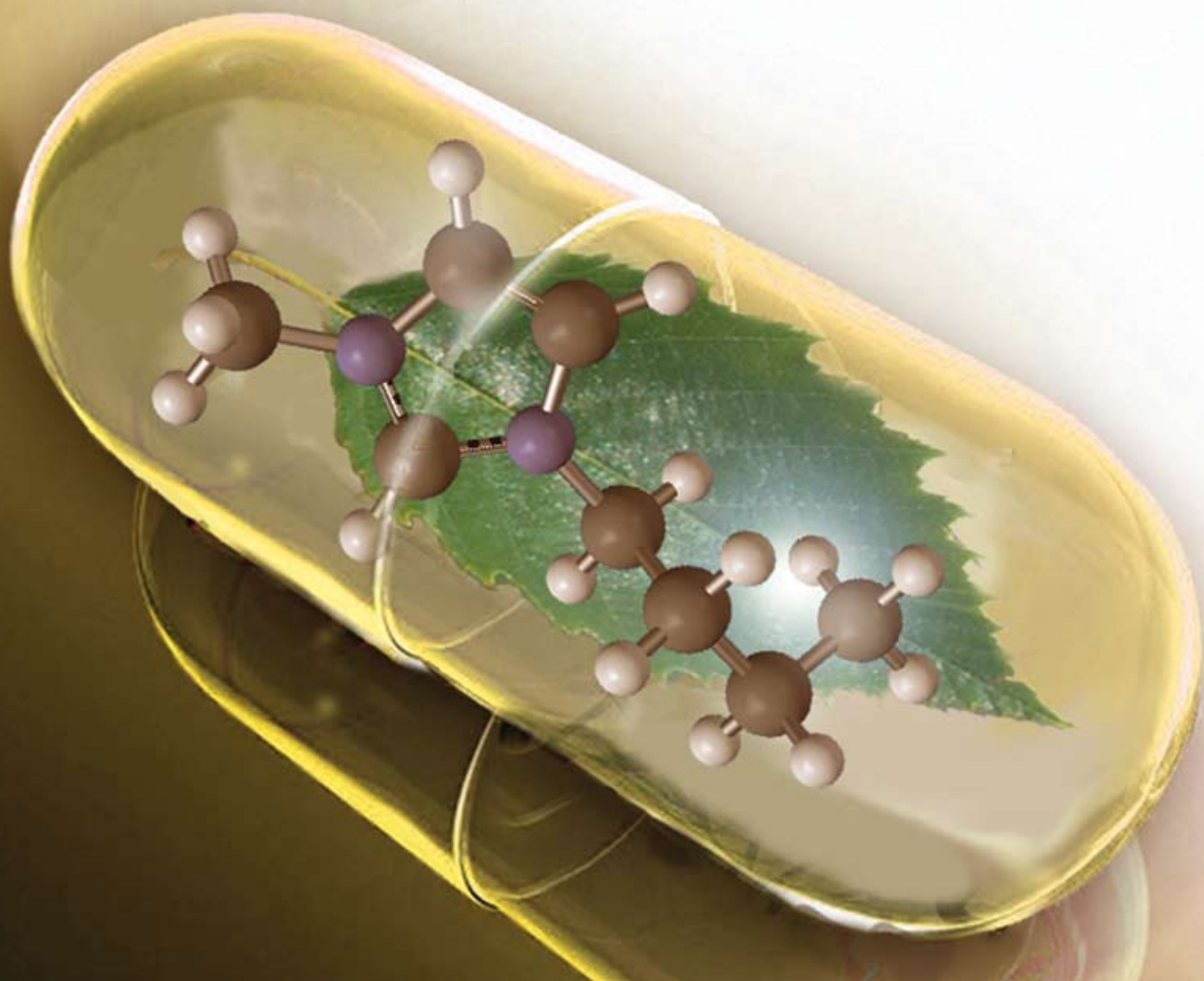


Green Chemistry

Cutting-edge research for a greener sustainable future

www.rsc.org/greenchem

Volume 10 | Number 9 | September 2008 | Pages 897–1012



ISSN 1463-9262

RSC Publishing

Peters *et al.*
High-pressure behaviour of ionic liquids
Beckman and Chen
One-pot synthesis of propylene oxide



1463-9262(2008)10:9;1-9

Number 1
in the field



years of publishing!

Green Chemistry...



- The most highly cited *Green Chemistry* journal, Impact factor = 4.836*
- Fast publication, typically <90 days for full papers
- Full variety of research including reviews, communications, full papers and perspectives.

Celebrating 10 years of publishing, *Green Chemistry* offers the latest research that reduces the environmental impact of the chemical enterprise by developing alternative sustainable technologies, and provides a unique forum for the rapid publication of cutting-edge and innovative research for a greener, sustainable future

...for a sustainable future!

* 2007 Thomson Scientific (ISI) Journal Citation Reports ®

Green Chemistry

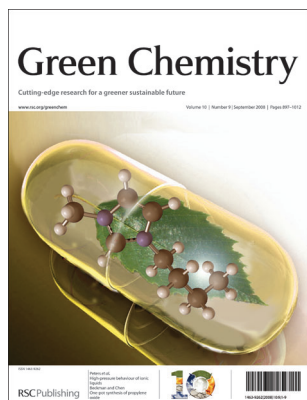
Cutting-edge research for a greener sustainable future

www.rsc.org/greenchem

RSC Publishing is a not-for-profit publisher and a division of the Royal Society of Chemistry. Any surplus made is used to support charitable activities aimed at advancing the chemical sciences. Full details are available from www.rsc.org

IN THIS ISSUE

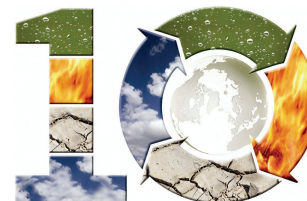
ISSN 1463-9262 CODEN GRCHFJ 10(9) 897–1012 (2008)



Cover

See Peters *et al.*, pp. 929–933. Design of processes based on single-phase reactions in ionic liquids and extraction by CO₂ under heterogeneous conditions is a novel step for synthesizing medicines in a greener way. Artwork designed in collaboration with Dr Sona Raeissi.

Image reproduced with permission of Eliane Kühne, from *Green Chem.*, 2008, **10**, 929.



CHEMICAL TECHNOLOGY

T65

Drawing together research highlights and news from all RSC publications, *Chemical Technology* provides a 'snapshot' of the latest applications and technological aspects of research across the chemical sciences, showcasing newsworthy articles and significant scientific advances.

Chemical Technology

September 2008/Volume 5/Issue 9

www.rsc.org/chemicaltechnology

COMMUNICATIONS

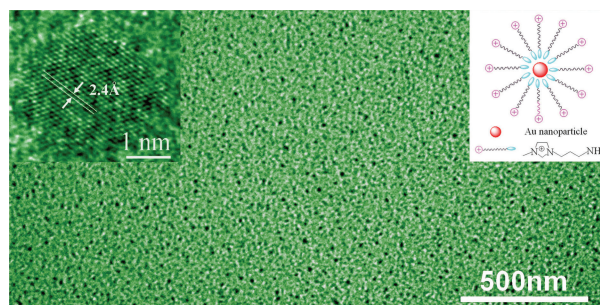
907



Green synthesis of 1–2 nm gold nanoparticles stabilized by amine-terminated ionic liquid and their electrocatalytic activity in oxygen reduction

Zhijuan Wang, Qixian Zhang, Daniel Kuehner, Ari Ivaska and Li Niu*

Stable gold nanoparticles with average size 1.7 nm were synthesized *via* a simple and green method using an amine-terminated ionic liquid as both reductant and stabilizer. The obtained gold nanoparticles showed enhanced electrocatalytic activity and high stability.



EDITORIAL STAFF

Editor

Sarah Ruthven

Assistant editor

Sarah Dixon

Publishing assistant

Ruth Bircham

Team leader, serials production

Stephen Wilkes

Technical editor

Edward Morgan

Production administration coordinator

Sonya Spring

Administration assistantsClare Davies, Donna Fordham, Kirsty Lunnon,
Julie Thompson**Publisher**

Emma Wilson

Green Chemistry (print: ISSN 1463-9262; electronic: ISSN 1463-9270) is published 12 times a year by the Royal Society of Chemistry, Thomas Graham House, Science Park, Milton Road, Cambridge, UK CB4 0WF.

All orders, with cheques made payable to the Royal Society of Chemistry, should be sent to RSC Distribution Services, c/o Portland Customer Services, Commerce Way, Colchester, Essex, UK CO2 8HP. Tel +44 (0) 1206 226050; E-mail sales@rscdistribution.org

2008 Annual (print + electronic) subscription price: £947; US\$1799. 2008 Annual (electronic) subscription price: £852; US\$1695. Customers in Canada will be subject to a surcharge to cover GST. Customers in the EU subscribing to the electronic version only will be charged VAT.

If you take an institutional subscription to any RSC journal you are entitled to free, site-wide web access to that journal. You can arrange access via Internet Protocol (IP) address at www.rsc.org/ip. Customers should make payments by cheque in sterling payable on a UK clearing bank or in US dollars payable on a US clearing bank. Periodicals postage paid at Rahway, NJ, USA and at additional mailing offices. Airfreight and mailing in the USA by Mercury Airfreight International Ltd., 365 Blair Road, Avenel, NJ 07001, USA.

US Postmaster: send address changes to Green Chemistry, c/o Mercury Airfreight International Ltd., 365 Blair Road, Avenel, NJ 07001. All despatches outside the UK by Consolidated Airfreight.

PRINTED IN THE UK

Advertisement sales: Tel +44 (0) 1223 432246; Fax +44 (0) 1223 426017; E-mail advertising@rsc.org

Green Chemistry

Cutting-edge research for a greener sustainable future

www.rsc.org/greenchem

Green Chemistry focuses on cutting-edge research that attempts to reduce the environmental impact of the chemical enterprise by developing a technology base that is inherently non-toxic to living things and the environment.

EDITORIAL BOARD

Chair

Professor Martyn Poliakoff
Nottingham, UK

Scientific Editor

Professor Walter Leitner
RWTH-Aachen, Germany

Associate Editors

Professor C. J. Li
McGill University, Canada

Members

Professor Paul Anastas
Yale University, USA
Professor Joan Brennecke
University of Notre Dame, USA
Professor Mike Green
Sasol, South Africa
Professor Buxing Han
Chinese Academy of Sciences,
China

Dr Alexei Lapkin
Bath University, UK
Professor Steven Ley
Cambridge, UK
Dr Janet Scott
Unilever, UK
Professor Tom Welton
Imperial College, UK

ADVISORY BOARD

James Clark, York, UK
Avelino Corma, Universidad
Politécnica de Valencia, Spain
Mark Harmer, DuPont Central
R&D, USA
Herbert Hugel, Lanxess Fine
Chemicals, Germany
Roshan Jachuck,
Clarkson University, USA
Makoto Misono, nite,
Japan

Colin Raston,
University of Western Australia,
Australia
Robin D. Rogers, Centre for Green
Manufacturing, USA
Kenneth Seddon, Queen's
University, Belfast, UK
Roger Sheldon, Delft University of
Technology, The Netherlands
Gary Sheldrake, Queen's
University, Belfast, UK

Pietro Tundo, Università ca
Foscari di Venezia, Italy

INFORMATION FOR AUTHORS

Full details of how to submit material for publication in Green Chemistry are given in the Instructions for Authors (available from <http://www.rsc.org/authors>). Submissions should be sent via ReSource: <http://www.rsc.org/resource>.

Authors may reproduce/republish portions of their published contribution without seeking permission from the RSC, provided that any such republication is accompanied by an acknowledgement in the form: (Original citation) – Reproduced by permission of the Royal Society of Chemistry.

© The Royal Society of Chemistry 2008. Apart from fair dealing for the purposes of research or private study for non-commercial purposes, or criticism or review, as permitted under the Copyright, Designs and Patents Act 1988 and the Copyright and Related Rights Regulations 2003, this publication may only be reproduced, stored or transmitted, in any form or by any means, with the prior permission in writing of the Publishers or in the case of reprographic reproduction in accordance with the terms of licences issued by the Copyright Licensing Agency in the UK. US copyright law is applicable to users in the USA.

The Royal Society of Chemistry takes reasonable care in the preparation of this publication but does not accept liability for the consequences of any errors or omissions.

The paper used in this publication meets the requirements of ANSI/NISO Z39.48-1992 (Permanence of Paper).

Royal Society of Chemistry: Registered Charity No. 207890

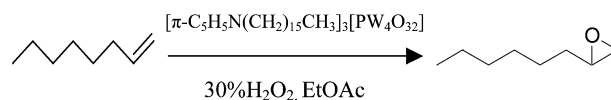
COMMUNICATIONS

910

**[π -C₅H₅N(CH₂)₁₅CH₃]₃[PW₄O₃₂]/H₂O₂/ethyl acetate/alkenes: a recyclable and environmentally benign alkenes epoxidation catalytic system**

Yong Ding,* Wei Zhao, Hui Hua and Baochun Ma*

A halide-free reaction-controlled phase transfer catalytic system for epoxidation of alkenes was reported. The epoxidation of alkenes was successfully catalyzed by a recyclable and environmentally benign catalytic system: [π -C₅H₅N(CH₂)₁₅CH₃]₃[PW₄O₃₂]/H₂O₂/ethyl acetate/olefin.

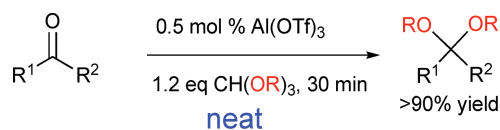


914

**Highly atom efficient aluminium triflate catalysed acetal formation**

D. Bradley G. Williams* and Michelle C. Lawton

Al(OTf)₃ at low concentration catalyses remarkably efficient acetal formations in high yields at room temperature using only 1.2 equivalents of an orthoester, and is readily recyclable.

R = Me or Et; R¹ = Aryl or Alkyl; R² = Alkyl or H

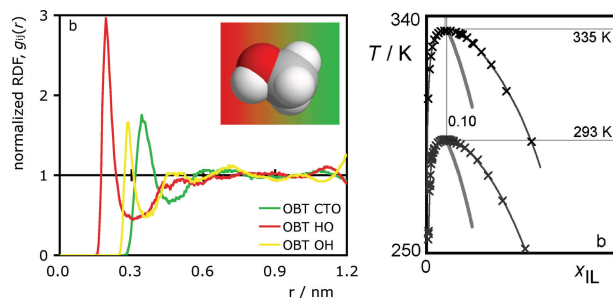
PAPERS

918

Solubility of fluorinated compounds in a range of ionic liquids. Cloud-point temperature dependence on composition and pressure

Rui Ferreira, Marijana Blesic, Joana Trindade, Isabel Marrucho, José N. Canongia Lopes* and Luís Paulo N. Rebelo*

Ionic liquids and fluorinated organic molecules are perceived as relatively benign media. Blending them poses very interesting challenges both from the theoretical and the applied chemistry points of view.

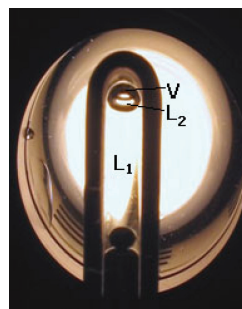


929

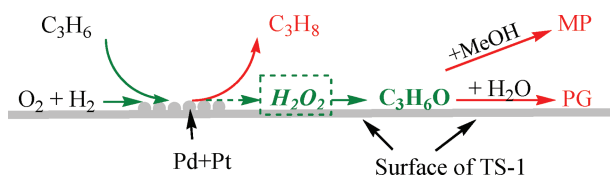
High-pressure phase behavior of ternary mixtures with ionic liquids, part I: the system bmim[BF₄]+4-isobutylacetophenone + CO₂

Eliane Kühne, Geert-Jan Witkamp and Cor J. Peters*

The influence of CO₂ pressure on the miscibility of the ternary system bmim[BF₄] + 4-isobutylacetophenone + CO₂ is presented. An increase in CO₂ composition gradually reduces the extension and influences the location of the one-phase liquid region, finally resulting in its complete disappearance.



934

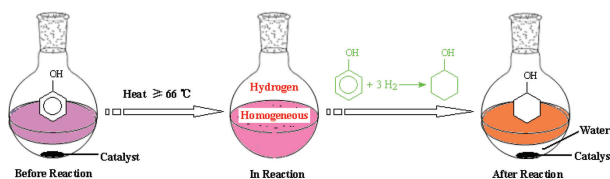


One-pot green synthesis of propylene oxide using *in situ* generated hydrogen peroxide in carbon dioxide

Qunlai Chen and Eric J. Beckman*

Propylene oxide was synthesized using *in situ* generated hydrogen peroxide in carbon dioxide (supercritical or liquid) with the addition of small amounts of polar co-solvent. Side reactions were effectively suppressed by using a selected inhibitor.

939

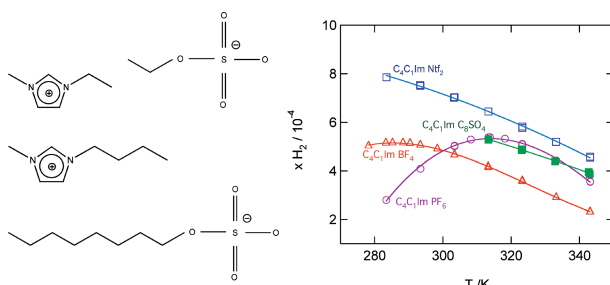


Aqueous system for the improved hydrogenation of phenol and its derivatives

Yizhi Xiang, Lei Ma, Chunshan Lu, Qunfeng Zhang and Xiaonian Li*

An aqueous reaction system, in which complete aqueous miscibility of phenol is achieved, separation of the products from water is simplified, and the recovered aqueous solvent could be reused.

944

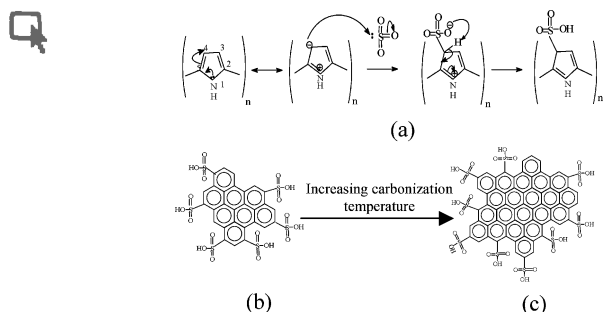


Thermophysical properties, low pressure solubilities and thermodynamics of solvation of carbon dioxide and hydrogen in two ionic liquids based on the alkylsulfate anion

Johan Jacquemin, Pascale Husson, Vladimir Majer, Agilio A.H. Padua and Margarida F. Costa Gomes*

The solubility of carbon dioxide and hydrogen in two 1-alkyl-3-methylimidazolium alkylsulfates are presented and compared to that obtained for other ionic liquids.

951



Sulfonated polypyrrole nanospheres as a solid acid catalyst

Xiaoning Tian, Fabing Su and X. S. Zhao*

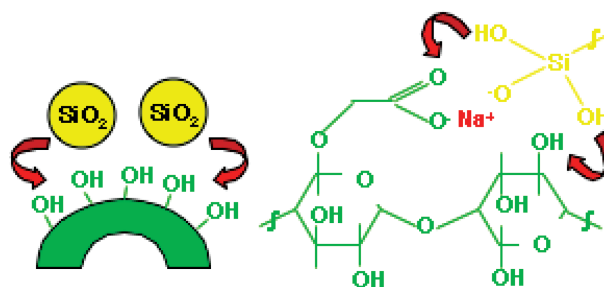
The prepared sulfonated polypyrrole (SPNs) and carbonized polypyrrole nanosphere (SCPNs) sulfonic acid catalysts show high catalytic activity and good recyclability. This preparation shows a new way to find alternative solid acid catalysts.

957

Aqueous sol-gel routes to bio-composite capsules and gels

Namia Benmouhoub, Nicolas Simmonet, Nouria Agoudjil and Thibaud Coradin*

Aqueous silicates can be associated with agarose and carboxymethylcellulose to obtain biocomposites with improved stability and/or controlled diffusion properties following a sol-gel route that complies with Green Chemistry principles.

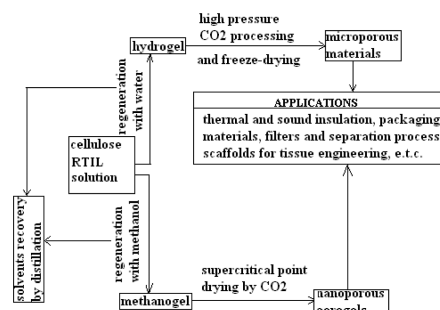


965

Development of micro- and nano-porous composite materials by processing cellulose with ionic liquids and supercritical CO₂

Costas Tsiptsias, Apostolis Stefopoulos, Ioannis Kokkinomalis, Lambrini Papadopoulou and Costas Panayiotou*

Combination of ionic liquids and supercritical carbon dioxide to produce porous cellulose and cellulose composite materials.

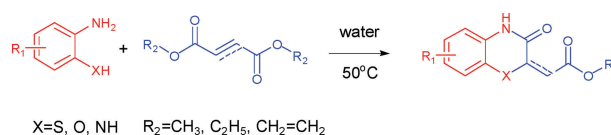


972

A green protocol for synthesis of benzo-fused *N,S*-, *N,O*- and *N,N*-heterocycles in water

Qing-Yi Zhang, Bo-Kai Liu, Wan-Qin Chen, Qi Wu and Xian-Fu Lin*

A fast and efficient protocol which is associated with readily available starting materials, mild conditions, excellent yields, and a broad range of the products in synthetic chemistry, was established for synthesis of benzo-fused heterocycles in water under catalyst-free conditions.

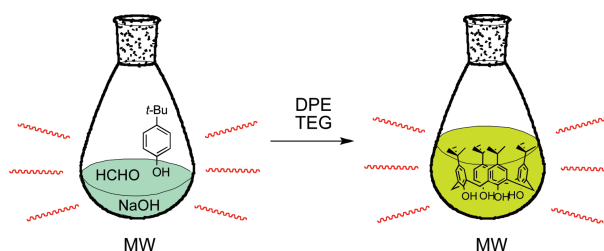


978

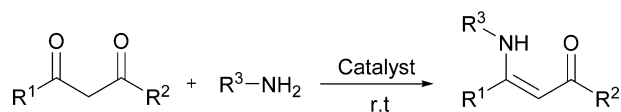
Rapid and convenient laboratory method for the preparation of *p*-*tert*-butylcalix[4]arene using microwave irradiation

Masafumi Takagaki, Asao Hosoda, Hajime Mori, Yasuhito Miyake, Keiichi Kimura, Hisaji Taniguchi and Eisaku Nomura*

Rapid preparation of *p*-*tert*-butylcalix[4]arene using microwave irradiation was studied and *p*-*tert*-butylcalix[4]arene was obtained as a pure form in modest yield with shortening the reaction time from hours to minutes.



982

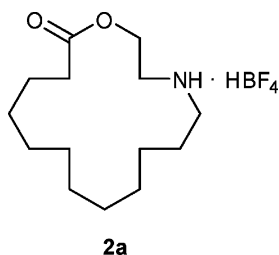


A revision for the synthesis of β -enaminones in solvent free conditions: efficacy of different supported heteropoly acids as active and reusable catalysts

Ezzat Rafiee,* Mohammad Joshaghani, Sara Eavani and Solmaz Rashidzadeh

Catalytic performance of different supported heteropoly acids for synthesis of β -enaminones and β -enamino esters in solvent and solvent free conditions has been investigated.

990

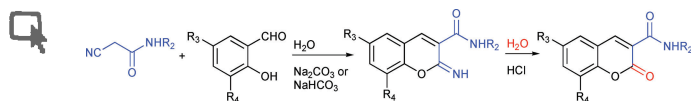


Potential green fungicide: 16-oxo-1-oxa-4-azoniacyclohexadecan-4-ium tetrafluoroborate

Yanhong Dong, Xiaomei Liang, Huizhu Yuan, Shuhua Qi, Fuheng Chen and Daoquan Wang*

16-Oxo-1-oxa-4-azoniacyclohexadecan-4-ium tetrafluoroborate (**2a**) was synthesized as a safe to human beings and low toxicological potential fungicide by a green process.

995

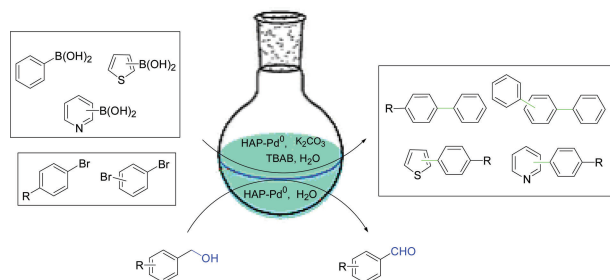


A simple and eco-friendly approach for the synthesis of 2-imino and 2-oxo-2H-chromene-3-carboxamides

Fernanda Proença* and Marta Costa

New 2-imino-2H-chromene-3-carboxamides were synthesized by the Knoevenagel condensation of salicylaldehyde derivatives and *N*-substituted cyanoacetamides. Addition of aqueous HCl led to the formation of 2-oxo-2H-chromene-3-carboxamides.

999



Hydroxyapatite-supported palladium (0) as a highly efficient catalyst for the Suzuki coupling and aerobic oxidation of benzyl alcohols in water

Navjot Jamwal, Monika Gupta and Satya Paul*

Hydroxyapatite-supported palladium (0) catalyst was prepared and employed for the Suzuki reaction and aerobic oxidation of benzyl alcohols in water.

PAPERS

1004

Improved chemoselective, ecofriendly conditions for the conversion of primary alkyl halides into nitroalkanes under PEG400

Roberto Ballini,* Luciano Barboni and Alessandro Palmieri

Treatment of primary alkyl halides with NaNO_2 at room temperature in PEG400, as an ecofriendly solvent, allows the chemoselective formation of primary nitroalkanes.



AUTHOR INDEX

Agoudjil, Nouria, 957
 Ballini, Roberto, 1004
 Barboni, Luciano, 1004
 Beckman, Eric J., 934
 Benmouhoub, Namia, 957
 Blesic, Marijana, 918
 Chen, Fuheng, 990
 Chen, Qunlai, 934
 Chen, Wan-Qin, 972
 Coradin, Thibaud, 957
 Costa Gomes, Margarida F., 944
 Costa, Marta, 995
 Ding, Yong, 910
 Dong, Yanhong, 990
 Eavani, Sara, 982
 Ferreira, Rui, 918
 Gupta, Monika, 999
 Hosoda, Asao, 978
 Hua, Hui, 910

Husson, Pascale, 944
 Ivaska, Ari, 907
 Jacquemin, Johan, 944
 Jamwal, Navjot, 999
 Joshaghani, Mohammad, 982
 Kimura, Keiichi, 978
 Kokkinomalis, Ioannis, 965
 Kuhner, Daniel, 907
 Kühne, Eliane, 929
 Lawton, Michelle C., 914
 Li, Xiaonian, 939
 Liang, Xiaomei, 990
 Lin, Xian-Fu, 972
 Liu, Bo-Kai, 972
 Lopes, José N. Canongia, 918
 Lu, Chunshan, 939
 Ma, Baochun, 910
 Ma, Lei, 939
 Majer, Vladimir, 944

Marrucho, Isabel, 918
 Miyake, Yasuhito, 978
 Mori, Hajime, 978
 Niu, Li, 907
 Nomura, Eisaku, 978
 Padua, Agilio A.H., 944
 Palmieri, Alessandro, 1004
 Panayiotou, Costas, 965
 Papadopoulou, Lambrini, 965
 Paul, Satya, 999
 Peters, Cor J., 929
 Proença, Fernanda, 995
 Qi, Shuhua, 990
 Rafiee, Ezzat, 982
 Rashidzadeh, Solmaz, 982
 Rebelo, Luís Paulo N., 918
 Simmonet, Nicolas, 957
 Stefanopoulos, Apostolis, 965
 Su, Fabing, 951

Takagaki, Masafumi, 978
 Taniguchi, Hisaji, 978
 Tian, Xiaoning, 951
 Trindade, Joana, 918
 Tsiptsias, Costas, 965
 Wang, Daoquan, 990
 Wang, Zhijuan, 907
 Williams, D. Bradley G., 914
 Witkamp, Geert-Jan, 929
 Wu, Qi, 972
 Xiang, Yizhi, 939
 Yuan, Huizhu, 990
 Zhang, Qing-Yi, 972
 Zhang, Qixian, 907
 Zhang, Qunfeng, 939
 Zhao, Wei, 910
 Zhao, X. S., 951

FREE E-MAIL ALERTS AND RSS FEEDS

Contents lists in advance of publication are available on the web *via* www.rsc.org/greenchem – or take advantage of our free e-mail alerting service (www.rsc.org/ej.alert) to receive notification each time a new list becomes available.



Try our RSS feeds for up-to-the-minute news of the latest research. By setting up RSS feeds, preferably using feed reader software, you can be alerted to the latest Advance Articles published on the RSC web site. Visit www.rsc.org/publishing/technology/rss.asp for details.

ADVANCE ARTICLES AND ELECTRONIC JOURNAL

Free site-wide access to Advance Articles and the electronic form of this journal is provided with a full-rate institutional subscription. See www.rsc.org/ejs for more information.

* Indicates the author for correspondence: see article for details.



Electronic supplementary information (ESI) is available *via* the online article (see <http://www.rsc.org/esi> for general information about ESI).

A new journal from RSC Publishing launching in 2009

Integrative Biology

Quantitative biosciences from nano to macro



Integrative Biology provides a unique venue for elucidating biological processes, mechanisms and phenomena through quantitative enabling technologies at the convergence of biology with physics, chemistry, engineering, imaging and informatics.

With 12 issues published annually, **Integrative Biology** will contain a mix of research articles including Full papers, Reviews (Tutorial & Critical), and Perspectives. It will be supported by an international Editorial Board, chaired by Distinguished Scientist Dr Mina J Bissell of Lawrence Berkeley National Laboratory.

The current issue of **Integrative Biology** will be freely available to all readers via the website. Free institutional online access to all 2009 and 2010 content of the journal will be available following registration at www.rsc.org/ibiology_registration

Contact the Editor, Harp Minhas, at ibiology@rsc.org or visit the website for more details.

060858

RSC Publishing

www.rsc.org/ibiology

Registered Charity Number 207890

Chemical Technology

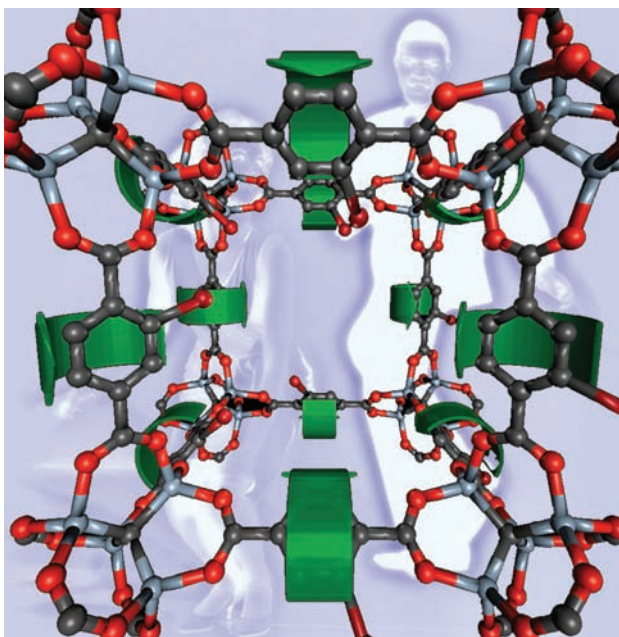
Solid-state rotors may replace liquid crystals

Metal organic frameworks do the twist

Rotating solid-state crystals could outperform liquid crystals for optoelectronic applications, claim US scientists.

John Price and colleagues from the University of Colorado, Boulder, have investigated metal organic framework crystals that can act as molecular rotors. Rotating or twisting molecules using an applied electric field is the principle behind liquid crystals, an important class of optoelectronic materials. However, solid-state crystals – such as metal organic framework (MOF) crystals – could lead to more robust materials for use in the data communications industry.

MOF crystals are metal clusters linked by organic groups to form 1-, 2- and 3-D frameworks. Price's team used an existing MOF containing octahedrally coordinated zinc oxide clusters and incorporated polar functional groups into the organic linker parts of the framework. They demonstrated that in the presence of an electric field, the effect on the polar group causes the molecule to



rotate. Rotation was not observed for an analogous MOF with no polar functional groups.

'MOFs have better structural predictability than we currently

Polar groups on the metal organic framework cause the molecule to rotate

have with other solid-state crystals which makes them particularly appealing,' says Erick Winston, a member of Price's group. However, more work is needed as the barrier to rotation of $7.3 \text{ kcal mol}^{-1}$ for this particular polar MOF means that it cannot compete with liquid crystals.

The Colorado group plan to keep searching for an MOF structure which can compete with liquid crystals. 'Dealing with these challenges does not appear to be a far off goal,' says Winston, 'particularly if the community becomes more interested in molecular rotation in MOF crystals.'

Miguel Garcia-Garibay, an expert in MOFs from the University of California, Los Angeles, US, says that the work of the Price group represents 'an important step forward' in the application of crystals as molecular rotors.

Ruth Doherty

Reference

E B Winston *et al*, *Phys. Chem. Chem. Phys.*, 2008, **10**, 5188 (DOI: 10.1039/b808104b)

In this issue

Artificial cells seek out disease

Polymers self-assemble into drug delivery vesicles that release contents on cue

Fabrics reveal their explosive secrets

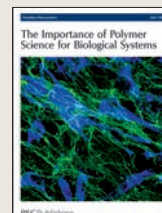
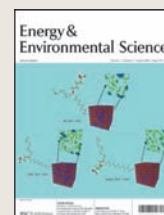
New detection method could improve airport security

Interview: Chemistry's gain

Ryong Ryoo tells Rachel Cooper how he took a risk and became an expert in mesoporous materials

Instant insight: The wonder of gold

Graham J Hutchings, Mathias Brust and Hubert Schmidbaur introduce the newly discovered allure of gold



The latest applications and technological aspects of research across the chemical sciences

Application highlights

Detection using surface plasmon resonance could save lives

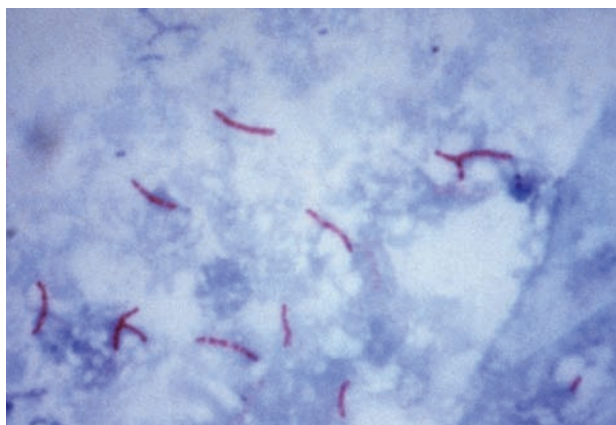
Faster test for tuberculosis

Early diagnosis of tuberculosis is now a step closer, say scientists from India and Japan.

Bansi Malhotra from the National Physical Laboratory in New Delhi, India and colleagues have made a detection device that is quick, precise and efficient to use.

According to the World Health Organization, tuberculosis kills nearly three million people every year. Patients suffer damage to their lungs, bones and central nervous system. Current detection techniques, such as the polymerase chain reaction (PCR) and immunoassays, although sensitive, can take from hours to days to complete and are expensive. A faster and cheaper test is an absolute necessity, says Malhotra.

Malhotra's sensor detects the DNA of the disease-causing



bacterium *Mycobacterium tuberculosis*. When a serum sample containing the bacterium passes over the sensor, the bacterial DNA binds to complementary nucleotide sequences fixed to a gold surface.

The disease-causing bacterium can be detected in about 12 minutes

This causes a change in optical properties which can be detected using surface plasmon resonance.

The device was so sensitive, it could detect *M. tuberculosis* DNA without PCR amplification or rigorous washing, decreasing the detection time to around 12 minutes. Malhotra says that the next step is to make a commercial sensor for clinical samples and miniaturise it for point-of-care use. But the research doesn't stop there: 'This technique has implications for the diagnosis of other diseases, such as cholera, and sexually transmitted infections like *Neisseria gonorrhoeae*,' he explains. Rebecca Brodie

Reference

N Prabhakar *et al*, *Analyst*, 2008, DOI:10.1039/b808225a

Microfluidic array allows complex biological experiments

On-chip sequential cell treatment

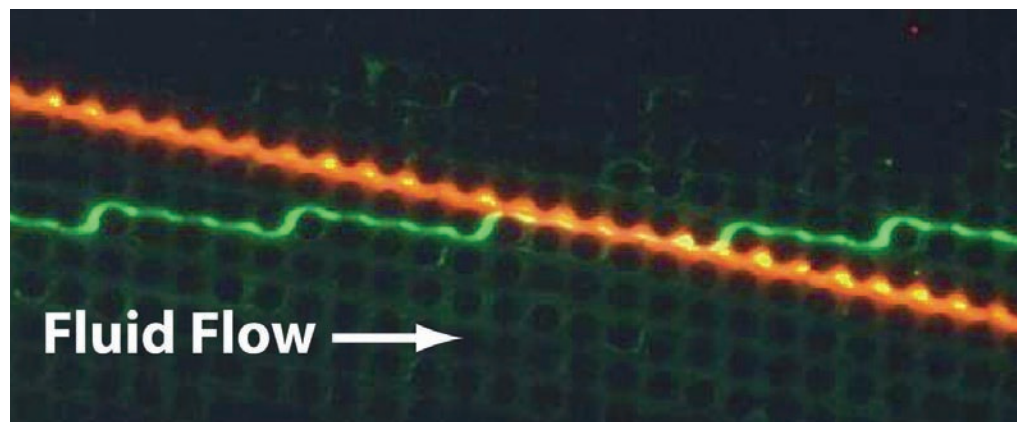
US scientists have designed a chip that can subject cells to different chemical treatments in a continuous sequence.

James Sturm and colleagues at Princeton University have tested a method that can handle complex sequential cell analyses.

On-chip experiments produce faster results than conventional approaches and use smaller sample and reagent volumes. But their application to biological systems is limited because sequential treatments are often required, causing reagent mixing that is difficult to reverse.

Sturm's chip has an asymmetric arrangement of posts that causes cells to move across the surface at an angle. Parallel streams of reagents, known as microfluidic channels, flow over the chip so that the cells pass through each chemical zone without any cross-contamination.

Sturm's team demonstrated the technique could be used for labelling and washing a blood cell, which proved to be much simpler



than other methods currently used. They also broke down a bacterial cell on the chip and removed the intact chromosome.

'For whole bacterial chromosome isolation, the method is without peer,' comments co-worker Keith Morton. He says he hopes the technique will advance whole chromosome research. The next challenge is to design a system capable of more complex reactions.

An asymmetric arrangement of posts directs particles across multiple reagent streams

Harold Craighead of Cornell University, Ithaca, US, an expert in biomolecule microfluidics, says, 'This approach presents exciting new possibilities for continuous analysis of cells, bacteria, and biomolecules.'

Harriet Brewerton

Reference

K J Morton *et al*, *Lab Chip*, 2008, **8**, 1448 (DOI: 10.1039/b805614e)

Polymers self-assemble into drug delivery vesicles that release contents on cue

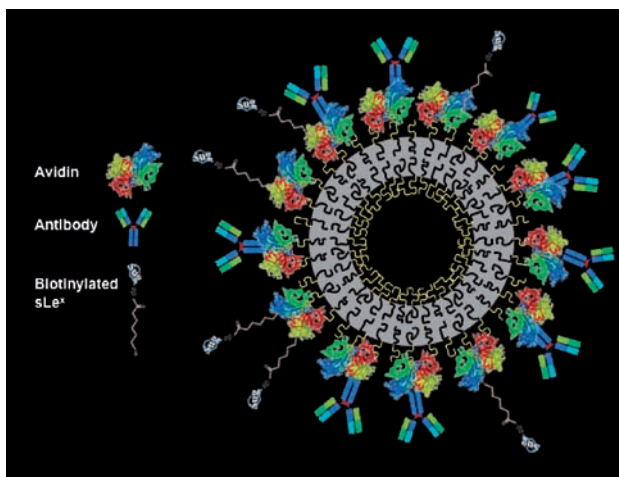
Artificial cells seek out disease

Scientists in the US have made an artificial cell that can locate sites of disease within the body.

Daniel Hammer and colleagues at the University of Pennsylvania, Philadelphia, and the University of Minnesota, Minneapolis, say they can engineer the cell to release its contents on cue, allowing it to deliver drugs directly to sites of disease. This approach could be useful in treating diseases such as cancer, they claim.

The artificial cells, known as leuko-polymerosomes, are made from polymers that can self-assemble into vesicles that can be used for drug delivery. Polymerosomes have been used in this way before but Hammer has now developed a way to make them behave like white blood cells. This lets them travel quickly and easily through blood vessels in the body.

'After the invention of polymerosomes, it seemed natural to make an artificial white blood cell from them because there are so many ways that one can engineer



the mechanical properties and release characteristics of polymerosomes,' says Hammer.

Hammer and his team now plan to use different types of ligands on the polymerosome's surface to target different locations within the body. 'These leuko-polymerosomes are designed to travel to sites of inflammation,' explains Hammer.

Leuko-polymerosomes can encapsulate drugs and deliver them to sites of disease

'However, with different homing ligands, we envision developing particles that could find sites of cancer or other diseases.'

'The leuko-polymerosome is a great example of biomimetics, and their tuneable strength and surface adhesion are proving useful for a range of clinical applications in drug delivery and medical imaging,' comments Michael King, an expert in biomedical engineering at the University of Rochester, US. 'Looking forward to the future, one could imagine the polymerosome as an important building block in the field of synthetic biology, for instance incorporating ion channels to produce "smart" polymerosomes which sense their surroundings, or encapsulating enzymatic cargo within circulating "micro-factories".'

Sarah Dixon

Reference

D A Hammer *et al*, *Faraday Discuss.*, 2008, **139**, 129 (DOI: 10.1039/b717821b)

New class of CO₂ binding agents could help reduce global warming

Organic liquids capture greenhouse gas

Carbon dioxide-binding organic liquids (CO₂BOLs) can hold more than twice as much CO₂ as current capture agents, say scientists in North America. The liquids could be used in coal power plants to capture the greenhouse gas from combustion exhaust.

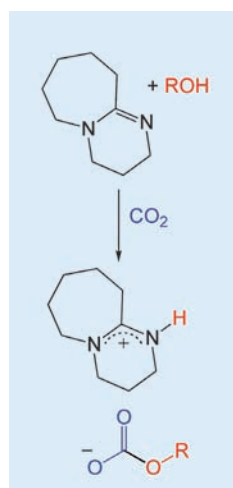
David Heldebrant at the Pacific Northwest National Laboratory, Richland, US, and colleagues, made CO₂BOLs from mixtures of organic alcohols and strong organic bases. They found that the CO₂BOLs can store up to 19 per cent of their weight in CO₂, much higher than the maximum of seven per cent achievable with current aqueous amine systems.

'The biggest obstacle in efficient chemical CO₂ capture and release is the cost of stripping CO₂ from the aqueous capture agent due to the

high specific heats associated with water,' says Heldebrant. Removing, or stripping, the CO₂ from the capture agent allows the liquid to be recycled and capture more CO₂. With CO₂BOLs, less fluid is needed to capture the same amount of CO₂, and less energy is needed to strip the CO₂, Heldebrant explains. 'Such a system can potentially offer large energy savings for CO₂ stripping when employed on an industrial scale,' he adds.

In addition, Heldebrant's group found that the CO₂BOLs, which were designed to be a direct replacement for the aqueous amines currently used in coal plants, could go through five cycles of capturing and releasing CO₂ without losing activity or selectivity.

'The release of CO₂ in a controlled fashion is important for permanent



Reference

D J Heldebrant *et al*, *Energy Environ. Sci.*, 2008, DOI: 10.1039/b809533g

sequestration of CO₂ or other applications such as carbonation in the beverage, dry cleaning or chemical industries,' explains Heldebrant. 'Just because CO₂ is a greenhouse gas doesn't mean it has no useful applications or market value.'

Kazunari Ohgaki, an expert in carbon capture and storage, from Osaka University, Japan, sees the potential of the study. 'In the future, these mixtures could replace aqueous amine solutions as a way of removing CO₂ from post-combustion waste gases,' he says.

Heldebrant's team are currently modelling the system to check for any obstacles to implementation and also plan to investigate whether CO₂BOLs could be used to capture CO₂ before the fuel is burned. *Christina Hodkinson*

New detection method could improve airport security

Fabrics reveal their explosive secrets

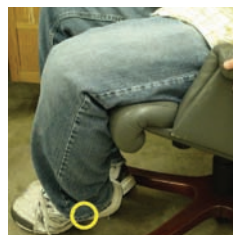
Explosives and drugs on fabrics can be detected within seconds using mass spectrometry, say US scientists. The method could be used to improve travel security in airports, they claim.

Graham Cooks and colleagues from Purdue University, West Lafayette, analysed a variety of fabrics for drugs and explosives using desorption electrospray ionisation (DESI) mass spectrometry. They showed they could identify compounds of interest in less than 10 seconds, even if the fabric also contained other chemicals, such as insect repellent or skin lotions.

Typically, scientists have to extract compounds from fabrics using time-consuming techniques, such as solvent extraction. In

DESI, charged droplets from an electrospray source are directed at the fabric. Compounds on the fabric's surface are picked up by the charged droplets and analysed in a mass spectrometer. The method, which can detect compounds at picogram levels, requires no sample preparation or work-up. It allows mass spectrometry to address important problems in forensics and public safety rapidly with the accuracy of slower traditional mass spectrometry methods, says Cooks.

Even though this method seems to overcome quite a few of the background and interference problems associated with other methods, further investigations are still needed, states Christopher Latkoczy, a specialist in the



Nowhere to hide: drugs and explosives on clothing can be identified within seconds

applications of mass spectrometry from the Swiss Federal Institute of Technology, Zurich. 'After overcoming some of the current limitations, in the future this method could be used as a rapid screening technique coupled to handheld devices for security people working, for example, at airports,' he says.

Cooks already plans to miniaturise the technique: 'The next challenge is to develop a handheld mass spectrometer capable of performing the same ambient ionisation experiments in situ,' he says.

Michael Brown

Reference

N Talaty et al, *Analyst*, 2008, DOI:10.1039/b807934j

No missing pieces

Chemistry World e-alerts are the perfect way to ensure you always see the complete picture.

Sign up now for free and keep up to date on all the latest chemistry news with a daily e-mail that lets you know what's new on the *Chemistry World* website.

chemistryworld
e-alerts

RSC | Advancing the
Chemical Sciences

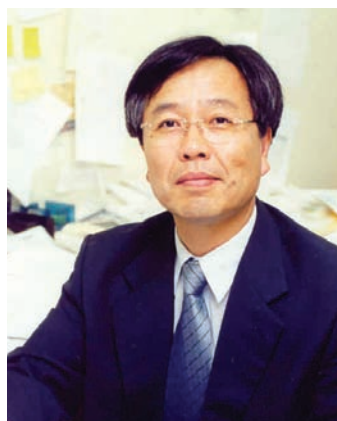
www.chemistryworld.org

Registered Charity Number 207890

Interview

Chemistry's gain

Ryong Ryoo tells Rachel Cooper how he took a risk and became an expert in mesoporous materials



Ryong Ryoo

Ryong Ryoo is a professor of chemistry at Korea Advanced Institute of Science and Technology and has been on the *Chemical Communications* editorial board since 2006. He has received numerous awards and was named Korea's national scientist by the Korean government in 2007.

What first attracted you to science?

In the second year of high school in Korea, students are divided into two groups. One group is taught science and engineering and the other is taught an advanced level of literature, such as English. I belonged to the non-science group, so I never thought I would become a scientist. When I was almost at the end of my high school studies, I realised that my ability was science-based, so I decided to risk taking the entrance exam for science at Seoul National University. Fortunately, I succeeded.

What made you choose chemistry as a career?

At university, I liked chemistry. I took the entrance exam for KAIST [Korea Advanced Institute of Science and Technology], a university that gave special exemption from military service. People graduating from KAIST could instead take a job in industry, a research institute or even in a university, with three years' regular salary. I would never have thought about being a chemist otherwise, as my parents could not afford to pay for my graduate studies. Korea was totally different 30 years ago – ordinary people couldn't think about sending their children to study. It cost too much.

Which area of chemistry did you work in?

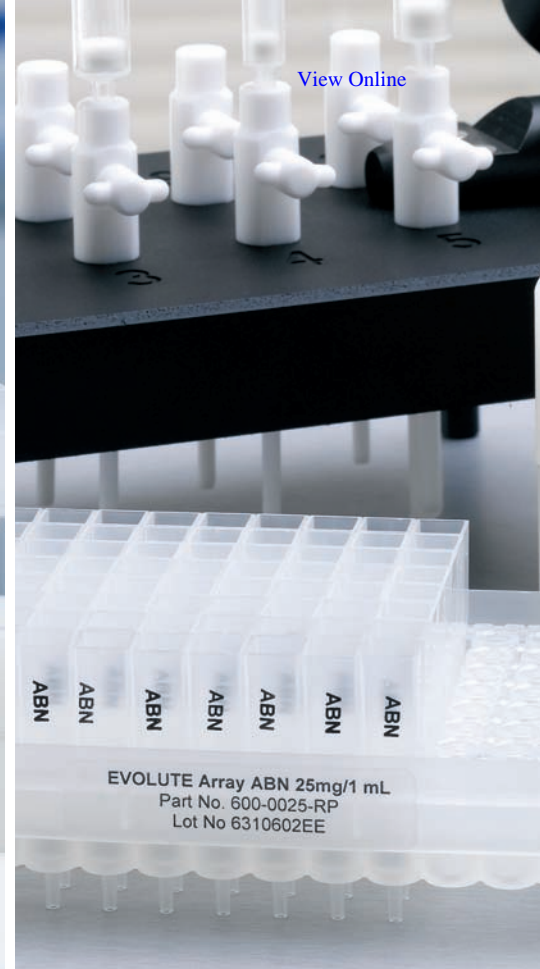
Initially, I chose computational chemistry, calculating thermodynamic properties of liquid helium and other liquids. After working at a national lab, the Korea Atomic Energy Research Institute, for three years, I went to Stanford University for my PhD. There, I chose more practical chemistry – heterogeneous catalysis. I learnt about xenon gas NMR, and its use on porous materials, such as zeolites, but I didn't learn how to synthesise porous materials at that time. I returned to Korea after a one-year post-doctoral stay at the University of California, Berkeley and I did the same kind of research as I had done in the US. I used zeolites as supports for platinum. I used xenon NMR, extended X-ray absorption fine structure and other physical tools to characterise porous zeolites and supported metal nanoparticles, at that time called clusters.

What is your favourite piece of research?

At a conference in Japan in 1993, I happened to hear about mesoporous silica MCM-41. I was fascinated by its structure and large pores. I wanted to use the material as a support for metal nanoparticles, but I couldn't obtain it then. Although I knew nothing about the chemistry of silica, I decided to synthesise it in my laboratory. I struggled for several years, and somehow became an expert in mesoporous materials. Because I hadn't been trained how to do it, I used my own ideas and this is what brings the field forwards. In 1999, I published a very important paper on the synthesis of ordered mesoporous carbon, using mesoporous silica as a template. Before that, there were no carbon materials showing ordered porosity, so my synthesis of the first ordered mesoporous carbon, named CMK (carbon metastructure at KAIST), was very surprising. It was the first material to exhibit Bragg X-ray diffraction peaks (due to the structural order) with porosity. People were fascinated by the material; they began to use it and to follow the synthesis. So that was my favourite, and best, work.

What do you see as the most important future applications for mesoporous materials?

These days, I work on zeolites with mesoporosity as well as the inherent microporosity. Microporous materials have pores smaller than two nanometres, and mesoporous materials have pores between two and 50 nanometres. Zeolites have micropores about one nanometre and normally they are synthesised as crystals, with no mesoporosity. However, if you synthesise zeolites with mesopores penetrating the crystals then you make a zeolite with both micropores and mesopores; these are called hierarchical zeolites. The advantage of such hierarchical zeolites is that molecular diffusion can take place very rapidly through large mesopores into small micropores. Without mesopores, the diffusion into micropores is very slow. The consequence of such facile diffusion is that zeolites, in many reactions, show dramatically increased lifetimes when they are used as catalysts. This is a great advantage, as you can continuously operate two or three times longer without catalyst replacement, saving money.



IST Sample Preparation • Bioanalysis • Clinical • Environmental • Forensic • Agrochemical • Food • Doping Control

EVOLUTE® CX **NEW!**

Mixed-mode selectivity, generic methodology and efficient extraction

EVOLUTE® CX mixed-mode resin-based SPE sorbent extracts a wide range of **basic drugs** from biological fluid samples. EVOLUTE CX removes matrix components such as proteins, salts, non-ionizable interferences and phospholipids, delivering cleaner extracts with reproducible recoveries for accurate quantitation.

EVOLUTE® ABN

Minimize matrix effects, reduce ion suppression and concentrate analytes of interest

EVOLUTE® ABN (Acid, Base, Neutral) is a water-wettable polymeric sorbent optimized for fast generic reversed phase SPE. Available in 30 μm columns and 96-well plates for bioanalysis and **NEW 50 μm columns** – ideally suited for environmental, food/agrochemical and industrial analysis as well as forensic and doping control applications.

Contact your local Biotage representative or visit www.biotage.com to request a **FREE** sample.

Instant insight

The wonder of gold

Graham J Hutchings, Mathias Brust and Hubert Schmidbaur introduce the newly discovered allure of gold

Gold is a material that has fascinated humankind since it was first discovered. It is the most noble of metals; it does not tarnish on exposure to the atmosphere and retains its beautiful lustre undiminished for millennia. It has been the inspiration for great artworks and also the cause of great conflicts. It is also a metal with high monetary value and, in these current times of high energy costs, gold has increased in value dramatically. Hence, from the perspective of the monetary, art and historical communities, gold is an important metal, something that has high value and is readily traded.

Gold was also the fascination of alchemists as they tried, in vain, to make gold from base metals. However, for mainstream chemists, until recently, gold has presented very little fascination. Its chemical inertness in a bulk state convinced chemists that few, if any, exciting chemistries awaited deeper investigation. Hence, the real wonders of gold chemistry have only recently been discovered and the observation that gold, when sub-divided to the nanoscale, can be exceptionally active as a catalyst, has spurred a great number of discoveries. In tandem with catalysis discoveries, there have been enormous developments in the fabrication and uses of gold nanoparticles that are underpinned by the growing field of structural and theoretical advances that are being made in gold chemistry.

Gold now fascinates material scientists, catalysis, surface and synthetic chemists and theoreticians in great numbers. From a catalysis viewpoint, gold has become the hot topic and is now the catalyst of choice for many reactions. Indeed, the observation that it can catalyse the oxidation of carbon monoxide at temperatures



JUPTER IMAGES

as low as minus 76 degrees Celsius has fascinated many researchers in the recent past.

In terms of application, gold catalysts are starting to show efficacy in selective oxidation and hydrogenation, often showing activities far higher than other previously tried catalysts. There still remains a fascination with carbon monoxide oxidation, since this is expected to find applications in fuel cells for removal of the last traces of carbon monoxide impurities in the hydrogen fuel, something that gold can readily achieve without oxidizing the valuable hydrogen. A key discovery has been the discovery that gold–palladium alloys can act as efficient catalysts for the direct formation of hydrogen peroxide by hydrogenation of oxygen, which we anticipate will find commercial application.

Although the field of gold chemistry and catalysis has been

Gold is a metal with high monetary value that is now finding new uses in chemistry

significantly advanced in recent years, many key challenges remain. In the case of gold chemistry, we now need to gain precise control in the preparation strategies of the particle shape. Most effort has gone into controlling particle size, but controlling shape will be more challenging. In the field of catalysis, the remaining main challenge concerns the nature of the active site for supported gold nanoparticles. This has proved to be a highly controversial topic and a number of key debates concern the electronic nature of the active species. It is most likely that different gold species will be active for the myriad of reactions that gold can catalyse. However, as yet the active site for most reactions remains an area of intense activity.

Reference
G J Hutchings, M Brust and H Schmidbaur, *Chem. Soc. Rev.*, 2008, **37**, 1759 (DOI: 10.1039/b810747p)

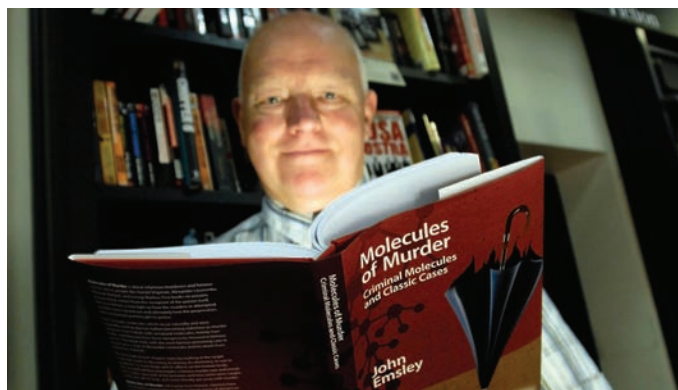
Read more in 'Gold - an introductory perspective' in issue 9 of Chemical Society Reviews.

Essential elements

Molecules of Murder book launch

On 30 July the RSC, with Waterstone's bookshop Gower Street London, were delighted to host the launch of John Emsley's highly anticipated book *Molecules of Murder: Criminal Molecules and Classic Cases*. John Emsley is a great science communicator, best known for his series of highly readable books about everyday chemistry. His latest book looks at 10 toxic molecules, discusses their chemistry and effects in humans, and re-examines their deliberate misuse in high profile murder cases.

At the book launch, guests were joined by two actors in Victorian costume, posing as the murderer and victim from Chapter 2 of the book: Hyoscine and the Murder of Belle Elmore (Mrs Crippen). The infamous Edwardian killer Dr Crippen poisoned his wife, Belle Elmore, then dissected and buried her under the cellar floor. The victim was a minor celebrity noted for her flamboyant clothing, and had appeared at



music halls around the country at that time. The two came to life in the basement of Waterstone's bookshop, and intrigued guests with spine chilling tales of poison and murder!

John Emsley signed copies of the book, described his reasons for embarking on the project and then read a piece of the work. Guests reading the book for the first time were interested to find out about other murder cases, such as the use of ricin in a rolled

umbrella to assassinate Georgi Markov 30 years ago, and most recently the murder of Alexander Litvinenko in London by polonium. *Molecules of Murder* is a gripping read with appeal to chemists and non-chemists alike. Anyone with an interest in popular science and crime will be enthralled by this exciting new book.

For more information please visit www.rsc.org/books

A science feast in Philadelphia

It was an action-packed few days at the ACS Fall 2008 National Meeting in Philadelphia. The first print issue of *Energy & Environmental Science* generated a lot of interest, with its impressive range of articles on solar cells, hybrid fuel cells, hydrogen storage, biofuel production, sustainable energy, and more. *Integrative Biology* and *Metallomics*, the two new journals launching in 2009, were in the spotlight and grabbed

the attention of many visitors to the RSC booth. RSC Publishing staff were on hand as people signed up for journal e-alerts, hoping to win a solar-powered charger for mobile devices. The book sale proved popular, and authors John Emsley (*Molecules of Murder*) and Stephen Beckett (*The Science of Chocolate*) signed copies of their recent books for an appreciative audience. Other activities included stimulating

talks on science writing and chocolate – and the arrival of cookies, cakes and other goodies, gave everyone a chance to boost their energy levels!

The RSC Reception, held at a nearby Philadelphia hotel, gave assembled guests the opportunity to hear from RSC President Dave Garner about developments across the whole of the RSC, including how the RSC Roadmap will shape future RSC strategy.

Need a guiding hand?

Walk through an enhanced online journal article and discover the wealth of additional information available to you using our new RSC Prospect User Guide. RSC Prospect is the award-winning service that structures the science within our journal articles.

Our user-friendly guide shows you how to make the most of our enhanced articles by demonstrating all of the special features available to you, including:

- biomedical terms linked to definitions and related papers
- RSS feeds containing biomedical terms and compound structures
- hyperlinked compound information in text
- downloadable compound structures
- searching for articles by compound structure

Each step is illustrated with screenshots taken from actual enhanced articles and a glossary of terms helps you get to grips with new terminology. Download the full guide at www.rsc.org/prospectguide



Chemical Technology (ISSN: 1744-1560) is published monthly by the Royal Society of Chemistry, Thomas Graham House, Science Park, Milton Road, Cambridge UK CB4 0WF. It is distributed free with *Chemical Communications*, *Journal of Materials Chemistry*, *The Analyst*, *Lab on a Chip*, *Journal of Atomic Absorption Spectrometry*, *Green Chemistry*, *CrystEngComm*, *Physical Chemistry Chemical Physics*, *Energy & Environmental Science* and *Analytical Abstracts*. *Chemical Technology* can also be purchased separately. 2008 annual subscription rate: £199; US \$396. All orders accompanied by payment should be sent to Sales and Customer Services, RSC (address above). Tel +44 (0) 1223 432360, Fax +44 (0) 1223 426017. Email: sales@rsc.org

Editor: Joanne Thomson
Deputy editor: Michael Spencelayh
Associate editors: Celia Gitterman, Nina Notman
Interviews editor: Elinor Richards
Web editors: Nicola Convine, Michael Townsend, Debora Giovanelli
Essential elements: Sarah Day, Rebecca Jeeves and Valerie Simpson

Publishing assistant: Jackie Cockrill
Publisher: Graham McCann

Apart from fair dealing for the purposes of research or private study for non-commercial purposes, or criticism or review, as permitted under the Copyright, Designs and Patents Act 1988 and the copyright and Related Rights Regulations 2003, this publication may only be reproduced, stored or transmitted, in any form or by any means, with the prior permission of the Publisher or in the case of reprographic reproduction in accordance with the terms of licences issued by the Copyright Licensing Agency in the UK. US copyright law is applicable to users in the USA.

The Royal Society of Chemistry takes reasonable care in the preparation of this publication but does not accept liability for the consequences of any errors or omissions.

Royal Society of Chemistry: Registered Charity No. 207890.

RSC Publishing

Green synthesis of 1–2 nm gold nanoparticles stabilized by amine-terminated ionic liquid and their electrocatalytic activity in oxygen reduction†

Zhijuan Wang,^{a,b} Qixian Zhang,^a Daniel Kuehner,^a Ari Ivaska^b and Li Niu^{*a,b}

Received 16th April 2008, Accepted 15th July 2008

First published as an Advance Article on the web 29th July 2008

DOI: 10.1039/b806453a

Stable gold nanoparticles with average size 1.7 nm synthesized by an amine-terminated ionic liquid showed enhanced electrocatalytic activity and high stability.

Electrocatalytically active gold nanoparticles are enjoying increasing applications in electrochemistry, electroanalysis and bioelectronics.¹ Catalytic activity has been shown to depend strongly on the gold oxidation state, nanoparticle size and surface properties.² For example, 1.3 nm gold nanoparticles exhibited superior activity in catalysis of aerobic alcohol, relative to larger (9.5 nm) particles.³ An established method for generating 1–3 nm gold nanoparticles is reduction of AuCl₄⁻ by sodium borohydride in the presence of an alkanethiol in water–toluene biphasic reaction systems.⁴ While the resulting nanoparticles are very stable, the reagents are hazardous. A “greener” route, reduction by citrate in water, yields particles of only limited stability.⁵ In general, preparation of gold particles with narrow size distribution in the 1–3 nm range and long-term electrocatalytic activity is difficult, and reports of suitable novel syntheses are few.^{6–8}

Room-temperature ionic liquids (RTILs) seem well positioned to address the challenge of preparing stable, active gold nanoparticles, due to their high chemical and thermal stability, negligible vapor pressure, recyclability, high conductivity and wide electrochemical window.⁹ Moreover, low interfacial tensions result in high nucleation rates, allowing formation of very small particles because Ostwald ripening occurs only weakly.¹⁰ RTILs have been successfully employed in “green” preparations of Cu₂O crystals,⁹ gold nanosheets,¹¹ and nanoparticles of silver, gold or platinum.^{12–14} In this work, a functionalized RTIL, 1-(3-aminopropyl)-3-methylimidazolium bromide (IL-NH₂),¹⁵ was applied to simultaneously reduce aqueous HAuCl₄ and stabilize the resulting gold nanoparticles, which had an average diameter 1.7 nm and retained long-term stability without special protection. These IL-stabilized gold nanoparticles (Au-IL) showed better electrocatalytic activity in reduction of oxygen

than similarly prepared gold nanoparticles stabilized by thiol⁴ or citrate.¹⁶

The resulting orange gold suspension did not show a plasmon band in the range of 500–550 nm (Fig. 1A), qualitatively indicating average particle size less than 2 nm.¹⁷ The UV-vis analysis is verified easily by TEM (Fig. 1B) and HRTEM (Fig. 1C) measurements. The TEM image revealed well-dispersed gold nanoparticles with average diameter ~1.7 nm. Several particles with diameter > 2.0 nm are also present, but it was suspected that these particles arise from overlapping of two or more small particles. The formation of 1–2 nm gold nanoparticles resulted from two factors. Firstly, in the presence of ILs, gold nanoparticles undergo weak Ostwald ripening and easily formed very small gold nanoparticles. Further, the chemical and physical interaction between the ionic liquid and the metal plays a decisive role in controlling the size and structure of the nanoparticles. Fig. 1C shows a representative HRTEM image of a gold nanoparticle. Clear lattice fringes indicate high crystallinity, and d-spacing of 2.4 Å corresponds to the (111) lattice planes of gold. The selective-area-electron-diffraction (SAED) pattern (Fig. S1, ESI†) and XRD results (Fig. S2, ESI†) indicates the small Au nanoparticles possess (111) facets. Fig. 1D shows a typical XPS spectrum of Au-IL particles. While

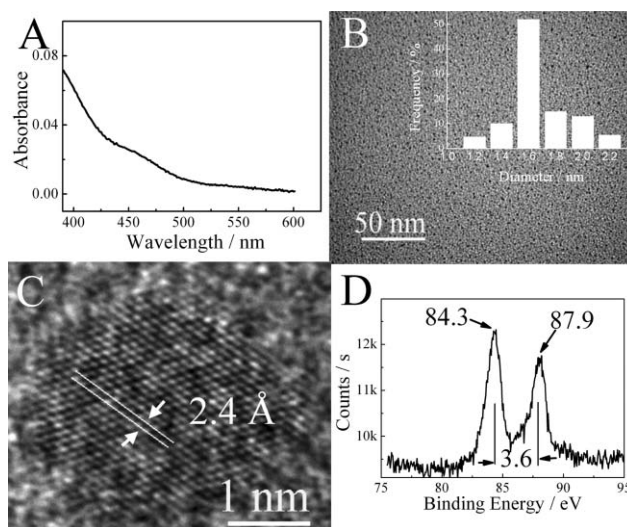


Fig. 1 (A) UV-vis spectrum of the resulting suspension after 8 h, (B) TEM image of the gold nanoparticles prepared in the presence of IL-NH₂ with size-distribution histogram obtained from measuring 240 randomly selected particles, (C) HRTEM image showing lattice spacing and (D) XPS pattern of the resulting product.

^aState Key Laboratory of Electroanalytical Chemistry, Changchun Institute of Applied Chemistry and Graduate School of the Chinese Academy of Sciences, Chinese Academy of Sciences, Changchun, 130022, P. R. China. E-mail: lniu@ciac.jl.cn; Fax: +86-431-85262800; Tel: +86-431-85262074

^bLaboratory of Analytical Chemistry, Process Chemistry Centre, Åbo Akademi University, Biskopsgatan 10, Åbo-Turku, 20500, Finland

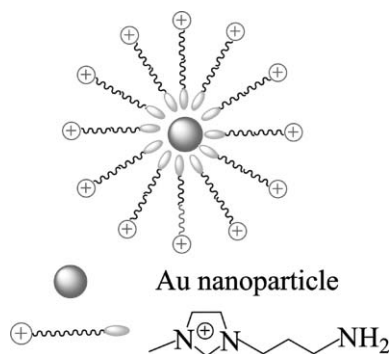
† Electronic supplementary information (ESI) available: Instrumentation details and Fig. S1–S8. See DOI: 10.1039/b806453a

the line shape and peak-to-peak distance of the Au 4f doublet is consistent with the Au⁰ state, the binding energies 84.3 (Au 4f_{7/2}) and 87.9 (Au 4f_{5/2}) were slightly higher than expected for bulk Au (Au 4f_{7/2} 84.0 eV and Au 4f_{5/2} 87.6 eV). This difference might be a consequence of the small size of these nanoparticles^{18a} and the presence of the IL-NH₂ ligands.^{18b} The increase in values of the binding energy with the decrease in the size is consistent with the previous reports.^{18a,b} However, other opposite results showed that the binding energy of small gold nanoparticles decreased compared to the bulk Au.^{18c,d}

To investigate the role of the IL-NH₂ terminal amine group, IL-NH₂ was replaced by [C4mim]⁺BF₄⁻ (Fig. S3, ESI[†]) in a control reaction. Here, no change happened even after two days stirring, indicating that the terminal amine reduces [AuCl₄⁻]. At the same time, the disappearance of the primary amine peak in the control reaction's NMR spectrum (inset of Fig. S4, ESI[†]), compared with the NMR spectra of IL-NH₂ (Fig. S5, ESI[†]) and Au-IL (Fig. S4, ESI[†]), confirms the reaction of the amine group.

After dialysis of Au-IL solution, the originally *ca.* 1.7 nm Au nanoparticles evolved into larger particles (*ca.* 9 nm) and hexagonal gold sheets (Fig. S6, ESI[†]). Removal of IL units by dialysis destabilized the nanoparticles by exposing surface area for further crystallization. This observation also confirms that IL-NH₂ plays an active role in stabilizing the gold nanoparticles, by the weak interaction of Au⁰/N.¹⁹

In addition, the ζ potential of aqueous Au-IL suspensions were as high as 35 ± 0.5 mV, which further indicated that imidazole positive termini are exposed to the outside of gold nanoparticles, illustrated in Scheme 1.



Scheme 1 Structure illustration of the resulting Au-IL nanoparticles.

Fig. 2A shows typical cyclic voltammograms (CV) for the reduction of oxygen at electrodes functionalized with Au-IL (Au-IL f-electrode) in O₂- and N₂-saturated acidic electrolyte solutions. A well-defined peak for oxygen reduction is present at 0.28 V, while in the nitrogen-saturated systems no peak is apparent. Oxygen reduction at a naked GC electrode gave a peak at -0.50 V (inset of Fig. 2A). The 780 mV positive peak shift achieved with the functionalized electrode indicates the significant electrocatalytic effect of the Au-IL nanoparticle coating.

For comparison, CV in the same system was also conducted using Au-SH and Au-cit f-electrodes. Fig. 2B shows that oxygen reduction at the Au-SH f-electrode began at a potential of -0.51 V, approximately the same as at the naked electrode, while the Au-cit f-electrode showed a reduction peak

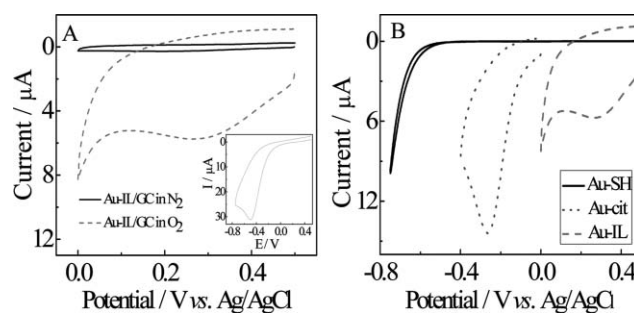


Fig. 2 Cyclic voltammograms from: (A) Au-IL f-electrode in aqueous 0.5 M H₂SO₄ electrolyte solution saturated with O₂ (dashed) and N₂ (solid); inset shows voltammogram from bare GC electrode in aqueous 0.5 M H₂SO₄ solution saturated with O₂; (B) Au-IL (dashed), Au-cit (dotted) and Au-SH (solid) f-electrodes in aqueous 0.5 M H₂SO₄ solution saturated with O₂. Scan rates: 0.05 V s⁻¹.

at -0.26 V. These results indicate that the electrocatalytic activity of Au-IL nanoparticles is higher than that of thiol- and citrate-stabilized gold. Since the particle sizes of Au-IL, Au-SH and Au-cit were all quite similar, the clear difference in their voltammograms suggests that the type of the stabilizing group contributes strongly to the catalytic activity. The too strong interaction between Au and -SH reduced the catalytic activity of gold nanoparticles greatly,²⁰ the presence of -SH even prevents oxygen from reacting on the f-GC electrode surface. However, the good electrocatalysis might be attributed to the unique properties of IL, such as the high conductivity²¹ and the weak interaction of Au⁰/N.

Samples of the stabilized-gold products were kept in air without any special protection, and UV-vis absorbance was monitored over a period of more than eight months (Fig. 3). At no point did the absorbance spectrum of Au-IL change significantly, indicating that aggregation did not occur. However, in Au-cit suspensions, peak shifting was apparent after only 2.5 h (Fig. S7, ESI[†]) due to significant aggregation.

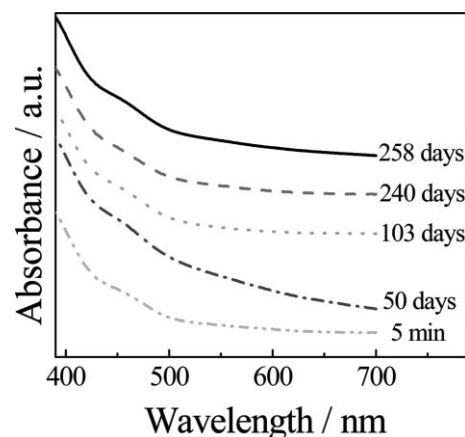


Fig. 3 UV-vis spectra of Au-IL nanoparticles kept at room temperature over time.

In conclusion, Au nanoparticles (1.7 nm average diameter) were synthesized and stabilized by 1-(3-aminopropyl)-3-methylimidazolium bromide through a one-step green method. Despite their small size, the obtained nanoparticles are very stable in air, compared to similarly prepared Au-cit particles

of comparable size. Moreover, Au-IL nanoparticles showed significant electrocatalytic activity towards O₂ reduction (780 mV positive peak shift in cyclic voltammetry). Control experiments with Au-cit and Au-SH indicated that the presence of 1-(3-aminopropyl)-3-methylimidazolium bromide plays a unique role in improving the electrocatalysis of the gold nanoparticles.

Materials

Methylimidazole ($\geq 98\%$) was distilled under a nitrogen atmosphere at reduced pressure prior to use. H₂AuCl₄·3H₂O (99.9+%, Aldrich), 3-bromopropylamine hydrobromide (98%, Aldrich), 1-butyl-3-methylimidazolium tetrafluoroborate, [C₄mim]⁺BF₄⁻ (99%, Lanzhou Institute of Chemical Physics, Chinese Academy of Sciences), ethanol (99.8%, Beijing Chemicals Company) and ethyl acetate (99.7%, Beijing Chemicals Company) were used as received. All aqueous solutions were prepared with ultra-pure water ($> 18 \text{ M}\Omega$) from a Milli-Q Plus system (Millipore). All experiments were carried out at room temperature.

Preparation of IL-NH₂:

IL-NH₂ was prepared following our previous report.¹⁵ Briefly, 3-bromopropylamine hydrobromide (1.1000 g, 5 mmol) and 1-methylimidazole (0.395 mL, 5 mmol) were added to 12.5 mL ethanol, forming a colourless solution which was refluxed under nitrogen for 24 h. The resulting turbid mixture was purified by recrystallization from ethanol, with ethyl acetate as anti-solvent. Finally, the resulting white powder was dried overnight at 60 °C under vacuum and purity verified by ¹H NMR (Fig. S5, ESI[†]).

Preparation of Au-IL:

Ionic-liquid stabilized gold nanoparticles (Au-IL) were typically prepared by dissolving 0.2096 g IL-NH₂ (0.95 mmol) in 5.000 mL ultra-pure water, followed by dropwise addition of 1.000 mL of aqueous H₂AuCl₄·3H₂O (containing 0.0080 g, 0.02 mmol) over several minutes. During addition, the colour of the resulting solution changed from yellow to orange to deep red, indicating formation of gold nanostructures. After stirring for an additional 8 h, the colour remained deep red, and some precipitate was evident, which was collected by centrifugation, washed several times with ultra-pure water and dried overnight at 60 °C under vacuum. After the re-suspension into distilled water, the colour was orange.

Preparation of gold nanoparticles stabilized by thiol (Au-SH) and citrate (Au-cit):

Au-SH (Fig. S8, 1–3 nm, ESI[†]) and Au-cit (3.5 nm) were prepared following Brust⁴ and Gao,¹⁶ respectively.

Preparation of Au-IL, Au-SH and Au-cit-functionalized glassy carbon electrode:

Au-IL, Au-SH and Au-cit samples were suspended in ethanol, respectively. And then, these suspensions were dropped onto

separate 3 mm-diameter glassy carbon electrodes. After ethanol evaporated, these functionalized-Au-nanoparticle electrodes (f-electrodes) were applied in reduction of molecular oxygen.

Acknowledgements

We thank Hui Wei and Wen Yang for their invaluable discussions and Prof. Jixue Li for his analysis of the results of HRTEM. Moreover, we gratefully acknowledge NSFC and Department of Science and Technology of Jilin Province, China for their financial supports (No.20475053, No.20673109 and No.20050102).

Notes and references

- 1 C. R. Raj and B. K. Jena, *Chem. Commun.*, 2005, 2005.
- 2 N. Hickey, P. A. Larochette, C. Gentilini, L. Sordelli, L. Olivi, S. Polizzi, T. Montini, P. Fornasiero, L. Pasquato and M. Graziani, *Chem. Mater.*, 2007, **19**, 650.
- 3 H. Tsunoyama, H. Sakurai, Y. Negishi and T. Tsukuda, *J. Am. Chem. Soc.*, 2005, **127**, 9374.
- 4 M. Brust, M. Walker, D. Bethell, D. J. Schiffrin and R. Whyman, *J. Chem. Soc., Chem. Commun.*, 1994, 801.
- 5 J. A. Dahl, B. L. S. Maddux and J. E. Hutchison, *Chem. Rev.*, 2007, **107**, 2228.
- 6 Y. Negishi, K. Nobusada and T. Tsukuda, *J. Am. Chem. Soc.*, 2005, **127**, 5261.
- 7 Y. Shichibu, Y. Negishi, T. Tsukuda and T. Teranishi, *J. Am. Chem. Soc.*, 2005, **127**, 13464.
- 8 C.-C. Huang, Z. Yang, K.-H. Lee and H.-T. Chang, *Angew. Chem., Int. Ed.*, 2007, **46**, 6824.
- 9 H. Li, R. Liu, R. X. Zhao, Y. F. Zheng, W. X. Chen and Z. D. Xu, *Cryst. Growth Des.*, 2006, **6**, 2795.
- 10 M. Antonietti, D. B. Kuang, B. Smarsly and Y. Zhou, *Angew. Chem., Int. Ed.*, 2004, **43**, 4988.
- 11 Z. H. Li, Z. M. Liu, J. L. Zhang, B. X. Han, J. M. Du, Y. N. Gao and T. Jiang, *J. Phys. Chem. B*, 2005, **109**, 14445.
- 12 G. Shemer, O. Krichevski, G. Markovich, T. Molotsky, I. Lubitz and A. B. Kotlyar, *J. Am. Chem. Soc.*, 2006, **128**, 11006.
- 13 H. Itoh, K. Naka and Y. Chujo, *J. Am. Chem. Soc.*, 2004, **126**, 3026.
- 14 Z. W. Zhao, Z. P. Guo, J. Ding, D. Wexler, Z. F. Ma, D. Y. Zhang and H. K. Liu, *Electrochem. Commun.*, 2006, **8**, 245.
- 15 Y. J. Zhang, Y. F. Shen, J. H. Yuan, D. X. Han, Z. J. Wang, Q. X. Zhang and L. Niu, *Angew. Chem., Int. Ed.*, 2006, **45**, 5867.
- 16 J. X. Gao, C. M. Bender and C. J. Murphy, *Langmuir*, 2003, **19**, 9065.
- 17 Y.-G. Kim, S.-K. Oh and R. M. Crooks, *Chem. Mater.*, 2004, **16**, 167.
- 18 (a) M. J. Hostetler, J. E. Wingate, C. J. Zhong, J. E. Harris, R. W. Vachet, M. R. Clark, J. D. Londono, S. J. Green, J. J. Stokes, G. D. Wignall, G. L. Glish, M. D. Porter, N. D. Evans and R. W. Murray, *Langmuir*, 1998, **14**, 17; (b) X. Y. Fu, Y. Wang, N. Z. Wu, L. L. Gui and Y. Q. Tang, *J. Colloid Interface Sci.*, 2001, **243**, 326; (c) J. Radnik, C. Mohr and P. Cluz, *Phys. Chem. Chem. Phys.*, 2003, **5**, 172; (d) B. Balamurugan and T. Maruyama, *Appl. Phys. Lett.*, 2005, **87**, 143105.
- 19 D. V. Leff, L. Brandt and J. R. Heath, *Langmuir*, 1996, **12**, 4723.
- 20 H. Lee, S. E. Habas, S. Kwekin, D. Butcher, G. A. Somorjai and P. D. Yang, *Angew. Chem., Int. Ed.*, 2006, **45**, 7824.
- 21 Y. F. Shen, Y. J. Zhang, Q. X. Zhang, L. Niu, T. Y. You and A. Ivaska, *Chem. Commun.*, 2005, 4193.

$[\pi\text{-C}_5\text{H}_5\text{N}(\text{CH}_2)_{15}\text{CH}_3]_3[\text{PW}_4\text{O}_{32}]/\text{H}_2\text{O}_2/\text{ethyl acetate}/\text{alkenes}$: a recyclable and environmentally benign alkenes epoxidation catalytic system†

Yong Ding,* Wei Zhao, Hui Hua and Baochun Ma*

Received 19th May 2008, Accepted 2nd July 2008

First published as an Advance Article on the web 16th July 2008

DOI: 10.1039/b808404a

The epoxidation of alkenes was successfully catalyzed by a recyclable and environmentally benign catalytic system: $[\pi\text{-C}_5\text{H}_5\text{N}(\text{CH}_2)_{15}\text{CH}_3]_3[\text{PW}_4\text{O}_{32}]/\text{H}_2\text{O}_2/\text{ethyl acetate}/\text{olefin}$.

Epoxides are well known as one of the most valuable building blocks that can be used as intermediates and precursors for chemical production. The oxidation of alkenes with aqueous hydrogen peroxide¹ is very attractive from the viewpoint of industrial production and synthetic organic chemistry, since aqueous hydrogen peroxide is cheap, environmentally clean and easy to handle. Polyoxometalates have drawn wide attention in the last two decades as effective catalysts for epoxidation of alkenes.^{1–13} Among all the reported polyoxometalates, tungsten-based catalytic systems showed high efficiency of H_2O_2 utilization and high selectivity to the epoxides.^{2–12} Many groups have been involved in this topic in the world, and in particular, groups of Venturello and Ishii have contributed significantly to the developments of tungsten-based catalysts. In 1983, Venturello *et al.*² reported epoxidation of alkenes with a dilute H_2O_2 solution (15%) as an oxidant using a complex consisting of tungstate and phosphate as the catalyst. A combination of $\text{H}_3\text{PW}_{12}\text{O}_{40}$ and cetylpyridinium chloride was then developed in 1988 by Ishii *et al.*³ for epoxidation of alkenes using a commercially available H_2O_2 solution (35%) as an oxidant. However, the Venturello–Ishii epoxidation system had the following drawbacks: (1) the use of toxic and carcinogenic chlorocarbons (chloroform and 1,2-dichloroethane) as solvents; (2) separation and reuse of the catalysts are extremely difficult.

Later, many improvements based on tungsten-based catalysts were developed.^{4–9} Despite the high activity and excellent selectivity obtained in epoxidation of alkenes using the improved catalysts, difficulty of recovery and reuse of those homogeneous metal species has restricted their wide applications in industrial and laboratory synthesis. Xi¹⁰ explored a reaction-controlled phase transfer catalyst to resolve the recovery of the catalyst, however, to facilitate the reaction and recovery of the catalyst, Xi's catalyst has to be used in chlorinated solvents.

Herein, we report our preliminary result on this endeavor in which a new tungsten-based polyoxometalate, cetylpyridium heteropolyoxotungstates ($[\pi\text{-C}_5\text{H}_5\text{N}(\text{CH}_2)_{15}\text{CH}_3]_3[\text{PW}_4\text{O}_{32}]$, abbreviated as **I**), was synthesized and used as a reaction-controlled phase transfer catalyst for epoxidation of alkenes with H_2O_2 as the oxidant. This new system was not only capable of catalyzing homogeneous epoxidation of alkenes with unique reaction-controlled phase transfer characters, but also avoids the use of chlorinated solvents. The reactions were conducted in a biphasic mixture of aqueous H_2O_2 /ethyl acetate, and many kinds of alkenes can be converted to the corresponding epoxides in high to excellent yields. The catalyst could be easily recovered and reused after reaction. Therefore, this catalytic system possesses the advantages of both homogeneous and heterogeneous catalysts. In addition, our system was further extended to epoxidation of some dienes. Good to excellent reaction yields over catalyst **I** were obtained, further indicating the usefulness of this new system.

When using 30% H_2O_2 as an oxidant and ethyl acetate as a solvent to carry out the epoxidation of olefins, catalyst **I** precipitates from the reaction medium after epoxidation and can be recovered and reused. In an aqueous/oil biphasic system, catalyst **I** itself is not soluble in the oil phase, but it dissolves slowly under the action of H_2O_2 and the increase of the reaction temperature, which subsequently leads to homogeneous catalytic epoxidation of olefins. During the reaction, the system gradually changes from turbid to clear. When the reaction stops, with temperature dropping, catalyst **I** precipitates gradually. This phenomenon manifests a solid–liquid–solid phase transfer of catalyst **I**, which is controlled by the reaction conditions, and so these catalysts are called “reaction-controlled phase transfer catalysts.”

Table 1 summarises the catalytic epoxidation of 1-octene in ethyl acetate with 30% H_2O_2 using different catalysts prepared. It was found that the epoxidation does occur upon all the catalysts, but the yield of 1,2-epoxyoctane depends on different organic counter cations of heteropolyoxotungstates and anions of the quaternary ammonium salts that were used to prepare the catalysts. For catalysts containing a small quaternary ammonium cation such as tetra-butyl ammonium, they were insoluble in the reaction system during epoxidation, so the yield of epoxide was low (entry 3). Those catalysts containing a bigger quaternary ammonium cation, such as 1-dodecylpyridinium, cetylpyridinium, were a reaction-controlled phase transfer catalyst with high activity and selectivity (entry 1, 2). The activity of catalysts synthesized with quaternary ammonium bromide is

State Key Laboratory of Applied Organic Chemistry, College of Chemistry and Chemical Engineering, Lanzhou University, Lanzhou, 730000, China. E-mail: dingyong1@lzu.edu.cn, mabaochun@lzu.edu.cn; Fax: (+86)-931-8912582

† Electronic supplementary information (ESI) available: Instruments, syntheses and characterization of polyoxometalates and oxidation products. See DOI: 10.1039/b808404a

Table 1 Epoxidation of 1-octene on different catalysts^a

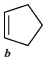
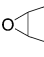
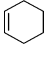
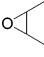
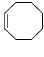
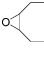
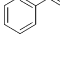
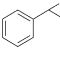
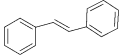
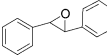

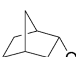
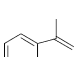
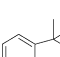
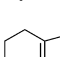
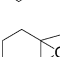
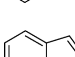
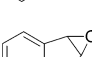


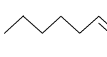
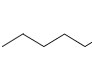

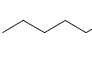

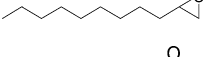
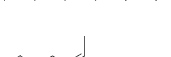
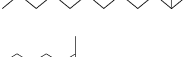

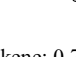
Entry	Catalyst	Selectivity (mol%)	Yield (mol%)
1	[π -C ₃ H ₅ N(CH ₂) ₁₅ CH ₃] ₃ PW ₄ O ₃₂ (I)	99	98
2 ^b	[π -C ₃ H ₅ N(CH ₂) ₁₁ CH ₃] ₃ -Cat	99	89
3 ^b	{[CH ₃ (CH ₂) ₃ N] ₃ -Cat	99	3
4 ^c	[π -C ₃ H ₅ N(CH ₂) ₁₅ CH ₃] ₃ -Cat	74	28
5 ^d	[π -C ₃ H ₅ N(CH ₂) ₁₅ CH ₃] ₃ [PW ₄ O ₁₆]	99	69
6	[π -C ₃ H ₅ N(CH ₂) ₁₅ CH ₃] ₃ [PW ₁₂ O ₄₀]	99	6

^a Reaction conditions: 3 mmol alkene; 0.75 mmol H₂O₂; 30 mg catalyst; 3 ml ethyl acetate; reaction temperature: 65 °C, reaction time: 2 h. Yield (%) = products (mol)/H₂O₂ used (mol) × 100. Conversions and selectivities were determined by gas chromatography using an internal standard technique and were based on H₂O₂. ^b Quaternary ammonium salts are quaternary ammonium chloride. ^c Quaternary ammonium salts are quaternary ammonium bromide. ^d Xi's catalyst.

inferior to that prepared with quaternary ammonium chloride (entry 4). Hence, the structure and anion of the quaternary ammonium salts play an important effect on forming an efficient reaction-controlled phase transfer catalyst.

The heteropolyoxotungstates catalyst **I** could be applicable to the epoxidation of various olefins (such as linear terminal olefins, internal olefins, cyclic olefins, styrene, and unactivated alkenes) with 30% H₂O₂ (Table 2). Excellent catalytic activity and selectivity, as well as the same property of reaction-controlled phase transfer catalysis, were also observed in the epoxidation of such olefins. Bulky cyclic olefins such as cyclohexene, styrene, cyclooctene, and norbornene were epoxidized with ~90% yield of epoxides. Nonactivated terminal C₇–C₁₆ alkenes such as 1-heptene, 1-octene, 1-undecene, 1-dodecene, and 1-hexadecylene could be transformed to the corresponding epoxide specifically with about 90% yield after 2 h reaction. For the epoxidation

Table 2 Epoxidation of various olefins catalyzed by **I**/H₂O₂/ethyl acetate^a

Substrate	Product	Reaction time/h	Selectivity (mol%)	Yield (mol%)
		1.5	91	80
		1.5	92	83
		1	99	98
		1	97	96
		1	98	97
		1	96	95
		1	97	96
		1	94	92
		2	96	67
		2	98	74
		1	97	94
		1	99	98
		2	98	90
		2	97	96
		1	99	98

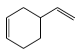
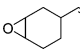
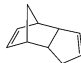
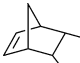
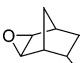
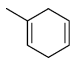
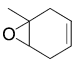
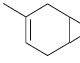
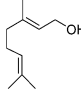
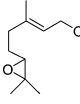
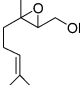
^a Reaction conditions: 3 mmol alkene; 0.75 mmol H₂O₂; 30 mg catalyst of **I**; 3 ml ethyl acetate; reaction temperature: 65 °C, Yield (%) = products (mol)/H₂O₂ used (mol) × 100. Conversions and selectivities were determined by gas chromatography using an internal standard technique and were based on H₂O₂. ^b Reaction temperature: 55 °C.

of *cis*-2-heptene, the configuration around the C=C bond was retained in the corresponding epoxide (*cis*-2,3-epoxyheptane was obtained with a 98% yield).

The $[\pi\text{-C}_5\text{H}_5\text{N}(\text{CH}_2)_{15}\text{CH}_3]_3\text{PW}_4\text{O}_{32}/\text{H}_2\text{O}_2/\text{ethyl acetate}$ catalytic system was also effective for the epoxidation of dienes (Table 3). After 1.5 h reaction, conversion of 99% for all substrates was obtained, but the selectivity for monoepoxide was not high enough. Only 4-vinyl-1-cyclohexene, a C=C moiety with higher electron density was epoxidized regioselectively to give the corresponding monoepoxide without the successive epoxidation of the other C=C fragment (entry 1).

To evaluate the stability and reuse of the solid catalysts of $[\pi\text{-C}_5\text{H}_5\text{N}(\text{CH}_2)_{15}\text{CH}_3]_3\text{PW}_4\text{O}_{32}$, we investigated the epoxidation of 1-octene over **I**/ H_2O_2 /ethyl acetate system (Table 4). The solid catalyst can be easily recovered by filtration and dry in air. After the catalytic epoxidation of 1-octene in the medium of **I**/ H_2O_2 /ethyl acetate system, catalyst **I** is self-precipitated with a 95% recovery yield (by weight). From Table 4, even after nine consecutive cycles of the reaction, a 70% yield of the epoxide with 99% selectivity was still kept for the epoxidation of 1-octene in this catalytic system, but the epoxide yield decreased gradually from cycle to cycle. From the spectra of ^{31}P MAS NMR, the recycled catalysts have almost the same chemical shift. The similarity between the catalyst of cycle 1, cycle 2 and cycle 3 suggests that from the second catalytic cycle, the structure of the quaternary ammonium heteropolyoxotungstates catalyst was stable and unchanged (see Fig. S4 in the ESI).† The IR spectra also indicates the catalyst remains stable from

Table 3 Epoxidation of dienes by **I**/ H_2O_2 /ethyl acetate^a

Entry	Dienes	Product	Selectivity (mol%)	Yield (mol%)
1			98	97
2			29	28
			71	70
3			53	52
			35	34
4			40	39
			60	60

^a Reaction conditions: 3 mmol alkene; 0.75 mmol H_2O_2 ; 30 mg catalyst of **I**; 3 ml ethyl acetate; reaction temperature: 65 °C, reaction time: 1.5 h; Yield (%) = products (mol)/ H_2O_2 used (mol) × 100. Selectivity (%) = monoepoxide (mol)/all products (mol). The products were identified by GC-MS and ^1H NMR.

Table 4 Epoxidation of 1-octene on catalyst **I**^a

Cycle times	Reaction time/h	Conversion (mol%)	Yield (mol%)
1	1	99	98
2	1	83	82
3	2	91	90
4	2	86	85
5	3	86	85
6	3	85	84
7	3	84	83
8	3	76	75
9	3	71	70
10 ^b	4	93	92

^a Reaction conditions: 3 mmol alkene; 0.75 mmol H_2O_2 ; 30 mg catalyst of **I**; 3 ml ethyl acetate; reaction temperature: 65 °C. Yield (%) = products (mol)/ H_2O_2 used (mol) × 100. Selectivity of epoxide was more than 99% for all cycles. ^b Reaction temperature: 70 °C.

the second cycle (see Fig. S6 in the ESI).† The decrease of the catalyst activity should be attributed to the leaching of W after each catalytic run (see Table 2 in the ESI).† The reason for the catalyst being easily recoverable after each reaction could be associated with the unique solvent of ethyl acetate and reaction temperature.

In summary, we developed a halide-free reaction-controlled phase transfer catalytic system consisting of $[\pi\text{-C}_5\text{H}_5\text{N}(\text{CH}_2)_{15}\text{CH}_3]_3\text{PW}_4\text{O}_{32}/\text{H}_2\text{O}_2/\text{ethyl acetate}$, and can efficiently catalyze many kinds of alkene epoxidations in high yield with an environmentally benign character. The catalyst could be easily recovered and reused after the reaction. This halide-free catalytic system overcomes the drawbacks of previously reported tungsten-based catalysts, which were difficult to recover and used toxic and carcinogenic chlorocarbons as solvents.

Experimental

Preparation catalyst of $[\pi\text{-C}_5\text{H}_5\text{N}(\text{CH}_2)_{15}\text{CH}_3]_3\text{PW}_4\text{O}_{32}$ (**I**). $\text{H}_3\text{PW}_{12}\text{O}_{40}$ (3.0 g, *ca.* 1.0 mmol) in 30% H_2O_2 (10 ml) was dropwise added to a solution of cetylpyridinium chloride (1.1 g, 3.1 mmol) in 30% H_2O_2 (40 ml) with intense stirring over 30 min. White precipitate was produced with the reaction of the above three reactants, and the mixture was stirred at 40 °C for 5 h. The suspended mixture was cooled to room temperature. After filtration, the precipitate was washed repeatedly with water and dried under air. Analytically pure catalyst **I** was obtained as a white powder. Yield: 1.9 g (87%). Anal. calcd for $[\pi\text{-C}_5\text{H}_5\text{N}(\text{CH}_2)_{15}\text{CH}_3]_3\text{PW}_4\text{O}_{32}$: C, 34.51; H, 5.20; N, 1.92; P, 1.42; W, 33.57; Found: C, 36.16; H, 5.59; N, 1.74; P, 1.23; W, 32.33; Raman spectra (cm^{-1}): 213, 235, 324, 556, 647, 862, 953, 988, 1006, 1029, 1064, 1174, 1217, 1299, 1440, 1582, 1633. IR spectrum (KBr, cm^{-1}): 2920, 2851, 2334, 1711, 1633, 1484, 1173, 1088, 1060, 984, 915, 846, 773, 723, 683, 650, 572, 549, 526, 440. UV-vis spectrum (in dichloromethane) showed shoulder bands at 227 nm, 260 nm. ^{31}P MAS NMR: 3.5, 0.7, -15.8 ppm. (Detailed characterizations see the ESI).†

Catalysts of $[\pi\text{-C}_5\text{H}_5\text{N}(\text{CH}_2)_{11}\text{CH}_3]_3\text{-Cat}$, $\{[\text{CH}_3(\text{CH}_2)_3\text{N}]\}_3\text{-Cat}$, $[\pi\text{-C}_5\text{H}_5\text{N}(\text{CH}_2)_{15}\text{CH}_3]_3\text{-Cat}$ were synthesized similarly according to above (detailed characterizations see the ESI).†

$[\pi\text{-C}_5\text{H}_5\text{N}(\text{CH}_2)_{15}\text{CH}_3]_3\text{PW}_4\text{O}_{16}$ was synthesized by the method reported in ref. 12a.

[π -C₅H₅N(CH₂)₁₅CH₃]₃[PW₁₂O₄₀]

A solution of cetylpyridinium bromide (5.2 mmol) in 70 ml of distilled water was added dropwise to H₃PW₁₂O₄₀ (1.7 mmol) in 10 ml of distilled water with stirring at ambient temperature to form a white precipitate immediately. After being stirred continuously for 3.5 h, the resulting mixture was filtered, washed several times with distilled water, and then dried at room temperature.

The catalytic reactions were performed in a 25 ml two-necked round-bottomed flask equipped with a septum, a magnetic stirring bar, and a reflux condenser. The epoxidation was carried out as follows: catalyst (30 mg), solvent (3 ml), substrate (3 mmol), and H₂O₂ (30% aq., 0.75 mmol) were charged in the reaction flask. The reaction was carried out at 338 K and detected by TLC accompanied with GC. After the reaction was over, the organic layer was analyzed by GC. The yield of products were calculated from the peak areas by using an internal standard method. The products were identified by GC-MS (Finnigan Trace DSQ). The carbon balance in each experiment was in the range of 95–100%. The amount of H₂O₂ remaining after the reaction was analyzed by normal iodometric methods. After reaction, the catalyst was precipitated from the solvent and was separated by centrifugation. For the characterization products of dienes as follows:

The precipitate was removed by centrifugation and filtration, and the filtrate extracted with EtOAc (30 ml \times 3), the organic layer was collected and washed with water and brine, then dried with anhydrous Na₂SO₄. After evaporation of the solvent under reduced pressure, the residue was purified by column chromatography with eluent (petroleum ether/ethyl acetate, 10/1) to give epoxides as a colorless liquid. The structure of the epoxides were determined by ¹H NMR, MS(EI).

Acknowledgements

This work was partly supported by the Natural Science Foundation of China (Grant No. 20702021). We gratefully thank Prof. W. Wang for the measurement of solid state NMR, GC-MS and GC.

References

- (a) B. Notari, *Adv. Catal.*, 1996, **41**, 253–334; (b) M. Klawonn, M. K. Tse, S. Bhor, C. Döbler and M. Beller, *J. Mol. Catal. A: Chem.*, 2004, **218**, 13–19; (c) T. Sakamoto and C. Pac, *Tetrahedron Lett.*, 2000, **41**, 10009–10012; (d) E. G. Ankudey, H. F. Olivo and T. L. Peeples, *Green Chem.*, 2006, **8**, 923–926.
- (a) C. Venturello, E. Alneri and M. Ricci, *J. Org. Chem.*, 1983, **48**, 3831–3833; (b) C. Venturello, R. D. Aloisio, J. C. J. Bart and M. Ricci, *J. Mol. Catal.*, 1985, **32**, 107–110; (c) C. Venturello and R. D'Aloisio, *J. Org. Chem.*, 1988, **53**, 1553–1557.
- (a) Y. Ishii, K. Yamawaki, T. Ura, H. Yamada, T. Yoshida and M. Ogawa, *J. Org. Chem.*, 1988, **53**, 3587–3593; (b) Y. Matoba, H. Inoue, J. Akagi, T. Okabayashi, Y. Ishii and M. Ogawa, *Synth. Commun.*, 1984, **14**, 865–873; (c) H. Yamamoto, M. Tsuda, S. Sakaguchi and Y. Ishii, *J. Org. Chem.*, 1997, **62**, 7174–7177.
- (a) R. Noyori, M. Aoki and K. Sato, *Chem. Commun.*, 2003, 1977; (b) K. Sato, M. Aoki, M. Ogawa, T. Hashimoto, D. Panyella and R. Noyori, *Bull. Chem. Soc. Jpn.*, 1997, **70**, 905–915.
- (a) K. Kamata, K. Yonehara, Y. Sumida, K. Yamaguchi, S. Hikichi and N. Mizuno, *Science*, 2003, **300**, 964; (b) K. Kamata, M. Kotani, K. Yamaguchi, S. Hikichi and N. Mizuno, *Chem.–Eur. J.*, 2007, **13**, 639; (c) T. Okuhara, N. Mizuno and M. Misono, *Adv. Catal.*, 1996, **41**, 113; (d) Y. Nakagawa, K. Kamata, M. Kotani, K. Yamaguchi and N. Mizuno, *Angew. Chem., Int. Ed. Engl.*, 2005, **44**, 5136; (e) K. Yamaguchi, C. Yoshida, S. Uchida and N. Mizuno, *J. Am. Chem. Soc.*, 2005, **127**, 530.
- (a) R. Neumann and M. Gara, *J. Am. Chem. Soc.*, 1994, **116**, 5509; (b) R. Neumann, *Prog. Inorg. Chem.*, 1998, **47**, 317; (c) A. Khenkin, D. Kumar, S. Shaik and R. Neumann, *J. Am. Chem. Soc.*, 2006, **128**, 15451; (d) R. Neumann and M. Cohen, *Angew. Chem., Int. Ed. Engl.*, 1997, **36**, 1738; (e) M. Vasylyev and R. Neumann, *J. Am. Chem. Soc.*, 2004, **126**, 884.
- (a) C. Aubry, G. Chottard, N. Platzter, J. M. Bregeault, R. Thouvenot, F. Chauveau, C. Huet and H. Ledon, *Inorg. Chem.*, 1991, **30**, 4409; (b) L. Salles, C. Aubry, R. Thouvenot, F. Robert, C. Doremieux-Morin, G. Chottard, H. Ledon, Y. Jeanin and J. M. Bregeault, *Inorg. Chem.*, 1994, **33**, 871; (c) L. Salles, J. Y. Piquemal, R. Thouvenot, C. Minot and J. M. Bregeault, *J. Mol. Catal. A: Chem.*, 1997, **117**, 375; (d) J. M. Bregeault, M. Vennat, L. Salles, J. Y. Piquemal, Y. Mahha, E. Briot, P. C. Bakala, A. Atlamsani and R. Thouvenot, *J. Mol. Catal. A: Chem.*, 2006, **250**, 177; (e) L. Salles, R. Thouvenot and J. M. Brégeault, *Dalton Trans.*, 2004, 904.
- (a) N. M. Gresley, W. P. Griffith, A. C. Laemmel, H. I. C. Nogueira and B. C. Parkin, *J. Mol. Catal. A: Chem.*, 1997, **117**, 185; (b) W. P. Griffith, B. C. Parkin, A. J. P. White and D. J. Williams, *J. Chem. Soc., Chem. Commun.*, 1995, 2183; (c) N. J. Campbell, A. C. Dengel, C. J. Edwards and W. P. Griffith, *J. Chem. Soc., Dalton Trans.*, 1989, 1203; (d) A. C. Dengel, W. P. Griffith and B. C. Parkin, *J. Chem. Soc., Dalton Trans.*, 1993, 2683; (e) W. P. Griffith, B. C. Parkin, A. J. P. White and D. J. Williams, *J. Chem. Soc., Dalton Trans.*, 1995, 3131.
- D. C. Duncan, R. C. Chambers, E. Hecht and C. L. Hill, *J. Am. Chem. Soc.*, 1995, **117**, 681.
- (a) Z. Xi, N. Zhou, Y. Sun and K. Li, *Science*, 2001, **292**, 1139; (b) J. Li, S. Gao, M. Li, R. Zhang and Z. Xi, *J. Mol. Catal. A: Chem.*, 2004, **218**, 247; (c) S. Zhang, S. Gao, Z. Xi and J. Xu, *Catal. Commun.*, 2007, **8**, 531; (d) Z. Xi, H. Wang, Y. Sun, N. Zhou, G. Cao and M. Li, *J. Mol. Catal. A: Chem.*, 2001, **168**, 299.
- (a) Y. Ding, Q. Gao, G. Li, H. Zhang, J. Wang, L. Yan and J. Suo, *J. Mol. Catal. A: Chem.*, 2004, **218**, 161; (b) Y. Ding, B. Ma, Q. Gao, G. Li, L. Yan and J. Suo, *J. Mol. Catal. A: Chem.*, 2005, **230**, 121; (c) Y. Ding, Q. Gao, G. Li, J. Wang, L. Yan and J. Suo, *Acta Chim. Sin.*, 2005, **63**, 1167; (d) Y. Ding, B. Ma, Q. Gao and J. Suo, *J. Chem. Res.*, 2006, 499; (e) G. Li, Y. Ding, J. Wang, X. Wang and J. Suo, *J. Mol. Catal. A: Chem.*, 2007, **262**, 67.
- (a) J. Gao, Y. Chen, B. Han, Z. Feng, C. Li, N. Zhou, S. Gao and Z. Xi, *J. Mol. Catal. A: Chem.*, 2004, **210**, 197; (b) Y. Chen, J. Zhuang, X. Liu, J. Gao, X. Han, X. Bao, N. Zhou, S. Gao and Z. Xi, *Catal. Lett.*, 2004, **93**, 41.
- (a) M. Misono, N. Mizuno, K. Katamura, A. Kasai and Y. Konishi, *Bull. Chem. Soc. Jpn.*, 1982, **55**, 400; (b) M. Hashimoto, K. Itoh, K. Y. Lee and M. Misono, *Top. Catal.*, 2001, **15**, 265.

Highly atom efficient aluminium triflate catalysed acetal formation†

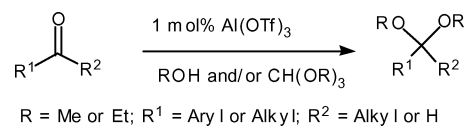
D. Bradley G. Williams* and Michelle C. Lawton

Received 4th April 2008, Accepted 28th July 2008

First published as an Advance Article on the web 5th August 2008

DOI: 10.1039/b805748f

Aromatic and aliphatic acetals are formed in excellent yields under solventless conditions at room temperature within 30 minutes by treating aldehydes and ketones with 0.5 mol% Al(OTf)₃ as a recyclable catalyst in the presence of only 1.2 equivalents of an orthoester as reagent.



Scheme 1

Introduction

Acetalisation is probably the most important protection strategy for carbonyl groups.¹ Acetal formation is achieved by treating aldehydes or ketones with an excess (10 equivalents or more) of an alcohol or diol in the presence of a drying reagent and a Lewis or Brønsted acid,² or by removing water through the formation of an azeotrope with the solvent and the use of a Dean–Stark trap.¹

Copper(II) tetrafluoroborate is an effective catalyst for the formation of acetals,³ but the BF₄⁻ counter ion is harmful to the environment. Metal triflates have previously been reported to catalyse acetalisation reactions.^{4,5} In particular, Bi(OTf)₃ and In(OTf)₃ effectively catalyse this process. While efficient, there are drawbacks with these catalysts: Bi(OTf)₃ requires the reactions to be carried out under reflux and suffers from relatively long reaction times.⁵ When reactions are carried out using In(OTf)₃, an aqueous work-up cannot be used as the acetal under goes rapid hydrolysis back to the corresponding carbonyl,⁴ making recycling of the catalyst difficult. On a slightly different note, polystyrene-supported Al(OTf)₃ has been used to catalyse dithioacetalisation and *trans*-dithioacetalisation reactions.⁶ Perhaps the biggest drawback of these Lewis acid catalysts is that they require the presence of either a solvent such as CH₂Cl₂, an alcohol in excess, or two or more equivalents of the orthoester.

Our previous successes working with aluminium triflate, which we have found to be an air and moisture tolerant compound that is a remarkably efficient catalyst at low concentrations,^{7–9} led us to investigate the efficacy of Al(OTf)₃ in the formation of acetals from a variety of aryl and alkyl aldehydes and ketones. Herein, we report a mild procedure for the conversion of aldehydes and ketones into the corresponding acetals in excellent yields, at room temperature, using just 0.5–1 mol% of Al(OTf)₃ as catalyst (Scheme 1). The reaction is efficient in the absence of solvent or added alcohol and it is possible to limit the orthoester reagent to only 1.2 equivalents with respect to the carbonyl

substrate. Excellent yields were obtained in the majority of cases under these atom-efficient conditions.

Results and discussion

Acetal formation reactions were initially carried out in the presence of 10 equivalents of an alcohol (MeOH or EtOH) as solvent and two equivalents of the corresponding orthoester (Table 1).†‡ It is clear from Table 1, column A that, with few exceptions, the reactions afforded good to excellent yields of the anticipated acetals. Acetals of aromatic compounds substituted with activating groups (Table 1, entries 1 and 2) or deactivating groups (Table 1, entries 3–8) were readily formed in high yields. α,β -Unsaturated aldehydes (Table 1, entries 9–10) and aliphatic aldehydes (Table 1, entries 11–14) underwent smooth transformation to the corresponding methyl or ethyl acetals in good to excellent yields.

All reactions were also successfully carried out under solventless conditions (*i.e.* in the presence of only the catalyst and 2 equivalents of the orthoester) with very little difference in the product yields (Table 1, column B). In fact, the yields generally improved slightly under these conditions as was especially evident in Table 1, entries 2, 6, 10. This aspect alone (*i.e.* the ability to omit the alcohol) implies less waste from the use of solvents and reduces our reliance upon volatile organic compounds.

Triflic acid is unlikely to be the causative agent in the catalysis. Our previous^{7,9} work comparing aluminium triflate and triflic acid using equimolar amounts of the two compounds, respectively, shows distinct differences in the outcomes of those reactions. Furthermore, amine bases, which should quench triflic acid, have been used by us⁸ and others¹⁰ with aluminium triflate without deleterious effects on the outcomes of the reactions. Also, the very different outcomes of the reactions with Al(OTf)₃ or HOTf making use of the acid-sensitive silyl protecting groups (see below in Schemes 2 and 3) provide convincing indirect evidence that triflic acid is generated only in very small (not equimolar) amounts if at all.

Encouraged, we performed the reactions using only 1.2 equivalents of the orthoester (*versus* the aldehyde or the ketone) in the presence of 1 mol% of the catalyst. The yields (Table 1, column C) were generally improved over those obtained in the presence of two equivalents of the orthoester (Table 1, column B). In the case of 4-nitroacetophenone (Table 1, entries

Department of Chemistry, University of Johannesburg, P.O. Box 524, Auckland Park, 2006, South Africa. E-mail: bwilliams@uj.ac.za; Fax: +27(0)11 559-2819; Tel: +27(0)11 559-3431

† Electronic supplementary information (ESI) available: Literature references for known compounds prepared, analytical data and NMR spectra for new compounds. See DOI: 10.1039/b805748f

Table 1 Al(OTf)₃-catalysed acetal formation of aldehydes and ketones

Entry	Product	A ^{a,b,c} yield (%)	B ^{a,c,d} yield (%)	C ^{a,e,f} yield (%)
1	R = CH ₃ , R ¹ = OCH ₃ , R ² = H	88 ^g	97 ^h	75 (90) ^g
2	R = CH ₂ CH ₃ , R ¹ = OCH ₃ , R ² = H	—	90 ^h	72 (80) ^g
3	R = CH ₃ , R ¹ = Cl, R ² = H	76	88	>98 ⁱ
4	R = CH ₂ CH ₃ , R ¹ = Cl, R ² = H	79	90	>98 ⁱ
5	R = CH ₃ , R ¹ = H, R ² = NO ₂	57	96	95
6	R = CH ₂ CH ₃ , R ¹ = H, R ² = NO ₂	64	92	>98 ⁱ
7		97	94 ⁱ	72 ^k (94) ⁱ
8		92	91 ^h	57 ^k (75) ^h
9		92	99	>98 ⁱ
10		72	93	96
11	<i>n</i> -C ₉ H ₁₉ CH(OMe) ₂	90	96	>98 ⁱ
12	<i>n</i> -C ₉ H ₁₉ CH(OEt) ₂	85	96	>98 ⁱ
13	Cy-CH(OMe) ₂ ^j	78	74 ^g	>98 ⁱ
14	Cy-CH(OEt) ₂ ^j	81	73 ^g	>98 ⁱ

^a 1 h reaction, 1 mol% Al(OTf)₃ catalyst unless otherwise noted. ^b 10 eq ROH, and 2 eq orthoester. ^c Isolated yields. ^d 2 eq orthoester, no ROH. ^e 1.2 eq of orthoester were used. ^f Yields determined by ¹H NMR spectroscopy. ^g 2 hour reaction. ^h 5 h reaction. ⁱ >98% implies quantitative reaction with no other products detected in concentrated samples in which spinning side bands are observable. ^j Cy = cyclohexyl. ^k 0.5 mol% Al(OTf)₃ used.

7 and 8) the reaction mixture formed a biphasic mixture necessitating longer reaction times. Nonetheless, even under these unfavourable conditions, a yield of 72% was obtained after two hours when the trimethyl orthoester was used (Table 1, entry 7), and 57% when triethyl orthoester was used (Table 1, entry 8). The yields improved to 94% and 75%, respectively, after five hours (see yields in parentheses). These aspects point to an atom-efficient process and less waste from the use of solvents and excess reagents.

Pertinently, one equivalent of orthoester provides both alkoxy groups resident on the acetal or ketal products, in the process scavenging the one equivalent of water that is produced, generating methyl or ethyl formate as the only major by-products. That this process is extremely high yielding, and makes use only of minimal amounts of reagents, implies that the amount of material to be purified is dramatically reduced, further enhancing its attractiveness.

As noted, reactions carried out in alcohols as solvents generally afforded slightly lower yields than those carried out using only the orthoester (compare Table 1, columns **A** and **B**) by omitting the solvent. Al(OTf)₃ is a hard Lewis acid and is oxophilic. Quite possibly, the oxygen atom of the MeOH or EtOH solvent competes with the carbonyl group of the aldehyde or ketone for the aluminium metal centre, thereby reducing the activity of the catalyst.

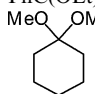
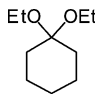
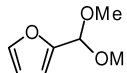
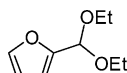
This putative competition would be largely removed by the absence of the alcohol solvent. Incidentally, the Lewis donor

strength of various solvents has previously been measured¹¹ and methanol was found to be one of the stronger donors for both hard and soft Lewis acids.

The taming effect of the alcohols on the reaction can be better seen from the results in Table 2 (compare columns **A** and **B**). Here, reactions performed in the presence of the alcohol (MeOH and EtOH) and the corresponding orthoester gave good results, while those reactions performed under solventless conditions (*i.e.* in the presence of the orthoester only) afforded lower yields or in some cases no desired product at all. In these latter instances, the reactivity of the system was high, leading to a significant initial exotherm, presumably giving rise to the substantial by-product formation observed. To circumvent this problem the reactions were performed at -20 °C with slow warming to room temperature. In this way, the yields were much improved, as is clear from Table 2, column **C**. Here, too, the outcomes of the reactions were similar to or better than those performed in the alcohol solvent. Under these conditions (*i.e.* in the absence of alcohol solvent, -20 °C) acetophenone repeatedly failed to afford any product (Table 2, entry 4) when using triethylorthoformate as reagent. On the other hand, furan derivatives are notoriously prone to polymerisation, yet, importantly in this context, the procedure was readily applicable to furfural to afford excellent yields of the required products (Table 2, entries 7 and 8).

The positive results obtained for reactions shown in Table 1 using only 1.2 equivalents of the orthoester led us to apply

Table 2 Al(OTf)₃-catalysed acetal formation of aldehydes and ketones

Entry	Product	A ^{a,b,c} Yield (%)	B ^{a,c,d} Yield (%)	C ^{a,c,e} Yield (%)	D ^{f,g} Yield (%)
1	PhCH(OMe) ₂	96	63	98	92
2	PhCH(OEt) ₂	83 ^h	75	89	92
3	PhC(OMe) ₂ CH ₃	94 ^{hi}	0	92	73 (92) ^j
4	PhC(OEt) ₂ CH ₃	77	0	0	75 (82) ^j
5		80	33	77	90
6		83	33	80	93
7		86	0	>98 ^k	96
8		74	0	82 ^l	92

^a 1 h reactions, 1 mol% Al(OTf)₃ catalyst unless otherwise noted. ^b 10 eq ROH, and 2 eq orthoester. ^c Isolated yields. ^d 2 eq orthoester, no ROH. ^e Reactions carried out at -20 °C. ^f 1.2 eq of orthoester and 0.5 mol% Al(OTf)₃, 30 min reaction time. ^g Yields determined by ¹H NMR spectroscopy. ^h 5 h reaction. ⁱ 5 mol% Al(OTf)₃ used. ^j 2 h reaction. ^k >98% implies quantitative reaction with no other products detected in concentrated samples. ^l If the reaction was allowed to proceed beyond 1 h the product curiously reverted to starting material.

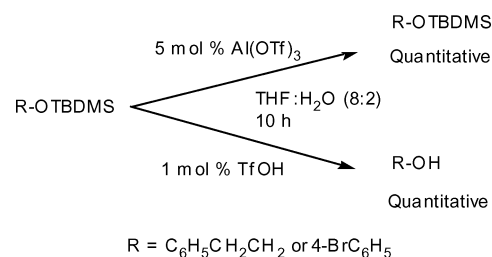
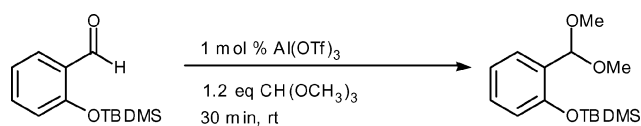
the same conditions to the more reactive substrates (Table 2), with unsurpassed results. By lowering the catalyst loading to only 0.5 mol% of Al(OTf)₃ and performing the reactions under solventless conditions (*i.e.* 1.2 equivalents of the orthoester), we were able to obtain yields of greater than 90% *within 30 minutes* at room temperature in all but two cases. In those two cases (acetophenone substrate), slightly longer reaction times afforded high yields of products. Unlike other metal triflate catalysts that have been used,^{4,5} acetal formation with Al(OTf)₃ could be carried out at or below room temperature in all cases. The only by-product of the reaction was the corresponding formate ester (confirmed by NMR spectroscopy) derived from the orthoester.

We have previously shown Al(OTf)₃ to be recyclable.^{8,9} In the present instance, a simple process of product distillation from the non-volatile catalyst allowed the Al(OTf)₃ to be reused without loss of activity over four runs (Table 3), when converting benzaldehyde into its dimethyl acetal. This feature provides a significant benefit (environmental and cost) over traditional Lewis and Brønsted acids.

Table 3 Al(OTf)₃ recycling experiments using benzaldehyde as substrate

Run	Yield (%) ^{a,b,c}
1	> 98
2	> 98
3	96
4	95

^a 30 min reaction time, 0.5 mol% Al(OTf)₃ catalyst, 1.2 eq trimethylorthoformate. ^b Determined by ¹H NMR spectroscopy. ^c >98% implies quantitative reaction with no other products detected in concentrated samples.

**Scheme 2****Scheme 3**

Pleasingly, neither aliphatic nor aromatic (Scheme 2) silyl ethers were cleaved under conditions *more forcing* (5 mol% Al(OTf)₃) than those required for acetal formation. This bodes well for the use of Al(OTf)₃ for acetal formation in the presence of such acid-sensitive groups. This is in contrast to the use of triflic acid at *lower* concentrations which rapidly led to quantitative deprotection to afford the respective free alcohols.

In order to more directly determine the stability of the acid-sensitive *t*-butyldimethylsilyl (TBDMS) protecting group during acetal formation we used a silyl-protected salicylaldehyde (Scheme 3) as substrate. The acetal was formed in greater than 98% yield (determined by ¹H NMR) within 30 minutes using 1 mol% Al(OTf)₃ and only 1.2 equivalents of the orthoester, without removing the TBDMS group. This outcome once again highlighted the efficacy and selectivity of Al(OTf)₃ for this transformation.

Conclusions

This paper describes the use of Al(OTf)₃ as a mild active catalyst for the formation of acetals from various aldehydes and ketones at ambient temperature. The reaction may be performed in the presence of the alcohol/orthoester mixture or using neat orthoester, the latter solvent-free procedure of which is preferred and produces the least waste. Simple distillation of the products allowed their isolation in excellent yields. The reaction was found to be highly effective even when only 1.2 equivalents of the orthoesters were used and is tolerant of the TBDMS protection group on aliphatic and aromatic systems under these conditions. It was possible to recycle the catalyst several times without loss of activity in reactions that excluded the reliance upon volatile organic solvents. Overall, the procedures described here provide the opportunity to perform the acetal protection reaction, which is so frequently used in organic synthesis, in a manner that significantly reduces waste while maintaining very good outcomes indeed.

Acknowledgements

We thank Sasol, THRIP and the University of Johannesburg for financial support.

Notes and references

‡ Typical experimental procedure for the formation of acetals: *Dimethoxymethylbenzene* (Table 2, entry 1, column D). 1.2 eq (15 mmol)

of trimethyl orthoformate were added under nitrogen to 0.0625 mmol (0.5 mol% with respect to benzaldehyde) of Al(OTf)₃. To this solution was added 12.5 mmol (1.32 g) of benzaldehyde. The mixture was allowed to stir for 30 min at room temperature. The product was isolated by subjecting the reaction mixture to vacuum distillation without any work-up procedure. This also allowed for ready catalyst recycling. Work-up of the reaction mixture could be carried by passing the reaction solution through neutral alumina with no loss of product. This procedure is not useful for catalyst recycling. It was also possible to quench the reaction by addition of a saturated sodium bicarbonate solution followed by extraction with a suitable solvent such as Et₂O (preferred) or CH₂Cl₂. The volatile component was removed under vacuum and the residue subjected to high vacuum (0.05 mmHg) at ambient temperature. Where necessary, higher temperatures of up to 60 °C were applied to remove less volatile substrate residues from the acetal products. Product characterisation was carried out using NMR spectroscopy and other standard analytical techniques. Procedures using alcohol solvents were similarly performed.

- 1 P. J. Kociński, *Protecting Groups*, Thieme, New York, 1994.
- 2 D. S. Torok, J. J. Fiueroa and W. J. Scott, *J. Org. Chem.*, 1993, **58**, 7274.
- 3 R. Kumar and A. K. Chakraborti, *Tetrahedron Lett.*, 2005, **46**, 8319.
- 4 N. M. Leonard, M. C. Oswald, D. A. Freiberg, B. A. Nattier, R. C. Smith and R. S. Mohan, *J. Org. Chem.*, 2002, **67**, 5202.
- 5 B. M. Smith and A. E. Graham, *Tetrahedron Lett.*, 2006, **47**, 9317.
- 6 K. P. Borujeni and A. R. Massah, *React. Funct. Polym.*, 2006, **66**, 1126.
- 7 D. B. G. Williams and M. Lawton, *Org. Biomol. Chem.*, 2005, **3**, 3269.
- 8 D. B. G. Williams and M. Lawton, *Tetrahedron Lett.*, 2006, **47**, 6557.
- 9 D. B. G. Williams, M. L. Shaw, M. J. Green and C. W. Holzapfel, *Angew. Chem., Int. Ed.*, 2008, **47**, 560.
- 10 L. Coulombel, M. Rajzmann, J. -M. Pons, S. Olivero and E. Duñach, *Chem.-Eur. J.*, 2006, **12**, 6356.
- 11 M. Sandström, I. Persson and P. Persson, *Acta Chem. Scand.*, 1990, **44**, 653.

Solubility of fluorinated compounds in a range of ionic liquids. Cloud-point temperature dependence on composition and pressure

Rui Ferreira,^a Marijana Blesic,^a Joana Trindade,^a Isabel Marrucho,^b José N. Canongia Lopes^{*a,c} and Luís Paulo N. Rebelo^{*a}

Received 8th April 2008, Accepted 17th June 2008

First published as an Advance Article on the web 11th August 2008

DOI: 10.1039/b805902k

In this work, we explore the mutual solubility of a number of mixtures of commonly used ionic liquids (imidazolium, pyridinium, phosphonium and ammonium ionic liquids) with partially fluorinated *n*-alcohols (C₇ to C₁₀) or perfluoroheptane. The corresponding *T*-*x* diagrams at atmospheric pressure were measured through cloud-point temperature determinations. For some selected systems under near-critical isopleth conditions, pressure effects were also studied. The results are discussed in terms of (i) shifts in the immiscibility envelopes as the cation alkyl-chain length is changed, (ii) the nature of the cation or the anion, (iii) the increasing length of the fluorinated/alkylic moiety of the partially fluorinated alcohol, or (iv) comparisons with similar systems involving normal alcohols.

1. Introduction

One of the key-issues concerning the current importance of ionic liquids is the fact that they can simultaneously act as sophisticated solvation or reaction media while avoiding dramatic impacts in the environment due to their general low volatility and flammability combined with high thermal stability. Ionic liquids are able to dissolve (at least partially) a wide range of polar or nonpolar, organic or inorganic compounds,¹ providing new ways to carry out chemical reactions or industrial separations.²

It was recently reported in different molecular simulation studies³ that neat ionic liquids exhibit medium-range ordering, in other words, there are persistent microscopic domains in the liquid phase. Other simulation studies⁴ on the microscopic dynamics of ionic liquids have also pointed out their slow dynamics and the persistence of local environments, typical of the glassy state.

The segregation in polar and nonpolar domains at a nanoscale level in ionic liquids with alkyl side chains of intermediate length (for instance in 3-alkyl-1-methylimidazolium-based ionic liquids with alkyl groups larger than hexyl), has changed the way in which solvation in these liquids is understood. Some solutes dissolve preferentially in low electrical charge-density domains, while others prefer the Coulomb environment of high electrical-charge density regions, whereas some can even “be dissolved” at the interface between these polar and non-polar territories.⁵ These facts account for the extraordinary versatility of ionic liquids as solvents.

Fluorinated organic compounds also display many exceptional physico-chemical properties that have been used in many commercial applications. Similar to ionic liquids, they are also perceived as alternative substances towards the development of

more environmentally friendly processes. Industrial production of these compounds has increased significantly since the early 1980s and fluorinated organics are commonly used as refrigerants, surfactants, polymers, as components of pharmaceuticals, fire retardants, lubricants, and insecticides.⁶ In recent years the possibility of their use as gas-carriers (including the possibility of their use as synthetic blood substitutes),⁷ and as solubility-promoters in supercritical extraction media⁸ has also been explored. From a molecular point of view, the properties of fluorinated organic compounds can be rationalized in terms of the unique interactions they perform with different molecules: fluorocarbons generally exhibit low-intensity interactions with normal organic compounds⁹ or water, a fact related not only to their “reversed” quadrupole moment (note that the carbon backbone of a perfluorocarbon molecule carries a partially positive charge, due to the high electronegativity of the fluorine atom, unlike the situation in hydrocarbons or water) but also due to their relatively rigid structure (that inhibits the existence of different conformers and introduces entropic-driven factors in mixtures with other substances).

Functionalized fluorocarbons were also studied in recent years due to their amphiphilic behaviour and their possible use as separation media or surfactant agents. Examples of such compounds are the hydrofluorocarbon molecules,¹⁰ the hydrocarbon-fluorocarbon diblock molecules¹¹ and the fluorinated alcohols.¹² The rationale behind the synthesis and use of such molecules is the introduction of an interacting group in the otherwise inert perfluorinated chain, that will promote the “docking” of the fluorinated compound in the midst of other molecules (with the possible self-organization of the former in micelles or similar structures) or the formation of emulsions between fluorinated and organic or aqueous domains.

Systems where both types of compound, ionic liquids and fluorinated organic molecules, are inherently appealing as they are perceived as relatively benign media, combining two “clean” substances. This blend also poses very interesting challenges both from the theoretical and the applied chemistry points of

^aInstituto de Tecnologia Química e Biológica, UNL, 2780 901, Oeiras, Portugal. E-mail: luis.rebelo@itqb.unl.pt

^bCICECO, Universidade de Aveiro, 3810 193, Aveiro, Portugal

^cCentro de Química Estrutural, IST, 1049 001, Lisboa, Portugal. E-mail: jnlopes@ist.utl.pt

view. As an example of the former aspect, one can hope to gain some insight about the interactions between the fluorinated molecules and the parts of the ionic liquid that are themselves fluorinated (generally present in anions such as bistriflamide, triflate or hexafluorophosphate). An example of the latter issue can be, for instance, the possibility of using partially fluorinated alcohols or diblock molecules to promote the miscibility (through the formation of micro-emulsions) between bistriflamide-based ionic liquids and aqueous solutions.

In this work, we explore the fluid phase diagrams of mixtures of commonly used ionic liquids with partially fluorinated alcohols. The systems are analyzed in terms of the two-phase envelopes (immiscibility regions) of the corresponding $T-x$ diagrams at atmospheric pressure, which in turn have been determined by the measurement of cloud-point temperatures as a function of the mixture compositions. Pressure effects were also studied for some selected systems under near-critical isopleth conditions. The results are discussed in terms of shifts in those envelopes as the alkyl side chains of the cations get longer, the nature of the cation or the anion is changed, the length of the fluorinated moiety of the partially fluorinated alcohol is increased, or by comparison with systems involving normal alcohols (ethanol and propanol). We have also noticed the essentially total immiscible behaviour of a range of ionic liquids studied in this work with a linear perfluorinated alkane.

2. Experimental

Materials

Table 1 shows the compounds involved in the detailed determination of the fluid phase behaviour of mixtures of ionic liquids with fluorinated alcohols. In addition to the compounds listed in Table 1, other ionic liquids and other fluorinated alcohols were used in preliminary solubility tests (see Table 2). The complete list, including name and/or commercial name (abbreviated name; CAS number, source and grade if available), is as follows: 1-ethyl-3-methylimidazolium ethylsulfate, ECOENGTM 212 ($C_2mimEtSO_4$; 342573-75-5; Solvent Innovation; >99%); trioctylmethylammonium chloride, ALIQUATTM 336 ($N_{888}Cl$; 63393-96-4; Aldrich; n/a); trihexyl-(tetradecyl)phosphonium chloride ($P_{66614}Cl$; 258864-54-9; Cytec; >96%); trihexyl(tetradecyl)phosphonium bis[(trifluoromethyl)sulfonyl]imide ($P_{66614}NTf_2$; 460092-03-9; QUILL†; n/a); trihexyl(tetradecyl)-phosphonium trifluoromethanesulfonate ($P_{66614}OTf$; CAS number; QUILL†; n/a); trihexyl(tetradecyl)-phosphonium acetate ($P_{66614}Ac$; 460092-04-0; QUILL†; n/a); 1-ethyl-3-methylimidazolium bis-[(trifluoromethyl)sulfonyl]imide ($C_2mimNTf_2$; 174899-82-2; QUILL†; n/a); 1-propyl-3-methylimidazolium bis[(trifluoromethyl)sulfonyl]imide ($C_3mimNTf_2$; 216299-72-8; QUILL†; n/a); 1-pentyl-3-methylimidazolium bis[(trifluoromethyl)sulfonyl]imide ($C_5mimNTf_2$; 280779-53-5; QUILL†; n/a); 1-octyl-3-methylimidazolium bis[(trifluoromethyl)sulfonyl]imide ($C_8mimNTf_2$; 178631-04-4; QUILL†; n/a); 1-decyl-3-methylimidazolium bis[(trifluoromethyl)sulfonyl]imide ($C_{10}mimNTf_2$; 433337-23-6; QUILL†; n/a); 1-dodecyl-3-methylimidazolium bis-

[(trifluoromethyl)sulfonyl]imide ($C_{12}mimNTf_2$; unknown CAS; QUILL†; n/a); acetyl-cholinium bis[(trifluoromethyl)sulfonyl]imide ($AcChNTf_2$; unknown CAS; QUILL†; n/a); 1-hexyl-3-methylimidazolium chloride (C_6mimCl ; 171058-17-6; QUILL†; n/a); 1-dodecyl-3-methylimidazolium chloride ($C_{12}mimCl$; 114569-84-5; QUILL†; n/a); 1-butyl-3-methylimidazolium hexafluoroborate (C_4mimBF_4 ; 174501-65-6; Solvent Innovation GmbH; >99%); 1-butyl-3-methylimidazolium hexafluorophosphate (C_4mimPF_6 ; 174501-64-5; QUILL†; n/a); 1-octyl-3-methylimidazolium hexafluorophosphate (C_8mimPF_6 ; 304680-36-2; QUILL†; n/a); 1-decyl-3-methylpyridinium bis-[(trifluoromethyl)sulfonyl]imide ($C_{10}MePyNTf_2$; unknown CAS; QUILL†; n/a); 1-dodecyl-3-methylpyridinium bis[(trifluoromethyl)sulfonyl]imide ($C_{12}MePyNTf_2$; unknown CAS; QUILL†; n/a); 1-tetradecyl-3-methylpyridinium bis[(trifluoromethyl)sulfonyl]imide ($C_{14}MePyNTf_2$; unknown CAS; QUILL†; n/a); 1-tetradecyl-3-methylpyridinium bromide ($C_{14}MePyBr$; unknown CAS; QUILL†; n/a); 1-butyl-3-methylimidazolium thiocyanate ($C_4mimSCN$; 344790-87-0; Fluka; >95%) e 1-butyl-3-methylimidazolium methylsulfate ($C_4mimMeSO_4$; 401788-98-5; Fluka; >97%).

All ionic liquids used in solubility tests were used without any further purification. Ionic liquids used in cloud-point data measurements were previously dried and degassed under vacuum conditions (1 to 10 Pa) at moderate temperatures (80–100 °C) for periods longer than 24 hours.

The list of alcohols used is as follows: ethanol (64-17-5; Pronalab; 99.8%); 1-propanol (71-23-8; Aldrich; 99.7%); 1*H*,1*H*,7*H*-perfluoroheptanol (117-C₇FOH; 335-99-9; Apollo Scientific; 98%); 1*H*,1*H*,2*H*,2*H*-perfluorooctanol (1122-C₈FOH; 647-42-7; ABCR; 98%); 1*H*,1*H*-perfluorooctanol (11-C₈FOH; 307-30-2; Apollo Scientific; 98%); 1*H*,1*H*-perfluorononanol (11-C₉FOH; 423-56-3; Apollo Scientific; 98%); 1*H*,1*H*-perfluorodecanol (11-C₁₀FOH; 307-37-9; Apollo Scientific; 98%); 1*H*,1*H*,2*H*,2*H*,3*H*,3*H*-perfluorononanol (112233-C₉FOH; 80806-68-4; Fluorochem; 98%) and perfluoroheptane (C₇F₁₆; 335-57-9; Apollo Scientific, 98%). All fluorinated alcohols were used without further purification.

Preliminary solubility tests

Solubility tests were performed by adding small amounts (*ca.* 100 μL) of IL and fluorinated compound into a glass (Pyrex) conical vessel containing a magnetic stirrer. Any phase separation (if present) was visually detected. Different composition ranges were tested at temperatures from *ca.* –10 °C up to 70 °C.

Cloud-point measurements

All cloud-point determinations on the temperature–composition phase diagrams of the ionic liquid plus fluorinated alcohol systems at a nominal pressure of 0.1 MPa were performed using a dynamic method with visual detection of the solution turbidity. For this purpose, Pyrex glass view cells with magnetic stirring were used. Samples were gravimetrically prepared directly inside the cells using an analytical high precision balance (±0.01 mg). The cells were then immersed in a thermostatic bath. Providing continuous stirring, we cooled off or heated the solutions usually in two or three runs with the two last runs being carried out very slowly (the

† Queen's University Ionic Liquids Laboratories.

Table 1 Description of the ionic liquids and fluorinated alcohols used in the cloud-point determinations

Formal Name	Structure	Abbreviation
1-Alkyl-3-methylimidazolium bis(trifluoromethylsulfonyl)imide (alkyl = octyl, decyl and dodecyl)		$C_8mimNTf_2$ $C_{10}mimNTf_2$ $C_{12}mimNTf_2$
Acetylcholinium bis(trifluoromethylsulfonyl)imide		$AcChNTf_2$
Trihexyltetradecylphosphonium bis(trifluoromethylsulfonyl)imide		$P_{66614}NTf_2$
1-Alkyl-3-methylpyridinium bis(trifluoromethylsulfonyl)imide (alkyl = decyl, dodecyl and tetradecyl)		$C_{10}MePyNTf_2$ $C_{12}MePyNTf_2$ $C_{14}MePyNTf_2$
1-Octyl-3-methylimidazolium hexafluorophosphate		C_8mimPF_6
1-Butyl-3-methylimidazolium tetrafluoroborate		C_4mimBF_4
1 <i>H</i> ,1 <i>H</i> ,2 <i>H</i> ,2 <i>H</i> -Perfluorooctanol ($n = 2$) 1 <i>H</i> ,1 <i>H</i> ,2 <i>H</i> ,2 <i>H</i> ,3 <i>H</i> ,3 <i>H</i> -Perfluorononanol ($n = 3$)		1122- C_8FOH 112233- C_9FOH

rate of temperature change near the cloud point was no more than 5 K h^{-1}). Beginning in the homogeneous region, upon cooling, the temperature at which the first sign of turbidity appeared was taken as the temperature of the liquid-liquid phase transition. Temperature was monitored using a four-wire platinum resistance thermometer coupled to a Yokogawa 7561 multimeter. The thermometer was calibrated against high accuracy mercury thermometers (0.01 K precision). The overall accuracy in the determination of the cloud-point temperatures is estimated to be $\pm 0.3 \text{ K}$.

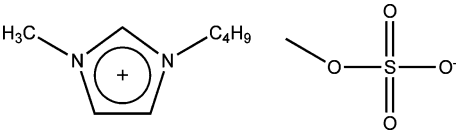
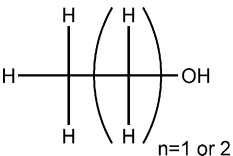
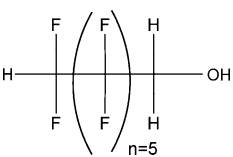
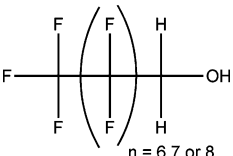
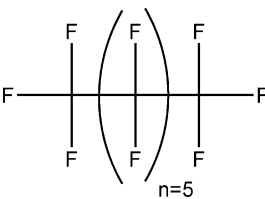
Pressure effects on the cloud-point temperature were obtained by a He-Ne laser light scattering technique. The apparatus and

the methodology used for the determination of phase transitions have already been described in detail.¹³ Here, only a brief description is provided. The cell (with an internal volume of *ca.* 1.0 cm^3 and an optical length of *ca.* 2.6 mm) is a thick-walled Pyrex glass tube that is connected to a pressurization line and separated from it by a mercury plug. The intensity of the scattered light is captured at a very low angle ($2^\circ < 2\theta < 4^\circ$) in the outer portion of a bifurcated optical cable, whereas transmitted light is captured in the inner portion of this cable. The intensity of scattered light (I_{sc}) and transmitted light (I_{tr}) are corrected for density fluctuations, reflections, and multiple scattering effects. The cloud-point is the point on the

Table 2 Description of other compounds, not listed in Table 1, which were used in preliminary solubility tests

Formal Name	Structure	Abbreviation
1-Ethyl-3-methylimidazolium ethylsulfate (ECOENG TM 212)		<i>C</i> ₂ <i>mimEtSO</i> ₄
Trioctylmethylammonium chloride (ALIQAT TM 336)		<i>N</i> ₈₈₈₁ Cl
Trihexyl(tetradecyl)phosphonium chloride		<i>P</i> ₆₆₆₁₄ Cl
Trihexyl(tetradecyl)phosphonium trifluoromethanesulfonate		<i>P</i> ₆₆₆₁₄ <i>OTf</i>
Trihexyl(tetradecyl)phosphonium acetate		<i>P</i> ₆₆₆₁₄ <i>Ac</i>
1-Alkyl-3-methylimidazolium bis-[(trifluoromethyl)sulfonyl]imide (alkyl = ethyl, propyl and pentyl)		<i>C</i> ₂ <i>mimNTf</i> ₂ <i>C</i> ₃ <i>mimNTf</i> ₂ <i>C</i> ₅ <i>mimNTf</i> ₂
1-Alkyl-3-methylimidazolium chloride (alkyl = hexyl, dodecyl)		<i>C</i> ₆ <i>mimCl</i> <i>C</i> ₁₂ <i>mimCl</i>
1-Butyl-3-methylimidazolium hexafluorophosphate		<i>C</i> ₄ <i>mimPF</i> ₆
1-Tetradecyl-3-methylpyridinium bromide		<i>C</i> ₁₄ <i>MePyBr</i>
1-Butyl-3-methylimidazolium thiocyanate		<i>C</i> ₄ <i>mimSCN</i>

Table 2 (Contd.)

Formal Name	Structure	Abbreviation
1-Butyl-3-methylimidazolium methylsulfate		$C_4mimMeSO_4$
Ethanol ($n = 1$) Propanol ($n = 2$)		C_2H_5OH C_3H_7OH
1H,1H,7H-dodecafluoroheptanol		117- C_7FOH
1-(Perfluoroheptyl)methanol ($n = 6$) 1-(Perfluorooctyl)methanol ($n = 7$) 1-(Perfluorononanol)methanol ($n = 8$)		11- C_8FOH 11- C_9FOH 11- $C_{10}FOH$
Perfluoroheptane		C_7F_{16}

least-squares fits of $(I_{sc,corr})^{-1}$ against pressure (p) or temperature (T) where the slope changes abruptly. Temperature accuracy is typically ± 0.01 K in the range $240 \text{ K} < T < 380 \text{ K}$. As for pressure, accuracy is ± 0.01 MPa in the range $0.1 \text{ MPa} < p < 5 \text{ MPa}$. The cell can be operated in the isobaric or isothermal mode. Whenever possible, isothermal runs are preferred over isobaric ones. Pressure transmission (isothermal mode) is many orders of magnitude faster than thermal equilibration (isobaric mode). Also, the rate at which one is able to change pressure is much greater than that for temperature. Nonetheless, many runs had to be performed in the isobaric mode due to the common low T - p slope presented by the binary mixtures being studied here.

3. Results and discussion

The preliminary solubility tests are given in Table 3. These results were used to select the systems that would be more promising in terms of a richer fluid phase behaviour, *i.e.*, systems exhibiting liquid–liquid partial immiscibility (LLE) ending at an upper critical solution temperature, UCST, as

the temperature is increased. For systems presenting this type of phase diagrams one can easily switch between one-phase and two-phase situations either by composition or temperature change. It is important to note that not all systems exhibiting LLE behaviour were selected for the subsequent cloud-point measurements (those that were selected are highlighted in grey in Table 3). There were different types of reasons for the rejection of some of the systems: some systems contained ionic liquids with rather high melting points (an LLE line interrupted by a solid–liquid equilibrium (SLE) line), which can cause problems in terms of turbidity detection; others exhibited degradation problems at temperatures near the UCST; *etc.* The solubility tests were also used to select the “best” fluorinated alcohol—that presenting LLE behaviour in mixtures with different ionic liquids at experimentally convenient conditions. In this case, it was found that a higher number of hydrogenated carbon atoms near the hydroxyl function decreased the miscibility between the ionic liquids and the fluorinated alcohols, promoting the appearance of larger immiscibility domains. The selected fluorinated alcohol was thus 1122- C_8FOH (or 112233- C_9FOH in just one case, for comparison purposes only). Tests with two normal (hydrogenated) alcohols, ethanol and propanol, were

Table 3 Solubility tests in (ionic liquid + fluorinated alcohol) and (ionic liquid + perfluoroalkane) mixtures. M: miscible (one fluid phase system); PM: partially miscible; LPM: low partial miscibility; I: immiscible; LLE: liquid–liquid equilibria; SLE: solid–liquid equilibria. Note that all these fluorinated alcohols are water immiscible. The cells highlighted in bold correspond to systems where the determination of the corresponding fluid phase diagrams was possible

	117-C ₇ FOH	1122-C ₈ FOH	11-C ₈ FOH	112233-C ₉ FOH	11-C ₉ FOH	11-C ₁₀ FOH	C ₇ F ₁₆
P ₆₆₆₁₄ NTf ₂	M	PM (LLE)	M	—	—	M	I to LPM
P ₆₆₆₁₄ Cl	M	M	—	—	—	—	I
P ₆₆₆₁₄ OTf	M	—	M	—	M	M (SLE)	I
P ₆₆₆₁₄ Ac	—	—	M (SLE)	—	M	foam (LLE)	—
C ₂ mimNTf ₂	M	—	M	—	M	M	—
C ₃ mimNTf ₂	—	PM (LLE)	—	—	—	—	I to LPM
C ₃ mimNTf ₂	M	—	—	—	—	—	I to LPM
C ₈ mimNTf ₂	—	PM (LLE)	—	—	—	—	—
C ₁₀ mimNTf ₂	M	PM (LLE)	M	PM (LLE)	—	M	I to LPM
C ₁₂ mimNTf ₂	M	PM (LLE)	—	—	—	—	I
AcChNTf ₂	—	PM (LLE)	—	—	—	—	—
C ₆ mimCl	—	M	—	—	M	M	—
C ₁₂ mimCl	M	—	—	—	—	—	I
C ₄ mimBF ₄	M	PM (LLE)	M (SLE)	—	—	M (SLE)	—
C ₄ mimPF ₆	M	PM (LLE)	—	—	—	—	I to LPM
C ₈ mimPF ₆	—	PM (LLE)	—	—	—	—	—
C ₁₀ MePy NTf ₂	—	PM (LLE)	—	—	—	—	—
C ₁₂ MePy NTf ₂	—	PM (LLE)	—	—	—	—	—
C ₁₄ MePy NTf ₂	—	PM (LLE)	M	—	—	M	—
C ₁₄ MePy Br	—	PM (LLE)	—	—	—	—	—
ECOENG 212	M	M	M	—	M	gel-like (LLE)	—
AMMOENG 102	—	M	—	—	—	—	I
ALQUAT 336	—	M	M	—	M	M	—
C ₄ mim SCN	—	M	—	—	—	—	—
C ₄ mim SO ₄	—	M	—	—	—	—	—

also performed in order to compare the fluid phase behaviour of their mixtures with ionic liquids.

It should be noted that M. Shiflett and A. Yokozeki^{10,14–16} determined a series of phase diagrams of several small-molecule hydrofluorocarbons with C₂mimNTf₂, C₄mimPF₆, C_nmimBF₄ (*n* = 2 or 4).

The results of the cloud-point determinations are given in Table 4 for the thirteen selected (ionic-liquid + alcohol) systems: ten systems with 1122-C₈FOH (highlighted in Table 3), one system with 1-decyl-3-methylimidazolium bistriflamide plus 112233-C₉FOH, and two with acetylcholinium bistriflamide plus ethanol or propanol.

Fig. 1 (a to d) depicts the fluid phase behaviour of mixtures of dialkylimidazolium bistriflamide ionic liquids with 1122-C₈FOH or 112233-C₉FOH. The figure shows that the fluid phase behaviour is affected by the length of the alkyl side-chains connected to the imidazolium ring of the ionic liquid and by the length of the hydrogenated segment between the perfluorinated chain and the hydroxyl group of the alcohol. It must be stressed that the scale (*x*- and *y*-axes ranges) in Fig. 1 was adjusted to the scale of all subsequent figures that depict the fluid phase behaviour in ionic liquid plus alcohol mixtures (Fig. 3 to 5), in order to facilitate comparisons between them—hence the apparently unused space in panels (a to d) in Fig. 1.

The general trend depicted in Fig. 1 can thus be summarized as follows: (i) ionic liquids with longer alkyl-side chains (in the imidazolium cation) show a larger immiscibility domain with fluorinated alcohols than their shorter-chain counterparts—a behaviour opposite of that shown when *n*-alcohols are mixed with these same ionic liquids,^{17,18} or *N*-alkyl-3-methylpyridinium-

based ionic liquids;¹⁷ (ii) a longer hydrogenated carbon chain—a kind of “spacer”—between the fluorinated chain and the hydroxyl group of the alcohol also decreases the miscibility between the two components of the mixture; and (iii) larger immiscibility regions (an increase in the *T*_{UCST}) are accompanied by a shift in the critical composition to mixtures richer in the fluorinated alcohol.

Trend (i) can be interpreted taking into account the recently discovered nano-structure of ionic liquids, exhibiting high-charge (polar) and low-charge (non-polar) density regions,³ and also their dual nature as they interact with a given solute either *via* the non-polar or polar regions, or (in the latter case) *via* the charged parts of the anion or of the cation.¹ Previous simulation studies,⁵ supported by experimental evidence have shown that the hydroxyl group of alcohols interact strongly with the anions of ionic liquids and also with the hydrogen atoms directly connected to the imidazolium ring (especially the one at C2) and that the alkyl side chain of the alcohol orients itself away from the polar region and towards the non-polar domains of the ionic liquid. To confirm these facts for bistriflamide-based ionic liquids, new Molecular Dynamics simulations were performed within the scope of the present work: methanol and tetrafluoromethane molecules acting as test-solutes and C₄mimNTf₂ acting as the solvent were modelled by explicit-atom force fields.^{19–22} Details of the simulations were similar to those adopted for pure ionic liquids.²³ Due to the slow dynamics of this type of system, special care was taken to ensure that equilibrium conditions were reached, including the proper diffusion of the solutes in the ionic liquid. Equilibration and production runs were implemented for 1 ns and multiple re-equilibrations through the use of temperature annealing

Table 4 Cloud-point temperatures as a function of the ionic liquid mole fraction in different (ionic liquid + alcohol) systems. All systems include the alcohol 1122-C₈FOH, except where stated

x_{IL}	T/K	x_{IL}	T/K	x_{IL}	T/K	x_{IL}	T/K	x_{IL}	T/K	x_{IL}	T/K	x_{IL}	T/K
$C_8mimNTf_2$		$C_{12}mimNTf_2$		$C_{10}MePyNTf_2$		$C_{14}MePyNTf_2$		$AcChNTf_2^b$		$AcChNTf_2^c$		C_5mimPF_6	
0.155	263.9	0.533	282.0	0.575	269.4	0.460	292.1	0.008	308.6	0.268	285.4	0.065	320.0
0.220	266.5	0.060	273.7	0.616	269.0	0.426	292.7	0.017	319.8	0.231	288.1	0.092	323.5
0.302	268.3	0.136	283.2	0.655	266.8	0.378	293.2	0.023	324.7	0.202	290.0	0.115	325.1
0.384	268.3	0.199	284.8	0.694	263.9	0.340	293.5	0.031	328.2	0.179	291.1	0.145	326.0
0.670	264.5	0.739	267.3	0.736	263.0	0.314	293.5	0.041	331.0	0.160	291.8	0.183	327.0
0.569	268.5	0.623	277.2	0.066	259.4	0.270	293.5	0.051	332.5	0.122	292.6	0.232	327.6
0.466	269.2	$C_{10}mimNTf_2^a$		0.097	265.7	0.239	293.4	0.063	333.5	0.088	292.7	0.284	328.1
0.346	268.9	0.093	280.8	0.118	267.8	$AcChNTf_2$		0.076	334.1	C_4mimBF_4		$P_{6,6,14}NTf_2$	
$C_{10}mimNTf_2^b$		0.118	283.3	$C_{12}MePyNTf_2$		0.006	282.6	0.093	334.3	0.313	284.3	0.015	283.8
0.038	252.3	0.141	285.5	0.050	267.7	0.017	304.6	0.108	334.4	0.371	287.7	0.021	290.3
0.052	261.2	0.174	287.1	0.083	275.4	0.028	313.6	0.125	334.3	0.404	290.1	0.035	295.9
0.083	267.5	0.222	287.9	0.120	278.5	0.045	319.6	0.153	333.9	0.439	291.9	0.048	300.0
0.102	270.4	0.273	288.3	0.163	281.0	0.064	323.6	0.173	333.4	0.480	294.8	0.063	302.4
0.760	259.9	0.350	287.8	0.200	281.9	0.087	326.1	0.190	332.9	0.508	297.0	0.084	303.6
0.690	266.2	0.406	286.1	0.227	282.7	0.106	327.9	0.181	333.2	0.538	299.1	0.134	305.5
0.625	270.7	0.048	270.3	0.269	283.0	0.129	329.6	0.212	331.8	0.572	301.2	0.180	306.1
0.045	256.9	0.072	276.6	0.331	283.1	0.169	330.7	0.248	329.5	0.601	302.8	0.234	306.1
0.067	262.9	0.062	274.3	0.418	282.5	0.202	331.4	0.289	326.4	0.621	303.7	0.381	303.2
0.080	266.0	0.078	278.1	0.638	273.6	0.227	331.8	0.629	275.7	0.609	303.5	0.445	300.7
0.094	268.6	0.291	288.2	0.560	278.0	0.255	332.0	0.553	292.3	0.645	304.8	0.518	295.8
0.121	270.8	0.329	288.0	0.508	281.0	0.286	332.3	0.422	311.5	0.696	306.5	0.634	284.3
0.139	272.2	0.388	286.6	$C_{14}MePyNTf_2$		0.318	332.2	0.340	321.4	0.744	307.8	0.686	278.2
0.168	274.1	0.451	284.9	0.020	267.2	0.348	332.4	0.242	329.8	0.805	308.7	0.013	280.9
0.185	274.4	0.501	283.0	0.034	277.5	0.374	332.0	$AcChNTf_2^c$		0.846	309.4	0.028	293.6
0.219	275.0	0.573	279.3	0.045	281.2	0.412	332.0	0.009	255.3	0.986	301.3	0.058	301.7
0.261	275.6	0.648	273.0	0.066	286.7	0.311	332.8	0.011	258.4	0.942	307.5	0.085	303.9
0.313	276.0	0.703	269.3	0.082	288.5	0.394	332.4	0.014	273.4	0.794	307.1	0.114	305.3
0.260	275.9	$C_{10}MePyNTf_2$		0.106	290.7	0.456	332.2	0.018	275.5	0.818	307.1	0.163	306.0
0.329	276.1	0.111	266.8	0.126	291.7	0.519	331.2	0.019	276.5	0.851	307.3	0.215	306.0
0.382	275.8	0.146	271.0	0.153	292.6	0.559	330.5	0.024	283.8	0.890	306.4	0.268	305.8
0.436	275.6	0.183	273.0	0.191	293.1	0.594	329.9	0.027	285.5	0.982	296.1	0.315	304.8
0.480	274.1	0.220	273.7	0.222	293.2	0.630	328.8	0.030	286.8	0.959	303.0	0.770	263.3
0.527	273.1	0.278	274.5	0.820	263.5	0.671	326.8	0.034	288.3	0.924	304.9	0.568	292.0
0.565	272.2	0.313	274.6	0.768	271.1	0.712	323.4	0.041	289.7	0.691	304.2		
0.605	270.6	0.349	274.0	0.705	278.1	0.749	320.4	0.072	292.2	0.479	294.2		
0.653	268.3	0.386	273.9	0.647	283.6	0.910	280.4	0.104	292.8	0.591	300.5		
0.730	263.0	0.424	273.0	0.610	286.2	0.853	302.5	0.143	292.2	0.405	293.2		
$C_{12}mimNTf_2^c$		0.438	273.6	0.569	288.4	0.801	314.5	0.520	251.6	0.645	306.6		
0.273	285.8	0.483	273.0	0.528	290.0	0.831	308.8	0.400	269.8	C_8mimPF_6			
0.393	285.2	0.529	272.2	0.493	291.2	0.722	322.8	0.325	279.4	0.041	314.3		

^a 112233-C₉FOH. ^b Propanol. ^c Ethanol.

and/or switching off and on of the Coulomb interactions were performed. The temperature, pressure and low concentration of the solutions ensured that they were performed in the one-phase region of each system. Solvent–solute radial distribution functions (RDFs) for selected atoms from each species (solute, cation and anion) were calculated from the structural simulation data and are shown in Fig. 2. Fig. 2a describes the position of the hydroxyl hydrogen atom of methanol (HO) relative to different atoms of the ionic liquid. The strong interaction of HO with the oxygen atom of bistriflamide (OBT) is obvious and confirms the statements produced at the beginning of this paragraph. On the other hand, the RDFs of Fig. 2b show how the methanol molecule orients itself in relation to the strong interaction centre OBT: the succession of the three peaks clearly shows that the hydrogen points towards the oxygen atom (possibly forming an hydrogen bond), while the methyl group points in the opposite direction (towards the less polar regions of the ionic liquid, *cf.* below). Finally, Fig. 2c shows the RDFs describing the position of the carbon atom of CF₄ (CFC) relative to different atoms of

the anion or cation of the ionic liquid. The changes are dramatic in relation to Fig. 2a: the solute is now positioned in the non-polar domains of the ionic liquid, as denoted by the RDF of CFC with the end-carbon of the butyl group of the cation, CT. However the different RDFs also show that there is a certain degree of affinity between CFC and the fluorine atoms of the CF₃ groups of bistriflamide (*cf.* the CFC-FBT radial distribution function), which means that probably the perfluorinated solutes will prefer to stay away from the polar regions of the ionic liquid but as close as possible to the CF₃ groups of bistriflamide. We must keep in mind that the interactions of perfluorocarbons with hydrocarbons are quite unfavourable and in this particular case the position of the perfluorinated solute is dictated simply by the less unfavourable position, a situation that can be partially mitigated by some (favourable) interactions with other (not so dissimilar) CF₃ groups.

Returning to the discussion of the systems studied experimentally, in the case of the fluorinated alcohols with an ethyl or propyl “spacer” group, 1122-C₈FOH or 112233-C₉FOH,

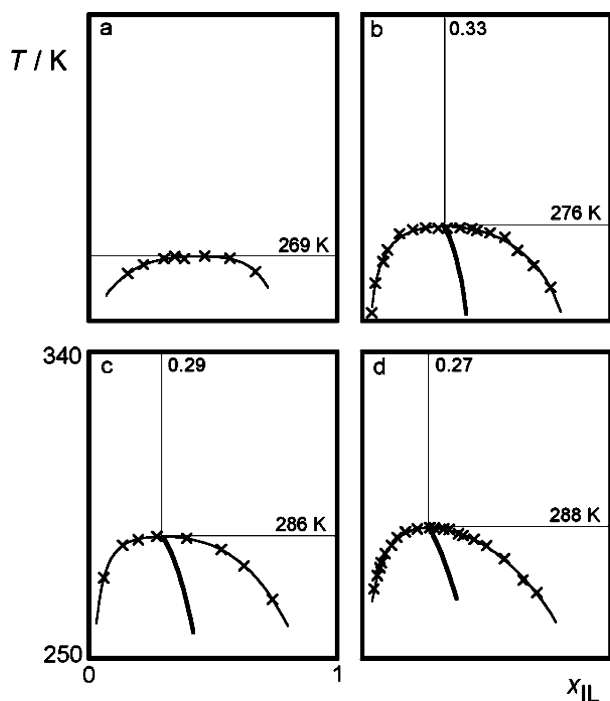


Fig. 1 Cloud-point temperature, T , as a function of composition (mole fraction of ionic liquid, x_{IL}) in (a) $\text{C}_8\text{mimNTf}_2 + 1122\text{-C}_8\text{FOH}$; (b) $\text{C}_{10}\text{mimNTf}_2 + 1122\text{-C}_8\text{FOH}$; (c) $\text{C}_{12}\text{mimNTf}_2 + 1122\text{-C}_8\text{FOH}$; and (d) $\text{C}_{10}\text{mimNTf}_2 + 112233\text{-C}_9\text{FOH}$. (x): experimental cloud-point data; black lines represent fittings to each side of the liquid–liquid equilibrium envelope; grey lines represent the average composition as determined by the rectilinear diameter law. Also shown are the estimated values for the upper critical solution temperature, T_{UCST} , and critical composition.

respectively, the perfluorinated segment will be thrown by the hydrogenated segment deep into the non-polar region of the ionic liquid, where the interactions are unfavourable and the driving force towards phase separation is larger. When the alkyl side-chains of the cation are longer, the nano-segregation is more noticeable and the non-polar domains are larger, which means that the immiscibility regions will also increase, as can be observed in the series of mixtures depicted in Fig. 1a to 1c.

Trend (ii) is noticeable not only by the comparison between Fig. 1b and 1d—a T_{UCST} upwards shift of ~ 12 K—but also by the fact that fluorinated alcohols with just one hydrogenated atom of carbon exhibit complete miscibility with the ionic liquid (*cf.* Table 3). Conversely, perfluorinated alkanes—with no spacer and no hydroxyl group—exhibit large immiscibility walls (complete immiscibility or very limited partial miscibility, *cf.* last column of Table 3) with different ionic liquids.²⁴ This trend can also be interpreted by the “dual-nature” arguments presented in the previous paragraphs. In fact, the increased miscibility of perfluorinated alcohols or fluorinated alcohols with short spacers (such as methyl) can be better understood if one also recognizes the presence of “fluorinated-friendly” residues included in (or adjacent to) the polar domains of the ionic liquid: the perfluoromethyl groups present at the ends of the bistriflamide anion. In the case of fluorinated alcohols with no or short spacers, the hydroxyl group will anchor the alcohol “head” near the polar regions and the short spacer will allow the perfluorinated chain to remain close to the polar domain

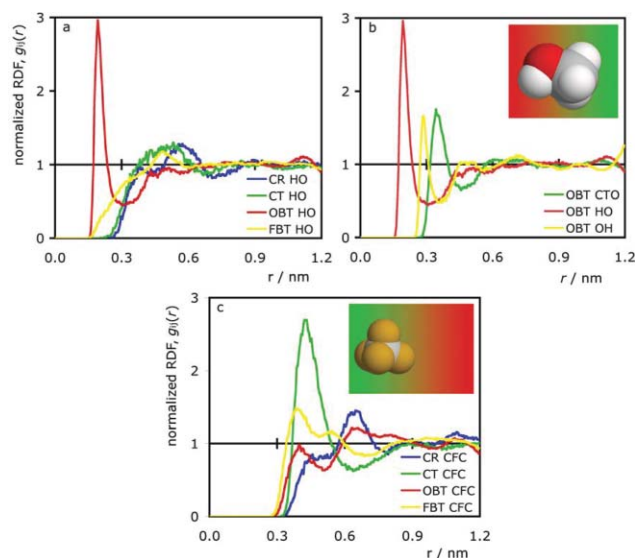


Fig. 2 Solute–solvent radial distribution functions showing the position and orientation of methanol (a and b) and tetrafluoromethane (c) dissolved in $[\text{C}_4\text{mim}][\text{NTF}_2]$. The insets indicate schematically the preference of each solute for the high-charge (red) or low-charge (green) regions of the ionic liquid. HO, OH and CTO represent the hydrogen (hydroxyl), oxygen and carbon atoms of methanol, respectively; CR the carbon atom between the two nitrogens of the imidazolium ring; CT the terminal carbon in the butyl chain of the cation; and OBT and FBT the oxygen and fluorine atoms of the anion, respectively. CFC holds for the carbon atom of tetrafluoromethane.

where it can orient itself towards the end groups of bistriflamide, thus increasing the mutual miscibility of the alcohol and the ionic liquid. When the hydroxyl group is absent (as in the case of perfluoroalkanes) no anchoring process is possible and the perfluorinated compound (that has no driving force to stay close to the polar regions) will exhibit large immiscibility windows in mixtures with ionic liquids.

Trend (iii) will be discussed below, when other ionic liquids and alcohols with different volume ratios are presented.

In Fig. 3 mixtures with a different family of ionic liquids—*N*-alkyl-3-methylpyridinium bistriflamide—are shown. The only difference between the previous systems and the present ones is the “head” of the cation that was “switched” from a methyl-imidazolium ring to a methyl-pyridinium one (*cf.* Table 1).

The differences between Fig. 1 and 3, especially when ionic liquids with the same alkyl side-chain length are compared (Fig. 1b and 3a; Fig. 1c and 3b), are very small both in terms of the upper critical solution temperatures and concentrations. This lends support to the view that no specific interactions between the fluorinated alcohol and the charged part of these two particular ionic liquid cations are present in the mixture. The structural similarity between the two head groups of the cations (both alkyl-substituted hetero-aromatic rings) also explains the similarity of the fluid phase behaviour.

The acetylcholinium cation was tested in the systems represented in Fig. 4. The most obvious difference in relation to the systems presented in Fig. 1 and 3 is that by changing the structural nature of the cation (the long alkyl side chain was changed into a shorter, functionalized one; the hetero-aromatic head group was replaced by a tetra-alkyl ammonium cation)

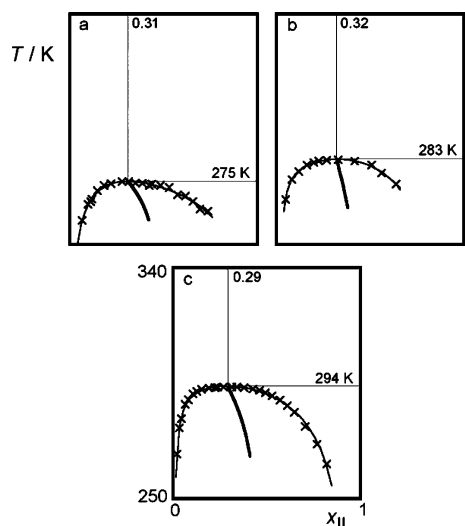


Fig. 3 Cloud-point temperature as a function of composition (mole fraction of ionic liquid) in (a) $C_{10}MePyNTf_2$ + 1122- C_8FOH ; (b) $C_{12}MePyNTf_2$ + 1122- C_8FOH ; and (c) $C_{14}MePyNTf_2$ + 1122- C_8FOH . Symbols and lines as in Fig. 1.

the immiscibility window with the fluorinated alcohol increases dramatically.

It is hard to interpret these results in terms of the polar/non-polar structure of the ionic liquid and of the specific interactions of the fluorinated alcohol with the anion. In acetylcholinium-based ionic liquids one can argue that the functionalization of the alkyl side-chain with an ester group increases the charge density of the non-polar regions, eventually reducing the segregated character of the ionic liquid and decreasing the size of its non-polar domains. This can be discussed in terms of the results presented in Fig. 4b, where the solubility of ethanol and propanol in $AcChNTf_2$ is shown. At room temperature (298 K) ethanol is completely miscible with $AcChNTf_2$, exhibiting an upper critical solution temperature at around 293 K. The corresponding value for the propanol mixtures is 338 K, signalling a much larger immiscibility domain. This can be easily understood in terms of the inability of the ionic liquid to accommodate the longer alkyl moieties of the propanol among its functionalized, high charge-density, alkyl side-chains. However, the increased immiscibility of the fluorinated alcohol in $AcChNTf_2$ cannot be understood considering only the partial destruction of the non-polar regions of the latter substance. In fact, we saw in previous systems that a smaller non-bonded region increased

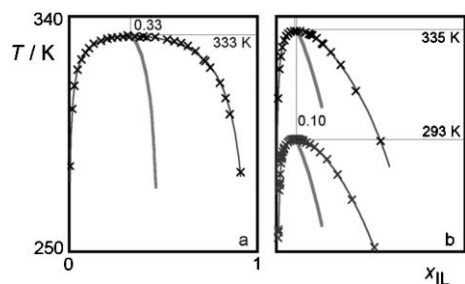


Fig. 4 Cloud-point temperature as a function of composition (mole fraction of ionic liquid) in (a) $AcChNTf_2$ + 1122- C_8FOH ; (b) $AcChNTf_2$ + C_3H_8OH (top); $AcChNTf_2$ + C_2H_5OH (bottom). Symbols and lines as in Fig. 1.

the miscibility. The detail that is missing is that now the hydroxy group of the fluorinated alcohol can interact not only with the oxygen atoms of bistriflamide (and orient its fluorinated moiety towards the CF_3 end-groups of that anion) but also interact with the oxygen atoms of the ester group (which implies the presence of the fluorinated residue in the midst of the alkyl side chain of the cation). This competition will promote the immiscibility of the fluorinated alcohol in the acetylcholinium-based ionic liquid.

Fig. 5 presents the results for mixtures of different types of ionic liquid with the fluorinated alcohol 1122- C_8FOH . In this case both the cation and the anion were changed.

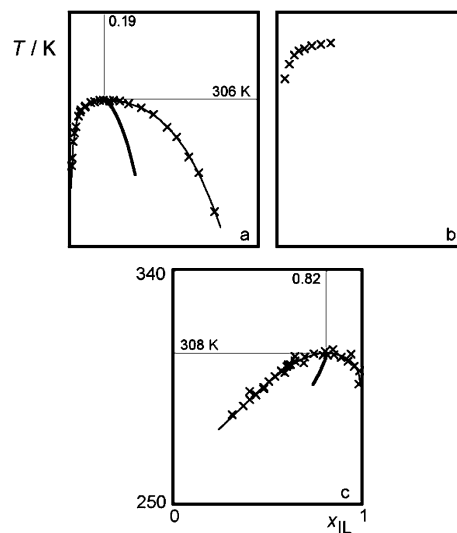


Fig. 5 Cloud-point temperature as a function of composition (mole fraction of ionic liquid) in (a) $P_{66614}NTf_2$ + 1122- C_8FOH ; (b) C_8mimPF_6 + 1122- C_8FOH ; (c) C_4mimBF_4 + 1122- C_8FOH . Symbols and lines as in Fig. 1.

In Fig. 5a we show the fluid phase diagram of mixtures of the fluorinated alcohol with a tetra-alkylphosphonium-based ionic liquid with bistriflamide as counter-ion. The immiscibility envelope lies somewhere in between those of imidazolium- and pyridinium-based ionic liquids (Fig. 1 and 3) and that of the acetylcholinium-based ionic liquid (Fig. 4a). Immiscibility is larger than in the former cases because the non-polar regions are bigger (four alkyl side-chains) and surround the charged part of the ionic liquid (the phosphorus atom in the cation and the bistriflamide anion), making it more difficult for the alcohol to anchor and orient itself favourably in the vicinity of the anion. On the other hand, miscibility is larger than in the acetylcholinium case due to the absence of the ester groups in the alkyl-side chains (*cf.* discussion above).

In Fig. 5b, the bistriflamide anion of the ionic liquid was substituted by the hexafluorophosphate anion. The fluid phase diagram is incomplete due to decomposition problems at the temperatures that needed to be attained to measure the corresponding cloud-points (one of the reasons behind the increasing popularity of bistriflamide as the “standard” anion in many recent studies involving ionic liquids is its enhanced thermal stability relative to other anions such as PF_6 or BF_4). Nevertheless, it is possible to conclude that the immiscibility is quite high, probably due to the size and rigidity of the anion

that while interacting with the hydroxyl group of the fluorinated alcohol does not allow at the same time the interaction of the fluorinated residue of the latter with the fluorinated atoms of the former.

In Fig. 5c, we tested a tetrafluoroborate anion-based ionic liquid. In order to decrease the working temperatures and avoid decomposition problems we decided to use an imidazolium cation with a shorter alkyl side-chain (as we saw in previous cases, smaller non-polar domains in the ionic liquid increase the solubility of the fluorinated alcohol). The fluid phase diagram of the mixture still exhibits a relatively high upper critical solution temperature (higher than the corresponding bistriflamide imidazolium-based ionic liquid of Fig. 1) for the same reasons pointed out in the previous paragraph.

However, the most interesting feature of the diagram in Fig. 5c is the shift to higher ionic liquid mole fraction of the upper critical solution concentration. Part of the shift can be attributed to the difference in size between the components of the mixture: components with similar size generally exhibit symmetrical $T-x$ immiscibility windows centred at the equimolar concentration, whereas mixtures with components very dissimilar in size will have the LLE envelope leaning towards the smaller component. This can explain trend (iii) observed in Fig. 1 (see above): as the alkyl side-chain of the ionic liquid is increased (its volume is larger) the diagrams shift to the side of the alcohol (lower ionic liquid mole fraction) and the corresponding critical concentration is decreased. The same applies to Fig. 4: when the fluorinated alcohol is substituted by (the much smaller) ethanol or propanol molecules, the corresponding diagrams and critical concentrations also shift (markedly) to more alcohol-rich compositions. In this case, we have the smallest of all studied ionic liquids, which means that we would anticipate a shift of the critical concentration to the ionic-liquid-rich side of the diagram. That is indeed the case, but the surprise is the magnitude of the shift: the molar volumes of the fluorinated alcohol and of C_4mimBF_4 are quite similar (216.7 and 187.6 $\text{cm}^3 \text{mol}^{-1}$, respectively, *cf.* Table 5), which would indicate a critical concentration close to the equimolar, not $x_{1L} = 0.82$.

Lattice models like the modified Flory–Huggins, FH, theory proved to be valuable tools to interpret liquid–liquid equilibrium behaviour, namely the prediction of the locus of the critical solution concentration in binary mixtures containing ionic liquids.³¹ According to those models, the critical solution concentration, expressed in mole fraction of component 1, can be expressed as $x_{1,c} = 1/(1 + r^{3/2})$, where r is the ratio between the molar volume of the components, $r = V_{m,1}/V_{m,2}$. The aforementioned relation was applied to the systems studied in this work and it was found (*cf.* Table 5) that the relation yields good results for all of them except for the $C_4mimBF_4 + 1122-C_8FOH$ mixtures. This fact suggests that there is some degree of association between the fluorinated molecules in the one-phase region above the USCT—the mixture is not completely random. For instance, if we consider that, on average, the fluorinated alcohol molecules form dimers (with a volume twice that of the isolated molecules) than the corresponding value of $x_{1,c}$ would rise from the 0.544 value presented in Table 5 to a value of 0.778, in better agreement with the experimental value. Such self-aggregation (possibly through the fluorinated “tails” of the alcohol) would compensate for the possible loss of F–F interactions when the anion of the ionic liquid is changed from bistriflamide to tetrafluoroborate and would explain the sudden change in the shape of the liquid–liquid immiscibility envelope in Fig. 5c.

The effect of pressure on the liquid–liquid immiscibility window of selected ionic liquid plus partially fluorinated alcohol was also investigated. The shift of the cloud point temperature as a function of pressure for four mixtures containing 1122- C_8FOH and $C_8mimNTf_2$, $C_{10}mimNTf_2$, $C_{12}mimNTf_2$, or $C_{12}MePyNTf_2$, each at their corresponding critical composition (*cf.* Fig. 1a–1c and 3b), is presented in Fig. 6. The graph shows that in these systems the cloud-point temperatures are almost not affected by pressure—less than 0.2 K per MPa increase in all cases (see caption to figure).

The fact that these slopes, dT/dp , are positive imply that the mixing process at temperatures near and above the UCST in these systems (fluorinated alcohols + bistriflamide- and imidazolium-based or pyridinium-based ionic liquids) is accompanied by a volume expansion (positive excess volume,

Table 5 Critical solution concentration (estimated, FH, and experimental, exp) in different (ionic liquid(1) + alcohol(2)) systems. All systems include the alcohol 1122- C_8FOH , except where stated. The molar volume of each component at 298 K is also given. Numbers as superscripts hold for references

	$C_8mimNTf_2$	$C_{10}mimNTf_2$	$C_{12}mimNTf_2$	$C_{10}MePyNTf_2$	$C_{12}MePyNTf_2$	$C_{14}MePyNTf_2$
$V_{m1}/\text{cm}^3 \text{mol}^{-1}$	362.1 ²⁵	404.1 ²⁵	429.8 ^{1,26, e}	407.6 ²⁷	440.1 ²⁷	473.2 ²⁷
$V_{m2}/\text{cm}^3 \text{mol}^{-1}$	216.4 ^d	216.4 ^d	216.4 ^d	216.4 ^d	216.4 ^d	216.4 ^d
$x_{1,c}$ (FH)	0.317	0.283	0.264	0.279	0.257	0.237
$x_{1,c}$ (exp)	0.47	0.330	0.294	0.309	0.323	0.291
	$C_{10}mimNTf_2^a$	$AcChNTf_2$	$AcChNTf_2^b$	$AcChNTf_2^c$	$P_{6,6,14}NTf_2$	C_4mimBF_4
$V_{m1}/\text{cm}^3 \text{mol}^{-1}$	404.1 ²⁵	287.4 ²⁸	287.4 ²⁸	287.4 ²⁸	716.3 ²⁶	187.6 ²⁹
$V_{m2}/\text{cm}^3 \text{mol}^{-1}$	234.2 ^d	216.4 ^d	75.2 ³⁰	58.7 ³⁰	216.4 ^d	216.4 ^d
$x_{1,c}$ (FH)	0.304	0.396	0.118	0.084	0.143	0.554
$x_{1,c}$ (exp)	0.269	0.334	0.109	0.101	0.186	0.815

All systems include the alcohol 1122- C_8FOH , except^a 112233- C_9FOH . ^b Propanol. ^c Ethanol. ^d Density measured in the present work using an Anton-Paar DMA 5000 vibrating-tube densimeter. ^e Molar volume estimated as the sum of the effective volumes occupied by the cation and anion (see ref. 1,26).

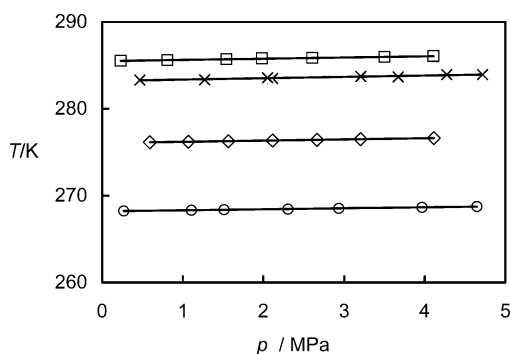


Fig. 6 Pressure dependence of cloud-point temperature in partially fluorinated alcohol plus ionic liquid systems near their critical composition. Values for the slope in mK/MPa are given between parentheses for each system. (□) 1122-C₈FOH + C₈mimNTf₂ (118); (◇) 1122-C₈FOH + C₁₀mimNTf₂ (140); (○) 1122-C₈FOH + C₁₂mimNTf₂ (138); (×) 1122-C₈FOH + C₁₂MePyNTf₂ (158).

$\Delta V^E > 0$). The rationale for this fact is found at the recently revisited^{32,33} Prigogine–Defay relation, which states that under some restrictive assumptions (in practice, the two excess properties, ΔV^E and ΔH^E , have to have a similar form in respect to composition and present no inflection points), one obtains a Clapeyron-type of relation, which can be expressed as:

$$\left(\frac{dT}{dp}\right)_c \cong T_c(p) \frac{\Delta V^E(T_c(p), x)}{\Delta H^E(T_c(p), x)} \quad (1)$$

Then, one should recognize that demixing upon cooling (UCST-type of phase diagram) is an exothermic process, thus, conversely, mixing is endothermic ($\Delta H^E > 0$).

4. Conclusions

In this work, liquid–liquid equilibria (cloud-point temperature determinations) of binary mixtures of fluorinated alcohols plus different ionic liquids were studied and measured by turbidimetry. These systems comprise two classes of fluids that, due to their unique characteristics, are very interesting both from the pure and applied chemistry points of view and have, in recent years, received increasing attention from the scientific community.

The corresponding T – x phase diagrams exhibit a rich fluid-phase behaviour that can be rationalized semi-quantitatively at the molecular level in terms of the different and complex interactions between the fluorinated alcohol—composed of a polar head group, an alkylated “spacer”, and a fluorinated moiety—and the ionic liquid—a micro-segregated fluid exhibiting non-polar domains permeated by a polar network.

The possibility of using fluorinated alcohols (or other diblock molecules with fluorinated residues) together with bistriflamide-based ionic liquids in order to promote the miscibility of the latter with water (and water-soluble molecules) is one of the potential future developments of the present work.

Acknowledgements

This work was supported by the *Fundação para a Ciência e Tecnologia (FC & T)*, Portugal (POCI/QUI/57716/2004 and PTDC/CTM/73850/2006). M. B. thanks *FC & T* for a Ph.D.

grant SFRH/BD/13763/2003. We would like to thank the QUILL team, Belfast, for the synthesis and characterization of several ionic liquids used in this work.

References

- L. P. N. Rebelo, J. N. Canongia Lopes, J. M. S. S. Esperança, J. Lachwa, V. Najdanovic-Visak and Z. P. Visak, *Acc. Chem. Res.*, 2007, **40**, 1114–1121.
- N. V. Plechkova and K. R. Seddon, *Chem. Soc. Rev.*, 2008, **37**, 123–150.
- J. N. Canongia Lopes and A. A. H. Pádua, *J. Phys. Chem. B*, 2006, **110**, 3330–3335.
- M. S. Kelkar and E. J. Maginn, *J. Chem. Phys.*, 2005, **123**.
- J. N. Canongia Lopes, M. F. Costa Gomes and A. A. H. Pádua, *J. Phys. Chem. B*, 2006, **110**, 16816–16818.
- R. E. Banks, B. E. Smart, J. C. Tatlow, *Organofluorine Chemistry – Principles and Commercial Applications*, Plenum Press, New York, 1994.
- J. G. Riess, *Chem. Rev.*, 2001, **101**, 2797–2919.
- C. A. Eckert, B. L. Knutson and P. G. Debenedetti, *Nature*, 1996, **383**, 313–318.
- M. J. P. de Melo, A. M. A. Dias, M. Blesic, L. P. N. Rebelo, L. F. Vega, J. A. P. Coutinho and I. M. Marrucho, *Fluid Phase Equilib.*, 2006, **242**, 210–219.
- M. B. Shiflett and A. Yokozeki, *Ind. Eng. Chem. Res.*, 2008, **47**, 926–934.
- P. Morgado, H. G. Zhao, F. J. Blas, C. McCabe, L. P. N. Rebelo and E. J. M. Filipe, *J. Phys. Chem. B*, 2007, **111**, 2856–2863.
- J. R. Trindade, A. M. A. Dias, M. Blesic, N. Pedrosa, L. P. N. Rebelo, L. F. Vega, J. A. P. Coutinho and I. M. Marrucho, *Fluid Phase Equilib.*, 2007, **251**, 33–40.
- H. C. de Sousa and L. P. N. Rebelo, *J. Chem. Thermodyn.*, 2000, **32**, 355–387.
- M. B. Shiflett and A. Yokozeki, *J. Chem. Eng. Data*, 2008, **53**, 492–497.
- M. B. Shiflett and A. Yokozeki, *Fluid Phase Equilib.*, 2007, **259**, 210–217.
- M. B. Shiflett and A. Yokozeki, *J. Chem. Eng. Data*, 2007, **52**, 2413–2418.
- J. M. Crosthwaite, M. J. Muldoon, S. Aki, E. J. Maginn and J. F. Brennecke, *J. Phys. Chem. B*, 2006, **110**, 9354–9361.
- J. M. Crosthwaite, S. Aki, E. J. Maginn and J. F. Brennecke, *J. Phys. Chem. B*, 2004, **108**, 5113–5119.
- W. L. Jorgensen, D. S. Maxwell and J. TiradoRives, *J. Am. Chem. Soc.*, 1996, **118**, 11225–11236.
- E. K. Watkins and W. L. Jorgensen, *J. Phys. Chem. A*, 2001, **105**, 4118–4125.
- J. N. C. Lopes, J. Deschamps and A. A. H. Padua, *J. Phys. Chem. B*, 2004, **108**, 11250.
- J. N. C. Lopes, J. Deschamps and A. A. H. Padua, *J. Phys. Chem. B*, 2004, **108**, 2038–2047.
- J. Lopes and A. A. H. Padua, *J. Phys. Chem. B*, 2006, **110**, 3330–3335.
- T. L. Merrigan, E. D. Bates, S. C. Dorman and J. H. Davis, *Chem. Commun.*, 2000, 2051–2052.
- J. N. C. Lopes, T. C. Cordeiro, J. Esperança, H. J. R. Guedes, S. Huq, L. P. N. Rebelo and K. R. Seddon, *J. Phys. Chem. B*, 2005, **109**, 3519–3525.
- J. Esperança, H. J. R. Guedes, M. Blesic and L. P. N. Rebelo, *J. Chem. Eng. Data*, 2006, **51**, 237–242.
- P. Natalia, *PhD Thesis*, Queens University of Belfast, 2007.
- G. W. Driver, *PhD Thesis*, Queens University of Belfast, 2007.
- R. G. de Azevedo, J. Esperança, V. Najdanovic-Visak, Z. P. Visak, H. J. R. Guedes, M. N. da Ponte and L. P. N. Rebelo, *J. Chem. Eng. Data*, 2005, **50**, 997–1008.
- G. C. Benson and H. D. Pflug, *J. Chem. Eng. Data*, 1970, **15**, 382.
- V. Najdanovic-Visak, J. Esperança, L. P. N. Rebelo, M. N. da Ponte, H. J. R. Guedes, K. R. Seddon, H. C. de Sousa and J. Szydowski, *J. Phys. Chem. B*, 2003, **107**, 12797–12807.
- L. P. N. Rebelo, *Phys. Chem. Chem. Phys.*, 1999, **1**, 4277–4286.
- H. C. De Sousa and L. P. N. Rebelo, *J. Polym. Sci., Part B: Polym. Phys.*, 2000, **38**, 632–651.

High-pressure phase behavior of ternary mixtures with ionic liquids, part I: the system bmim[BF₄]+4-isobutylacetophenone + CO₂

Eliane Kühne,^{a,b} Geert-Jan Witkamp^b and Cor J. Peters^{*b}

Received 24th January 2008, Accepted 30th June 2008

First published as an Advance Article on the web 11th August 2008

DOI: 10.1039/b801362d

Performing reactions in a homogeneous system is extremely important for the achievement of high reaction rates and yield. Since carbon dioxide can tune the miscibility of ionic liquid/organic mixtures, measurements on the phase behavior of these systems provide useful information for the selection of operational conditions for reactions and extractions. We investigated the phase behavior of ternary mixtures of the type bmim[BF₄] + solute + CO₂, in which the solute is an intermediary in the synthesis of ibuprofen. In this contribution, the influence of carbon dioxide pressure on the location of the homogeneous liquid phase region in the phase diagram of the ternary system bmim[BF₄] + 4-isobutylacetophenone + CO₂ is presented. We show that for CO₂ concentrations above 60 mol%, a narrow three-phase region can be found in the pressure *versus* temperature diagram, and that a further increase in CO₂ composition gradually reduces the extension and influences the location of the one-phase liquid region, finally resulting in its complete disappearance.

Introduction

Nowadays there is an increasing pressure on industry to reduce or even to eliminate pollution and the environmental impact of their activities. Rigorous governmental regulations and public awareness of ecological problems such as global climate change are driving the efforts of the scientific community towards the development of more green and efficient technologies in industrial processes.

Since the discovery that ionic liquids can efficiently replace common volatile organic solvents in synthesis and extraction processes,¹ the number of publications on ionic liquids increased remarkably. However, for the scale-up of processes and efficient design of industrial unit operations, knowledge of physico-chemical properties and thermodynamic fundamentals such as phase diagrams of the mixtures is prerequisite.

In that respect, most of the publications found on the phase behavior of mixtures with ionic liquids concern the solubility of gases.² From those gases, carbon dioxide is the most common one to be found in applications associated with ionic liquids.

In previous research performed by Gauter *et al.*,³ it was shown that mixtures of the type liquid₁ + liquid₂ + CO₂ present miscibility windows, *i.e.*, changes in carbon dioxide pressure are able to tune the miscibility of the phases.

This phenomenon has proven to hold also for mixtures of ionic liquid + organic + CO₂⁴ as well as ionic liquid + water + CO₂,⁵ in which it has been demonstrated that carbon dioxide is able

to induce phase separations, also in systems with ionic liquids. Additionally, the combination of ionic liquids (polar solvents) and carbon dioxide (non-polar solvent) generates a very flexible system applicable to a large number of compounds, both polar and non-polar.

When ionic liquids and CO₂ are combined for reactions and separations, the switch in miscibility caused by changes in pressure can be used to the advantage of the process: reactions can be performed in a homogeneous system, and by pressure changes, separation of the reaction mixture into two or more phases (usually one organic-rich and one ionic liquid-rich) is possible, leading to high reaction rates, reduced mass transfer barriers and a more efficient separation of the product. Since ionic liquids have negligible solubility in CO₂,⁶ the product can be extracted by the supercritical phase without any contamination from the solvents, achieving high purity levels of the final product.

Therefore, knowledge of the pressure and temperature conditions at which the phase split occurs as well as where the homogeneous phase is located, is extremely important in order to benefit from the miscibility switch in of synthesis and extractions.

In previous contributions we presented the phase diagrams of ternary mixtures of an ionic liquid, an organic solute and carbon dioxide, with CO₂ concentration ranging from about 10 mol% up to 50 mol%. At the experimental conditions applied, mostly liquid–vapor equilibria were found.⁷ However, additional solid–liquid equilibria occurred when the organic solute had a high melting point.⁸

From our measurements, however, we noticed that an increase in the concentration of carbon dioxide from about 50 mol% up to 60 mol% dramatically changed the complexity of the phase diagram. In order to have a deeper insight in this effect, we extended our measurements to ternary mixtures with concentrations of

^aDelft University of Technology - Faculty of Applied Sciences (DelftChemTech), Laboratory of Physical Chemistry and Molecular Thermodynamics, Julianalaan 136, 2628, BL, Delft, The Netherlands
^bDelft University of Technology - Faculty of Mechanical, Maritime and Materials Engineering, Laboratory for Process Equipment, Leeghwaterstraat 44, 2628, CA, Delft, The Netherlands.
E-mail: c.j.peters@tudelft.nl

carbon dioxide to above 60 mol%. The model reaction chosen to provide the solutes for the ternary system is a step reaction in the synthesis of the common non-steroidal anti-inflammatory drug ibuprofen (2-[4-(2-methylpropyl)phenyl]propanoic acid). In this step reaction, 4-isobutylacetophenone is hydrogenated into 1-(4-isobutylphenyl)-ethanol.

In this contribution the results of phase behavior measurements with the reactant 4-isobutylacetophenone as solute in the ternary system $\text{bmim}[\text{BF}_4] + 4\text{-isobutylacetophenone} + \text{CO}_2$ are presented. Our measurements were focused on the effect of CO_2 composition on the location of the homogeneous liquid phase region. Measurements were performed in the Cailletet apparatus, in a temperature range of 240 K up to 320 K, and maximum pressures of 14 MPa. Under these conditions, a very narrow three-phase liquid–liquid–vapor region was found, and the location of the phase boundary between the homogeneous liquid region and the liquid–liquid two-phase region was found to highly depend on the CO_2 concentration.

Experimental

Materials

The ionic liquid $\text{bmim}[\text{BF}_4]$ was synthesized in our facilities according to a known method.⁹ Water content was measured by Karl Fischer analysis as low as 0.046 mass%. Carbon dioxide was supplied by HoekLoos B.V., with 99.995 mol% purity. The solute 4-isobutylacetophenone (CAS number 38861-78-8) was purchased from Alfa Aesar GmbH & Co KG with 97% purity and 0.222 mass% water content according to Karl Fischer analysis.

All compounds were used without further purification.

In order to keep the ratio IL : solute constant for all samples, a solution with 9.425 mol% of 4-isobutylacetophenone in the ionic liquid $\text{bmim}[\text{BF}_4]$ was prepared. This solution was kept in a desiccator, reducing as much as possible the amount of absorbed water. During the time that the experiments were performed, the average water content detected in the solution by Karl Fischer analysis was 0.239 mass%.

Equipment

Phase behavior experiments were performed according to a synthetic method in the Cailletet apparatus, in which the phase transitions can be observed visually. The maximum pressure allowed in this equipment is 14 MPa, and the liquid used as heat-transfer fluid determines the operational temperature range. Since the phase transitions were located at low temperatures, ethanol 96% was used as heat-transfer fluid, allowing experiments to be carried out at temperatures from 240 K up to 320 K.

In the Cailletet apparatus, the sample with known overall composition is confined in a thick-walled Pyrex glass tube, which is placed inside a glass jacket. The tube is closed at one end, where the sample is contained, and mercury is used as a sealing and pressure transmitting fluid between the sample and the oil in the high-pressure equipment. The pressure is measured with a dead-weight gauge with an accuracy of $\pm 0.03\%$ of the reading.

A scheme of the Cailletet apparatus is shown in Fig. 1.

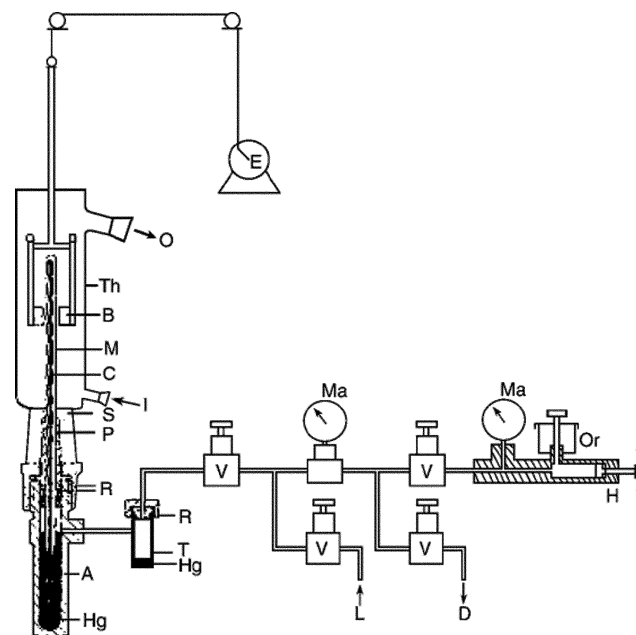


Fig. 1 The Cailletet apparatus. Legend: A, autoclave; B, magnets; C, capillary glass tube; D, drain; E, motor; H, rotating hand pump; Hg, mercury; I, thermostat liquid in; L, line to dead weight pressure gauge; M, mixture being investigated; Ma, manometers; O, thermostat liquid out; Or, hydraulic oil reservoir; P, closing plug; R, Viton O-rings; S, silicone rubber stopper; T, mercury trap; Th, glass thermostat; V, valve.

Methodology

The samples were prepared by inserting a known, weighted amount of the previously prepared solution $\text{bmim}[\text{BF}_4] + 4\text{-isobutylacetophenone}$ with a micro-syringe into the Cailletet tube. The tube containing the solution was then connected to the equipment in which degassing of the mixture is carried out, ensuring that no air remained present in the sample.

After deaeration of the sample, carbon dioxide was added volumetrically to the tube according to the desired molar fraction. The tube, now containing the three components, was sealed with mercury and mounted into the Cailletet equipment. Pressure and temperature data were taken for each phase transition, respecting the previously mentioned limitations of the equipment.

This procedure was repeated for five samples, varying the concentration of CO_2 in the ternary system from 60 mol% up to approximately 70 mol%.

For each sample the phase transitions were visualized in the Cailletet apparatus by slightly distinct measuring procedures. For bubble point measurements ($L+V \rightarrow L$) and $L_1+L_2+V \rightarrow L_1+L_2$ phase transitions, the temperature was set to a desired value and pressure was varied by means of a dead weight pressure gauge until the last bubble of gas disappears. Pressure was also the variable to determine $L_1+L_2 \rightarrow L$ phase transitions at a fixed temperature, but in that case the disappearance of the last tiny droplet of the lower-density liquid determined the boundary of the phase change.

In the case of $L+V \rightarrow L_1+L_2+V$ phase transitions, the temperature was kept constant but instead of increasing the pressure, it was decreased until the last droplet of liquid disappeared, and

a two-phase equilibrium L+V occurred. In this case, dew points were measured.

Results and discussion

Table 1 presents the experimental results for the various phase boundaries measured for the ternary system $\text{bmim}[\text{BF}_4] + 4\text{-isobutylacetophenone} + \text{CO}_2$, with the CO_2 composition varying from 60 mol% up to 67 mol%. Since emphasis was given to the location of the homogenous liquid region, measurements were performed at low temperatures, *i.e.* the region where the different phase transitions were located.

The location of each phase region in the pressure *versus* temperature diagram is demonstrated in Fig. 2, where data from Table 1 for the ternary system with a CO_2 composition of 62.38 mol% are presented graphically.

To interpret the data presented in Table 1 and to visualize how the $\text{L}_1 + \text{L}_2 \rightarrow \text{L}$ phase boundary evolves, in Fig. 3 the phase diagrams for different CO_2 compositions are represented.

From Fig. 3 it can be seen that the carbon dioxide concentration highly influences the location of the homogeneous liquid phase region. With an increase in the carbon dioxide composition, the $\text{L}_1 + \text{L}_2 \rightarrow \text{L}$ phase boundary shifts to lower temperatures and higher pressures (see diagrams A to D), until it completely disappears (diagram E).

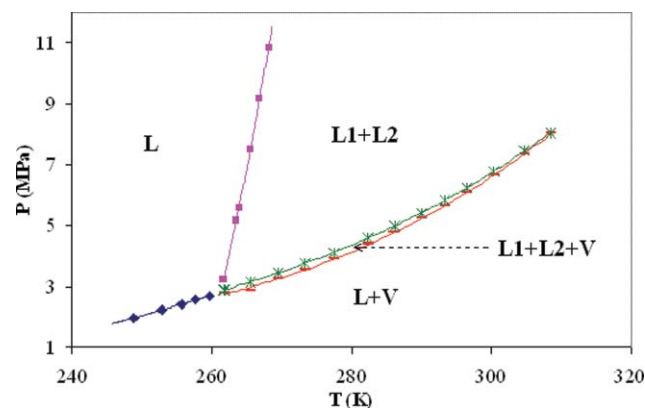


Fig. 2 Identification of the different miscibility regions measured for the ternary system $\text{bmim}[\text{BF}_4] + 4\text{-isobutylacetophenone} + \text{CO}_2$, with 0.6238 mol fraction of carbon dioxide. Lines are meant for eye-guidance only.

However, the region where the three phases $\text{L}_1 + \text{L}_2 + \text{V}$ coexist does not show any significant change with carbon dioxide composition. Investigation of the critical endpoints (CEP) as listed in Table 1, no conclusions could be drawn on the effect of CO_2 on the shape of this critical endpoint locus. Since the three-phase region is extremely narrow and the visualization of the CEP is quite cumbersome, considering the experimental errors,

Table 1 Experimental data obtained for the ternary system $\text{bmim}[\text{BF}_4] + 4\text{-isobutylacetophenone} + \text{CO}_2$. Values of pressure and temperature in bold are approximate experimental values for the critical endpoints

$x_{\text{CO}_2}^a$	Transition	<i>T</i> /K	<i>P</i> /MPa	<i>T</i> /K	<i>P</i> /MPa	<i>T</i> /K	<i>P</i> /MPa	<i>T</i> /K	<i>P</i> /MPa	<i>T</i> /K	<i>P</i> /MPa
0.6019	L + V → L	263.44	2.733	265.45	2.887	268.02	3.198				
	$\text{L}_1 + \text{L}_2 \rightarrow \text{L}$	269.81	3.307	273.08	4.949	275.09	6.648	278.08	9.423	279.68	11.397
	L + V → $\text{L}_1 + \text{L}_2 + \text{V}$	273.40	3.632	276.87	3.873	285.68	4.698	298.41	6.349	307.67	7.758
		276.01	3.747	279.47	4.124	292.14	5.473	304.36	7.238	308.54	8.023
	$\text{L}_1 + \text{L}_2 + \text{V} \rightarrow \text{L}_1 + \text{L}_2$	273.39	3.647	276.87	3.953	285.64	4.868	298.40	6.474	307.69	7.898
0.6238		276.01	3.857	279.47	4.239	292.10	5.633	304.15	7.348	308.54	8.023
	L + V → L	248.82	1.967	252.75	2.212	255.63	2.412	257.61	2.562	259.62	2.684
	$\text{L}_1 + \text{L}_2 \rightarrow \text{L}$	261.59	3.210	263.92	5.597	265.51	7.500	266.84	9.169	268.11	10.825
		263.51	5.160								
	L + V → $\text{L}_1 + \text{L}_2 + \text{V}$	261.79	2.795	273.39	3.549	286.08	4.767	296.42	6.061	304.72	7.331
		265.53	2.890	277.43	3.905	290.04	5.223	300.39	6.642	308.47	8.032
		269.47	3.235	282.41	4.386	293.34	5.643				
	$\text{L}_1 + \text{L}_2 + \text{V} \rightarrow \text{L}_1 + \text{L}_2$	261.59	2.890	269.43	3.441	282.41	4.595	293.34	5.824	304.73	7.446
		261.79	2.854	273.41	3.753	286.09	4.957	296.42	6.231	308.47	8.032
		265.54	3.150	277.43	4.110	290.04	5.406	300.39	6.782		
0.6496	$\text{L}_1 + \text{L}_2 \rightarrow \text{L}$	248.83	6.549	250.23	7.920	251.70	10.060	252.76	12.087		
	L + V → $\text{L}_1 + \text{L}_2 + \text{V}$	249.35	1.706	266.91	2.818	284.78	4.464	299.33	6.298	308.15	7.638
		254.78	1.997	273.56	3.363	290.62	5.130	303.30	6.893	309.47	7.988
		261.66	2.438	279.53	3.923	295.91	5.822				
	$\text{L}_1 + \text{L}_2 + \text{V} \rightarrow \text{L}_1 + \text{L}_2$	249.35	1.766	267.00	2.907	284.78	4.563	299.33	6.407	308.15	7.778
0.6570		254.75	2.066	273.58	3.452	290.62	5.242	303.30	6.992	309.47	7.988
		261.67	2.517	279.53	4.011	295.38	5.853				
	$\text{L}_1 + \text{L}_2 \rightarrow \text{L}$	249.00	9.406	250.35	10.528	251.14	11.490	251.59	12.421		
	L + V → $\text{L}_1 + \text{L}_2 + \text{V}$	249.33	1.715	265.67	2.767	281.09	4.146	297.97	6.201	305.79	7.401
		254.14	1.980	271.14	3.211	286.47	4.736	302.64	6.846	308.86	7.976
		260.61	2.400	276.77	3.716	292.87	5.517				
	$\text{L}_1 + \text{L}_2 + \text{V} \rightarrow \text{L}_1 + \text{L}_2$	249.33	1.744	265.68	2.803	281.10	4.190	297.97	6.254	308.27	7.886
		254.13	2.013	271.14	3.245	286.47	4.780	302.64	6.955	308.86	7.976
		260.61	2.433	276.77	3.759	292.87	5.560	305.80	7.461		
		249.38	1.716	267.29	2.900	283.84	4.422	297.47	6.152	308.70	7.953
0.6695	L + V → $\text{L}_1 + \text{L}_2 + \text{V}$	258.25	2.246	276.05	3.655	290.49	5.156	303.99	7.142		
		249.39	1.759	267.30	2.943	283.84	4.500	297.47	6.201	308.70	7.953
	$\text{L}_1 + \text{L}_2 + \text{V} \rightarrow \text{L}_1 + \text{L}_2$	258.25	2.289	276.04	3.703	290.49	5.276	303.99	7.182		

^a Molar fraction of carbon dioxide relative to ternary mixture.

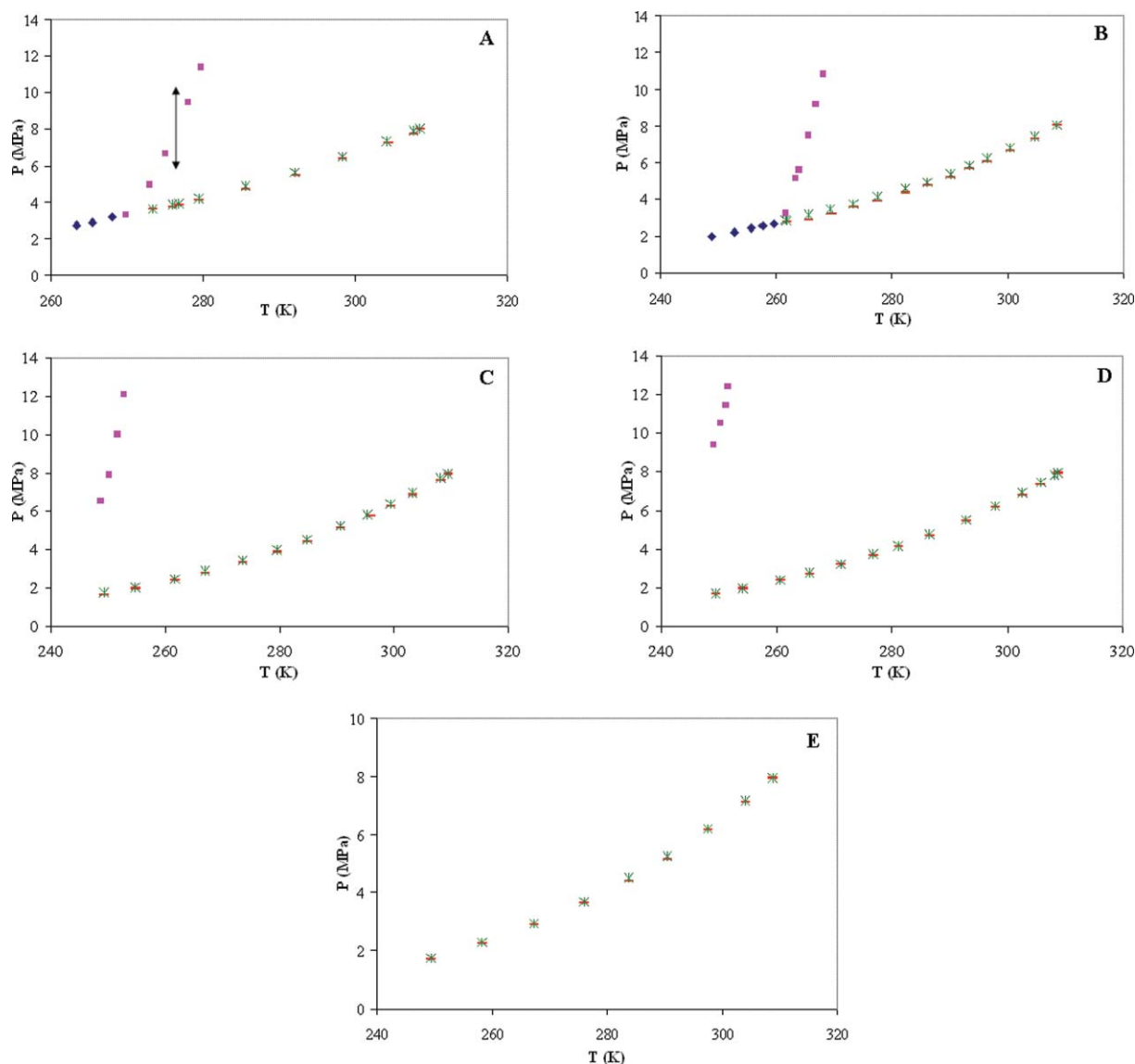


Fig. 3 Evolution of the phase boundaries in the system $\text{bmim}[\text{BF}_4] + 4\text{-isobutylacetophenone} + \text{CO}_2$. The vertical double arrow indicates where the switch in miscibility may occur. Diagrams are shown with increasing CO_2 concentration. A: 60.19 mol% CO_2 ; B: 62.38 mol% CO_2 ; C: 64.96 mol% CO_2 ; D: 65.70 mol% CO_2 and E: 66.95 mol% CO_2 . For identification of the location of the various phase regions, one is referred to Fig. 2.

the variation between the values presented in Table 1 is too small to show any trend related to the CO_2 composition. Therefore, those values are presented only as a close approximation of the critical endpoint.

The influence of carbon dioxide on the location and extension of the homogeneous liquid phase region is better visualized by representing the data from Table 1 in a 3D diagram, where pressure, temperature and CO_2 mol fractions are plotted. This diagram is depicted in Fig. 4.

In this figure, the dashed horizontal lines represent the area where the homogeneous liquid phase is found, and the circles are experimental values for the $L_1 + L_2 \rightarrow L$ phase transition. From Fig. 4 it is clear that an increase in CO_2 concentration decreases the extension of the one-phase region, and that the phase boundary is shifted to lower temperatures and higher pressures. This behavior is characteristic for the miscibility switch phenomenon, in which carbon dioxide is used to influence

the miscibility of the system. In our system, an increase in CO_2 composition caused a split in phases at constant pressure and temperature, but also a change in pressure at constant CO_2 concentration influenced the miscibility of the system.

In extraction processes, it is desirable that an increase in pressure will cause carbon dioxide to dissolve in the ionic liquid and “expel” the organic compound from the solvent mixture, creating an ionic liquid-rich phase and a lighter organic-rich phase. By comparing the phase boundaries of the three phase region measured in our system with the vapor pressure curve of pure carbon dioxide, as represented in Fig. 5, one can conclude that the less dense liquid phase is in fact a carbon dioxide-rich phase rather than organic-rich. Consequently, since ionic liquids do not dissolve in carbon dioxide, a very low solubility of the solute in the same phase explains the extremely small size of the three phase region. A higher solubility of 4-isobutylacetophenone in carbon dioxide would result in a

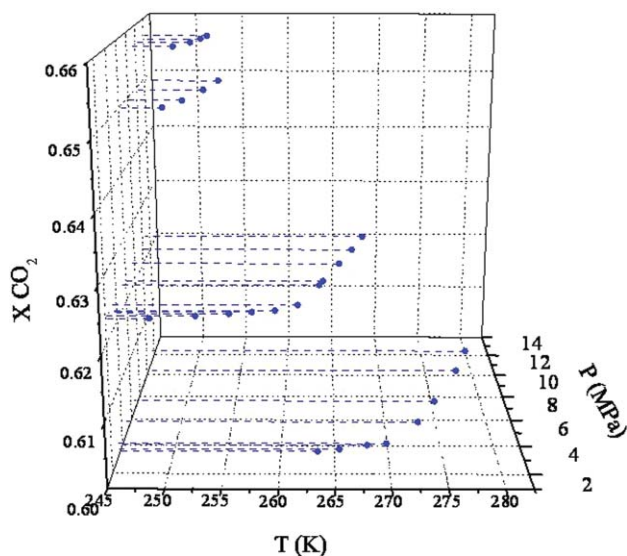


Fig. 4 Extension and location of the homogeneous liquid phase region in the ternary system $\text{bmim}[\text{BF}_4] + 4\text{-isobutylacetophenone} + \text{CO}_2$. Dots are experimental values for the $L_1+L_2 \rightarrow L$ phase transitions and the dashed lines represent the region where the homogeneous liquid phase is found.

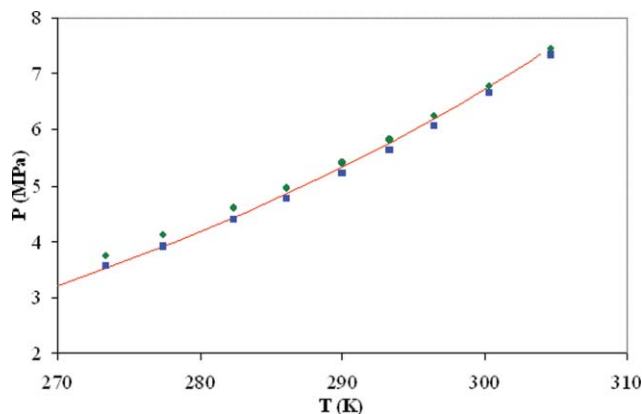


Fig. 5 Comparison between the vapor-pressure curve of pure CO_2 (continuous line) and the boundaries of the three-phase region measured in the system $\text{bmim}[\text{BF}_4] + 4\text{-isobutylacetophenone} + \text{CO}_2$ (with 66.95 mol% CO_2). Squares represent $L + V \rightarrow L_1+L_2+V$ phase transitions, and dots are $L_1+L_2+V \rightarrow L_1+L_2$ phase transitions.

more extended three-phase region, and a complete absence of solubility would cause the three-phase region to coincide with the vapor pressure curve of pure carbon dioxide in the pressure *versus* temperature diagram.

This conclusion is also supported by the proximity of the critical point of pure carbon dioxide (304.25 K and 7.3 MPa) and the experimentally critical endpoints found in our system. In summary, the three-phase region can be described as one dense ionic-liquid rich phase (with carbon dioxide and

4-isobutylacetophenone dissolved), one intermediary liquid phase rich in carbon dioxide and little 4-isobutylacetophenone dissolved, and finally, a vapor phase consisting mainly of carbon dioxide.

Conclusions

In this work the phase behavior of the ternary system $\text{bmim}[\text{BF}_4] + 4\text{-isobutylacetophenone} + \text{CO}_2$ was presented. At carbon dioxide compositions above 60 mol%, the diagram became more complex when compared with measurements performed at lower CO_2 compositions, where mostly $L+V \rightarrow L$ transitions were found. Although ternary systems may present a maximum of five co-existing phases according to the Gibbs phase rule, under our experimental conditions a maximum of three co-existing phases were found. The very narrow three-phase region is most likely composed by an intermediary liquid CO_2 -rich phase with little solute (4-isobutylacetophenone) dissolved, a denser ionic liquid-rich phase and a vapor phase composed mainly by carbon dioxide.

Additionally, the phase boundary $L_1+L_2 \rightarrow L$ was found to dramatically depend on the concentration of carbon dioxide. The homogeneous liquid phase region became smaller with increasing CO_2 composition until complete disappearance at approximately 67 mol% CO_2 .

Nevertheless, the location of the one-phase liquid region could be identified, together with the influence of CO_2 in its extension and location. The presence of the miscibility switch phenomenon in this ternary system has also been successfully demonstrated.

References

- 1 C. M. Gordon, *Appl. Catal., A*, 2001, **222**, 101; S. A. Forsyth, H. Q. Nimal Gunaratne, C. Hardacre, A. McKeown and D. W. Rooney, *Org. Process Res. Dev.*, 2006, **10**(1), 94; P. Lozano, T. de Diego, D. Carrié, M. Vaultier and J. L. Iborra, *Chem. Commun.*, 2002, **7**, 692; R. D. Rogers and K. R. Seddon, *Science*, 2003, **302**, 792.
- 2 A. Shariati, K. Gutkowski and C. J. Peters, *AIChE J.*, 2005, **51**(5), 1532; S. N. V. K. Aki, B. R. Mellein, E. M. Saurer and J. F. Brennecke, *J. Phys. Chem. B*, 2004, **108**, 20355; M. F. Jacquemin, Costa Gomes, P. Husson and V. Majer, *J. Chem. Thermodyn.*, 2006, **38**(4), 490; D. Camper, P. Scovazzo, C. Koval and R. Noble, *Ind. Eng. Chem. Res.*, 2004, **43**, 3049.
- 3 C. J. Peters and K. Gauter, *Chem. Rev.*, 1999, **99**, 419; K. Gauter, C. J. Peters, A. L. Scheidgen and G. M. Schneider, *Fluid Phase Equilib.*, 2000, **171**, 127.
- 4 A. M. Scurto, S. N. V. K. Aki and J. F. Brennecke, *J. Am. Chem. Soc.*, 2002, **124**(35), 10276.
- 5 A. M. Scurto, S. N. V. K. Aki and J. F. Brennecke, *Chem. Commun.*, 2003, **5**, 572.
- 6 L. A. Blanchard, Z. Gu and J. F. Brennecke, *J. Phys. Chem. B*, 2001, **105**(12), 2437.
- 7 E. Kühne, E. Perez, G. J. Witkamp and C. J. Peters, *J. Supercrit. Fluids*, 2008, **45**, 27; E. Kühne, E. Saez Calvo, G. J. Witkamp and C. J. Peters, *J. Supercrit. Fluids*, 2008, **45**, 293.
- 8 E. Kühne, S. Santarossa, G. J. Witkamp and C. J. Peters, *Green Chem.*, 2008, **10**, 762.
- 9 E. Kühne, C. J. Peters, J. van Spronsen and G. J. Witkamp, *Green Chem.*, 2006, **8**, 287.

One-pot green synthesis of propylene oxide using *in situ* generated hydrogen peroxide in carbon dioxide

Qunlai Chen and Eric J. Beckman*

Received 5th March 2008, Accepted 27th June 2008

First published as an Advance Article on the web 31st July 2008

DOI: 10.1039/b803847c

In the one-pot green synthesis of propylene oxide using *in situ* generated hydrogen peroxide, a propylene oxide yield of 23% with 82% selectivity was achieved over a (0.2%Pd + 0.02%Pt)/TS-1 catalyst by using compressed (supercritical or liquid) carbon dioxide as the solvent and small amounts of water and methanol as co-solvents. The addition of an inhibitor effectively suppressed a number of common side-reactions, including the hydrogenation of propylene, the hydrolysis of propylene oxide and the reaction between propylene oxide and methanol. This suppression effect is due to the interaction between the inhibitor and TS-1 leading to the neutralization of its surface acidity.

Introduction

Propylene oxide (PO), an important bulk chemical with a global annual capacity of 7 million metric tons,¹ is currently produced by two methods,² namely the chlorohydrin and hydroperoxide processes. In the chlorohydrin process, propylene is reacted with chlorine, water and a base to generate PO and stoichiometric amounts of salt waste. The hydroperoxide process uses either *tert*-butyl or ethylbenzene hydroperoxides as the oxidant to epoxidize propylene, and co-produces *tert*-butanol or styrene as a result. In order to avoid the generation of waste and co-products (3–4 pounds of *tert*-butanol or 2.4 pounds of styrene/pound of propylene oxide³), extensive studies^{2–4} have been conducted to find means by which to use hydrogen peroxide (H₂O₂), a “greener” oxidant. The drive to replace the use of chlorine and hydroperoxides increased significantly after the discovery of the selective oxidation catalyst titanium silicalite (TS-1) in the 1980s.⁵

TS-1 is a ZSM-5 type molecular sieve with an MFI structure in which small numbers of tetrahedral Si atoms are substituted by Ti atoms in an otherwise purely siliceous framework. TS-1 catalyzes the selective oxidation of various organic compounds by aqueous H₂O₂, especially the epoxidation of lower olefins. Experimental results³ have shown an almost quantitative yield of PO (from propylene) under mild reaction conditions using a dilute methanol solution of H₂O₂. Recently, Dow and BASF¹ announced the construction of the first commercial PO plant using pre-manufactured H₂O₂ to epoxidize propylene. Nevertheless, there are several issues associated with using pre-manufactured H₂O₂. As described in our earlier study,⁶ the current industrial method for producing H₂O₂, the anthraquinone auto-oxidation (AO) process, is not as green as one would prefer due to the generation of wastes, use of large volumes of organic solvents, low efficiency and high energy consumption.

More seriously, the production of major raw materials [2-alkylanthraquinone, trioctylphosphate (TOP) and tetrabutyl urea (TBU)] used in the AO process uses toxic chemicals and generates various wastes. For example, the production of 1 pound of 2-ethylanthraquinone will consume about 2 pounds of aluminium chloride anhydride and 4–5 pounds of oleum (20% in SO₃) and generates tens of pounds of wastewater (containing AlCl₃, H₂SO₄ and various organics). The production of TOP uses phosphorus oxychloride and generates hydrogen chloride (HCl) as waste. The production of TBU uses phosgene⁷ and also generates HCl. Therefore, using pre-manufactured H₂O₂ to produce PO would mean the shift of environmental and human health burden from the manufacture of PO (by either the chlorohydrin or hydroperoxide processes) to the production of H₂O₂ and the raw materials used in the AO process.

From both environmental and economic points of view, it is attractive to use *in situ* generated H₂O₂ (synthesized from O₂ and H₂) to replace pre-manufactured H₂O₂ and hence this route has been investigated extensively over the past decade.^{8–11} Here, precious metal (Pd, Pt, Au or their combination) loaded on a “support” functions as the catalyst for the *in situ* generation of H₂O₂ from O₂ and H₂, while the “support”, usually TS-1, catalyzes the epoxidation of propylene. Typically methanol or a mixture of methanol and water is used because, as proposed by Clerici *et al.*,¹² methanol could interact with the active site of TS-1 to enhance the selectivity of epoxidation. Propylene conversion is usually limited to less than 10% in order to achieve PO selectivities sufficient to merit further work. For example, recent results given by Chowdhury *et al.*¹¹ showed *ca.* 7% propylene conversion and *ca.* 90% PO selectivity with a PO production rate of 0.064–0.08 g h⁻¹ (g cat)⁻¹ when trimethylamine was used as a promoter. Attempts to increase propylene conversion usually led to a considerable decrease in PO selectivity due to the hydrogenation of propylene and other side-reactions. Laufer and Hoelderich¹³ reported that at a propylene conversion of 21%, the PO selectivity was only 71% in a semi-batch reactor.

We previously proved that compressed (supercritical or liquid) carbon dioxide is an effective solvent for the direct synthesis of

Department of Chemical & Petroleum Engineering, University of Pittsburgh, Pittsburgh, PA, 15261, USA.
E-mail: beckman@engr.pitt.edu; Fax: +1-412-624-7820;
Tel: +1-412-624-4828

H₂O₂ from O₂ and H₂.⁶ In this study, we use this *in situ* generated H₂O₂ in CO₂ to epoxidize propylene for a one-pot green synthesis of PO. Besides the advantages mentioned in our previous study, using compressed CO₂ as the solvent has special benefit over conventional solvents in that O₂, H₂, propylene and CO₂ will form a homogeneous single phase under reaction conditions. This will significantly reduce or even eliminate mass transfer resistance during the epoxidation of propylene. By adding small amounts of polar solvents to compressed CO₂ and using a selected inhibitor to suppress common side-reactions during the epoxidation of propylene, we experimentally proved that propylene oxide could be effectively synthesized using *in situ* generated H₂O₂ in compressed CO₂.

Results and discussion

Catalyst characterization

The catalytic activity of TS-1 is due to the incorporation of Ti atoms into the framework of silicalite, which is characterized by a fingerprint band at 960 cm⁻¹ in its FT-IR spectrum. The FT-IR spectra of TS-1 and (0.2%Pd + 0.02%Pt)/TS-1 are shown in Fig. 1 (the FT-IR spectrum of mineral oil used in sample preparation is also shown as a reference). It can be seen that there was no change in the fingerprint bands of TS-1 after the impregnation of precious metals, suggesting that the effect of impregnating Pd and Pt on the functional groups of TS-1 was negligible.

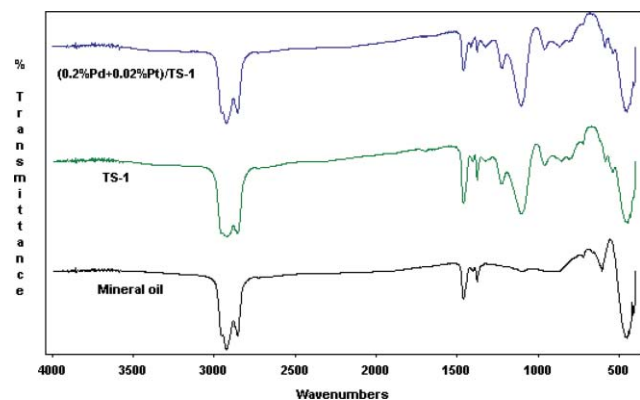


Fig. 1 FT-IR spectra of TS-1 and (0.2%Pd + 0.02%Pt)/TS-1.

The XRD spectra of TS-1 and (0.2%Pd + 0.02%Pt)/TS-1 are presented in Fig. 2. It can be seen that (0.2%Pd + 0.02%Pt)/TS-1 maintains all of the “fingerprint” peaks of a TS-1 molecular sieve as provided previously by Taramasso *et al.*⁵ Similar XRD patterns for TS-1 and precious metal loaded TS-1 suggest that the MFI crystal structure of TS-1 did not change appreciably as a result of impregnation with precious metal. The crystallinities of TS-1 and (0.2%Pd + 0.02%Pt)/TS-1 were calculated according to the equation given by Szostak¹⁴ using the intensity of five strong reflections ($2\theta = 7.99^\circ, 8.91^\circ, 23.21^\circ, 24.01^\circ, 24.47^\circ$)^{5,15} and two other fingerprint peaks ($2\theta = 29.33^\circ, 30.07^\circ$) of TS-1.⁵ The change in degree of crystallinity of TS-1 after impregnation was less than 5%, again suggesting that the effect of impregnation on the crystallinity of TS-1 was relatively minor.

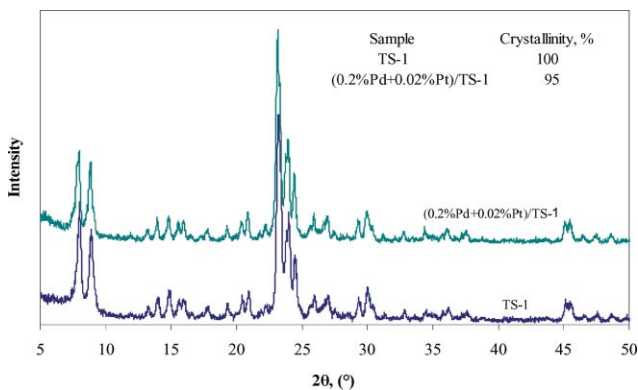


Fig. 2 XRD spectra of TS-1 and (0.2%Pd + 0.02%Pt)/TS-1.

One-pot green synthesis of PO using *in situ* generated H₂O₂ in CO₂

Using CO₂ as the sole solvent, Danciu *et al.*¹⁰ in our research group found that attempts to increase propylene conversion resulted in a substantial decrease in PO selectivity. For example, when propylene conversion was increased from 7.5% to 9.5%, the PO selectivity decreased considerably from 94.3% to 77.1%. CO₂ is an environmentally benign solvent, but it is also a feeble one, as indicated by a low dielectric constant.¹⁶ As such, addition of a small amount of polar co-solvent can enhance CO₂'s solvent strength significantly. In this study, we examined the effect of adding a small amount of polar co-solvent (water, methanol or their combination) to compressed CO₂ on the direct synthesis of PO. The catalyst used in this study was (0.2%Pd + 0.02%Pt)/TS-1, an effective catalyst in carrying out the direct synthesis of H₂O₂ from O₂ and H₂ in compressed CO₂.⁶ The experimental results are listed as entries 1–3 in Table 1: when water, methanol and their mixture were used as the co-solvent, hydrogenation of propylene to propane became the dominant reaction at higher propylene conversion. Although the addition of methanol enhanced the formation of PO (in agreement with the observations of Clerici *et al.*),³ it also led to side-reactions between generated PO and methanol to form methoxypropanols (MP). Further, the presence of water caused the hydrolysis of PO to form propylene glycols (PG). It is known² that acidic conditions favour the hydrolysis of PO and also the reaction between PO and methanol. Considering the existence of surface acidity in TS-1,^{17,18} we hypothesized that this surface acidity contributed to promoting these side-reactions. In order to verify this hypothesis, ammonium acetate (pH value of the mixture of ammonium acetate, water and methanol in this study was 7.6 at room temperature) was added to the reactor as an inhibitor; the experimental results are given as entries 4–6 in Table 1. We observed that addition of ammonium acetate could significantly inhibit not only the hydrolysis of PO and the reaction between PO and methanol, but also the hydrogenation of propylene, especially when small amounts of methanol and water were used as the co-solvent in compressed CO₂. Comparing entries 3 and 6, it can be seen that the addition of ammonium acetate led to the increase of PO yield from 9.4% to 23.5% and a significant increase in PO selectivity (from 21.7% to 81.8%); while the propane, MP and PG selectivities all decreased considerably. The PO production rate for entry 6 reached 0.343 g h⁻¹ (g cat)⁻¹ due

Table 1 Experimental results for the one-pot green synthesis of PO using *in situ* generated H₂O₂ in CO₂^a

Entry		1	2	3	4	5	6
Water/ml		0.25	—	0.25	0.25	—	0.25
Methanol/ml		—	0.25	0.25	—	0.25	0.25
NH ₄ COOCH ₃ /g		—	—	—	0.02	0.02	0.02
C ₃ H ₆ conv. (%)		22.8	54.9	43.1	16.0	27.3	28.7
PO yield (%)		1.7	10.4	9.4	10.0	20.3	23.5
Selectivity (%)	PO	7.6	18.9	21.7	62.7	74.6	81.8
	C ₃ H ₈	75.3	75.2	54.5	26.3	13.5	10.4
	MP	0	3.7	9.2	0	6.3	2.5
	PG	15.3	0.4	13.1	4.6	3.7	2.9
	Others	1.8	1.8	1.6	6.4	1.8	2.4

^a Other experimental conditions: (0.2%Pd + 0.02%Pt)/TS-1 = 0.05 g; C₃H₆ = 6.3 mmol, H₂/C₃H₆ = 1, O₂/H₂ = 1; T = 60 °C, P = 125 bar, reaction time = 5 h.

to the effective generation of H₂O₂ from O₂ and H₂ in CO₂⁶ and the likely decrease (or elimination) of mass transfer resistances.

Since the surface acidity of TS-1 is relatively weak, we believed that the selected inhibitor (ammonium acetate) could effectively interact with TS-1 and neutralize its surface acidity, and therefore, suppress side-reactions. In order to verify this hypothesis, a series of experiments was conducted using inhibitors with different pH values: ammonium trifluoroacetate (pH = 6.4) and ammonium carbonate (pH = 9.7). Experimental results and their comparison with ammonium acetate are given in Fig. 3. The addition of ammonium trifluoroacetate provided an acidic environment for the catalyst and could not neutralize the surface acidity of TS-1, and therefore, led to a substantial decrease in PO selectivity (although the conversion of propylene increased due to the enhancement of the hydrogenation of propylene and the hydrolysis of generated PO). The addition of ammonium carbonate provided a relatively stronger basic environment for the catalyst. As expected, a strong suppression effect was observed for all side-reactions. However, due to the relatively higher pH value (relatively stronger basic conditions can also cause the hydrolysis of PO),² the PO selectivity was lower than that when ammonium acetate (pH = 7.6) was used.

The second set of experiments used weak base inhibitors: Amberlyst A-21 (a weakly basic, macroreticular ion exchange resin with alkyl amine functionality), sodium acetate and sodium bicarbonate. The experimental results are shown in Table 2. Although Amberlyst A-21 is a weak base, it is bonded to the macroreticular structure of the ion exchange resin. As such, it

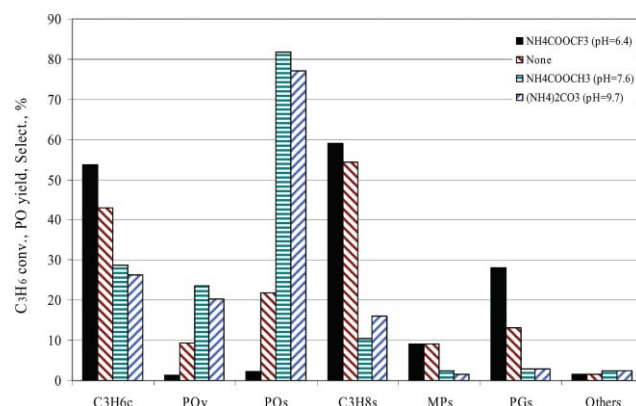


Fig. 3 Experimental results using inhibitors with different pH values on the green synthesis of PO using *in situ* generated H₂O₂ in CO₂ (low case “c” stands for conversion, “y” for yield and “s” for selectivity). Experimental conditions: (0.2%Pd + 0.02%Pt)/TS-1 = 0.05 g; water = 0.25 ml, methanol = 0.25 ml, inhibitor = 0.02 g; C₃H₆ = 6.3 mmol, H₂/C₃H₆ = 1, O₂/H₂ = 1; T = 60 °C, P = 125 bar, reaction time = 5 h.

clearly could not enter into the channels of TS-1 and interact with the surface acidity of TS-1. Therefore, no suppression effect was observed. Further increases to the amount of Amberlyst A-21 employed had no influence on the suppression of side reactions.

Surprisingly, when sodium acetate and sodium bicarbonate were used as the inhibitor, the PO yield and selectivity were low. One possible reason is that sodium ions could be strongly adsorbed onto the surface of TS-1's channels and could therefore

Table 2 Experimental results using inhibitors with different adsorption abilities on TS-1 for the green synthesis of PO using *in situ* generated H₂O₂ in CO₂^a

Inhibitor	Amberlyst A-21			NaCOOCH ₃		NaHCO ₃		
Amount/g	0.02	0.1	0.25	0.005	0.02	0.005	0.02	
C ₃ H ₆ conv. (%)	47.1	44.3	47.3	29.0	8.7	31.2	16.5	
PO yield (%)	10.2	11.6	8.2	8.2	4.6	6.7	4.0	
Selectivity (%)	PO	21.7	26.3	17.4	28.4	53.2	21.5	24.2
	C ₃ H ₈	68.9	67.5	78.9	67.4	35.1	75.4	69.2
	MP	5.3	3.9	2.0	2.2	0.0	1.7	3.1
	PG	3.6	1.9	1.2	1.5	9.3	0.8	2.3
	Others	0.5	0.4	0.4	0.3	2.4	0.7	1.2

^a Other experimental conditions: (0.2%Pd + 0.02%Pt)/TS-1 = 0.05 g; water = 0.25 ml, methanol = 0.25 ml; C₃H₆ = 6.3 mmol, H₂/C₃H₆ = 1, O₂/H₂ = 1; T = 60 °C, P = 125 bar, reaction time = 5 h.

block the adsorption of methanol, leading to the decrease in PO yield and selectivity. When examining the role of sodium ions as adsorption sites in silicalite-1, Matsumura *et al.*¹⁹ found a similar phenomenon in that the sodium ions located on the surface of the channels of silicalite-1 could block the adsorption of ethanol at its surface. Further increases to the amount of sodium ions led to a dramatic decrease in propylene conversion and PO yield, again possibly due to further blocking of TS-1's active sites. When using pre-manufactured H₂O₂ to epoxidize propylene, Li *et al.*²⁰ observed that small amounts of sodium salt enhanced the synthesis of PO, but excessive amounts poisoned the TS-1 catalyst. Hancu²¹ found that the presence of sodium ions had a negative impact on the direct synthesis of PO using a mixture of O₂ and H₂, consistent with the observations of this study.

In summary, to effectively suppress the side-reactions occurring during the synthesis of PO using *in situ* generated H₂O₂ from O₂ and H₂ in compressed CO₂, the selected inhibitor should be able to interact with TS-1 to neutralize its surface acidity, but the selected inhibitor should not be so strongly adsorbed on the surface of TS-1 so as to block the adsorption of methanol.

The effect of the amount of selected inhibitor (ammonium acetate in the range of 0.005 to 0.03 g) was also examined and the results are shown in Fig. 4. We can conclude that, in the range of this study, although the effect of the amount of inhibitor on the propylene conversion was minor, PO yield increased somewhat with the increase of the amount of inhibitor up to 0.02 g. Accordingly, we observed the increase in PO selectivity and the decrease in propane selectivity. The influence on the selectivities of MP, PG and others was not significant.

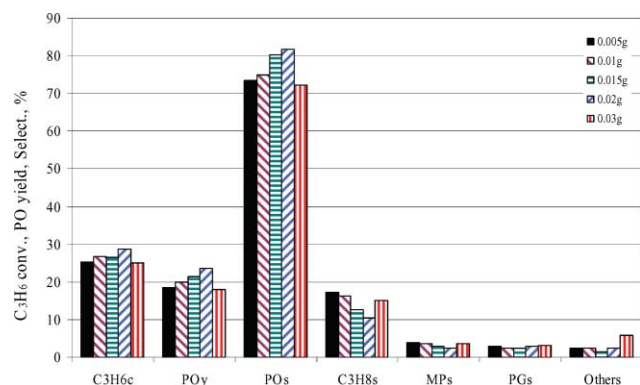


Fig. 4 Effect of the amounts of ammonium acetate on the green synthesis of PO using *in situ* generated H₂O₂ in CO₂. *Experimental conditions:* (0.2%Pd + 0.02%Pt)/TS-1 = 0.05 g; water = 0.25 ml, methanol = 0.25 ml; C₃H₆ = 6.3 mmol, H₂/C₃H₆ = 1, O₂/H₂ = 1; T = 60 °C, P = 125 bar, reaction time = 5 h.

The effect of reaction temperature on the green synthesis of PO using *in situ* generated H₂O₂ in CO₂ was investigated by maintaining constant amounts of reactants, CO₂ and co-solvents. It should be pointed out that, with a change of reaction temperature, reaction pressure will change accordingly. The corresponding pressures and experimental results under different reaction temperatures are listed in Table 3. As can be seen from Table 3, an increase in reaction temperature resulted in a considerable increase in propylene conversion and PO yield. For example, when reaction temperature was increased

Table 3 Effect of reaction temperature on the green synthesis of PO using *in situ* generated H₂O₂ in CO₂^a

Temperature/°C	40	50	60
Pressure/bar	100.5	113.1	125.0
C ₃ H ₆ conv. (%)	14.1	16.0	28.7
PO yield (%)	10.8	13.1	23.5
Selectivity (%)			
PO	77.0	81.5	81.8
C ₃ H ₈	9.2	10.6	10.4
MP	4.5	2.4	2.5
PG	6.1	1.9	2.9
Others	3.2	3.5	2.4

^a Other experimental conditions: (0.2%Pd + 0.02%Pt)/TS-1 = 0.05 g; water = 0.25 ml, methanol = 0.25 ml, NH₄COOCH₃ = 0.02 g; C₃H₆ = 6.3 mmol, H₂/C₃H₆ = 1, O₂/H₂ = 1; reaction time = 5 h.

from 50 °C to 60 °C, propylene conversion and PO yield almost doubled. When conducting the gas phase epoxidation of propylene over Au/TS-1, Taylor *et al.*²² also observed that temperature had strong effect on the production rate of PO. PO selectivity in this study also increased slightly with the increase of reaction temperature. The selectivity to by-products (PM and PG) were higher at lower temperature, implying that the hydrolysis of generated PO and the reaction between generated PO and methanol occurred more easily at lower temperature.

The effect of reaction time on the epoxidation of propylene using *in situ* generated H₂O₂ in compressed CO₂ with methanol and water as the co-solvent is shown in Fig. 5. It can be seen that propylene conversion, PO yield and selectivity were all increased with the increase of reaction time up to 5 hours, while by-product propane selectivity was decreased along with the increase of reaction time. After 5 hours, there were no significant changes in propylene conversion, PO yield and selectivity because of the insignificant generation of H₂O₂ after 5 hours. The reason⁶ is that, in 5 hours, most H₂ inside the reactor was consumed by the *in situ* generation of H₂O₂ (consumed immediately by the epoxidation of propylene) and associated side-reactions. Therefore, the concentration of H₂ in the reactor decreased significantly, which could lead to the further substantial decrease in H₂O₂ selectivity.

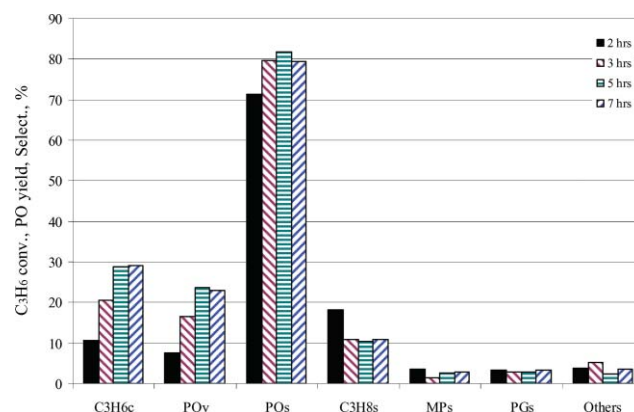


Fig. 5 Effect of reaction time on the green synthesis of PO using *in situ* generated H₂O₂ in CO₂. *Experimental conditions:* (0.2%Pd + 0.02%Pt)/TS-1 = 0.05 g; water = 0.25 ml, methanol = 0.25 ml, NH₄COOCH₃ = 0.02 g; C₃H₆ = 6.3 mmol, H₂/C₃H₆ = 1, O₂/H₂ = 1; T = 60 °C, P = 125 bar.

Experimental

TS-1 was obtained from the Lyondell Chemical Company. The preparation method of (0.2%Pd + 0.02%Pt)/TS-1 was as given by Chen and Beckman.⁶ FT-IR spectra of TS-1 and (0.2%Pd + 0.02%Pt)/TS-1 were recorded on a Genesis II FT-IR Spectrometer (Mattson Instruments, Wisconsin, USA) using a Nujol Mull technique for the sample preparation. X-Ray diffraction (XRD) patterns of TS-1 and (0.2%Pd + 0.02%Pt)/TS-1 were recorded on a Philips X'Pert PW3710 X-ray diffractometer using a Cu-K α radiation source ($\lambda = 1.54056 \text{ \AA}$). Bragg angles (2θ) between 5° and 50° were scanned with a step size of 0.02° .

The experiments for the one-pot green synthesis of PO were carried out in a 30 ml stainless steel high pressure reactor manufactured at the University of Pittsburgh. A glass liner was placed inside the reactor to prevent the possible decomposition of *in situ* generated H₂O₂ by the metal walls. The passivation method for the reactor and liner was the same as that given by Chen and Beckman.⁶ A Teflon-coated stir bar was placed inside the glass liner to keep the reactants mixing well. Known amounts of catalyst, inhibitor and co-solvent were then added to the reactor, followed by the addition of known amounts of propylene, oxygen, hydrogen, and carbon dioxide. The final pressure was adjusted to the desired value by adding more carbon dioxide. The reaction temperature was achieved using a stirrer/hotplate and monitored *via* a thermocouple inside the reactor. A pressure relief valve was installed for safety. Experiments were allowed to run for 2 to 7 hours and the amount of generated PO, propane and un-reacted propylene were analyzed using an online 5890A Series II gas chromatography (GC) equipped with a TCD detector and HayeSep D packed column (20 ft \times 1/8") and controlled by a HP ChemStation. The reactor was then ice-cooled down to 0–5 °C and its pressure was slowly released by venting the gas mixture through an acetone solution. This acetone solution was then used to extract any organics remaining inside the reactor and analyzed by another 5890A Series II GC equipped with a DB-1 capillary column (30 m \times 0.253 mm \times 0.50 μm) to determine the quantity of MP, PG and other by-products.

Conclusions

According to our experimental results, compressed carbon dioxide can be used as an environmentally benign solvent in the one-pot green synthesis of PO using *in situ* generated H₂O₂ from O₂ and H₂ over (0.2%Pd + 0.02%Pt)/TS-1. For the first time, a PO yield over 20% with an 80%+ selectivity was achieved by using small amounts of polar co-solvents (methanol and water) and adding an inhibitor (ammonium acetate) to suppress side-reactions (the hydrogenation of propylene, the hydrolysis of generated PO and the reaction between PO and methanol).

The experimental results using different inhibitors verified that this suppression effect was due to an interaction between the inhibitor and TS-1 leading to the neutralization of its surface acidity. The selected inhibitor should be able to interact with TS-1 to neutralize its surface acidity, but this interaction should not be strong enough to block the adsorption of methanol. Reaction temperature had strong effect on propylene conversion and PO yield in the range of 40 °C to 60 °C: increasing reaction temperature resulted in an increase in both propylene conversion and PO yield.

Acknowledgements

The authors gratefully acknowledge the US Environmental Protection Agency (EPA) for its grant R831533. We also want to thank the staff and faculty associated with the Materials Micro-Characterization Laboratory of the Department of Mechanical Engineering and Material Science at the University of Pittsburgh for assistance with the X-ray diffraction conducted during this study.

References

- 1 A. H. Tullo and P. L. Short, *Chem. Eng. News*, 2006, **84**(41), 22–23.
- 2 Propylene oxide in *Kirk-Othmer Encyclopedia of Chemical Technology*, ed, D. L. Trent, John Wiley & Sons, Inc., Hoboken, NJ, 2001.
- 3 M. G. Clerici, G. Bellussi and U. Romano, *J. Catal.*, 1991, **129**, 159–167.
- 4 G. F. Thiele and E. Roland, *J. Mol. Catal. A: Chem.*, 1997, **117**, 351–356.
- 5 M. Taramasso, G. Perego and B. Notari, *US Pat.* 4 410 501, 1983.
- 6 Q. Chen and E. J. Beckman, *Green Chem.*, 2007, **9**, 802–808.
- 7 J. Henkelmann, T. Weber, T. Rohde and R. Busch, *US Pat.* 7 053 244, 2006.
- 8 R. Meiers, U. Dingerdissen and W. F. Holderich, *J. Catal.*, 1998, **176**, 376–386.
- 9 G. Jenzer, T. Mallat, M. Maciejewski, F. Eigenmann and A. Baiker, *Appl. Catal., A*, 2001, **208**, 125–133.
- 10 T. Danciu, E. J. Beckman, D. Hancu, R. N. Cochran, R. Grey, D. M. Hajnik and J. Jewson, *Angew. Chem., Int. Ed.*, 2003, **42**, 1140–1142.
- 11 B. Chowdhury, J. J. Bravo-Suarez, M. Date, S. Tsubota and M. Haruta, *Angew. Chem., Int. Ed.*, 2006, **45**, 412–415.
- 12 M. G. Clerici and P. Ingallina, *J. Catal.*, 1993, **140**, 71–83.
- 13 W. Laufer and W. F. Hoelderich, *Appl. Catal., A*, 2001, **213**, 163–171.
- 14 R. Szostak, *Molecular Sieves Principles of Synthesis and Identification*, Van Nostrand Reinhold, New York, 1989, p. 290.
- 15 C. T. Wu, Y. Q. Wang, Z. T. Mi, L. Xue, W. Wei, E. Z. Min, S. Han, F. He and S. B. Fu, *React. Kinet. Catal. Lett.*, 2002, **77**, 73–81.
- 16 E. J. Beckman, *J. Supercrit. Fluids*, 2004, **28**, 121–191.
- 17 J. Q. Zhuang, Z. M. Yan, X. M. Liu, X. C. Liu, X. W. Han, X. H. Bao and U. Mueller, *Catal. Lett.*, 2002, **83**, 87–91.
- 18 R. S. Drago, S. C. Dias, J. M. McGilvray and A. Mateus, *J. Phys. Chem. B*, 1998, **102**, 1508–1514.
- 19 Y. Matsumura, K. Hashimoto, H. Kobayashi and S. Yoshida, *J. Chem. Soc., Faraday Trans.*, 1990, **86**, 561–565.
- 20 G. Li, X. Wang, H. Yan, Y. Chen and Q. Su, *Appl. Catal., A*, 2001, **218**, 31–38.
- 21 D. Hancu, *US Pat.* 6 399 794 B1, 2002.
- 22 B. Taylor, J. Lauterbach, G. E. Blau and W. N. Delgass, *J. Catal.*, 2006, **242**, 142–152.

Aqueous system for the improved hydrogenation of phenol and its derivatives

Yizhi Xiang, Lei Ma, Chunshan Lu, Qunfeng Zhang and Xiaonian Li*

Received 25th February 2008, Accepted 10th June 2008

First published as an Advance Article on the web 23rd July 2007

DOI: 10.1039/b803217c

The hydrogenation of phenol to cyclohexanol under mild conditions (~340 K) was achieved over Raney Ni catalyst in the aqueous phase. The adsorption–desorption properties of the reactants (phenol and H₂) and the products (cyclohexanone and cyclohexanol) on the Raney Ni catalyst are different in the aqueous phase and the organic phase. The hydrogenation rate of phenol is improved because the Raney Ni catalyst adsorbs more H₂ and phenol in water than in methanol. Meanwhile, the higher uptakes of H₂ and the lower desorption rates for cyclohexanone on the Raney Ni catalyst in the aqueous system result in the further hydrogenation of cyclohexanone to cyclohexanol.

Introduction

Catalytic hydrogenation of phenol is of commercial and environmental significance for the synthesis of cyclohexanone and cyclohexanol (KA oil) as the intermediate for Nylon 6 and 66.¹ On the other hand, phenol is an established environmental toxin. Therefore, hydrogenation of phenol for cyclohexanone and cyclohexanol is an important chemical process, and has been extensively studied.^{2–8} Generally the hydrogenation of phenol is mainly carried out in vapor phase using methanol, ethanol, cyclohexane *etc.*, volatile organic compounds (VOCs) as the solvent.^{2–4} Hydrogenation of phenol and cresol in supercritical carbon dioxide (scCO₂) has also been proposed recently,⁹ but it needs high H₂ and CO₂ pressure of 10 and 12 MPa. Hardly any work has been reported for the hydrogenation of phenol in the aqueous phase,¹⁰ through which the use of organic solvent could be eliminated. Water, as a replacement for more conventional organic solvents, has been extensively investigated recently, and been identified as a 'green' solvent.^{11–13} However, the solubility should be the key consideration when using water as the solvent for organic reactions. For hydrophilic organics, the separation of products from the solvents is critical, because the heat for the vaporization of water is higher than many other liquids. For hydrophobic organics, the products could be separated naturally from water,¹⁴ but the reaction rates is always limited due to the insolubility of organics in water.¹⁵

Currently, aqueous biphasic system for the homogeneous catalytic reaction process has been extensively studied,^{15–20} in which the separation and recovery of the catalyst could be simplified (*via* phase separation technique), but organic solvents are still used in the most cases, and the separation of products from the solvent is still critical. Jessop *et al.*²¹ have recently reported that a reversible nonpolar-to-polar solvent (smart solvent) should facilitate organic syntheses and separations by eliminating the need to remove and replace solvents after

each reaction or separation steps. In the present paper, an aqueous reaction system for the hydrogenation of phenol and its derivatives has been proposed, in which the complete aqueous solubility of the reactant (phenol) is achieved by temperature increase. On the other hand, the separation of the products from water is simplified by their low aqueous solubility. The sketch of mechanism for the aqueous system for the hydrogenation of phenol is shown in Fig. 1.

In the phenol hydrogenation reaction aqueous system, the reactant (phenol) is completely aqueous soluble at temperatures higher than 339 K, although it is aqueous insoluble at the room temperature (0.17 g_{phenol}/100 mL_{water}). The hydrogenation rate of phenol could not be limited by the solubility of phenol into water, because the hydrogenation reactions of phenol are always carried out at temperatures higher than 339 K.^{5–8} The products cyclohexanone or cyclohexanol are only slightly soluble in water (5 g_{cyclohexanone}/100 mL_{water} and 4.3 g_{cyclohexanol}/100 mL_{water}), which facilitates their separation from the aqueous phase. Furthermore, the Raney Ni catalyst adsorbs more H₂ and phenol in water than in methanol, while the desorption rates of cyclohexanone and cyclohexanol in methanol are higher than those in water (Table 1, and Fig. 3 and 4). The different adsorption–desorption properties of reactants and products on the catalyst in various solvents implies that organic reactions carried out in water might potentially increase the reaction rate and change the product selectivity.²²

Experimental

Catalyst preparation

The Raney Ni catalyst was prepared from metallic alloy powders of Ni and Al with a mass ratio of 9 : 11. The details of the processes are as follows: Ni–Al metallic alloy powders were slowly impregnated with 20% NaOH aqueous solution, while temperature was elevated from room temperature to 353 K, and then held at that temperature for 2–3 h to leach Al until the content of Al was less than 6 wt%. Subsequently, the sample was washed with distilled water at 343–353 K until the pH value

Resources & Environmental Catalysis Institute of Zhejiang University of Technology, State Key Laboratory Breeding Base of Green Chemistry Synthesis Technology, Hangzhou, 310032, P. R. China. E-mail: xnli@zjut.edu.cn; Fax: +86 571-88320409; Tel: +86 571-88320409

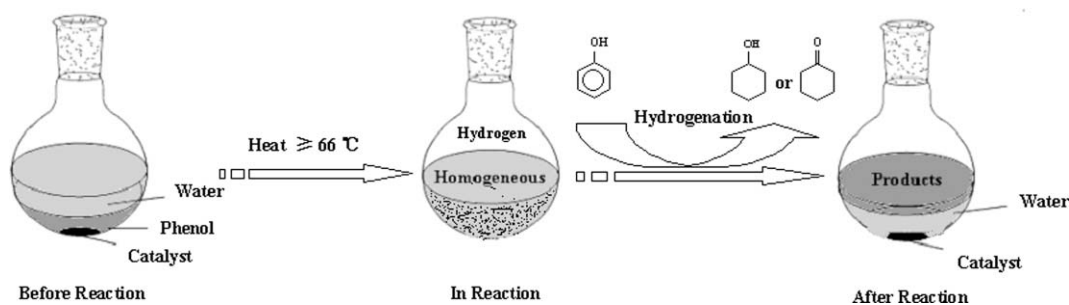


Fig. 1 Sketch of the mechanism for the aqueous reaction system for the hydrogenation of phenol.

reached at about 7–8. The obtained catalyst was reserved in water to avoid the oxidation of Ni by the air.

Hydrogenation study

Hydrogenation of phenol in water or methanol (AR/99.5%, Quzhou Juhua Reagents Co. Ltd.) solvent was carried out in a 200 mL stainless steel autoclave (Weihai Automatically-controlled Reaction Kettle Co. Ltd.). Appropriate amount of phenol (AR/99.5%, Hangzhou Shuanglin Chemical Reagents Factory), water and Raney Ni catalyst were added into the reactor together. The reactor system was then purged with N_2 (99.999%) three times followed by H_2 (99.999%) three times; subsequently, the autoclave was heated up to the required temperature and finally pressurized at the selected set point of H_2 . During the experiment, the stirring rate was fixed at 800 rpm. The products were separated from water by phase separation technique: firstly, the catalysts were removed from the liquid by filtration, the obtained liquid phase was then transferred to a separatory funnel, the aqueous phase was collected for circulation. The organic phase was collected and analysed by an instrument of Agilent-6890-GC-5973-MS equipped with 30mHP-5 capillary with the external standard method.

Adsorption and desorption study

The adsorption of phenol and the desorption of cyclohexanone and cyclohexanol on the Raney Ni catalyst in water and methanol, respectively, were determined according to the follows: Cyclohexanone (AR/99.5%, Quzhou Juhua Reagents Co. Ltd.) and cyclohexanol (CR/98%, Shanghai Linfeng Chemical Reagents Factory) were pre-adsorbed on the catalyst by intensively stirring of the Raney Ni in cyclohexanone or

cyclohexanol for 30min. Then the catalyst was filtrated, and dried in air at 373 K for 2 h. After that, 1 g of the pretreated catalyst, and 100 mL water or methanol were loaded together in a 250 mL flask. The liquid was stirred at 500 r.p.m to promote the desorption of cyclohexanone and cyclohexanol at room temperature. The concentrations of cyclohexanone or cyclohexanol in the liquid phase were determined every 10 s or 7 s by a Gas-Chromatograph (Japan Shimadzu GC-14B) equipped with 30mHP-5 capillary and FID detector, with the external standard method. The desorption rates of cyclohexanol and cyclohexanone were calculated by the following equation:

$$r = \frac{kV}{m}$$

where k represents the slope in the Fig. 3 and 4, V represents the volumetric of the liquid in the flask, and m represents the mass of the catalysts.

At room temperature, the adsorption of H_2 on the Raney Ni catalyst was tested by pulse chemisorption with a mass spectrometry (Omnistar TM), both in water and methanol.

Results and discussion

Catalyst characterization

The physical structure parameters and chemical composition of the Raney Ni catalyst and Ni–Al metallic alloy powders were characterized by BET, XRD and EDS, the experimental results are listed in Table 1, and the XRD results for the Raney Ni catalyst and Ni–Al metallic alloy powders are shown in Fig 2. The Raney Ni catalyst with nickel content of 94.1% showed three diffraction peaks of Ni 111, Ni 200 and Ni 220.

Table 1 Physical structure properties and chemical composition of Raney Ni catalyst and Ni–Al alloy

Catalyst	Mass content (%) ^c		Phenol uptake/ $\mu\text{mol g}^{-1}$	H_2 uptake/ $\mu\text{mol.g}^{-1}$	Particle size/nm	BET/ $\text{m}^2 \text{g}^{-1}$	Pore volume/ mL g^{-1}	Crystal size/ nm^d
	Al	Ni						
Raney Ni	5.9	94.1	/	159	22.1	131	0.204	6.4
Raney Ni ^a	5.9	94.1	283	117	22.1	131	0.204	6.4
Raney Ni ^b	5.9	94.1	29	69	22.1	131	0.204	6.4
Ni–Al alloy	45.0	55.0	/	/	41.2	15	0	/

^a Raney Ni in water. ^b Raney Ni in methanol. ^c Determined by EDS. ^d Determined by XRD.

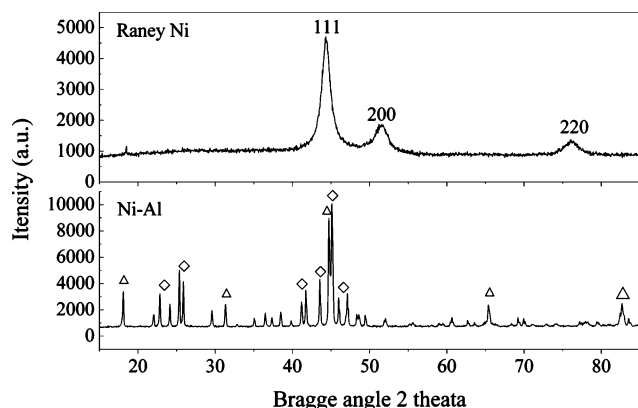


Fig. 2 X-ray diffraction patterns of Raney Ni catalyst and Ni–Al alloy (\diamond : Ni_3Al , \triangle : Ni_3Al_2).

Hydrogenation of phenol in water

The experimental results of solvent (water) recycling for phenol hydrogenation over the Raney Ni catalyst are summarized in Table 2. Hydrogenation of phenol at 340 K and atmospheric pressure in fresh water for 11 h obtains the phenol conversion degree of 96.1% and cyclohexanol selectivity of 99.6%. The organic phase (products) and water phase (solvent) were separated *via* phase separation technique; the water phase (containing 5% cyclohexanol and a trace amount of phenol) was collected for circulation. In the first circulation, the conversion degree

Table 2 Recycling of solvent (water) for the hydrogenation of phenol in the aqueous phase system^a

Water	Time/h	<i>X</i> (%)	<i>S</i> _{cyclohexanol}	<i>S</i> _{cyclohexanone}
Fresh	11	96.1	99.6	0.4
Cycle 1	11	96.4	99.8	0.2
Cycle 2	11.5	97.6	99.2	0.8
Cycle 3	12	95.6	99.1	0.9
Cycle 4	12	96.5	99.4	0.6

^a Reaction conditions: *t* = 340 K, *p* = 1 atm, Raney Ni : phenol : water = 10 g : 10 g : 20 mL. *X*: conversion rate of phenol, *S*: selectivity.

of phenol and the selectivity for cyclohexanol are 96.4% and 99.8%, respectively, and they change slightly compared to the fresh water. When the solvent was used for the second, third and fourth circulations, hardly any changes were observed for the conversion degree of phenol and the selectivity for cyclohexanol. The results indicated that the solvent water could be reused successfully. It is worthwhile to mention that the conversion degree of phenol in the above experimental is near 96%, which would result in the presence of phenol (~4%) in the products. However, 100% conversion of phenol could be reached at an elevated pressure or prolonged reaction time (see Table 3), which indicated that pure products (absence of phenol) could be obtained *via* the proposed aqueous system, thus providing an environmentally benign process.

The experimental results of the hydrogenation of phenol, *o*-cresol and *p*-*tert*-butylphenol in water or methanol, respectively, over the Raney Ni catalyst are summarized in Table 3. The conversion degrees of phenol, *o*-cresol and *p*-*tert*-butylphenol are 100, 95.8 and 82.4%, respectively (the selectivity to their corresponding alcohols is all 100%), in entries 1, 7 and 9. However, the conversion degrees of phenol, *o*-cresol and *p*-*tert*-butylphenol are only 5.2, 6.8 and 5.1%, respectively (the selectivity to their corresponding alcohols is 63, 95 and 100%), if the reactions were carried out in the methanol solvent (entries 2, 8 and 10) under the same conditions. The experimental results indicated that the hydrogenation rate of phenol, *o*-cresol and *p*-*tert*-butylphenol in water is significantly higher than that in methanol, and it follows the sequence of phenol > *o*-cresol > *p*-*tert*-butylphenol. The hydrogenation rate of *o*-cresol and *p*-*tert*-butylphenol in water was inhibited because the lower aqueous solubility of these phenol derivatives compared to phenol, which can not be improved much by temperature, inhibits their hydrogenation rate in water. For phenol and *o*-cresol, the selectivity to their corresponding ketones in methanol is higher than that in water.

The solvent-free hydrogenation of phenol at 413 K and 2 MPa for 2.5 h (Table 3, entry 6) obtains a phenol conversion degree of 100% with cyclohexanol selectivity of 93% and by-products selectivity of 7%. The selectivity for by-products is reduced to 3% if water was used as the solvent. These results implying that organic reactions carried out in

Table 3 Experimental results for the hydrogenation of phenol, *o*-cresol and *p*-*tert*-butylphenol over the Raney Ni catalyst in water and methanol, respectively^a

Entry	<i>t</i> /K	<i>p</i> /MPa	time/h	Solvent	Substrate	<i>X</i> (%)	Products [selectivity (%)]		
1	343	2	2	H ₂ O	1a	100	2a (100)	3a (0)	4a (0)
2	343	2	2	MeOH	1a	5.2	2a (63)	3a (37)	4a (0)
3	340	0.1	16	H ₂ O	1a	100	2a (100)	3a (0)	4a (0)
4	413	2	0.5	H ₂ O	1a	100	2a (97)	3a (0)	4a (3)
5	413	2	5	MeOH	1a	9.5	2a (60)	3a (38)	4a (2)
6	413	2	2.5	None	1a	100	2a (93)	3a (0)	4a (7)
7	363	2	5	H ₂ O	1b	95.8	2b (100)	3b (0)	4b (0)
8	363	2	6	MeOH	1b	6.8	2b (95)	3b (5)	4b (0)
9	373	2	5	H ₂ O	1c	82.4	2c (100)	3c (0)	4c (0)
10	373	2	6	MeOH	1c	5.1	2c (100)	3c (0)	4c (0)

^a Reaction conditions: Raney Ni : phenol : water = 5 g : 20 g : 40 mL **1a**: phenol, **1b**: *o*-cresol, **1c**: *p*-*tert*-butylphenol, **2(a–c)**: alcohol, **3(a–c)**: ketone, **4(a–c)**: other.

water could potentially improve the selectivity for the desired products.

Effect of solvent water

The reversible uptakes of phenol and H₂ on the Raney Ni catalyst are 283 and 117 μmol g⁻¹ (Table 1), respectively, in water, while they are 29 and 69 μmol g⁻¹, respectively, in methanol. These results could be attributed to the competitive adsorption of methanol on the catalyst.

Fig. 3 and 4 showed the desorption curves of cyclohexanol and cyclohexanone on the Raney Ni catalyst, in water and methanol. The results point out that the desorption rates of cyclohexanone and cyclohexanol on the catalyst in water are lower than those in methanol. The ratio $r_{\text{methanol}}/r_{\text{water}}$ for both cyclohexanone and cyclohexanol equals to approximately 1.5 (r_{water} and r_{methanol} represent the desorption rates of the products in water and methanol, respectively). Higher solubility of cyclohexanone and

cyclohexanol in methanol compared to that in water favors the desorption process.

The hydrogenation rates of phenol in water are higher than in methanol because phenol and H₂ are of higher reversible uptakes on the Raney Ni catalyst in water than those in methanol (Table 1). The selectivity for cyclohexanone is highly dependent upon the desorption rate of cyclohexanone and cyclohexanol on the Raney Ni catalyst. The lower desorption rates for cyclohexanol and cyclohexanone in water result in the further hydrogenation of cyclohexanone to cyclohexanol. Meanwhile, the higher H₂ uptakes on the Raney Ni catalyst in water could also favor the formation of cyclohexanol.

Conclusions

An aqueous reaction system for the hydrogenation of phenol and its derivatives has been proposed. The complete aqueous miscibility of liquid phenol is achieved by temperature increase. On the other hand, the separation of the products from water is simplified by their low aqueous solubility. The aqueous phase recovered after the reaction could be used repeatedly, thus providing an environmentally benign process. The hydrogenation rates of phenol in water are higher than that in methanol, because phenol and H₂ have higher reversible uptakes on the Raney Ni catalyst in water (117 and 283 μmol g⁻¹) than in methanol (69 and 29 μmol g⁻¹). The lower desorption rates for cyclohexanone in water result in the further hydrogenation of cyclohexanone to cyclohexanol. Meanwhile, the higher H₂ uptakes on the Raney Ni catalyst in water could also favor the formation of cyclohexanol.

Acknowledgements

The financial support by the Program for New Century Excellent Talents in the University of China (NCET-04-0557), and the Specialized Research Fund for the Doctoral Program of High Education of China (SRFDP-20060337001) are gratefully acknowledged.

References

- 1 *World Nylon 6 & 66 Supply/Demand Report*, PCI-Fibers & Raw Materials, Seaford, UK, 1998.
- 2 K. Weissermel and H. J. Arpe, in *Industrial Organic Chemistry*, VCH, New York, 2nd edn, 1993, p. 251.
- 3 J. F. Van Peppen, W. B. Fisher and C. H. Chan, in *Phenol, Hydrogenation Process in Catalysis of Organic Reactions*, ed. R. L. Augustine, Marcel Dekker, New York, 1980, p. 355.
- 4 W. B. Fisher and J. F. van Peppen, *Production of Cyclohexanone*, US Patent 4 162 267, 1978.
- 5 S. Scire, S. Minico and C. Crisafulli, *Appl. Catal., A*, 2002, **235**, 21.
- 6 S. G. Shore, E. Ding and C. Park *et al.*, *Catal. Commun.*, 2002, **3**, 77.
- 7 N. Mahata, K. V. Raghavan and V. Vishwanathan *et al.*, *Phys. Chem. Chem. Phys.*, 2001, **3**, 2712.
- 8 V. Vishwanathan, N. Mahata and M. A. Keane, *React. Kinet. Catal. Lett.*, 2001, **72**(2), 297.
- 9 C. V. Rode, U. D. Joshi, O. Sato and M. Shirai, *Chem. Commun.*, 2003, **15**, 1960.
- 10 E. Diaz, A. F. Mohedano, L. Calvo, M. A. Gilarranz, J. A. Casas and J. J. Rodríguez, *Chem. Eng. J.*, 2007, **131**, 65.
- 11 R. Breslow, *Green Chemistry*, ed. P. T. Anastas and T. C. Williamson, Oxford University Press, New York, 1998, ch. 13.
- 12 C. J. Li and T. H. Chan, *Organic Reactions in Aqueous Media*, John Wiley & Sons, New York, 1997.

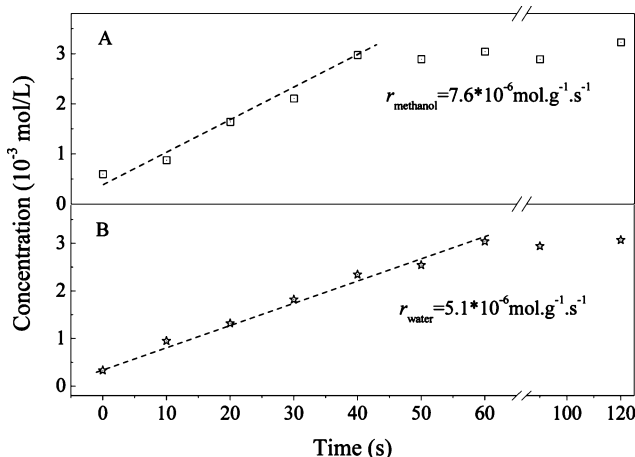


Fig. 3 The desorption properties of cyclohexanol on the Raney Ni catalyst in water and methanol. (A) Desorption in methanol, (B) desorption in water.

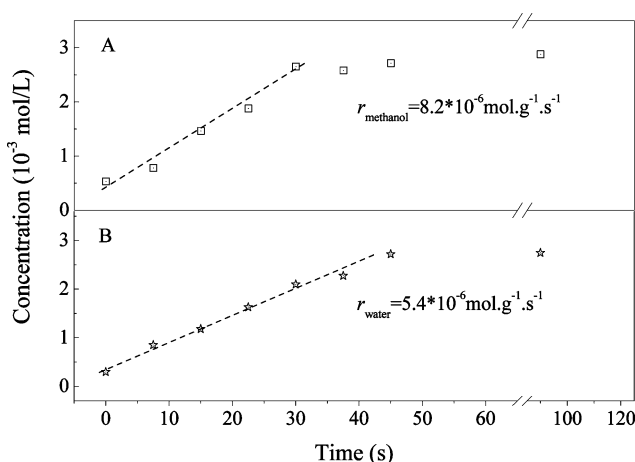


Fig. 4 The desorption properties of cyclohexanone on the Raney Ni catalyst in water and methanol. (A) Desorption in methanol, (B) desorption in water.

-
- 13 P. A. Grieco, *Organic Synthesis in Water*, Blackie Academic and Professional, London, 1998.
- 14 F. Joó, E. Papp and A. Kathó, *Top. Catal.*, 1998, **5**, 113.
- 15 R. T. Baker and W. Tumas, *Science*, 1999, **284**, 1477.
- 16 Z. W. Xi, N. Zhou, Y. Sun and K. L. Li, *Science*, 2001, **292**, 1139.
- 17 G. J. T. Brink, I. W. C. E. Arends and R. A. Sheldon, *Science*, 2000, **287**, 1636.
- 18 E. D. Bergbreiter, P. L. Osburn, T. Smith, C. M. Li and J. D. Frels, *J. Am. Chem. Soc.*, 2003, **125**, 6254.
- 19 F. Joo, *Acc. Chem. Res.*, 2002, **35**, 738.
- 20 J. H. Chen and H. Alper, *J. Am. Chem. Soc.*, 1997, **119**, 893.
- 21 P. G. Jessop, D. J. Heldebrant, X. W. Li, C. A. Eckert and C. L. Liotta, *Nature*, 2005, **436**, 1102.
- 22 M. C. Pirrung, *Chem.–Eur. J.*, 2006, **12**, 1312.

Thermophysical properties, low pressure solubilities and thermodynamics of solvation of carbon dioxide and hydrogen in two ionic liquids based on the alkylsulfate anion

Johan Jacquemin, Pascale Husson, Vladimir Majer, Agilio A.H. Padua and Margarida F. Costa Gomes*

Received 18th February 2008, Accepted 24th June 2008

First published as an Advance Article on the web 24th July 2008

DOI: 10.1039/b802761g

Densities and viscosities of the ionic liquid 1-butyl-3-methylimidazolium octylsulfate, $[\text{C}_4\text{C}_1\text{Im}][\text{C}_8\text{SO}_4]$ were measured as a function of temperature between 313 K and 395 K. Solubilities of hydrogen and carbon dioxide were determined, between 283 K and 343 K, and at pressures close to atmospheric in $[\text{C}_4\text{C}_1\text{Im}][\text{C}_8\text{SO}_4]$ and in another ionic liquid based on the alkylsulfate anion-1-ethyl-3-methylimidazolium ethylsulfate, $[\text{C}_2\text{C}_1\text{Im}][\text{C}_2\text{SO}_4]$. Density and viscosity were measured using a vibrating tube densimeter from Anton Paar and a rheometer from Rheometrics Scientific with accuracies of $10^{-3} \text{ g cm}^{-3}$ and 1%, respectively. Solubilities were obtained using an isochoric saturation technique and, from the variation of solubility with temperature, the partial molar thermodynamic functions of solvation, such as the standard Gibbs energy, the enthalpy, and the entropy, are calculated. The precision of the experimental data, considered as the average absolute deviation of the Henry's law constants from appropriate smoothing equations, is better than $\pm 1\%$.

Introduction

Much of the research on ionic liquids has been centred on their use as alternative solvents associating tuneable physical–chemical properties to a so-called green character that mainly rest on their negligible vapour pressure.¹ The possibility of changing the widely used volatile organic compounds by alternative solvents, like ionic liquids, implies not only the knowledge and understanding of the properties of this new family of compounds but also the search for less toxic species that are more biodegradable and obtainable from environmentally benign sources.^{1,2}

In 2002, Wasserscheid *et al.*³ have proposed the synthesis “of even ‘greener’” ionic liquids for catalytic applications. These ionic liquids should combine different environmentally favourable properties, namely a low melting point, a high chemical stability in the presence of water, the possibility of being disposed by combustion without formation of HF or HCl, a high temperature for thermal decomposition, a possibility of being biodegradable and being synthesized from cheap and available raw materials. Ionic liquids based on alkylsulfate anions seem to gather most of these desired properties and they are usually considered as cheaper,⁴ easily prepared with high purity⁴ and more adequate than other imidazolium-based ionic liquids in terms of chemical stability, toxicology, degradability and environmental effects.^{5–7}

A relatively small number of studies are available in the literature concerning the physical–chemical properties of alkylsulfate-based ionic liquids.⁸ Of the published studies, the large majority concern ionic liquids containing the lower homologues of alkylsulfate anions, namely methylsulfate and ethylsulfate,^{9–11} and their mixtures with molecular compounds like hydrocarbons^{12–14} and other organic compounds,¹⁵ alcohols^{16,17} or water.^{16,18} These ionic liquids, based on methylsulfate or ethylsulfate anions, are known for their sensitivity to hydrolysis,³ which is undesired for most applications. This sensibility tends to disappear with the increase of the anion alkyl-side chain, and the ionic liquid 1-butyl-3-methylimidazolium octylsulfate $[\text{C}_4\text{C}_1\text{Im}][\text{C}_8\text{SO}_4]$ is described as stable in the presence of water.³ For this ionic liquid, apart from the publication where its synthesis is firstly described,³ only two studies were found which report the thermodynamic properties of the pure ionic liquid⁸ and of its mixtures with alcohols or hydrocarbons.¹⁹ This liquid is described as being more viscous and having a higher melting point than those with the lower-alkyl chain homologues of the anion.

In the present paper we report the density and viscosity of $[\text{C}_4\text{C}_1\text{Im}][\text{C}_8\text{SO}_4]$ as a function of temperature and at atmospheric pressure. The solubility of carbon dioxide and hydrogen as a function of temperature and at pressures close to atmospheric are also reported for $[\text{C}_4\text{C}_1\text{Im}][\text{C}_8\text{SO}_4]$ and $[\text{C}_2\text{C}_1\text{Im}][\text{C}_2\text{SO}_4]$. The data obtained are compared to those for other ionic liquids based on different anions.

Results and discussion

Density and viscosity

The density of $[\text{C}_4\text{C}_1\text{Im}][\text{C}_8\text{SO}_4]$ was measured at atmospheric pressure and as a function of temperature from 313 K to

Laboratoire Thermodynamique et Interactions Moleculaires, Université Blaise Pascal Clermont-Ferrand/ CNRS, 24 avenue des Landais, 63177, Aubière Cedex, France. E-mail: margarida.c.gomes@univ-bpclermont.fr; Fax: +33 473407185; Tel: +33 473407205

Table 1 Experimental values of the density of $[\text{C}_4\text{C}_1\text{Im}][\text{C}_8\text{SO}_4]$ between (313 and 343) K. The percent deviations are relative to the fit of the data by eqn (1)

T/K	$\rho/\text{kg m}^{-3}$	Dev%
$[\text{C}_4\text{C}_1\text{Im}][\text{C}_8\text{SO}_4]$		
313.14	1058.0	-0.003
313.28	1057.8	+0.001
318.52	1054.5	+0.000
323.10	1051.5	+0.004
323.40	1051.4	-0.001
328.18	1048.3	-0.002
333.04	1045.3	-0.004
333.15	1045.0	+0.012
338.14	1042.1	-0.009
343.05	1038.9	-0.004
343.27	1038.6	+0.007

343 K. The melting point of $[\text{C}_4\text{C}_1\text{Im}][\text{C}_8\text{SO}_4]$ has been reported as being 34–35 °C³ but we have observed that this salt remains as a subcooled melt for several months at room temperature (around 20 °C). This behaviour has been reported by other authors that were able to measure the thermodynamic properties of the subcooled liquid.^{3,8} We have decided to measure the liquid density of $[\text{C}_4\text{C}_1\text{Im}][\text{C}_8\text{SO}_4]$ from 313 K, above its melting point temperature. The measured densities are listed in Table 1. The experimental values were correlated as a function of temperature following the equation:

$$\rho(\text{kg m}^{-3}) = 1257.9 - 6386.3 \times 10^{-4}(T/\text{K}) \quad (1)$$

The average absolute deviation of the fit is of 0.005%.

The density values obtained in this work are slightly higher than those measured by other authors. We can compare the present value at 25 °C (by extrapolating the present results)—1067.5 kg m^{-3} —with the ones published by Wasserscheid *et al.*³ measured with a pycnometer—1060.1 kg m^{-3} —and by Davila *et al.*⁸ obtained with a vibrating tube densimeter—1066.8 kg m^{-3} . The present values are 0.7% higher than the pycnometric values and less than 0.1% above those recently published by Davila *et al.*⁸

Compared with other ionic liquids, based on the 1-butyl-3-methylimidazolium cation, with the tetrafluoroborate, hexafluorophosphate, triflate or bis(trifluoromethanesulfonyl)imide anion, the $[\text{C}_4\text{C}_1\text{Im}][\text{C}_8\text{SO}_4]$ has a much lower density, as seen in Fig. 1, which is closer to that of classical organic solvents. It is also noteworthy that $[\text{C}_2\text{C}_1\text{Im}][\text{C}_2\text{SO}_4]$ ⁹ is significantly denser than the $[\text{C}_4\text{C}_1\text{Im}][\text{C}_8\text{SO}_4]$ studied here. This observation confirms the fact that ions with longer alkyl chains lead to less dense ionic liquids. This effect was observed before for the cation's alkyl chain⁹ and is also seen here for the anion.

The dynamic viscosity was measured for $[\text{C}_4\text{C}_1\text{Im}][\text{C}_8\text{SO}_4]$, previously dried, and is listed in Table 2 as a function of temperature from (314 to 395) K. It was first observed that the viscosity of the sample remained constant with increasing shear rates (from 0 to 500 s^{-1}). This linear relationship between the shear stress and the shear rate corresponds to a Newtonian behaviour that has been also reported by Wasserscheid *et al.*³ for $[\text{C}_4\text{C}_1\text{Im}][\text{C}_8\text{SO}_4]$.

In the temperature range studied, the viscosity drastically decreases with increasing temperature. This variation is very important for $[\text{C}_4\text{C}_1\text{Im}][\text{C}_8\text{SO}_4]$ which is 19 times more viscous

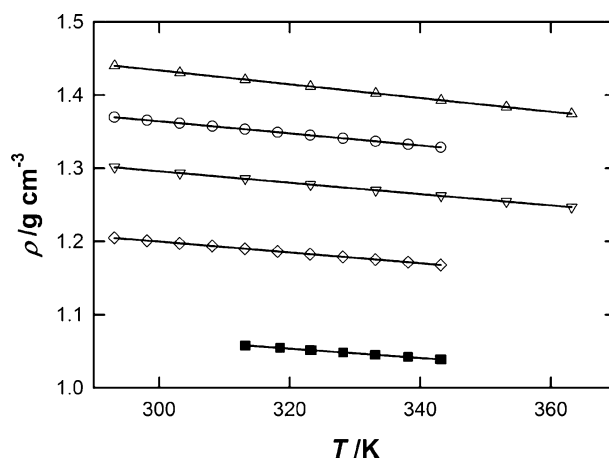


Fig. 1 Experimental density of $[\text{C}_4\text{C}_1\text{Im}][\text{C}_8\text{SO}_4]$: (■), as a function of the temperature. Comparison of this density with other $[\text{C}_4\text{C}_1\text{Im}]$ based ionic liquids:³⁸ (Δ), $[\text{C}_4\text{C}_1\text{Im}][\text{NTf}_2]$; (\circ), $[\text{C}_4\text{C}_1\text{Im}][\text{PF}_6]$; (∇), $[\text{C}_4\text{C}_1\text{Im}][\text{OTf}]$; (\diamond), $[\text{C}_4\text{C}_1\text{Im}][\text{BF}_4]$; as a function of temperature. The lines correspond to the linear fit of the data as a function of temperature.

Table 2 Experimental values of the viscosity of $[\text{C}_4\text{C}_1\text{Im}][\text{C}_8\text{SO}_4]$ between (314 and 395) K and of $[\text{C}_4\text{C}_1\text{Im}][\text{C}_8\text{SO}_4]$. The percent deviations are relative to the fit of the data by eqn (2)

T/K	$\eta/\text{mPa s}$	Dev%
$[\text{C}_4\text{C}_1\text{Im}][\text{C}_8\text{SO}_4]$		
314.25	281	-0.2
323.77	168	+0.0
333.04	108	+0.4
342.07	74.2	-0.0
352.98	49.5	-0.1
362.10	36.6	-0.0
373.90	25.9	-0.3
384.11	19.8	-0.2
395.32	15.1	+0.4

at 313 K than at 395 K. In Fig. 2, the viscosity of several ionic liquids, measured before in the same temperature range,⁹ is represented together with the values obtained in this work. The $[\text{C}_4\text{C}_1\text{Im}][\text{C}_8\text{SO}_4]$ is the most viscous of the ionic liquids studied, *circa* two times more viscous than $[\text{C}_4\text{C}_1\text{Im}][\text{PF}_6]$ at 314 K but having only a slightly more important viscosity at temperatures above 350 K. The $[\text{C}_2\text{C}_1\text{Im}][\text{C}_2\text{SO}_4]$, also based in an alkylsulfate anion, has a much lower viscosity as observed in Fig. 2. At 310 K, a large difference on the viscosities of the two liquids is observed—59 mPa s for $[\text{C}_2\text{C}_1\text{Im}][\text{C}_2\text{SO}_4]$ compared with 361 mPa s for $[\text{C}_4\text{C}_1\text{Im}][\text{C}_8\text{SO}_4]$. This difference decreases with temperature and at 395 K a viscosity of 7 mPa s for $[\text{C}_2\text{C}_1\text{Im}][\text{C}_2\text{SO}_4]$ has been measured,⁹ compared with 15 mPa s for $[\text{C}_4\text{C}_1\text{Im}][\text{C}_8\text{SO}_4]$.

The Vogel–Fulcher–Tamman (VFT) equation is used to correlate the experimental viscosities as a function of temperature:

$$\eta = (4.153 \times 10^{-3})T^{0.5}\exp(1149/(T - 174.9)) \quad (2)$$

with an average absolute deviation of 0.3% in the present case.

Gas solubility

For each pair gas–ionic liquid studied, multiple experimental data points were obtained in the temperature interval between 283 K and 343 K in steps of approximately 10 K. The

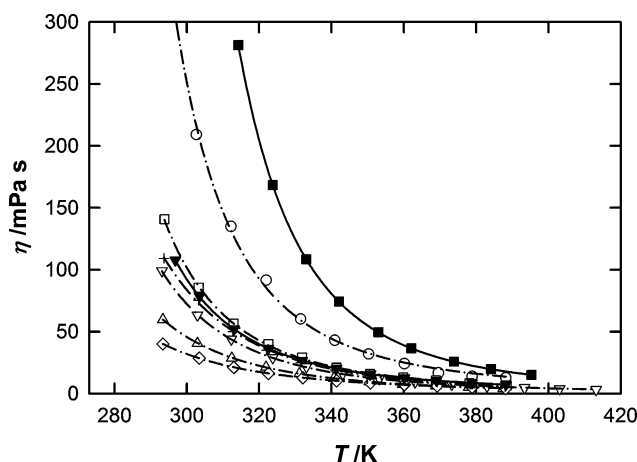


Fig. 2 Experimental viscosities as a function of temperature. (■), $[C_4C_1Im][C_8SO_4]$, this work; (▼), 1-ethyl-3-methylimidazolium ethylsulfate $[C_2C_1Im][C_2SO_4]$;⁹ (○), 1-butyl-3-methylimidazolium hexafluorophosphate $[C_4C_1Im][PF_6]$;⁹ (+), 1-methyl-3-butylimidazolium tetrafluoroborate $[C_4C_1Im][BF_4]$;⁹ (△), 1-methyl-3-butylimidazolium bis(trifluoromethylsulfonyl)imide $[C_4C_1Im][NTf_2]$;⁹ (▽), Butylmethylpyrrolidinium bis(trifluoromethylsulfonyl)imide $[C_4C_1Pyrro][NTf_2]$;⁹ (□), butyltrimethylammonium bis(trifluoromethylsulfonyl)imide $[N_{4111}][NTf_2]$;⁹ (◇), 1-ethyl-3-methylimidazolium bis(trifluoromethylsulfonyl)imide $[C_2C_1Im][NTf_2]$.⁹ The lines correspond to the fit of the data.

experimental gas solubilities in the two ionic liquids— $[C_2C_1Im][C_2SO_4]$ and $[C_4C_1Im][C_8SO_4]$ —are reported in Tables 3 and 4 for hydrogen and carbon dioxide, respectively. The solubility results are given both as Henry's law constants and as mole fractions of solute. These latter values are calculated from the experimental data on K_H (at slightly different total pressures) assuming a partial pressure of the gaseous solute equal to 0.1 MPa. The relative atomic masses used are the ones recommended by IUPAC²⁰ and the values of the second virial coefficients for all the gases, necessary for the calculation of the compressibility factor, were taken from the compilation by Dymond and Smith.²¹

To obtain representative values of the solubility, the raw experimental data were correlated as a function of temperature by an empirical equation of the type:

$$\ln[K_H(T)/10^5 \text{ Pa}] = \sum_{i=0}^n A_i (T/K)^{-i} \quad (3)$$

the optimized coefficients A_i are listed in Table 5 together with the average absolute deviations for each solute. These values can be regarded as an estimation of the precision of the experimental data, which is in the present case always less than 1%.

In Fig. 3 are represented the solubility data expressed in mole fraction, for carbon dioxide and hydrogen in the two ionic liquids as a function of temperature. As it can be observed by comparing both plots, carbon dioxide is at least one order of magnitude more soluble in both liquids than hydrogen. The solubility of both gases is higher in $[C_4C_1Im][C_8SO_4]$. As it has been observed before,^{22,23} the increase of the alkyl side chain in the cation causes a slight increase on the gas solubility. This effect seems to be even more pronounced in this case, where the alkyl side chain is also longer in the anion of the ionic liquid.

Table 3 Experimental values of H_2 in $[C_2C_1Im][C_2SO_4]$ and $[C_4C_1Im][C_8SO_4]$ expressed both as Henry's law constants, K_H and as H_2 mole fraction, x_2 , corrected for a partial pressure of solute of 0.1 MPa. p is the experimental equilibrium pressure and the percent deviation is relative to the correlations of the data reported in Table 5

T/K	$p/10^2 \text{ Pa}$	$K_H/10^5 \text{ Pa}$	$x_2/10^{-4}$	Dev/%
$[C_2C_1Im][C_2SO_4]$				
283.16	779.45	2492	4.015	-0.3
292.93	804.85	2143	4.669	+0.1
303.39	499.66	2056	4.866	+0.6
303.39	832.19	2062	4.853	+0.3
303.42	921.92	2071	4.831	-0.1
316.29	959.48	2280	4.389	-0.4
323.29	980.04	2544	3.933	-1.1
324.27	531.49	2516	3.976	+1.7
333.12	1008.87	3071	3.258	-0.4
333.22	545.39	3107	3.220	-1.3
343.13	937.32	3924	2.550	+0.1
343.13	1038.24	3894	2.569	+0.9
$[C_4C_1Im][C_8SO_4]$				
313.33	921.66	1892	5.288	+0.1
313.33	832.13	1891	5.292	-0.0
323.03	857.54	2062	4.853	+0.3
323.20	950.28	2047	4.887	-0.5
332.87	883.34	2279	4.390	+0.2
342.69	909.05	2531	3.953	-0.9
342.98	1007.71	2584	3.873	+0.8

Table 4 Experimental values of CO_2 in $[C_2C_1Im][C_2SO_4]$ and $[C_4C_1Im][C_8SO_4]$ expressed both as Henry's law constants, K_H and as CO_2 mole fraction, x_2 , corrected for a partial pressure of solute of 0.1 MPa. p is the experimental equilibrium pressure and the percent deviation is relative to the correlations of the data reported in Table 5

T/K	$p/10^2 \text{ Pa}$	$K_H/10^5 \text{ Pa}$	$x_2/10^{-4}$	Dev/%
$[C_2C_1Im][C_2SO_4]$				
283.32	380.10	62.13	160.0	-0.1
293.48	402.72	77.22	128.8	+0.2
303.38	836.77	94.28	105.6	+0.1
303.39	777.62	94.52	105.3	-0.1
313.28	869.49	113.2	88.00	+0.4
313.28	443.24	114.1	87.30	-0.4
314.68	813.40	117.0	85.15	-0.4
323.18	901.28	134.2	74.22	+0.6
323.24	839.67	135.7	73.41	-0.4
333.12	932.51	158.1	63.02	+0.5
333.14	869.20	159.0	62.68	-0.0
333.16	479.90	159.5	62.48	-0.3
343.08	898.46	186.0	53.58	-0.4
343.12	963.32	184.7	53.96	+0.3
$[C_4C_1Im][C_8SO_4]$				
313.15	682.01	64.84	153.6	+0.9
313.33	702.76	63.71	156.3	-1.0
322.31	725.63	70.81	140.7	-1.1
322.81	705.87	73.09	136.3	+1.5
323.27	728.35	80.51	123.8	-1.1
332.28	752.10	81.89	121.7	+0.6
342.23	778.22	94.57	105.4	+1.1
343.22	755.86	94.03	106.0	-0.9

The behaviour of $[C_4C_1Im][C_8SO_4]$ is compared, in Fig. 4, with that of other ionic liquids sharing the same cation, 1-butyl-3-methylimidazolium, but with different anions—tetrafluoroborate,²⁴ hexafluorophosphate²⁵ and bis(trifluoromethylsulfonyl)imide.²³ It is observed that both gases are approximately twice more soluble in $[C_4C_1Im][NTf_2]$ than in the three other ionic liquids. The solubility of carbon dioxide or of hydrogen is similar in $[C_4C_1Im][C_8SO_4]$ and in $[C_4C_1Im][PF_6]$,

Table 5 Parameters of eqn (3) used to smooth the experimental results on K_H from Table 3 and Table 4 along with the percent average absolute deviation of the fit (AAD)

Gas	A_0	A_1	A_2	AAD%
[C ₂ C ₁ Im][C ₂ SO ₄]				
H ₂	+51.46	-2.644 × 10 ⁴	+3.986 × 10 ⁶	0.6
CO ₂	+9.967	-1.505 × 10 ³	-4.229 × 10 ⁴	0.3
[C ₄ C ₁ Im][C ₈ SO ₄]				
H ₂	+23.28	-9.121 × 10 ³	+1.313 × 10 ⁶	0.4
CO ₂	+18.61	-7.959 × 10 ³	+1.075 × 10 ⁶	1.0

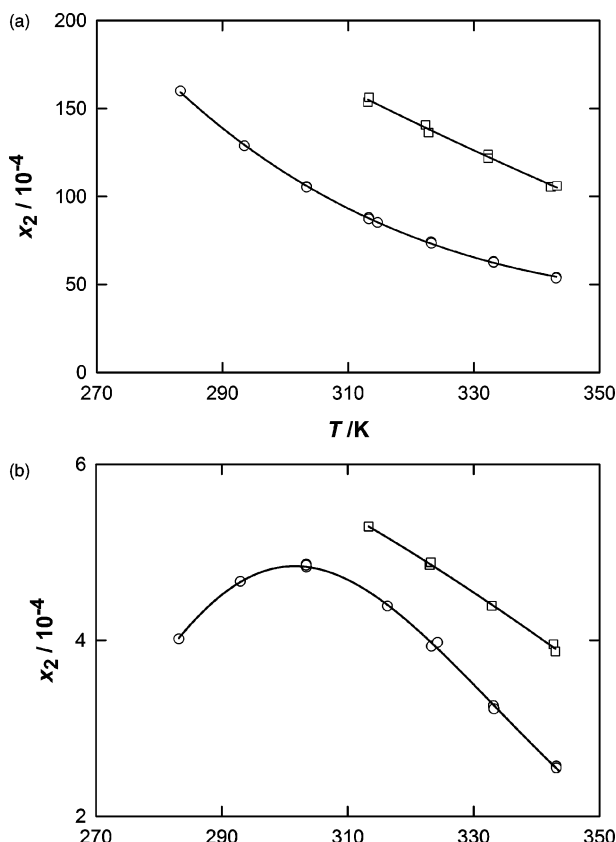


Fig. 3 Mole fraction gas solubilities of CO₂ (upper plot) and H₂ (lower plot) at 0.1 MPa partial pressure of the solute and as a function of temperature in: ○, [C₂C₁Im][C₂SO₄]; □, [C₄C₁Im][C₈SO₄]. Lines represent the smoothed data.

in spite of the quite different molecular structure of the anions. The lowest solubility is observed for the two gases for [C₄C₁Im][BF₄]. The solubility of hydrogen in [C₂C₁Im][C₂SO₄] has a peculiar behaviour with temperature as it was previously found in other ionic liquids like, for example, [C₄C₁Im][BF₄]²⁴ or [C₄C₁Im][PF₆]^{25,26} where the solubility is not monotonous in the temperature range studied^{24,25} or slightly increases with temperature.²⁶

The variation with temperature of gas solubility, expressed as Henry's law constant, is directly related to the thermodynamic properties of solvation which, in the case of gaseous solutes at low pressures, is practically identical to the thermodynamic properties of solution.²⁷ The Gibbs energy of solvation, corresponding to the change in Gibbs energy when the solute is transferred, at constant temperature, from the pure, perfect gas

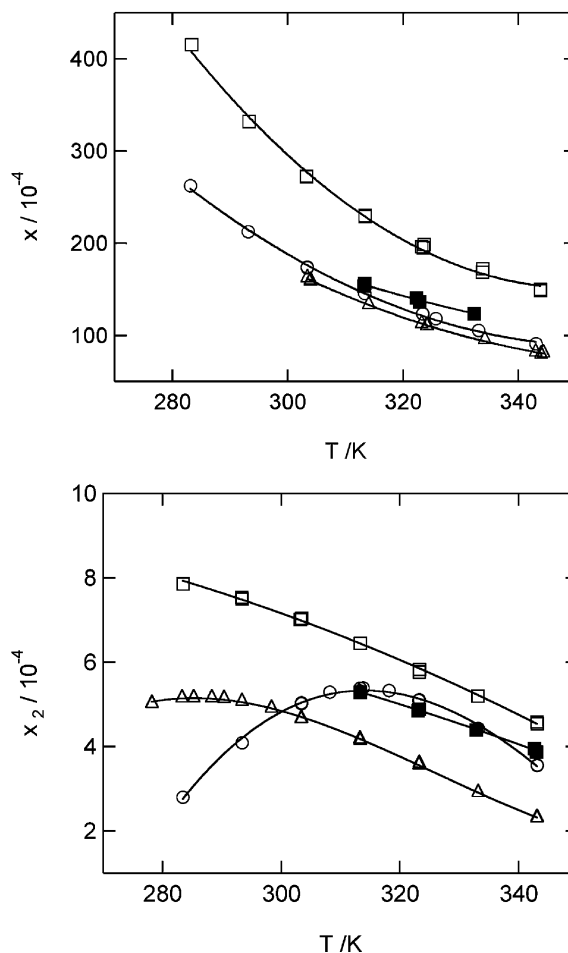


Fig. 4 Mole fraction gas solubilities of CO₂ (upper plot) and of H₂ (lower plot) in several ionic liquids based on the [C₄C₁Im] cation: ○, [C₄C₁Im][PF₆];²⁵ □, [C₄C₁Im][Ntf₂];²² △, [C₄C₁Im][BF₄];²⁴ ■, [C₄C₁Im][C₈SO₄], this work.

state at the standard pressure to the standard state of infinite dilution in the solvent, is given by

$$\Delta_{\text{solv}}G = RT \ln(K_H/p^0) \quad (4)$$

where p^0 is the standard-state pressure. The partial molar differences in enthalpy and entropy between the two states can be obtained by calculating the corresponding partial derivatives of the Gibbs energy with respect to temperature

$$\Delta_{\text{solv}}H = -T^2 \partial / \partial T (\Delta_{\text{solv}}G/T) = -RT^2 \partial / \partial T [\ln(K_H/p^0)] \quad (5)$$

$$\Delta_{\text{solv}}S = (\Delta_{\text{solv}}H - \Delta_{\text{solv}}G)/T = -RT \partial / \partial T [\ln(K_H/p^0)] - R \ln(K_H/p^0) \quad (6)$$

The values for the Gibbs energy, enthalpy and entropy of solvation are given in Table 6 for the two gases in the two ionic liquids at several discrete temperatures between 283 K and 343 K.

The analysis of the thermodynamic properties of solvation allows the interpretation of the values of gas solubility encountered. It is observed that, in the case of hydrogen, the higher solubility measured in [C₄C₁Im][C₈SO₄] corresponds both to a more favorable enthalpic term (the enthalpy of solvation is more negative for this ionic liquid) and a more favorable entropic term

Table 6 Thermodynamic functions of solvation for H₂ and CO₂ in [C₂C₁Im][C₂SO₄] and [C₄C₁Im][C₈SO₄] at several discrete temperatures between 283 K and 343 K. $\Delta_{\text{solv}}G$ is the Gibbs energy of solvation, $\Delta_{\text{solv}}H$ the enthalpy of solvation and $\Delta_{\text{solv}}S$ the entropy of solvation. The values are consistent with $p^0 = 0.1$ MPa

T/K	$\Delta_{\text{solv}}G/kJ mol^{-1}$	$\Delta_{\text{solv}}H/kJ mol^{-1}$	$\Delta_{\text{solv}}S/J mol^{-1} K^{-1}$
[C ₂ C ₁ Im][C ₂ SO ₄] + H ₂			
283	18.40	+14.4	-14.1
293	18.69	+6.43	-41.8
303	19.23	-1.04	-66.9
313	20.02	-8.03	-89.6
323	21.02	-14.6	-110
333	22.21	-20.7	-129
343	23.59	-26.6	-146
[C ₄ C ₁ Im][C ₈ SO ₄] + H ₂			
313	19.63	-6.08	-82.1
323	20.48	-8.24	-88.9
333	21.41	-10.3	-95.1
343	22.38	-12.2	-101
[C ₂ C ₁ Im][C ₂ SO ₄] + CO ₂			
283	9.698	-15.0	-87.3
293	10.57	-14.9	-87.0
303	11.44	-14.8	-86.7
313	12.30	-14.8	-86.5
323	13.17	-14.7	-86.2
333	14.03	-14.6	-86.0
343	14.89	-14.6	-85.9
[C ₄ C ₁ Im][C ₈ SO ₄] + CO ₂			
313	10.83	-9.05	-63.5
323	11.49	-10.8	-69.1
333	12.21	-12.5	-74.1
343	12.97	-14.0	-78.8

(the entropy of solvation is less negative). For the solubility of carbon dioxide, it is the entropic term that causes a higher solubility as, in this case, a less negative entropy of solvation explains the experimental result obtained for the gas solubility.

For the case of hydrogen, the thermodynamic properties of solvation reflect the variation of the solubility with temperature. In the lower temperature end, the enthalpy of solvation for hydrogen in [C₂C₁Im][C₂SO₄] is slightly positive which means that the solvation process is endothermic in these temperatures. This result has been found for the solubility of hydrogen in other ionic liquids, for example, in [C₄C₁Im][BF₄],²⁴ in [C₄C₁Im][PF₆]²⁵ and [N₄₁₁₁][NTf₂]²³ previously measured by the authors of the present work and in [C₄C₁Im][C₁SO₄],²⁸ [C₄C₁Im][PF₆]²⁶ and [C₆C₁Im][NTf₂]²⁹ formerly published by Kumelan *et al.*

Experimental

Samples

The samples of the alkylsulfate-based ionic liquids (minimum stated purity of 0.99 in mole fraction, as obtained by ¹H-NMR analysis) were supplied by the group of Prof. Wasserscheid at the University of Erlangen-Nürnberg, Germany.

1-Butyl-3-methylimidazolium octylsulfate, [C₄C₁Im][C₈SO₄]-CAS registry number 445473-58-5-was prepared *via* a metathesis reaction between 3-butyl-1-methylimidazolium chloride and sodium sulfate, according to the reported procedures by Wasserscheid *et al.*³ 1-Ethyl-3-methylimidazolium ethyl sulfate, [C₂C₁Im][C₂SO₄]-CAS registry number 342573-75-5-was

prepared by reaction of 1-methylimidazole with diethyl sulfate according to the reported procedures by Xu *et al.*³⁰

Before starting each measurement, the ionic liquids were kept under vacuum (pressure lower than 1 Pa) for at least 15 h at 323 K. Before being introduced to each apparatus, the samples were kept under nitrogen at 1 bar. This inert gas was chosen because of its very low solubility in the ionic liquids.²⁴ To avoid any contact of the sample with atmosphere, a septum adapted to the storage Schlenk flask and a syringe equipped with a *Luer-lock* valve were used to load the samples into the different instruments.

The water content was determined for each sample of ionic liquid before and after each series of measurements using a volumetric Karl Fisher titration method (Mettler Toledo DL31). No variation of the water content was found in the samples of ionic liquid used. For [C₂C₁Im][C₂SO₄], the water quantities measured were (100 ± 10) ppm and for [C₄C₁Im][C₈SO₄] they were (200 ± 10) ppm.

The halide content of the two ionic liquids was determined using suppressed ion chromatography (IC).³¹ The [C₂C₁Im][C₂SO₄] is an halogen-free ionic liquid. The sample of [C₄C₁Im][C₈SO₄] used contains less than 10 ppm of chloride.

Carbon dioxide and hydrogen used for this study come from to AGA/Linde Gaz with mole fraction purities of 0.99995 and 0.9998, respectively. All gases were used as received from the manufacturer.

Density

Densities were measured using a U-shape vibrating-tube densimeter (Anton Paar, model DMA 512) operating in a static mode, following the procedure described in a previous publication.⁹ The temperature was maintained constant to within ±0.01 K by means of a recirculating bath equipped with a PID temperature controller (Julabo FP40-HP). For measuring the temperature a 100 Ω platinum resistance thermometer (precision of ±0.02 K and accuracy of ±0.04 K) was used. Its calibration was performed against a 100 Ω platinum resistance Hart Scientific model 1502A.

The measured period of vibration (τ) of a U tube is related to the density (ρ) according to: $\rho = A\tau^2 + B$ where A and B are parameters that are a function of temperature. They were determined in the present work in the temperature range between (283 and 343) K. Three calibrating fluids were used: air, tridistilled water and two aqueous solutions of NaCl with accurate concentrations of approximately 1 mol kg⁻¹ and 3 mol kg⁻¹. These latter two fluids were chosen in order to cover a range of densities close to that of the ionic liquids studied. Measurements were performed in steps of 10 K and at least three independent values were obtained at each temperature. The precision of the density measurement is of the order 5×10^{-4} g cm⁻³, the results are expected to be accurate to 10^{-3} g cm⁻³.

It is worth noting that for the case of viscous fluids, such as the ionic liquid measured here ($\eta > 100$ mPa s), a correction for the effect of viscosity should also be included.^{8,9} Furthermore, due to the large effect of temperature on viscosity, this correction is only valid for narrow temperature ranges, close to room temperature. The effect of the viscosity on the density measurement was analyzed in order to validate the density measurements. In the

case of $[\text{C}_4\text{C}_1\text{Im}][\text{PF}_6]$, for which this effect will be greatest, the density was found to vary less than 0.1% and, therefore, the correction was considered to be negligible.

Viscosity

The viscosity was determined using a rheometer, Rheometrics Scientific SR200, that allows measurements from (293 to 393) K at atmospheric pressure and in a wide viscosity range (from 1 to 3000 mPa s) depending on the geometry used. A Couette geometry (concentric cylinders) was chosen for this study. Temperature was maintained constant to 0.01 K by means of a recirculating bath similar to that used for the density measurements and was measured with the same accuracy. To avoid any water contamination of the sample during the measurement, the rheometer was placed inside a glove-box in an isolating atmosphere of purified and dried air. The rheometer was calibrated with an oil of known viscosity (viscosity standard oil from Brookfield, 95 mPa s at 298 K). Measurements were performed in steps of 10 K and at least three independent values were obtained at each temperature. A statistical analysis of our results indicates a precision in the viscosities of 0.2% and an expected overall uncertainty lower than 1%.

Low-pressure gas solubility

The experimental method used for these gas solubility measurements is based on an isochoric saturation technique and has been described in previous publications.^{22–25,32–34} In this technique, a known quantity of gaseous solute is put in contact with a precisely determined quantity of degassed solvent at a constant temperature inside an accurately known volume. When thermodynamic equilibrium is attained, the pressure above the liquid solution is constant and is directly related to the solubility of the gas in the liquid.

The quantity of ionic liquid introduced in the equilibration cell, V_{liq} , is determined gravimetrically. The amount of solute present in the liquid solution, n_2^{liq} (subscript 2 stands for solute and subscript 1 stands for solvent), is calculated by the difference between two pVT measurements: first when the gas is introduced in a calibrated bulb with volume V_{GB} and second after thermodynamic equilibrium is reached:

$$n_2^{\text{liq}} = \frac{p_{\text{ini}} V_{\text{GB}}}{[Z_2(p_{\text{ini}}, T_{\text{ini}}) RT_{\text{ini}}]} - \frac{p_{\text{eq}} (V_{\text{tot}} - V_{\text{liq}})}{[Z_2(p_{\text{eq}}, T_{\text{eq}}) RT_{\text{eq}}]} \quad (7)$$

where p_{ini} and T_{ini} are the pressure and temperature in the first pVT determination and p_{eq} and T_{eq} the pressure and temperature at the equilibrium. V_{tot} is the total volume of the equilibration cell and Z_2 is the compressibility factor for the pure gas. The solubility can then be expressed in mole fraction:

$$x_2 = \frac{n_2^{\text{liq}}}{n_1^{\text{liq}} + n_2^{\text{liq}}} \quad (8)$$

or as Henry's law constant:

$$K_{\text{H}} = \lim_{x_2 \rightarrow 0} \frac{f_2(p, T, x_2)}{x_2} \cong \frac{\phi_2(p_{\text{eq}}, T_{\text{eq}}) p_{\text{eq}}}{x_2} \quad (9)$$

where f_2 is the fugacity of the solute and ϕ_2 its fugacity coefficient.

Conclusions

This paper presents original gas solubility data in two ionic liquids based on the alkylsulfate anion— $[\text{C}_2\text{C}_1\text{Im}][\text{C}_2\text{SO}_4]$ and $[\text{C}_4\text{C}_1\text{Im}][\text{C}_8\text{SO}_4]$. The two ionic liquids are believed to be promising alternatives to traditional volatile organic solvents^{3,8} and this work contributes to their physico-chemical characterization. The density and the viscosity of the two liquids studied were compared to those of other common ionic liquids. Although their viscosity is significantly higher than that of ionic liquids with the same cation but with other anions, like bis[(trifluoro)sulfonyl]imide or even hexafluorophosphate, it decreases dramatically with temperature and, above 350 K, the viscosities of all the liquids are much closer. These high values of viscosity can be considered as a drawback for chemical or catalysis purposes, around room temperature, of this family of ionic liquids but can constitute an advantage for their use in other fields of application.

Of the two liquids studied in this work, $[\text{C}_4\text{C}_1\text{Im}][\text{C}_8\text{SO}_4]$ is capable of dissolving larger quantities of carbon dioxide and of hydrogen. When compared with other ionic liquids based on the same cation but with other anions, it dissolves lesser quantities of gases than the ionic liquid based on the bis[(trifluoro)sulfonyl]imide anion and approximately as much as the ionic liquid based on the hexafluorophosphate anion.

It was also observed that $[\text{C}_4\text{C}_1\text{Im}][\text{C}_8\text{SO}_4]$ is more viscous than other ionic liquids at temperatures close to the ambient. In particular, it is significantly more viscous than $[\text{C}_2\text{C}_1\text{Im}][\text{C}_2\text{SO}_4]$ and, at 300 K, it exhibits a viscosity two times higher than that of $[\text{C}_4\text{C}_1\text{Im}][\text{PF}_6]$. $[\text{C}_4\text{C}_1\text{Im}][\text{C}_8\text{SO}_4]$ is also much less dense than other ionic liquids based on the same cation, with densities not far from those of common organic solvents.

The properties of the two ionic liquids studied here can be explained in light of their molecular structures.^{35,36} It has been recently shown that the fluid structure in $[\text{C}_4\text{C}_1\text{Im}][\text{C}_8\text{SO}_4]$ is dominated by the apolar domains formed by aggregation of the alkyl chains of the cation and the anion.⁸ This argument can contribute to explain the higher values of viscosity of $[\text{C}_4\text{C}_1\text{Im}][\text{C}_8\text{SO}_4]$ when compared to $[\text{C}_2\text{C}_1\text{Im}][\text{C}_2\text{SO}_4]$.

We have shown before, using molecular simulation, that the solvation properties of the ionic liquids can be explained by their peculiar molecular characteristics.³⁵ We have also shown that, when dissolved in $[\text{C}_4\text{C}_1\text{Im}][\text{PF}_6]$, carbon dioxide interacts preferentially with the anion³⁷ and is more probably located near the polar domains in the ionic liquid. The similar solubility of carbon dioxide in $[\text{C}_4\text{C}_1\text{Im}][\text{C}_8\text{SO}_4]$ and in $[\text{C}_4\text{C}_1\text{Im}][\text{PF}_6]$, an ionic liquid with a much smaller anion, supports the idea that, although the anion in $[\text{C}_4\text{C}_1\text{Im}][\text{C}_8\text{SO}_4]$ is much larger than in $[\text{C}_4\text{C}_1\text{Im}][\text{PF}_6]$, the electrostatic charge is concentrated in the SO_4 group which will preferentially interact with carbon dioxide. The solubility of CO_2 is then determined by this specific electrostatic interaction.

The analysis of the thermodynamic properties of solvation of CO_2 in $[\text{C}_4\text{C}_1\text{Im}][\text{PF}_6]$ (previously determined by Jacquemin *et al.*²⁵) and in $[\text{C}_4\text{C}_1\text{Im}][\text{C}_8\text{SO}_4]$ (calculated in this work) does not permit to confirm the arguments developed above, which

are related to structural features of the ionic liquids. It is observed that the enthalpy of solvation is slightly less negative in $[\text{C}_4\text{C}_1\text{Im}][\text{C}_8\text{SO}_4]$ than in $[\text{C}_4\text{C}_1\text{Im}][\text{PF}_6]$ and because the Gibbs energy of solvation is similar for carbon dioxide in the two ionic liquids, the entropy of solvation is also slightly less negative for the solvation of CO_2 in $[\text{C}_4\text{C}_1\text{Im}][\text{C}_8\text{SO}_4]$ than in $[\text{C}_4\text{C}_1\text{Im}][\text{PF}_6]$.

These arguments surely deserve to be further developed by associating new experimental measurements of the solubility of other gases, both apolar, like oxygen or ethane, or having an important dipole moment, like for example nitrous oxide, with molecular simulations that provide an interpretation of the thermodynamic properties at the atomic scale.

Acknowledgements

The authors thank the group of P. Wasserscheid from Erlangen-Nurnberg University for supplying the IL samples. This study was part of a CNRS-DFG cooperation project between France and Germany and was also supported by the ADEME France (PhD grant of J.J.).

References

- 1 T. Welton, *Green Chem.*, 2008, **10**, 483.
- 2 D. J. Adams, P. J. Dyson and S. J. Tavener, *Chemistry in Alternative Reaction Media*, Wiley, Chichester, 2004.
- 3 P. Wasserscheid, R. van Hal and A. Bösmann, *Green Chem.*, 2002, **4**, 400–404.
- 4 J. D. Holbrey, W. M. Reichert, R. P. Swatloski, G. A. Broker, W. R. Pitner, K. R. Seddon and R. D. Rogers, *Green Chem.*, 2002, **4**, 407–413.
- 5 C. Pretti, C. Chiappe, D. Pieraccini, M. Gregori, F. Abramo, G. Monni and L. Intorre, *Green Chem.*, 2006, **8**, 238–240.
- 6 N. Gathergood, M. T. Garcia and P. J. Scammells, *Green Chem.*, 2004, **6**, 166–175.
- 7 M. T. Garcia, N. Gathergood and P. J. Scammells, *Green Chem.*, 2005, **7**, 9–14.
- 8 M. J. Davila, S. Aparicio, R. Alcalde, B. Garcia and J. M. Leal, *Green Chem.*, 2007, **9**, 221–232.
- 9 J. Jacquemin, P. Husson, A. A. H. Padua and V. Majer, *Green Chem.*, 2006, **8**, 172–180.
- 10 J. Jacquemin, P. Husson, V. Majer and I. Cibulka, *J. Chem. Eng. Data*, 2007, **52**, 2204–2211.
- 11 A. Fernandez, J. S. Torrecilla, J. Garcia and F. Rodriguez, *J. Chem. Eng. Data*, 2007, **52**, 1979–1983.
- 12 R. Kato, M. Krummen and J. Gmehling, *Fluid Phase Equilib.*, 2004, **224**, 47–54.
- 13 G. W. Meindersma, A. J. G. Podt and A. B. de Haan, *Fluid Phase Equilib.*, 2006, **247**, 158–168.
- 14 U. Domanska, Z. Zolek-Tryznowska and M. Krolikowski, *J. Chem. Eng. Data*, 2007, **52**, 1872–1880.
- 15 A. B. Pereiro and A. Rodriguez, *J. Chem. Eng. Data*, 2007, **52**, 600–608.
- 16 E. Gomez, B. Gonzalez, N. Calvar, E. Tojo and A. Dominguez, *J. Chem. Eng. Data*, 2006, **51**, 2096–2102.
- 17 N. Calvar, E. Gomez, B. Gonzalez and A. Dominguez, *J. Chem. Eng. Data*, 2007, **52**, 2529–2535.
- 18 H. Rodriguez and J. F. Brennecke, *J. Chem. Eng. Data*, 2006, **51**, 2145–2155.
- 19 U. Domanska, A. Pobudkowska and A. Wisniewska, *J. Solution Chem.*, 2006, **35**, 311–334.
- 20 IUPAC Commission on Atomic Weights and Isotopic Abundances, *Pure Appl. Chem.*, 1986, **58**, 1677–1692.
- 21 J. H. Dymond and E. B. Smith, *The Virial Coefficients of Pure Gases and Mixtures*, Clarendon Press, Oxford, 1980.
- 22 G. Hong, J. Jacquemin, M. Deetlefs, C. Hardacre, P. Husson and M. F. Costa Gomes, *Fluid Phase Equilib.*, 2007, **257**, 27–34.
- 23 J. Jacquemin, P. Husson, V. Majer and M. F. Costa Gomes, *J. Solution Chem.*, 2007, **36**, 967–979.
- 24 J. Jacquemin, M. F. Costa Gomes, P. Husson and V. Majer, *J. Chem. Thermodyn.*, 2006, **38**, 490–502.
- 25 J. Jacquemin, P. Husson, V. Majer and M. F. Costa Gomes, *Fluid Phase Equilib.*, 2006, **240**, 87–95.
- 26 J. Kumelan, A. P.-S. Kamps, D. Tuma and G. Maurer, *J. Chem. Eng. Data*, 2006, **51**, 11–14.
- 27 J. H. Hildebrand, J. M. Prausnitz and R. L. Scott, *Regular and Related Solutions*, Van Nostrand Reinhold, New York, 1970.
- 28 J. Kumelan, A. P.-S. Kamps, D. Tuma and G. Maurer, *Fluid Phase Equilib.*, 2007, **260**, 3–8.
- 29 J. Kumelan, A. P.-S. Kamps, D. Tuma and G. Maurer, *J. Chem. Eng. Data*, 2006, **51**, 1364–1367.
- 30 W. Xu, L.-M. Wang, R. A. Nieman and C. A. Angell, *J. Phys. Chem. B*, 2003, **107**, 11749–11756.
- 31 C. Villagran, M. Deetlefs, W. R. Pitner and C. Hardacre, *Anal. Chem.*, 2004, **76**, 2118–2123.
- 32 P. Borg-Husson, V. Majer and M. F. Costa Gomes, *J. Chem. Eng. Data*, 2003, **48**, 480–485.
- 33 M. F. Costa Gomes, P. Husson, J. Jacquemin and V. Majer, *ACS Symp. Series Ionic Liquids III: Fundamentals, Progress, Challenges, and Opportunities*, ch. 16, ed. R. D. Rogers and K. R. Seddon, American Chemical Society Publications, Washington D.C., 2005.
- 34 M. F. Costa Gomes, *J. Chem. Eng. Data*, 2007, **52**, 472–475.
- 35 J. N. Canongia Lopes, M. F. Costa Gomes and A. A. H. Padua, *J. Phys. Chem. B*, 2006, **110**, 16816–16818.
- 36 A. A. H. Padua, M. F. Costa Gomes and J. N. A. Canongia Lopes, *Acc. Chem. Res.*, 2007, **40**, 1087–1096.
- 37 J. Deschamps, M. F. Costa Gomes and A. A. H. Padua, *ChemPhysChem*, 2004, **5**, 1049–1052.
- 38 J. Jacquemin, P. Ge, P. Nancarrow, D. Rooney, M. F. Costa Gomes, A. A. H. Padua and C. Hardacre, *J. Chem. Eng. Data*, 2008, **53**, 716–726.

Sulfonated polypyrrole nanospheres as a solid acid catalyst†

Xiaoning Tian,^a Fabing Su^b and X. S. Zhao^{*a}

Received 19th March 2008, Accepted 6th June 2008

First published as an Advance Article on the web 25th July 2008

DOI: 10.1039/b804743j

Polypyrrole nanospheres synthesized by using the ultrasonic method were sulfonated with concentrated H₂SO₄ at different temperatures. The catalytic performance of the sulfonated polypyrrole nanospheres in the esterification of methanol with acetic acid was evaluated and compared with that of sulfonated carbonized polypyrrole nanospheres. The surface chemistry and structure of the samples were investigated using X-ray diffraction, X-ray photoelectron spectroscopy, Fourier-transform infrared spectrometry, thermogravimetric analysis, nitrogen adsorption and elemental analysis techniques. The morphology of samples was characterized with field-emission scanning electron microscopy and transmission electron microscopy. The results showed that low carbonization and sulfonation temperatures are favorable for enhancing the catalytic activity and recyclability of the solid acid catalysts.

1. Introduction

Liquid sulfuric acid is widely used as a catalyst for many chemical reaction processes, such as hydration, esterification and hydrolysis. However, considering its toxicity, corrosiveness and the difficulty of separation from the reaction medium, environmentally friendly solid acid catalysts are highly desired. Recently, the sulfonation of solid materials such as incompletely carbonized polymers,¹ carbon nanotubes² and mesoporous silica^{3–5} has received a great deal of research attention because it is a potential approach to the preparation of novel solid acid catalysts.

Carbon-based solid sulfonic acid catalysts were first described by Hara and co-workers.¹ In their work, a carbon-based acid catalyst composed of small polycyclic aromatic carbon sheets with attached sulfonic acid groups (–SO₃H) was obtained by heating aromatic compounds (*e.g.*, naphthalene) in concentrated sulfuric acid. Lately, they employed sucrose as a carbon precursor to prepare carbon-based sulfonic acid catalysts and investigated their catalytic properties.^{6–8} Templated porous carbon materials were sulfonated and used as solid acid catalysts as well.^{9,10} Good stability and catalytic activity were observed when these carbons were prepared at high temperatures.

Polypyrrole (Ppy) synthesized by polymerization of pyrrole monomer in the presence of an oxidative catalyst is a technologically important, environmentally stable and biocompatible conducting polymer. In a recent study, we employed the ultrasonic method to prepare polypyrrole nanospheres (PNs) and carbonized polypyrrole nanospheres (CPNs).¹¹ In

this work, sulfonation of both PNs and CPNs was conducted to prepare sulfonated PNs (SPNs) and CPNs (SCPNs). The catalytic properties of the sulfonated materials were evaluated using the esterification of methanol with acetic acid. It was observed that the catalytic performance of the SPNs is better than that of the SCPNs, and the SPNs prepared at a lower sulfonation temperature possess a higher catalytic activity and a better recyclability.

2. Experimental

2.1. Preparation of PNs and CPNs

In a typical preparation, 4.0 g of decyl alcohol (1-decanol, 99%, Aldrich) and 120 ml of deionized water were mixed under stirring at room temperature for 40 min. Then, 6.0 g of dodecyltrimethylammonium bromide (DTAB, 99%, Aldrich) was added. After further stirring at 1 °C for 20 min, the emulsion system was transferred to an ultrasonicator (Elma Transsonic T460/H of capacity 2.75 litres and frequency of 35 kHz). Subsequently, 3.2 g of pyrrole (98%, Aldrich) was added dropwise. Polymerization was initiated by adding 8.0 g of FeCl₃ (99%, Aldrich). After ultrasonication for 3 h, the solid PNs were separated by filtration, washed with ethanol to remove the surfactant, and dried in an oven at 60 °C overnight. Carbonization of the PNs was conducted in a quartz tube under pure nitrogen flow (99.9995%, 50 cm³ min⁻¹) at a desired temperature for 5 h. The resultant carbonized PNs are denoted as CPNs(*x*), where *x* stands for the carbonization temperature.

2.2. Sulfonation of PNs and CPNs

0.3 g of PNs or CPNs was heated in 70 ml of concentrated H₂SO₄ (97%, Merck) at a given temperature (40–150 °C) for 4 h. After cooling down to room temperature, 1000 ml of ethanol was added. The black solid was collected by filtration, and washed repeatedly using ethanol until no sulfate ions were detected in the filtrate. The sulfonated PNs and CPNs are denoted as SPNs(*y*)

^aDepartment of Chemical and Biomolecular Engineering, National University of Singapore, 4 Engineering Drive 4, Singapore 117576. E-mail: chezxs@nus.edu.sg; Fax: +65-67791936; Tel: +65-65164727

^bApplied Catalysis, Institute of Chemical and Engineering Sciences, 1 Pesek Road, Jurong Island, Singapore 627833

† Electronic supplementary information (ESI) available: Fig. S1–S3 and Table S1: XRD, XPS, FTIR and TG analysis results. For ESI see DOI: 10.1039/b804743j

and SCPNs(x,y), respectively, where y stands for the sulfonation temperature.

The deactivation reasons for resultant catalysts were investigated by BaSO₄ sediment and UV techniques (UV-1601PC, UV-Visible spectrophotometer, Shimadzu).

2.3. Characterization

X-ray diffraction (XRD) patterns were collected on an XRD-6000 (Shimadzu, Japan) with Cu K α radiation ($\lambda = 0.15418$ nm). Field-emission scanning electron microscope (FESEM) images were obtained on a JSM-6700F (JEOL, Japan) operated at 10 kV. Field-emission transmission electron microscope images (HRTEM) were obtained from a JEM 2101F (JEOL, Japan) operated at 200 kV. X-ray photoelectron spectroscopy (XPS) spectra were recorded on an AXIS HIS 165 spectrometer (Kratos Analytical) with a monochromatized Al K α X-ray source. The operating pressure in the analysis chamber was maintained below 8×10^{-9} Torr. Wide-scan spectra in the binding energy range of 1100–0 eV were recorded in 1 eV step size with a pass energy of 80 eV. High resolution spectra of the C_{1s}, O_{1s}, S_{2p} and N_{1s} signals were recorded in a 0.05 eV step with a pass energy of 40 eV. The elemental compositions of the samples were analyzed using a CHNS-O Analyzer (FLASH EA 1112 series, Thermo electron corporation). Fourier-transform infrared (FT-IR) spectra were acquired using the KBr technique on a Bio-Rad FTS-3500 FT-IR (Digilab Instruments, USA) by averaging 64 scans in the frequency range of 400–4000 cm⁻¹ with a resolution of 4 cm⁻¹. The nitrogen adsorption/desorption isotherms were measured at the liquid-nitrogen temperature (–196 °C) on an automatic volumetric sorption analyzer (Quantachrome, NOVA1200). The specific surface areas of the samples were calculated using the Brunauer–Enmett–Teller (BET) method in the relative pressure range of 0.05–0.2.

2.4. Catalytic reactions

The catalytic properties of both SPNs and SCPNs were evaluated using the esterification of methanol with acetic acid. The reaction was carried out in a three-neck round bottom flask immersed in a silicon oil bath at 55 °C. 1.0 mol of methanol, 0.1 mol of acetic acid and 0.2 g of catalyst were added to the flask. After reaction for 5 h, the liquid phase was analyzed using a gas chromatograph (HP 6890 series GC) mass spectrometer (HP 5973 Mass selective detector) with a capillary column (HP 5MS, L 30 m, I.D. 0.25 mm, Film 0.25 μ m). After each reaction run, the catalyst was collected by filtration, washed with ethanol, and dried at 60 °C in an oven.

3. Results and discussion

3.1. FESEM observations

Fig. 1 shows the FESEM images of representative samples. It can be seen from Fig. 1a that the PN particles are spherical in shape with an average particle size of around 90 nm in diameter. Upon sulfonation at 40 °C (Fig. 1b), the particle surface and size are similar to that before sulfonation. When the sulfonation temperature was increased to 150 °C (Fig. 1c) to obtain sample SPNs(150), the particles became smaller

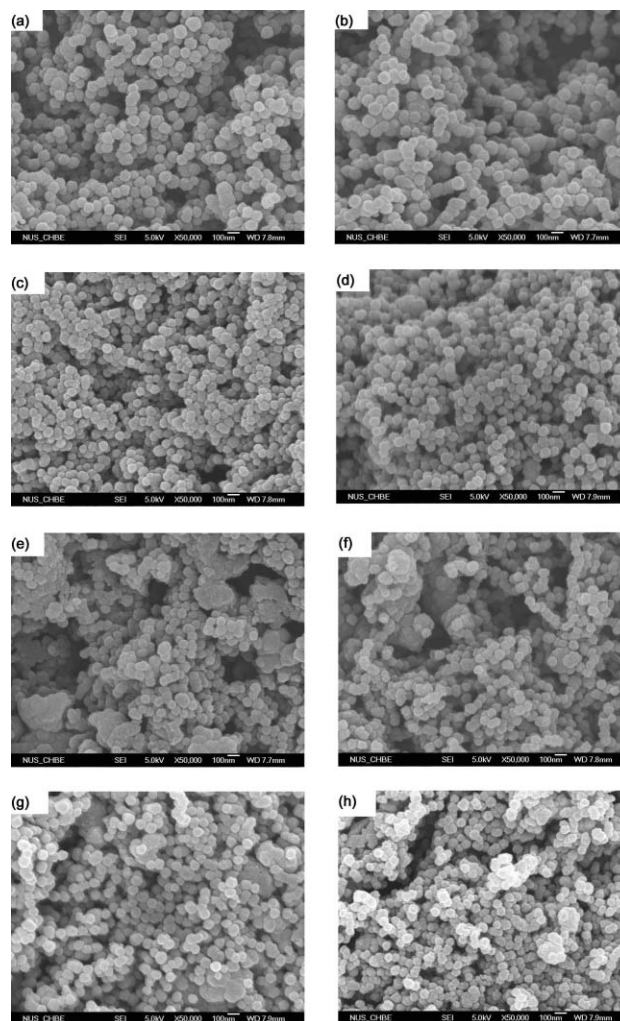


Fig. 1 FESEM images of (a) PNs, (b) SPNs(40), (c) SPNs(150), (d) SCPNs(400,40), (e) SCPNs(400,150), (f) SCPNs(900,150), (g) CPNs(400) and (h) CPNs(900).

with an average diameter of about 73 nm, showing that particle shrinkage occurred during the sulfonation process. The particle shrinkage is due to incomplete carbonization during the sulfonation process.¹ The particle diameters for samples CPNs(400) and CPNs(900) are about 77 and 74 nm, respectively, smaller than that of PNs but larger than that of SPNs(150). Such a shrinkage of PNs during carbonization is a result of the denitrogenation, dehydrogenation and aromatization in the carbonization process.¹² However, the particle diameters for SCPNs(400,40), SCPNs(400,150) and SCPNs(900,150) are similar to that of CPNs(400) and CPNs(900) (see Fig. 1g and h), indicating that sulfonation of CPNs carbonized in the temperature range of 400–900 °C did not lead to obvious particle shrinkage.

3.2. HRTEM observations

Fig. 2 shows the HRTEM images of SCPNs(400,150) and SCPNs(900,150). The increase of graphene stacking degree can be detected by the HRTEM technique. Graphene sheets can be clearly seen on sample SCPNs(900,150) (see Fig. 2a). In contrast, no obvious graphene layer can be found on sample

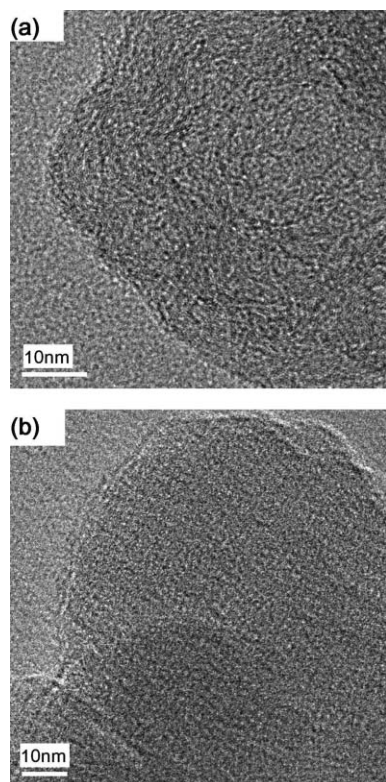


Fig. 2 HRTEM images of (a) SCPNs(900,150) and (b) SCPNs(400,150).

SCPNs(400,150) (see Fig. 2b). The increase of graphene stacking degree indicates that SCPNs(900,150) possesses a more compact structure than SCPNs(400,150) due to the higher carbonization temperature. However, the compact structure can be hardly sulfonated and the attached $-\text{SO}_3\text{H}$ groups are unstable.¹

The XRD patterns of samples PNs and SPNs(40) shown in Fig. S1 exhibit a broad peak at around $2\theta = 25^\circ$, indicating an amorphous structure, consistent with the previous report.¹³ The XRD pattern of sample SPNs(150) (see Fig. S1c†) shows a peak at $2\theta = 25^\circ$ with a slightly stronger intensity than that of PNs and SPNs(40), showing a more compact structure because of the higher sulfonation temperature, in agreement with the FE-SEM observation. The two carbonized samples, SCPNs(400,40) (Fig. S1d†) and SCPNs(400,150) (Fig. S1e†), possess a broad and low peak at around $2\theta = 25^\circ$, which is assigned to the (002) reflection of carbon material, indicating the low crystallinity. The peak for SCPNs(900,150) (Fig. S1f†) is higher than that of SCPNs(400,40) and SCPNs(400,150), indicating the increase of graphene stacking degree caused by the enhancement of carbonization temperature.¹⁴

3.3. XPS analysis

Shown in Fig. 3A are the N_{1s} XPS spectra of samples PNs, CPNs(400), CPNs(900), and SCPNs(900,150). The N_{1s} spectrum of sample PNs depicted in Fig. 3A-a shows one peak at a BE of 399.1 eV, corresponding to the N atoms within the pentagonal pyrrole rings of the Ppy.¹¹ However, the N_{1s} spectra of samples CPNs(900) and SCPNs(900,150) display two peaks, one at about 397.8 eV, corresponding to pyridine-type N atoms

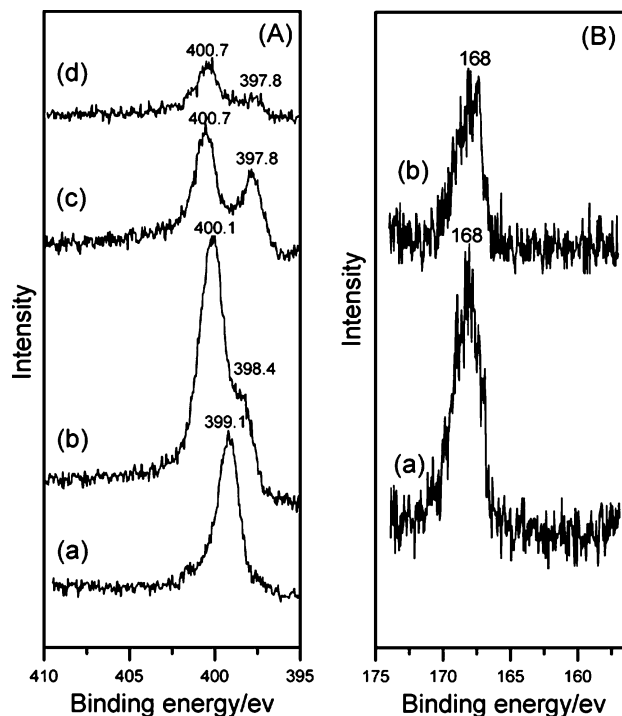


Fig. 3 (A) N_{1s} XPS spectra of (a) PNs, (b) CPNs(400), (c) CPNs(900), and (d) SCPNs(900,150) and (B) S_{2p} XPS spectra of (a) SPNs(40) and (b) SPNs(40) after the 4th reaction run.

at the edge of graphene sheets, and the other one at about 400.7 eV, associated with the quaternary N atoms incorporated in graphene sheets.^{11,15–17} These two peaks for sample CPNs(400) had a little shift compared with that of CPNs(900) and the peak according to N atoms at the edge of the graphene sheets is weaker than that of CPNs(900), indicating more graphene sheets exist in CPNs(900) than in CPNs(400). The above XPS results suggest that during the carbonization process pentagonal pyrrole rings had transferred to hexagonal carbon rings, which are the primary building units of graphene sheet. At the same time, the size of graphene sheets increased and many more graphene sheets stacked closely to form a more compact structure with the increase of carbonization temperature. It can be assumed that the graphitization degree increases with the increase in carbonization temperature and the backbone of the resultant material was transformed from polymer to carbon during the carbonization process.

Shown in Fig. 3B are the S_{2p} XPS spectra for sample SPNs(40) before the reaction and after the 4th reaction run. Both of the XPS spectra exhibit a single S_{2p} peak at 168 eV, attributed to S atoms in $-\text{SO}_3\text{H}$,¹ showing the presence of $-\text{SO}_3\text{H}$ groups in the samples. It can be seen that the S_{2p} peak for SPNs(40) is higher than that of SPNs(40) after the 4th reaction run, indicating the decrease of $-\text{SO}_3\text{H}$ groups after the 4th reaction run.

3.4. FT-IR spectra

Fig. 4 shows the FTIR spectra of the samples. The peak at around 1548 cm^{-1} (also see Fig. S2†) is attributed to the C=C stretching vibration of pyrrole.¹⁸ The peaks at 1708 and 1300 cm^{-1} are assigned to C=N and C–N vibrations in Ppy.¹⁸ Sample SPNs(40) before the reaction and after the 4th reaction

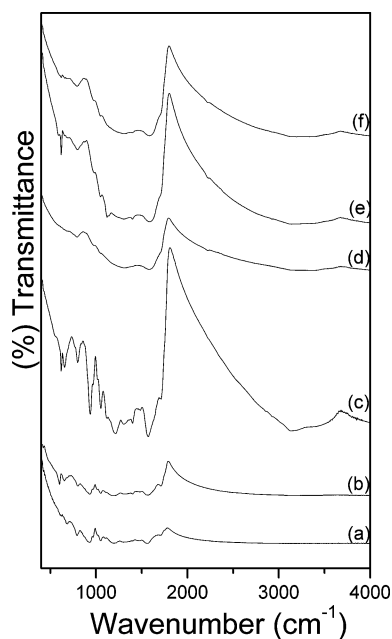


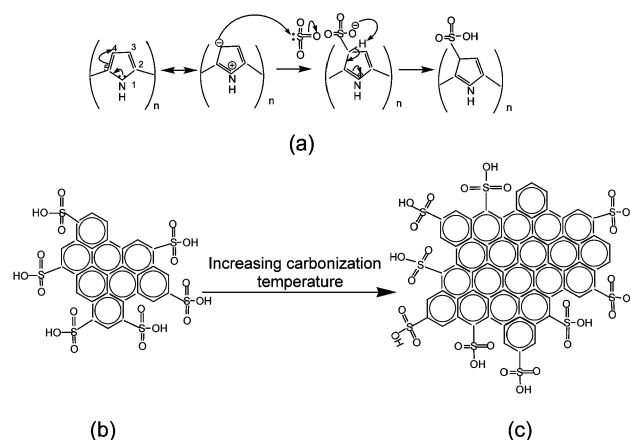
Fig. 4 FTIR spectra of (a) PNs, (b) SPNs(40), (c) SPNs 40 after the 4th reaction run, (d) CPNs(400), (e) SCPNs(400,40) and (f) SCPNs(400,40) after the 4th reaction run.

run exhibits a peak at around 1044 cm^{-1} (see Fig. S2†), which is due to the symmetric $\text{O}=\text{S}=\text{O}$ stretching vibrations, showing the presence of $-\text{SO}_3\text{H}$ groups. The peaks at around 798 and 650 cm^{-1} are responsible for $\text{S}-\text{O}$ and $\text{C}-\text{S}$ stretching vibrations, respectively.¹⁸ After the 4th reaction run, catalyst SPNs(40) still possessed these peaks, indicating a good catalyst recyclability of SPNs(40).

For sample CPNs(400), SCPNs(400,40) and SCPNs(400,40) after the 4th reaction run, the peak for $\text{C}=\text{C}$ also can be seen from Fig. 4. However, the peaks attributed to $\text{C}=\text{N}$ and $\text{C}-\text{N}$ are not obvious. The peaks at 1044 , 798 and 650 cm^{-1} attributed to $\text{O}=\text{S}=\text{O}$, $\text{S}-\text{O}$ and $\text{C}-\text{S}$, respectively, for sample SCPNs(400,40) can also be seen clearly from Fig. 4e. However, these three peaks are much weaker for sample SCPNs(400,40) after the 4th reaction run (see Fig. 4f), indicating the lose of the $-\text{SO}_3\text{H}$ group.

4. The formation of the $-\text{SO}_3\text{H}$ group

Sahin and Okamura have proved that $-\text{SO}_3\text{H}$ groups are attached on the C atom of carbon sheets both on the pentagonal pyrrole rings¹⁹ and hexagonal carbon rings.⁶ This attachment of the $-\text{SO}_3\text{H}$ group on the C atom can be confirmed by the FTIR spectra. The FTIR spectra of SPNs(40) (Fig. 4b) and SCPNs(400,40) (Fig. 4e) show the $\text{S}-\text{O}$ and $\text{O}=\text{S}=\text{O}$ stretching vibrations, indicating the existence of $-\text{SO}_3\text{H}$ groups. The stretching vibration of $\text{C}-\text{S}$ for SPNs(40) and SCPNs(400,40) were also detectable, confirming that $-\text{SO}_3\text{H}$ groups were attached on the C atom both on the pentagonal pyrrole rings (Scheme 1a) and on the hexagonal carbon rings (Scheme 1b).



Scheme 1 The formation of $-\text{SO}_3\text{H}$ groups on (a) a pentagonal pyrrole ring, (b) a small carbon sheet and (c) a big carbon sheet.

As discussed above, the pentagonal pyrrole rings were transferred to the hexagonal carbon rings, resulting in the bulk of catalysts transforming from polymer to carbon during the carbonization process. The compact graphene structure appeared under the higher-temperature carbonization process. The $-\text{SO}_3\text{H}$ groups can be attached only on the edge of carbon sheets.⁶ However, the carbon sheet will grow with the increase in the carbonization temperature, as shown in Scheme 1b and c. Therefore, the S content decreased with the increase in the carbonization temperature (Table 1).

Table 1 Elemental compositions of samples analyzed using the CHNS technique

Sample	C (wt%)	N (wt%)	O (wt%)	S (wt%)	H (wt%)
PNs	47.0	14.6	35.3	0	2.9
SPNs(40)	40.8	13.1	34.9	8.0	3.2
SPNs(40) after the 4th run	47.1	11.6	35.4	2.2	3.7
SPNs 55	42.5	13.5	33.7	6.9	3.4
SPNs(55) after the 4th run	47.4	14.3	30.6	4.4	3.3
SPNs(70)	42.0	13.2	34.9	6.9	3.0
SPNs(70) after the 4th run	46.0	13.5	32.0	5.3	3.2
SPNs(150)	47.3	13.3	34.2	2.6	2.6
SPNs(150) after the 4th run	48.7	13.3	34.3	1.1	2.5
CPNs(400)	62.7	17.4	26.4	0	2.5
SCPNs(400,40)	54.0	15.0	26.4	2.2	2.4
SCPNs(400,40) after the 4th run	55.8	15.3	25.2	1.1	2.6
SCPNs(400,150)	49.8	12.9	32.8	1.8	2.7
SCPNs(400,150) after the 4th run	52.3	13.7	30.6	0.6	2.8
CPNs(900)	58.5	4.1	36.4	0	1.0
SCPNs(900,150)	72.6	5.5	18.9	2.0	1.0

5. Catalytic performance

According to Okamura *et al.*,⁶ sulfonated carbons contain $-\text{SO}_3\text{H}$ groups, and all S atoms exist in the $-\text{SO}_3\text{H}$ groups. Therefore, the more the S content and the more stable the $-\text{SO}_3\text{H}$ groups, the higher the catalytic activity and the better the recyclability. It can be seen from Table 1 that the S content for prepared catalysts decreased with the increase of sulfonation and carbonization temperatures. Therefore, the activity and recyclability for the polymer-based catalysts decreased with the increase in sulfonation temperature, while the activity and recyclability for the carbon-based catalysts decreased with the increase in both carbonization and sulfonation temperatures.

It is also seen from Table 1 that the S content detected using the CHNS method is higher than that measured using the XPS technique (see Table S1†), indicating that $-\text{SO}_3\text{H}$ groups were attached on both the surface and bulk of the samples. Comparing the S contents in Table 1 and Table S1,† one can see that after the 4th reaction run the decrease on the bulk S content is almost equal to that of the surface S content expected for sample SPNs(40). Therefore, it can be concluded that the decrease in the S content is mainly caused by the loss of the surface-attached $-\text{SO}_3\text{H}$ groups.

Sample SPNs(40) shows the highest S content, which accounts for the highest catalytic activity (Fig. 5). While the S content for SPNs(40) after the 4th reaction run decreased greatly, its recyclability was the best among the catalysts studied. On the other hand, although the S contents of samples SPNs(55) and SPNs(70) after the 4th reaction run were higher than that of SPNs(40), their recyclabilities were worse than that of SPNs(40). As discussed above, particle shrinkage occurred during the sulfonation and carbonization processes at relatively high temperatures. Those $-\text{SO}_3\text{H}$ groups attached in shrunken bulk spheres are hardly accessible to the reactants,⁶ thus causing the observed bad recyclability. However, the $-\text{SO}_3\text{H}$ groups attached on both surface and bulk of sample SPNs(40), which has a more flexible structure due to the lower sulfonation temperature, can be easily reached by the reactants.

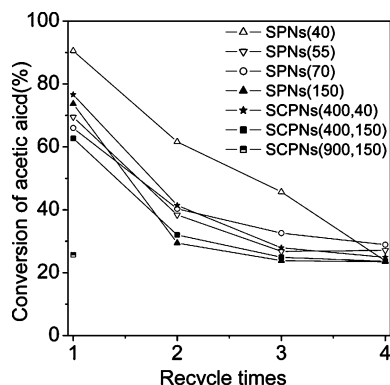


Fig. 5 Catalytic conversion of acetic acid over various catalysts.

The carbon-based catalyst, SCPNs(900,150), displayed the lowest S content among all of the CPNs samples, showing it was hard to sulfonate. While both CPNs(400,150) and CPNs(900,150) possessed similar bulk and surface S contents (see Table 1), the catalytic activity and recyclability

of CPNs(900,150) were worse than that of CPNs(400,150), indicating the unstable attachment of the $-\text{SO}_3\text{H}$ group on CPNs(900,150). Therefore, it can be concluded that graphene sheets are hard to sulfonate and the $-\text{SO}_3\text{H}$ groups attached on graphene sheets are unstable.¹ SCPNs(400,40) showed a better activity and recyclability than SCPNs(400,150) because of the higher sulfonation temperature used in preparing the latter.

Fig. 5 shows the catalytic conversion of acetic acid of various catalysts after the first, second, third and fourth reaction runs. It is seen that the catalytic activity decreased with the number of recycles. For the polymer-based catalysts there are two main reasons for the deactivation. One is the hydrolysis of $-\text{SO}_3\text{H}$ groups,^{19,20} which can be detected by using BaCl_2 .²² The other one is the leaching of polycyclic pentagonal pyrrole rings, similar to the leaching of polycyclic aromatic hydrocarbons,²¹ which can be detected by using the UV technique.²³ For the carbon-based sulfonic acid catalysts, the main reason for the deactivation is the hydrolysis of $-\text{SO}_3\text{H}$ groups. From the data of surface area for the resultant sample (Table S1†), we can see that the surface area of prepared polymer and carbon based catalysts decreased after sulfonation and then increased after the 4th reaction run, except for sample SCPNs(400,150). Therefore, pore blockage is not the main reason for deactivation.

6. Conclusions

In summary, we have demonstrated the potential of using sulfonated polypyrrole nanospheres and carbonized polypyrrole nanospheres as a solid sulfonic acid catalyst. For the polymer-based solid catalysts, the high temperature sulfonation reaction was an incomplete carbonization process that would result in a compact structure, and this compact structure impeded the transport of reactants to the bulk active sites. Therefore, SPNs created under low sulfonation temperature showed the best activity and recyclability. For carbon-based acid catalysts, the stability of the attached $-\text{SO}_3\text{H}$ groups decreased with the increase of carbonization and sulfonation temperature, since the high temperature carbonization process can introduce compact graphene structures. The low carbonization and sulfonation temperature may be more helpful in enhancing the activity and recyclability of solid acid catalysts derived from polypyrrole in the esterification reaction of methanol with acetic acid.

Acknowledgements

This work was financially supported by Ministry of Education's AcRF Tier 1 funding (grant number R279000235112).

References

- M. Hara, T. Yoshida, A. Takagaki, T. Takata, J. N. Kondo, S. Hayashi and K. Domen, *Angew. Chem., Int. Ed.*, 2004, **43**, 2955.
- F. Peng, L. Zhang, H. Wang, P. Lv and H. Yu, *Carbon*, 2005, **43**, 2397.
- W. M. Van Rhijn, D. E. De Vos, B. F. Sels, W. D. Bossaert and P. A. Jacobs, *Chem. Commun.*, 1998, **3**, 317.
- W. D. Bossaert, D. E. De Vos, W. M. Van Rhijn, J. Bullen, P. J. Grobet and P. A. Jacobs, *J. Catal.*, 1999, **182**, 156.
- K. Wilson, A. F. Lee, D. J. Macquarrie and J. H. Clark, *Appl. Catal.*, 2002, **228**, 127.
- M. Okamura, A. Takagaki, M. Toda, J. N. Kondo, K. Domen, T. Tatsumi, M. Hara and S. Hayashi, *Chem. Mater.*, 2006, **18**, 3039.

- 7 M. Toda, A. Takagaki, M. Okamura, J. N. Kondo, S. Hayashi, K. Domen and M. Hara, *Nature*, 2005, **438**, 178.
- 8 A. Takagaki, M. Toda, M. Okamura, J. N. Kodo, S. Hayashi, K. Domen and M. Hara, *Catal. Today*, 2006, **116**, 157.
- 9 X. Wang, R. Liu, M. M. Waje, Z. Chen, Y. Yan, K. N. Bozhilov and P. Feng, *Chem. Mater.*, 2007, **19**, 2395.
- 10 R. Xing, Y. Liu, Y. Wang, L. Chen, H. Wu, Y. Jiang, M. He and P. Wu, *Microporous Mesoporous Mater.*, 2007, **105**, 41.
- 11 Y. Wang, F. Su, C. D. Wood, J. Y. Lee and X. S. Zhao, *Ind. Eng. Chem. Res.*, 2008, **47**, 2294.
- 12 J. Jang, J. H. Oh and X. L. Li, *J. Mater. Chem.*, 2004, **14**, 2872.
- 13 Y. S. Chen, Y. Li, H. C. Wang and M. J. Yang, *Carbon*, 2007, **45**, 357.
- 14 J. Jang, J. H. Oh and L. Xiang, *J. Mater. Chem.*, 2004, **14**, 2872.
- 15 F. Su, X. S. Zhao, Y. Wang, L. Wang and J. Y. Lee, *J. Mater. Chem.*, 2006, **16**, 4413.
- 16 P. X. Hou, H. Orikasa, T. Yamazaki, K. Matsuoka, A. Tomita, N. Setoyama, Y. Fukushima and T. Kyotani, *Chem. Mater.*, 2005, **17**, 5187.
- 17 F. Su, X. S. Zhao, L. Lv and Z. Zhou, *Carbon*, 2004, **42**, 2821.
- 18 Y. Sahin, A. Aydin, Y. A. Udum, K. Pekmez and A. Yildiz, *J. Appl. Polym. Sci.*, 2004, **93**, 526.
- 19 J. M. Aragon, J. M. R. Vegas and L. G. Jodra, *Ind. Eng. Chem. Res.*, 1994, **33**, 592.
- 20 L. Petrus, E. J. Stamhuls and G. E. H. Joosten, *Ind. Eng. Chem. Prod. Res. Dev.*, 1981, **20**, 366.
- 21 X. Mo, D. E. Lopez, K. Suwannakarn, Y. Liu, E. Lotero, J. G. G., Jr. and C. Lu, *J. Catal.*, 2008, **254**, 332.
- 22 The hydrolysis of sulfonate groups was examined by using a BaCl₂ solution, which was added to the liquid phase after catalytic reaction. White precipitate BaSO₄ was immediately observed, showing the presence of sulfonate groups in the liquid phase, and thus the leaching of sulfonate groups from the catalyst. It was observed that both the polymer-based and the carbon-based solid sulfonic acid catalysts suffered from hydrolysis of sulfonate groups. This is one of the reasons for catalyst deactivation.
- 23 The decomposition of the sulfonated solid catalysts was characterized using the UV-Vis technique. It was experimentally observed that the mixture of pyrrole monomer, methanol, acetic acid and methylacetate showed a UV peak at around 253 nm. For the liquid phase after catalytic reaction, a peak at about 265 nm was seen. This peak can be attributed to polymerized pyrrole segments. The liquid phases after the first, second, third and fourth catalytic reaction runs in the presence of catalyst SPNs(40) all displayed the 265 nm peak, showing the decomposition of polypyrrole during the catalytic reaction. However, the 265 nm peak was very weak for the liquid phase after the first reaction run in the presence of catalyst SPNs(900,150), showing negligible decomposition of the carbon based catalyst.

Aqueous sol-gel routes to bio-composite capsules and gels†

Namia Benmouhoub,^{a,b} Nicolas Simmonet,^b Nouria Agoudjil^a and Thibaud Coradin^{*b,c}

Received 14th April 2008, Accepted 9th June 2008

First published as an Advance Article on the web 31st July 2008

DOI: 10.1039/b806313c

Due to their solvent-free chemistry and low environmental impact, aqueous silicates appear as promising alternative precursors to silicon alkoxides for the development of a greener sol-gel process. In this context, aqueous routes to silica/biopolymer composite materials are described here, allowing the formation of silica-coated agarose capsules and hybrid silica/carboxymethyl-cellulose hybrid gels. Infra-red spectroscopy and thermogravimetric analyses suggest that the silica-polymer interface is controlled by hydrogen bond formation. In addition, scanning electron microscopy suggests limited modification of the agarose surface and of carboxymethylcellulose network organization. However, the presence of silica has a significant impact on the release of rhodamine B, a cationic dye, from the biocomposites. These materials not only comply with several requirements of Green Chemistry but also open new perspectives in the field of hybrid drug carrier design and plant silicification mimicry.

Introduction

Since the establishment of the Green Chemistry principles, the contribution of inorganic materials to this domain has mainly consisted in the development of more efficient heterogeneous catalysts for improving the yields of organic reactions (9th principle).¹ In contrast, very few studies have been devoted to the green synthesis of inorganic materials.² One main reason is that glasses and ceramics are usually obtained at high temperature and/or high pressure, from inorganic powders, so that the possibility to improve these processes from a 'green' point of view appears rather limited. However, in the case of nanocomposites and/or hybrid materials, where the inorganic phase is usually formed in mild conditions (soft chemistry, sol-gel, ...) and in the presence of (bio)-organic systems, recent examples suggest that there is plenty of room to design alternative, eco-friendly processes.³⁻⁴

Traditional sol-gel chemistry makes use of metal alkoxides $M(OR)_n$. However, these precursors are synthetic molecules obtained by organic/organometallic chemistry involving the use of solvents and release of toxic by-products.⁵ In contrast, it is possible to perform sol-gel chemistry from aqueous salts but their reactivity is usually more difficult to control.⁶ In the case of silica, the most widespread material obtained *via* sol-gel reactions, these aqueous precursors consist of alkaline

silicate solutions, also called 'waterglass', that are obtained from siliceous sand in basic conditions.⁷ Silicates therefore constitute a cheap source of silica precursors obtained from a widely available natural resource. Moreover, their toxicity is weak and their presence in the environment of limited impact.⁸ It was therefore recently proposed that the use of aqueous silicates as an alternative to silicon alkoxides could contribute to the development of a greener sol-gel chemistry.⁹

Many bio-composites associating natural macromolecules and silica have already been described with potential applications in biotechnology and medicine.¹⁰ These biocomposites can be obtained either by the silicification of a pre-formed biopolymer-based material¹¹ or from silica precursor/biopolymer mixed solutions.¹² Until now, most of these processes involves silicon alkoxides and much less has been done using aqueous silicates.^{9,10} However, it was already demonstrated that silicate-based materials and, on a more general level, aqueous sol-gel processes were particularly well-adapted for the design of cell-containing materials.¹³

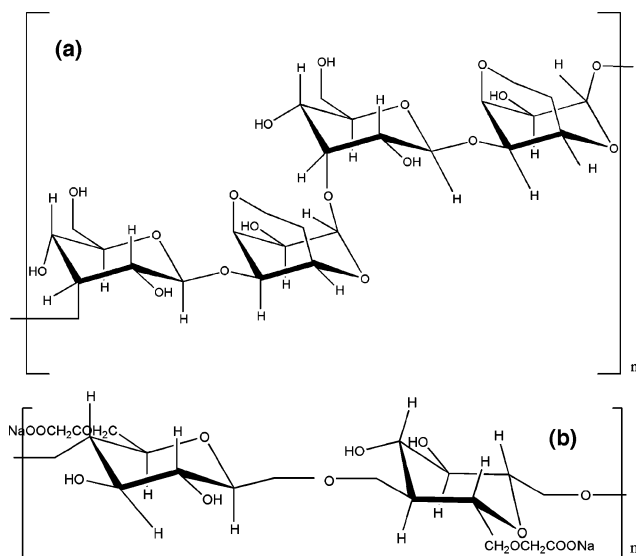
Herein, we describe the synthesis of two novel biocomposite systems through the controlled association of polysaccharides, agarose and carboxymethylcellulose (CMC) (Scheme 1) with silicates. The first system consists of pre-formed agarose capsules coated with silica. In fact, similar capsules have already been described with polylysine-coated alginic acid and gelatin beads.¹⁴ However, in both cases, the deposition of the silica layer was favoured by electrostatic interactions between the negatively-charged silicates and the positively-charged surface of the capsule. In contrast, the direct deposition of silicates on uncharged capsules have never been reported so far. The second system consists of hybrid gels obtained from CMC/silicate mixtures. Indeed, Shchipunov and Karpenko already described the formation of bio-composite formed by associating several biopolymers with silicon alkoxides.¹⁵ However, the substitution of alkoxides by silicates is challenging, as the reactivity of aqueous precursors towards bio-macromolecules may strongly

^aLaboratoire de physico-chimie des matériaux et application à l'environnement, Faculté de Chimie, USTHB, BP 32, 16111, El-Alia, Bab-Ezouar, Alger, Algeria

^bUPMC Univ Paris 06, UMR 7574, Chimie de la Matière Condensée de Paris, F-75005, Paris, France

^cCNRS Univ Paris 06, UMR 7574, Chimie de la Matière Condensée de Paris, F-75005, Paris, France. E-mail: thibaud.coradin@upmc.fr; Fax: +33 1 44274769; Tel: +33 1 44275517

† Electronic supplementary information (ESI) available: TGA curve of the initial CMC powder; TGA curves of selected SiO_2 /CMC systems; selected SEM images of silica-coated beads. See DOI: 10.1039/b806313c



Scheme 1 Chemical structures of (a) agarose and (b) carboxymethylcellulose (CMC).

differ from that of organosilanes,⁵⁻⁷ leading in many instances to the precipitation of silica/biopolymer aggregates rather than to bulk material formation.⁹ In both cases, the identification of the mechanisms by which silicates can interact with neutral and negatively charged biopolymers would significantly extend the range of macromolecules that could be associated with silicates for a rational design of functional bio-composites.

We show that silicates can interact with these two polysaccharides and form hybrid silica/biopolymer materials. In the case of agarose capsules, a hybrid membrane is formed that leads to the modification of the capsule diffusion properties. The condensation of silicates within a CMC solution leads to hybrid gels whose stability and affinity for a cationic dye can be tailored. In both cases, the possibility for silicates to form hydrogen bonds with the biopolymer is suggested to be responsible for the cohesion of the composite structure. Overall, these results indicate that aqueous silicates are attractive alternative precursors to silicon alkoxides for the design of hybrid materials in the context of green material chemistry and, more specifically, well-adapted to aqueous sol-gel routes for the design of novel bio-composites.

Experimental

Silica-coated agarose capsule synthesis

The synthesis of agarose capsules was performed by adaptation of the Zvitov method.¹⁶ Agarose Type I-B (gel point (1.5 wt%) = 36 ± 1.5 °C, melting temperature = 87 ± 2 °C, from Sigma) with high gel strength and low sulfate content was selected to favor capsule stability and avoid the occurrence of negative charges on the bead surface. An agarose aqueous solution, 2.5 wt%, was prepared by dissolving the polymer powder in water at 80 °C. This solution was added dropwise through a 0.9 mm needle to a 250 mL beaker placed in an ice bath at 5 °C and containing 100 mL of water topped with a 5 mm thick hexane layer. This solution was maintained under moderate stirring (*i.e.* without perturbation of the hexane layer) during addition and

for another 15 min. The obtained capsules were left to settle and the hexane layer carefully withdrawn. Capsules were then recovered by paper filtration. The silica coating was performed by adding the agarose beads to silicate solutions (10% NaOH, 27% SiO₂ from Riedel-de Haen) at various pH and concentration under mild stirring.

Silica/CMC hybrid gel synthesis

The synthesis of silica-CMC hybrid gels was performed by dissolving the carboxymethylcellulose, sodium salt powder (Sigma-Aldrich, $M_w = 250\,000\text{ g mol}^{-1}$, degree of substitution = 1.20) in a silicate solution at pH 7 in a phosphate buffer saline (PBS, 25 mM phosphate buffer, 300 mM NaCl) under stirring and moderate heating (30 °C). The final CMC concentration was 10 wt% and the SiO₂ : CMC weight ratio was varied between 2 wt% and 10 wt%. The stirring was maintained over 3.5 h and the resulting solutions/gels were left for 24 h in the fridge before characterization.

Characterization

All samples were freeze-dried before characterization. X-ray energy dispersive spectrometry (EDX) was performed using a IXRF system intergrated to a JEOL JSM-5510LV scanning electron microscope (SEM) operating at 20 kV. Atomic compositions (At%) were obtained using the IXRF software from multiple analyses of 10 μm × 10 μm area. Infra-red (IR) spectra of samples diluted in KBr pellets were recorded on a Nicolet Magna IR-550 spectrophotometer. Thermogravimetric analyses (TGA) were performed on a NETZCH STA 409 apparatus with a 5.0 °C min⁻¹ heating step under Ar atmosphere.

Release properties

Uncoated and coated agarose beads were impregnated for 30 min in a 0.1 mg ml⁻¹ rhodamine B aqueous solution. After filtration, 50 beads were placed in 30 mL of water or in 30 mL of a 100 mM silicate solution at pH 7. The kinetics of rhodamine B release was followed by sampling 100 mL of the solution, adding 2.4 mL of water and measuring the optical density at λ = 554 nm using a Uvikon XS UV-visible spectrophotometer.

These data were fitted using an analytical solution of the second Fick law previously developed for polymer microspheres (eqn (1)):¹⁷

$$\frac{M_{\infty} - M_t}{M_{\infty}} = \frac{6}{\pi^2} \sum_{n=1}^{\infty} \frac{1}{n^2} \exp\left(-\frac{n^2 \pi^2}{R^2} Dt\right) \quad (1)$$

with M_{∞} and M_t being the cumulated amount of released dye at equilibrium and time t , respectively, R corresponding to the capsule radius and D is the apparent diffusion coefficient of the dye within the capsules.

Silica/CMC hybrid materials incorporating rhodamine B were prepared as described above except for the presence of the dye at a 1.2 mg L⁻¹ concentration in the PBS solution. After 24 h ageing in the fridge, 4 mL of PBS was deposited over the gel surface and the dye release was monitored using a similar method.

Due to the low volume fraction between the gel and the supernatant, these data were fitted using a model initially developed for a solid/liquid extraction process (eqn (2)):¹⁸

$$C_s = K_1(1 - e^{-k_2 t}) \quad (2)$$

with

$$K_1 = \frac{k_1 C_g^0}{K_2} \text{ and } K_2 = k_2 + 2k_1 \quad (3)$$

with k_1 and k_2 corresponding to the first order kinetic constant of dye transfer from the gel to the supernatant (extraction) and from the supernatant to the gel (sorption), respectively and C_g^0 is the initial dye concentration in the gel.

Results and discussion

Silica-coated agarose capsules

Agarose capsule preparation

Agarose was selected as a model biopolymer in order to evaluate the possibility to coat macrocapsules with neutral surfaces in conditions similar to our previous reports.¹⁴ Agarose is a common, cheap natural polymer exhibiting thermoreversible gelation properties that can be easily shaped as films or particles, with wide applications in biotechnology.¹⁹

The principle of agarose beads preparation, as described by Zvitov and Nussinovitch,¹⁶ is the following: the agarose solution is prepared by dissolution of the polymer powder above its melting point. It is then added dropwise to a cold water solution covered by an hexane layer. The low temperature allows the agarose hydrogel to form whereas the hexane layer avoids the spreading of the agarose droplet during the few milliseconds that are necessary for the thermotropic sol-gel transition to occur (*i.e.* from 90 °C to 36 °C, corresponding to the gel point).

However, it was found that several parameters had to be optimized. The polymer concentration impacts on solution viscosity, gel point and capsule stability. For concentrations higher than 2.5 wt%, the high viscosity renders the solution difficult to extrude through the needle and leads to elongated drops sometimes presenting a tail-like extension. For concentrations below 2 wt%, the polymer sol-gel transition was too slow and the resulting beads too soft to obtain spherical particles. Another key parameter was the hexane layer thickness. Above 5 mm, the capsules are formed within the organic phase and tend to aggregate due to the hydrophobic nature of the solvent. Thinner layers do not allow a sufficient resident time for the hydrogel to form and flat, uneven particles are recovered.

The capsules obtained after optimization of the procedure are shown in Fig. 1. Spherical beads *ca.* 2.5 mm (\pm 0.5 mm) in diameter are recovered (Fig. 1a). Freeze-dried capsules show very similar dimensions, suggesting a limited shrinkage during water withdrawal (Fig. 1b). The capsule surface appears wrinkled with a network of polymer fibers and layers (Fig. 1c). At higher magnification, the wrinkled surface appears rather smooth (Fig. 1d).

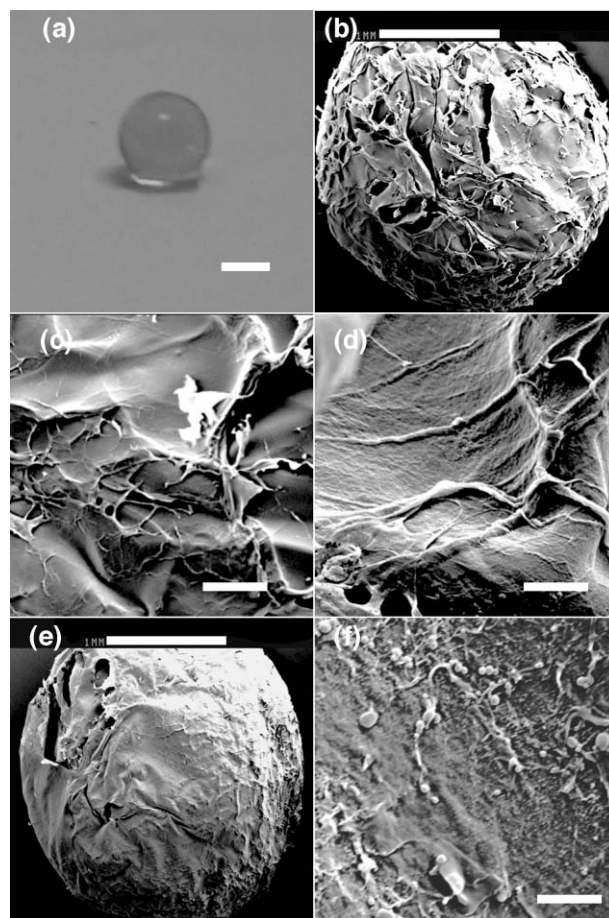


Fig. 1 (a) Photograph of wet agarose beads (scale bar = 1 mm). (b) SEM image of a freeze-dried agarose capsule (scale bar = 1 mm). (c), (d) SEM images of agarose bead surface (scale bars = 100 μ m and 10 μ m respectively). (e), (f) SEM images of silica-coated agarose beads (pH 5, 100 mM silicates, 5 h reaction time) (scale bars = 1 mm and 10 μ m, respectively).

Silica coating of agarose beads

For silica deposition, agarose beads were placed in a silicate solution. Silicate concentrations were varied between 50 and 200 mM since higher concentrations would lead to silica formation in the whole solution volume. Considering pH conditions, it has already been suggested elsewhere⁹ that a balance has to be found between neutral or slightly alkaline conditions where silicates bear a significant negative charge and have a strong tendency to react one with another through condensation, at the detriment of their interaction with the biopolymer, and slightly acid conditions where condensation is slow and silicates are more available to interact with the macromolecules. In the present case, where hydrogen bonding is the main kind of interaction that should arise between agarose and silica precursors, more acidic conditions lead to higher silanol-to-silanolate ratios⁷ and are therefore expected to be more favourable to silica deposition. Hence, two pH conditions, *i.e.* pH = 5 and 7, were evaluated. Finally, the reaction time was varied between 1 h and 5 h.

After 5 h reaction time, whatever the silicate concentration and pH value, the modification of the capsule surface as observed by SEM suggested the presence of a silica coating.

At low magnification, the surface appears more contrasted and smoother than pristine agarose beads with wrinkles and fibers being less apparent (Fig. 1e, to be compared with Fig. 1b). At higher magnification, the presence of particles *ca* 0.2 μm –2 μm in diameter is observed together with a network of fibers/layers that appear coated with a granular deposit (Fig. 1f and ESI†).

In these conditions, the presence of silica could be confirmed by IR studies (Fig. 2). After contact with silicates, the main modifications of the agarose beads IR spectra are the following: (i) in the 3300–3600 cm^{-1} region, the vibration bands at 3580 cm^{-1} and 3330 cm^{-1} (OH (agarose) stretching mode)²⁰ are now modified by the presence of Si–OH groups as well as the result of a modification of the OH bond network; (ii) in the 1000–1260 cm^{-1} region, the agarose vibration bands 1160 cm^{-1} (C–O stretching mode), 1080 cm^{-1} (glycosidic link) appear to overlap with triply degenerated stretching vibration mode of the $[\text{SiO}_4]$ tetrahedron (1100 cm^{-1}).²¹ The presence of the 945 cm^{-1} Si–OH mode and the 800 cm^{-1} inter-tetrahedral Si–O–Si bending vibration mode are difficult to ascertain due to their weak intensity and proximity with the 930 cm^{-1} (corresponding to 3,6-anhydrogalactose) and 890 cm^{-1} (CH bending of the β -anomeric carbon) bands of agarose. Finally, the presence of a band at 480 cm^{-1} corresponding to the bending vibration mode of the $[\text{SiO}_4]$ tetrahedron suggests silica formation, although agarose exhibits a vibration band of similar intensity at 520 cm^{-1} .

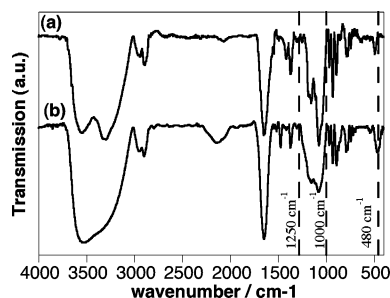


Fig. 2 Infra-red spectra of freeze-dried (a) agarose and (b) silica-coated agarose beads (pH 5, 100 mM silicates, 5 h reaction time).

The kinetics of silica deposition were studied at fixed silicate concentration (50 mM), at pH 7. After 1 h, silica nanoparticles are seen on the bead surface (Fig. 3a) whereas larger particles and fibers/layers are observed after 2 h (Fig. 3b) that do not seem to evolve further. A similar trend was observed at pH 5 (not shown). In parallel, an increase in silicate concentration from 50 mM to 200 mM at pH 5 induces the extension of the fiber/particle network on the capsule surface (Fig. 3c, 1f and 3d). At pH 7, only the first two concentrations could be studied as a 200 mM initial silica content leads to silica formation in the bulk solution within less than 1 h, but a similar trend was observed (not shown).

Further quantification of the silica deposition revealed to be difficult. Determination of the silica content by TGA was unsuccessful due to a SiO_2 : agarose weight ratio below the detection limit of the technique (*i.e.* 1 wt%). The beads were not easily sectioned and corresponding SEM observations did not allow to clearly observe a silica layer, in contrast with previous studies.¹⁴ These results suggest that the silica deposition is limited in thickness and/or do not form an homogeneous layer. Thus

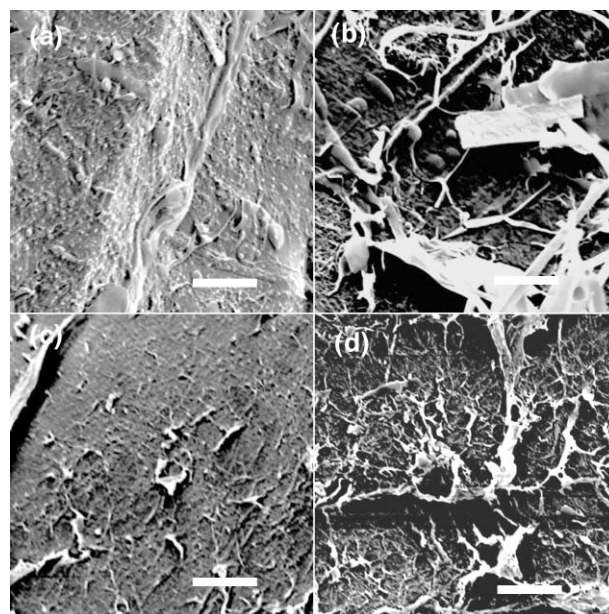


Fig. 3 SEM images of silica-coated agarose beads at pH 7, with 50 mM silicates after 1 h (a) and 2 h (b) and at pH 5 after 5 h with 50 mM (c) and 200 mM (d) silicates (scale bar = 10 μm).

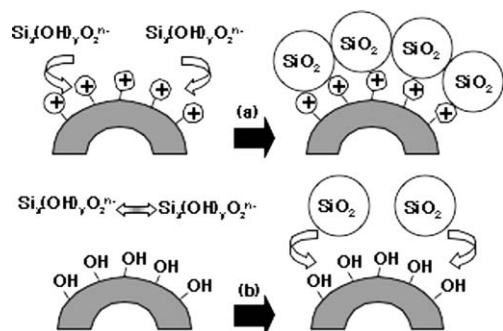
Table 1 Silicon–carbon (Si : C) atomic ratio for bead surface as a function of pH and silicate concentration, as obtained from EDX

pH	$[\text{SiO}_2]/\text{mM}$	Si : C (At%)
5	50	1.5 ± 0.5
	100	4.7 ± 1.0
	200	8.1 ± 2.0
7	50	5.1 ± 0.5
	100	4.9 ± 1.0

EDX measurements were used to estimate silica concentration on the bead's surface (Table 1). These data suggest that the silica coating density increases with silicate concentration at pH 5 but not at pH 7 and is independent of pH at high silicate concentration. It is worth noting that the experimental error in Si : C determination increases with silica content. Such an increase correlates well with SEM observations (Fig. 3c, 1f, 3d) as EDX measurements are sensitive to surface roughness and heterogeneity. Moreover, it is known that EDX penetration depth depends on the accelerating voltage and on the nature of the investigated material, ranging from 1 μm to 5 μm for polymeric systems.²² Hence, although the SiO_2 : agarose ratio can be estimated to vary between *ca* 3 wt% and 20 wt%, it is difficult to get a real insight on the thickness of the silica coating.

These data suggest that, in contrast to electrostatic interaction-induced silica deposition already performed on polylysine coated alginate and gelatine beads,¹⁴ the presence of an uncharged surface does not strongly favor silica formation. The fact that the deposition increases with pH at low silicate concentration, corresponding to an increased ionization of the inorganic precursors, indicate that the hydrogen bond interaction between the polymer and the initial silicates is not the main driving force for the coating process. In contrast, the observed effect of the increase in silicate concentration suggests that the kinetics of silica condensation in solution (*i.e.*

silicate–silicate interactions) is the predominant factor that influences this reaction.⁹ Therefore, whereas the previous electrostatic model implies the adsorption of negative silicates on positively-charged surface that favor their condensation (Scheme 2a),²³ it can be proposed here that the pre-condensation of silicates should occur in solution before they can interact *via* hydrogen bonding (as suggested by IR data) with the uncharged polymer surface (Scheme 2b). In this context, the fact that the silica coating is not continuous but consists of dispersed particles, fibers or layers suggests that deposition more easily occurs on surface heterogeneities.



Scheme 2 Comparison of the proposed mechanism of silica deposition on (a) cationic surfaces where silicates first interact with positively-charged groups *via* electrostatic bonding and then condense of the surface, and (b) neutral surfaces where silicates first condense in solution and then interact with hydroxyl groups *via* hydrogen bonding.

Release properties of silica-coated agarose capsules

In order to study the possible impact of the silica deposition on agarose beads diffusion properties, the release of rhodamine from dye-impregnated uncoated or coated (100 mM silicate, pH 7, 5 h reaction time) capsules was studied. As shown in Fig. 4, the presence of silica modifies the release profile. Both materials show a first rapid dye liberation within five minutes up to 50% release, followed by a second regime which is slower for coated capsules than for uncoated ones with maximum release being obtained after 35–40 minutes for the former and 15–20 minutes for the latter. Fitting these data following

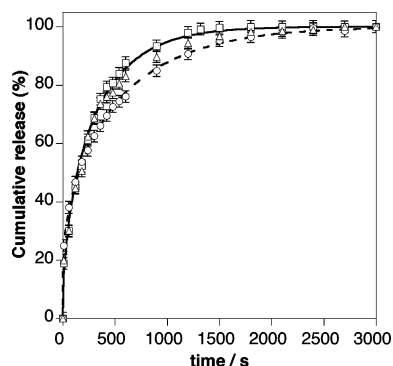


Fig. 4 Cumulative release of rhodamine B from agarose capsules in water (squares) and in a 100 mM silicate solution (triangles) as well as from silica-coated agarose capsules in water (open circles). Open symbols indicate experimental data and plain/dashed lines correspond to the result of the fitting procedure following eqn (1).

eqn (1), diffusion coefficients could be extracted leading to $D = 125 \pm 5 \cdot 10^{-7} \text{ cm}^2 \text{ s}^{-1}$ and $75 \pm 5 \cdot 10^{-7} \text{ cm}^2 \text{ s}^{-1}$ for agarose and silica–agarose capsules, respectively, reflecting the slowing down of the release kinetics due to the silica coating. As a comparison, rhodamine release from agarose beads was studied in a solution containing silicates at a 100 mM concentration and pH 7. Interestingly, the first part of the release process appears unmodified when compared to agarose beads in water. However, after about 10 minutes, the rhodamine concentration progressively gets closer to the data obtained for the silica-coated agarose beads. Overall, these release tests suggest that silicates are deposited on the agarose capsule surface within one hour. Moreover, the deposited silica layer can modify the diffusion properties of the polymer beads.

Silica/CMC hybrid gels

Silica/CMC hybrid gel synthesis and characterization

Cellulose and its derivatives present a wide diversity of structure and properties which, together with their large natural abundance, make them promising candidates for the development of green materials and processes.²⁴ In fact, the possibility to prepare hybrid silica/cellulose derivatives materials has already been described using silicon alkoxides,^{10,15,25} and we wished to evaluate the ability of silicate precursors to act similarly, while avoiding organic reagents and by-products.

Looking for a water-soluble cellulose derivative, we first selected hydroxypropylcellulose (HPC) as a neutral biopolymer. However, we observed that addition of silicate solutions to HPC solutions led to the rapid formation of a precipitate, even at low precursor concentration. We then turned our attention to CMC that could be mixed with silicates to yield clear solutions. Moreover, the fact that this polymer was anionic at neutral pH allowed us to investigate the possibility to form a stable interface between organic and inorganic components that bear a charge of similar sign.

First attempts were made to prepare CMC solutions to which silicate solutions were added. However, even under moderate heating (*i.e.* 30 °C), the polymer solution viscosity was too high to allow suitable mixing with the inorganic precursors. Hence, silicate solutions were first prepared and the CMC powder was then slowly added. After 3h 30 min under stirring, homogeneous solutions are obtained provided that the CMC concentration was lower than 10 wt% and the final SiO_2 : CMC weight ratio smaller than 10 wt%. After 24 h in the fridge, gels (*i.e.* materials that can be turned upside-down without flowing) were obtained for SiO_2 : CMC ratios larger than 6 wt% (Fig. 5a). Noticeably, in the same conditions but without CMC addition, silicate solutions were found to form gels above a similar silica concentration.

The extent of silica incorporation and condensation was studied by IR spectroscopy on freeze-dried solutions/gels (Fig. 6). The spectra of the pure CMC (Fig. 6a) is reminiscent of the agarose spectra.²⁶ For SiO_2 : CMC ratios up to 4 wt%, the modification of the IR spectra upon silica addition is hardly observed (Fig. 6b). However, for a 6 wt% ratio, a broadening of the 1000–1250 cm^{-1} band and the appearance of a new band at 480 cm^{-1} , corresponding to the bending vibration

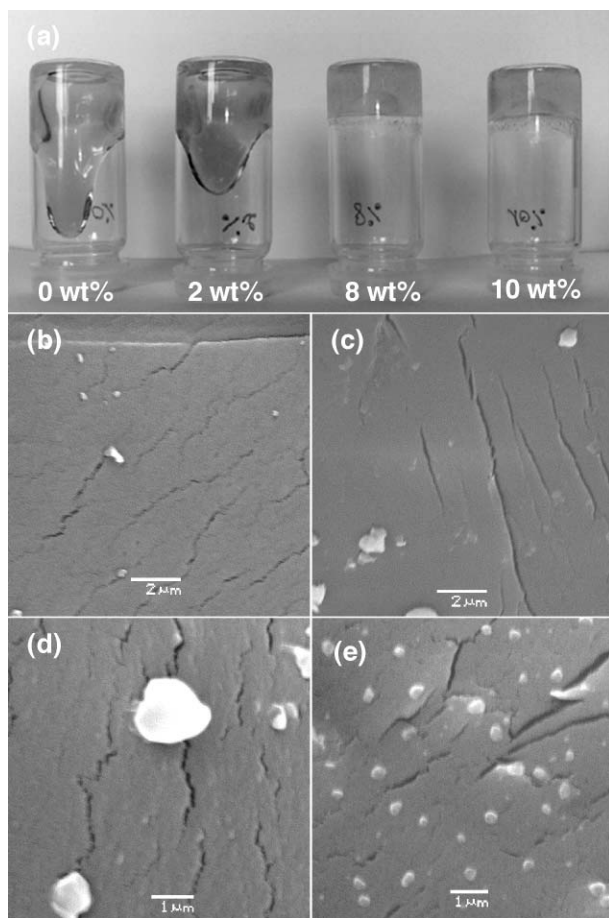


Fig. 5 (a) Optical micrograph of SiO_2/CMC solutions/gels with increasing silicate content showing the sol-to-gel transition. ‡ SEM images of freeze-dried solutions and gels obtained for $\text{SiO}_2 : \text{CMC} =$ (b) 0 wt%, (c) 2 wt%, (d) 8 wt% and (e) 10 wt%.

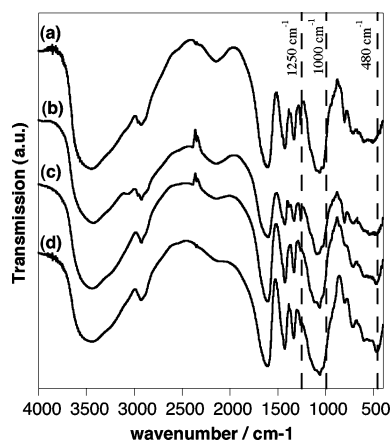


Fig. 6 Infra-red spectra of freeze-dried solutions and gels obtained for $\text{SiO}_2 : \text{CMC} =$ (a) 0 wt%, (b) 4 wt%, (c) 6 wt% and (d) 10 wt%.

mode of the $[\text{SiO}_4]$ tetrahedron, can be observed (Fig. 6c), the latter modification being more evident at a higher silica content (Fig. 6d).

‡ Rhodamine B was added to the initial silicate solution to improve the image contrast.

The hybrid silica/CMC gels were also studied by SEM. At low magnification, all materials appear dense and featureless, as previously reported. At high magnification, the material surface appears smooth and easily cracks under the electron beam (Fig. 5b). No significant modification are observed for $\text{SiO}_2 : \text{CMC}$ content up to 8 wt% (Fig. 5c, d). However, at 10 wt%, particles, *ca* 500 nm in size, are clearly visible on the gel surface, that may correspond to silica particles (Fig. 5e).

TGA analyses of the pure CMC solution and $\text{SiO}_2 : \text{CMC} = 10$ wt% hybrid gels are shown on Fig. 7. For the polymer alone, a first weight loss of 17 wt% is observed between room temperature and *ca* 200 °C, corresponding to weakly adsorbed water departure. The degradation of the polymer mainly occurs between 220 °C and 300 °C, corresponding to a 26 wt% weight loss.²⁶ Additional 10 wt% and 8 wt% losses are observed in the 300 °C–500 °C and 500 °C–800 °C ranges, respectively. By comparison with the initial CMC powder (see ESI), the remaining *ca* 40% corresponds to remaining mineral phase originating from initial sodium content of the polymer as well as from the PBS buffer salts. In the presence of silicates, the residual mass is now *ca* 45 wt%, in agreement with the increased mineral content of the material. Considering the first degradation step of the polymer, it can be noticed that the onset temperature of degradation is shifted from 220 °C to 228 °C. This effect being rather small, the TGA analyses for intermediate silicate content were performed and confirm this trend (see ESI†). In fact, the observed upshift of the onset temperature of degradation can be interpreted as an effect of CMC cross-linking by silica through hydrogen bonding, as already observed in activated carbon/CMC composites.²⁷

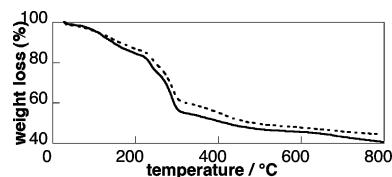
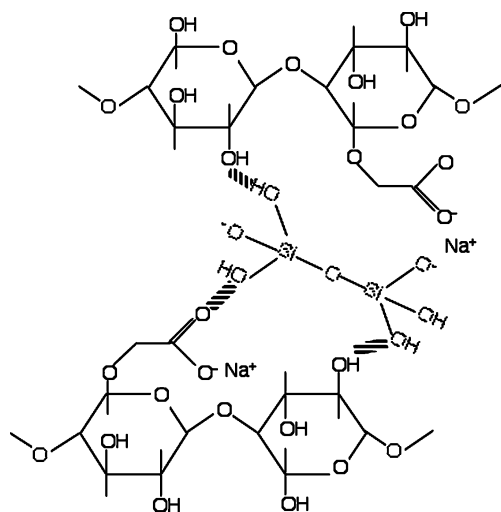


Fig. 7 Thermogravimetric analyses of the CMC solution (plain line) and $\text{SiO}_2 : \text{CMC} = 10$ wt% gel (dashed line).

Silica and CMC being both negatively charged at neutral pH, the only possible mode of interaction within the hybrid system is hydrogen bonding between polymer hydroxyl groups and silanol groups (Scheme 3). However, it may be hypothesized that silica/CMC electrostatic repulsion could be partially screened by sodium ions (Scheme 3) that are initially associated to the polymer chain but can also originate from the silicate solution.

Release properties of silica/CMC hybrid gels

The curves of rhodamine B release from $\text{SiO}_2 : \text{CMC}$ mixtures are shown in Fig. 8. All systems show a progressive diffusion of the dye, whose apparent rate (*i.e.* un-normalized) decreases with increasing silicate concentration so that, after 24 hours, the amount of released dye decreases with the relative polymer content. These curves could be fitted with eqn (2), supporting the hypothesis that the rhodamine release follows a solid/liquid extraction process. This also indicates that, although low silicate concentration leads to viscous solutions rather than gels (see Fig. 5a), inter-molecular interactions exist which provide



Scheme 3 Proposed mode of interaction between silicates and CMC : silanol groups of silicates can form hydrogen bonds with hydroxyl and carbonyl groups of CMC whereas silanolate–carboxylate electrostatic repulsion is screened by sodium ions.

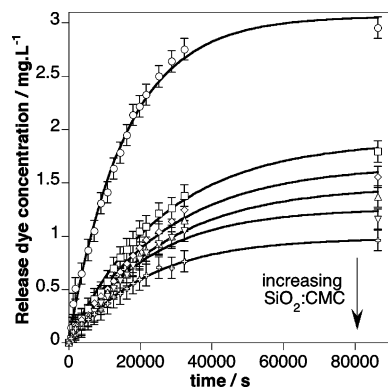


Fig. 8 Rhodamine release from hybrid solution/gels with SiO_2 : CMC ratio = (○) 0 wt%, (□) 2 wt%, (◇) 4 wt%, (Δ) 6 wt%, (▽) 8 wt% and (+) 10 wt%. Open symbols indicate experimental data and plain lines correspond to the result of the fitting procedure following eqn (2).

cohesion to these systems.²⁸ Extracted K_1 , K_2 and calculated k_1 , k_2 parameters (from eqn (3)) are gathered in Table 2. K_1 , which represents the dye concentration at equilibrium and k_1 , which corresponds to the gel-to-supernatant mass transfer, both undergo a strong decrease from pure CMC gels to SiO_2 : CMC = 2 wt% hybrid materials and then decrease with silicate content. In contrast, the values of k_2 , which corresponds to the supernatant-to-gel mass transfer, increases with mineralization

rate. Finally, K_2 , which characterizes the whole extraction rate (*i.e.* reflecting the time necessary to reach equilibrium), is maximal for pure CMC gels, significantly decreases for lowest silica content and then increases with SiO_2 : CMC.

The observed decrease in k_1 is in agreement with the observed enhanced stability of the hybrid gels with silicate content due to CMC interaction with silica, that should slow down the diffusion of the dye from the gel to the supernatant. Interpretation of K_1 and k_2 variations should take into account that rhodamine B is a cationic molecule whereas both CMC and silicates are negatively charged and therefore have a strong tendency to adsorb the dye. Thus, an increase in k_2 and decrease in K_1 with increasing silica content suggest that silica is more efficient than CMC for rhodamine adsorption. Finally, for pure CMC gels, corresponding to loose networks with low dye adsorption capability, the gel-to-supernatant transfer is fast (*i.e.* high k_1) and the dye retention is low (low k_2), so that the equilibrium is quickly reached (high K_2). With silicate addition, dye sorption increases (k_2 increases) so that less rhodamine is available for diffusion out of the gel. We observe here that the equilibrium is reached all the more rapidly as the silica content is high (K_2 increases), suggesting that the decrease in the amount of diffusing species is not compensated by the decrease in the gel-to-supernatant transfer kinetics (k_1 decrease). Overall, it is possible to form homogeneous hybrid materials where silicate/CMC interactions lead to stable gel formation. Moreover, the presence of silica allows the modulation of its affinity towards molecular species.

Conclusions

The combination of aqueous precursors of silica and biopolymer allows the formation of novel bio-composites following a procedure that complies with some of the key requirements of Green Chemistry, in particular design of safer routes involving eco-friendly aqueous inorganic precursors as an alternative to metal–organic alkoxides (2nd and 8th principles) and use of biomacromolecules from vegetal origin (3rd principle).²⁹ Within these hybrid materials, the inorganic phase modulates the stability and/or diffusion properties of the polymer network. The two examples presented here suggest that such bio-composites can be obtained, although no strong interaction are expected to arise between the negatively-charged silicates and the neutral or anionic macromolecules. In both cases, hydrogen bonding, a key mode of interaction in biological systems and in aqueous chemistry, appears to be responsible for the polymer/silica association.

Table 2 K_1 and K_2 parameters for SiO_2 /CMC systems obtained by fitting rhodamine release curves with eqn (2) and corresponding k_1 and k_2 values obtained from eqn (3)

SiO_2 : CMC (wt%)	K_1 ^a /mg L ⁻¹	K_2 ^b /10 ⁻⁵ s ⁻¹	k_1 /10 ⁻⁵ s ⁻¹	k_2 /10 ⁻⁵ s ⁻¹
0	3.06	6.4	2.06 ± 0.07	2.3 ± 0.4
2	2.10	3.8	0.80 ± 0.05	2.7 ± 0.3
4	1.66	3.7	0.61 ± 0.04	2.6 ± 0.2
6	1.46	3.8	0.56 ± 0.03	2.6 ± 0.2
8	1.25	4.5	0.56 ± 0.03	3.4 ± 0.2
10	0.98	4.6	0.22 ± 0.02	4.1 ± 0.2

^a ±0.02. ^b ±0.2.

Noticeably, the silica/CMC bio-composites bear some relevance in the context of silica formation in plants. It is known that silicon can be present in plant tissues, mostly composed of cellulose, in amounts that can vary from 0.1 wt% to 10–15 wt%.³⁰ Silica appears to play a role for the protection of the plant against biotic and abiotic stresses but its mode of action is still poorly understood.³¹ In this context, we are currently evaluating these silica/CMC biocomposites as hosts for the encapsulation and stabilization of enzymes from vegetal origin. As far as agarose capsules are concerned, the successful deposition of silica suggests that our strategy to design hybrid pharmaceutical nanovectors, already developed for anionic and cationic biopolymers,³² can be extended to neutral macromolecules. Thus, the formation of hybrid nanocarriers from poly(lactide-co-glycolide) (PLGA), one of the most popular candidate for drug delivery material design nowadays,³³ is currently under study.

Acknowledgements

NB thanks the Ministère de l'Enseignement Supérieur et de la Recherche Scientifique (Algeria) for its financial support in the frame of the PNE program.

References

- 1 A. Sheldon, I. Arends, and U. Hanfled, *Green Chemistry and Catalysis*, Wiley-VCH, Weinheim, 2007.
- 2 (a) J. W. Phair, *Green Chem.*, 2006, **8**, 763; (b) A. K. Mohanty, M. Misra and L. T. Drzal, *J. Polym. Environ.*, 2002, **10**, 19; (c) M. Y. A. Mollah, R. Schennach, J. Patscheider, S. Promreuk and D. L. Cocke, *J. Hazard. Mater.*, 2000, **79**, 301; (d) D. J. Macquarrie, *Green Chem.*, 1999, **4**, 195.
- 3 (a) M. Darder, P. Aranda and E. Ruiz-Hitzky, *Adv. Mater.*, 2007, **19**, 1309; (b) N. Ma, E. H. Sargent and S. O. Kelley, *J. Mater. Chem.*, 2008, **18**, 954; (c) C. Sanchez, H. Arribart and M. M. Giraud-Guille, *Nat. Mater.*, 2005, **4**, 277; (d) D. Avnir, T. Coradin, O. Lev and J. Livage, *J. Mater. Chem.*, 2006, **16**, 1013.
- 4 (a) H. C. Greenwell, W. Jones, D. N. Stammers, P. O'Connor and M. F. Brady, *Green Chem.*, 2006, **8**, 1067; (b) Y. Yang and T. Coradin, *Green Chem.*, 2008, **10**, 183; (c) V. L. Budarin, J. H. Clark, R. Luque, D. J. Macquarrie and R. J. White, *Green Chem.*, 2008, **10**(4), 382.
- 5 C. J. Brinker and G. W. Scherrer, *Sol-Gel Science*, Academic Press, San Diego, 1990.
- 6 J. P. Jolivet, *Metal Oxide Chemistry and Synthesis*, Wiley, Chichester, 2000.
- 7 R. K. Iler, *The Chemistry of Silica*, Wiley-Interscience, New York, 1979.
- 8 H. P. Van Dokkum, J. H. J. Hulskotte, K. J. M. Kramer and J. Wilmot, *Environ. Sci. Technol.*, 2004, **38**, 515.
- 9 T. Coradin and J. Livage, *Acc. Chem. Res.*, 2007, **40**, 819.
- 10 For a review, see: T. Coradin, J. Allouche, M. Boissière and J. Livage, *Curr. Nanosci.*, 2006, **2**, 219.
- 11 (a) K. Molvinger, F. Quignard, D. Brunel, M. Boissière and J.-M. Devoisselle, *Chem. Mater.*, 2004, **16**, 3367; (b) T. Coradin, N. Nassif and J. Livage, *Appl. Microbiol. Biotechnol.*, 2003, **61**, 429.
- 12 Y. A. Shchipunov, in *Bio-inorganic Hybrid Materials*, ed. E. Ruiz-Hitzky, K. Ariga and Y. M. Lvov, Wiley-VCH, Weinheim, 2007, pp. 75–112.
- 13 (a) N. Nassif, O. Bouvet, M. N. Rager, C. Roux, T. Coradin and J. Livage, *Nat. Mater.*, 2002, **1**, 42; (b) N. Nassif, C. Roux, T. Coradin, O. M. M. Bouvet and J. Livage, *J. Mater. Chem.*, 2004, **14**, 203; (c) C. Gautier, J. Livage, T. Coradin and P. J. Lopez, *Chem. Commun.*, 2006, 4611; (d) M. Amoura, N. Nassif, C. Roux, J. Livage and T. Coradin, *Chem. Commun.*, 2007, 4015.
- 14 (a) T. Coradin, E. Mercey, L. Lisnard and J. Livage, *Chem. Commun.*, 2001, 2496; (b) T. Coradin and J. Livage, *Mater. Sci. Eng., C*, 2005, **25**, 201.
- 15 Y. A. Shchipunov and T. Y. Karpenko, *Langmuir*, 2004, **20**, 3882.
- 16 R. Zvitov and A. Nussinovitch, *Food Hydrocolloids*, 2003, **17**, 255.
- 17 S. R. Van Tomme, B. D. De Geest, K. Braeckmans, S. C. De Smedt, F. Siepman, J. Siepman, F. van Nostrum and W. E. Hennink, *J. Controlled Release*, 2005, **110**, 67.
- 18 V. Ferreira, I. Jarauta and J. Cacho, *J. Agric. Food Chem.*, 2006, **54**, 3047.
- 19 R. Armisen, *Hydrobiologia*, 1991, **221**, 157.
- 20 D. Jhurry, A. Bhaw-Luximon, T. Mardamootoo and A. Ramanjooloo, *Macromol. Symp.*, 2006, **231**, 16.
- 21 A. Gendron-Badou, T. Coradin, J. Maquet, F. Frölich and J. Livage, *J. Non-Cryst. Solids*, 2003, **316**, 331.
- 22 (a) H. Younan, *Instrum. Sci. Tech.*, 2004, **32**, 115; (b) T. Imakoma, Y. Suzuki, O. Fujii and I. Nakajima, *Proceedings of the 4th International Conference on Properties and Applications of Dielectric Materials*, Brisbane, 3–8 Jul 1994, vol. 1, pp. 306–308, 10.1109/IC-PADM.1994.414000.
- 23 T. Coradin, O. Durupthy and J. Livage, *Langmuir*, 2002, **18**, 2331.
- 24 D. Klemm, B. Heublein, H.-P. Fink and A. Bohn, *Angew. Chem., Int. Ed.*, 2005, **44**, 3358.
- 25 S. Sequeira, D. V. Evtuguin, I. Portugal and A. P. Esculas, *Mater. Sci. Eng., C*, 2007, **27**, 172.
- 26 H. M. Said, S. G. Abd Alla and A. W. M. El-Naggar, *React. Funct. Polym.*, 2004, **61**, 397.
- 27 J. Qiu, L. Xu, J. Peng, M. Zhai, L. Zhao, J. Li and G. Wei, *Carbohydr. Polym.*, 2007, **70**, 236.
- 28 U. Kästner, H. Hoffmann, R. Dönges and J. Hilbig, *Colloids Surf., A*, 1997, **123–124**, 307.
- 29 P. Anastas and J. Warner, *Green Chemistry: Theory and Practice*, Oxford University Press, New York, 1998.
- 30 E. Epstein, *Annu. Rev. Plant Physiol. Plant Mol. Biol.*, 1990, **50**, 641.
- 31 K. E. Richmond and M. Sussman, *Curr. Opin. Plant Biol.*, 2003, **6**, 268.
- 32 (a) M. Boissière, P. J. Meadows, R. Brayner, C. Hélyary, J. Livage and T. Coradin, *J. Mater. Chem.*, 2006, **16**, 1178; (b) J. Allouche, M. Boissière, C. Hélyary, J. Livage and T. Coradin, *J. Mater. Chem.*, 2006, **16**, 3121.
- 33 T. Govender, S. Stolnik, M. C. Garnett, L. Illum and S. S. Davis, *J. Controlled Release*, 1999, **57**, 171.

Development of micro- and nano-porous composite materials by processing cellulose with ionic liquids and supercritical CO₂†

Costas Tsiptsias,^a Apostolis Stefopoulos,^a Ioannis Kokkinomalis,^a Lambrini Papadopoulou^b and Costas Panayiotou^{*a}

Received 5th March 2008, Accepted 17th June 2008

First published as an Advance Article on the web 7th August 2008

DOI: 10.1039/b803869d

Three lines of green chemistry were combined in this study, in order to produce porous materials with pore size distributions in the micro- and nano-scales. These lines are: (i) the renewable and biodegradable sources (cellulose), (ii) ionic liquids, and (iii) supercritical fluids. By dissolving cellulose in a room temperature ionic liquid and regenerating with water or methanol we obtained cellulose hydrogels and methanogels. The liquid mixtures were separated by vacuum distillation with high yield of recovery. The obtained gels were processed by supercritical carbon dioxide to give porous materials. A novel foaming procedure was applied to hydrogels in order to obtain microporous structures of cellulose and cellulose composites, while in alcogels the supercritical point drying method resulted in nanoporous aerogels. For elucidating physicochemical aspects involved in the two processes and for characterization of the produced materials, X-ray diffraction, sorption measurements (by a modified mass loss analysis and the BET method) and scanning electron microscopy were used. The role of various process parameters on the final porous structure was investigated.

Introduction

Environmental pollution has become an unquestionable threat for the planet and the quality of human life. Thus, novel environmentally friendly processes and materials have been sought that will minimize this threat. In this respect, biodegradable polymers (synthetic or natural) are gaining increasing interest in recent years. An important category of materials among natural polymers is polysaccharides (*e.g.* chitin, cellulose, *etc.*). Cellulose is the most abundant organic compound found on earth and is known to have very attractive properties such as biocompatibility, biodegradability, thermal and chemical stability. Also, it is a renewable and a major biomass source.¹

Often an environmentally friendly material (*e.g.* biodegradable packaging material) is produced by an environmentally damaging process (by using toxic and volatile organic solvents). Thus, alternative solvents have been proposed and supercritical fluids are among these. The good solvating properties of these fluids arise from their unique combination of having a density closer to a liquid's density and viscosity and diffusivity closer to those of a gas.² Carbon dioxide is probably the most commonly

used supercritical fluid due to its low cost, low toxicity, non-flammability, and low critical point (low energy demand).^{2,3} It has been widely used in polymer science and technology in areas such as chemical synthesis/polymerization, gelation, production of porous materials or particles.^{2–5} Supercritical carbon dioxide (ScCO₂)–polymer interactions have been both experimentally studied^{6,7} and modeled.^{8,9}

Besides supercritical fluids, ionic liquids (ILs) have attracted much interest recently as alternative benign solvents. ILs are organic salts with relative polar character and relative low melting point.^{10,11} They exhibit thermal and chemical stability and have very low vapor pressure (practically non-detectable) which is the main reason for their utilization as green solvents.^{10,11} When they are in the liquid state at room temperature they are called room temperature ionic liquids (RTILs). ILs have been very recently used for the dissolution of cellulose and for the production of bioactive films or for other biomedical purposes.^{12,13} ILs have opened new ways for the otherwise difficult treatment of cellulose that arises from the inter- and intra-molecular hydrogen bonds in its crystalline structure. Solutions of cellulose are usually quite viscous and have a gel formation ability or tendency.

Gels are colloidal dispersions of liquids in solid networks. When the solvent is water, the gels are called hydrogels. A number of polymers can form hydrogels. These materials are used in food and cosmetic industry, in drug delivery, and in tissue engineering applications.^{14,15} In contrast to the case of pure polymers, reports on treatment of polymeric hydrogels with ScCO₂ are almost absent in the literature.^{16,17} Besides water, alcohols are common solvents for gels. In this case the gels are called alcogels.

^aDepartment of Chemical Engineering, Aristotle University of Thessaloniki, 54124, Thessaloniki, Greece. E-mail: cpanayio@auth.gr; Fax: +30 2310 996232; Tel: +30 2310 996223

^bDepartment of Geology, Aristotle University of Thessaloniki, 54124, Thessaloniki, Greece

† Electronic supplementary information (ESI) available: TGA thermographs, XRD patterns, and additional SEM figures of the cellulose composite materials and of regenerated cellulose; TGA and DSC thermograms of the synthesized AmimCl; AFM image of the cellulose aerogel. See DOI: 10.1039/b803869d

Alcogels have been extensively used for the production of a specific category of nanoporous materials called aerogels. Aerogels exhibit unusual characteristics, such as high porosity and surface area, low density, transparency and low heat conductivity.¹⁸ They find applications in quite different fields such as transparent, super-thermal and sound insulators, electronics, space and particle research.¹⁸ Of course, they can be used in fields where common porous materials are used (catalysis, separation processes, packaging materials, *etc.*).³

By far, the most common technique for the production of aerogels is the supercritical point drying (SPD).^{18,19} The SPD method lies on removing the solvent from the gel in the absence of vapor–liquid interface in order to avoid collapse of the structure driven by the surface tension of the liquid. At supercritical conditions, surface tension is zero and this prevents the pore structure from collapsing.¹⁸

In this study, porous cellulose materials were prepared by two green processes. Besides the well-known SPD method, a novel method is also applied, namely, the hydrogel foaming. Thus, the use of a RTIL as a solvent for cellulose, the use of water or methanol for the regeneration process, and the final processing of the gels with ScCO₂ results in the production of useful biodegradable and biocompatible materials in an environmentally friendly manner.

Experimental

Materials and instruments

Cellulose (soft pulp, degree of polymerization, DP = 1283) was purchased from Lenzing Aktiengesellschaft (Austria). Hydroxyapatite (>97%) nano-powder (~100 nm) was purchased from Sigma-Aldrich. SiO₂ nanoparticles (~14 nm) were purchased from Sigma-Aldrich. Carbon dioxide (purity >99.98%) and nitrogen (purity >99.99%) were purchased from Air Liquide Mediterranee. All other chemicals were of analytical quality and were used as received.

The morphology of porous samples was examined using a Jeol JSM-840A scanning electron microscope. During the experiments an ultra-sonicator (HEAT SYSTEMS-ULTRASONICS, INC, W-375), a Rigaku Miniflex X-ray diffractometer (Cu, $\lambda = 1.5405 \text{ \AA}$), a Buchi RE 111 rotavapor with a BUCHI 461 water bath, and a Sartorius scale of $\pm 0.1 \text{ mg}$ accuracy were used. The apparatus used for the high pressure sorption experiments is described elsewhere in detail.⁴ Briefly, it consists of a high pressure cell of internal volume of 40 cm³, an ISCO syringe pump for pumping ScCO₂, and pressure and temperature controllers for keeping pressure and temperature constants at the desired values. The freeze drying setup consisted of a Haake constant temperature bath (model G) with a D1 circulator, a Savant refrigerated condensation trap (model RT-100A), and a rotary vane vacuum pump (Vacuubrand, type RZ5). Surface area measurements were carried out by the BET method (N₂ adsorption at 77 K).

Synthesis of 1-allyl-3-methylimidazolium chloride

1-Allyl-3-methylimidazolium chloride (AmimCl) was synthesized according to the literature.²⁰ Briefly, allyl-chloride and 1-methylimidazole in a mole proportion of 1.25 : 1 were

mixed and left to react for 8 h at 55 °C. The reaction was carried out in a glass flask with reflux. Liquid–liquid extraction with ethyl acetate was used for the purification process, followed by vacuum distillation until an odourless liquid was obtained.

Dissolution of cellulose and gel preparation

Cellulose was dissolved in AmimCl under magnetic stirring for 5 h. To accelerate the process, dissolution was carried out at the temperature range of 80–90 °C. It was dissolved in three different concentrations (1.5, 1.73 and 2.86% w/w). The 1.5 solution was used from the production of the aerogel as described below. In a certain amount of the 1.73% solution, hydroxyapatite particles were added in order to obtain a composite material of ~30% hydroxyapatite and 70% cellulose. Also, SiO₂ nanoparticles were dispersed in another solution to obtain a composite material of ~28% SiO₂ and 72% cellulose. The dispersion of the particles was accomplished by ultra-sonication. Special care was taken in order to avoid thermal degradation of AmimCl due to local overheating. Solutions were cast in cylinder glass or polypropylene molders and allowed to stand at low temperature (<8 °C) for 1–2 h. The plates with the obtained gel-like materials were immersed in excess of pre-cooled water or methanol. Extensive washings were carried out (mass of water or methanol to mass of AmimCl >15). The obtained hydrogels and alcogels were stored in excess of their solvent at room temperature. The mixtures of AmimCl with water and methanol from the regeneration process were separated by vacuum distillation at 85 °C for the aqueous mixture and at 45 °C for the methanol–AmimCl mixture in order to recover the ionic liquid.

Sorption of CO₂ by cellulose hydrogels

Cellulose hydrogels (from 1.73% solution) were wiped to remove surface water, weighed, and placed in the high pressure cell for 2 h at the desired conditions of pressure (65–125 bar) and at constant temperature at 80 °C in order to avoid freezing during expansion. The 2 h exposure of the hydrogels to ScCO₂ atmosphere was followed by a rapid depressurization (< 10 s). Within another 10–14 s the hydrogels were placed on the scale and weighed for 510 s (8.5 min), in total, at room temperature. During the first 70 s, one reading every 2 s was made, and for the rest of the period (70–510 s) the readings were taken every 5 s. For the first set of measurements and for the time range between 24–50 s (10–15 points) a linear fit with a correlation coefficient $r^2 > 0.99$ was obtained. This line describes the mass loss of the hydrogel due to, both, humidity loss and CO₂ desorption. For the time range between 200–510 s (~60 points) a linear fit of a different slope was again obtained, with $r^2 > 0.99$ describing the mass loss of the hydrogel due to humidity loss only. By subtracting the two equations for the time range between 24 and 50 s the mass loss of the hydrogels due to CO₂ desorption was calculated. The calculated points were plotted against the square root of time and the sorption was calculated by extrapolating the mass measurements to zero time as in classical mass loss analysis.^{7,21}

Preparation of microporous cellulose materials by hydrogel foaming

Hydrogels (from 1.73 and 2.86% solutions) were placed in the high pressure cell at the desired conditions of temperature and pressure for 2 h. After rapid depressurisation the foamed hydrogels were frozen and kept overnight at $-15\text{ }^{\circ}\text{C}$. Two samples, prepared at freezing conditions upon expansion (125 bar and $40\text{ }^{\circ}\text{C}$), were immersed in water. All samples were freeze dried, at $-2\text{ }^{\circ}\text{C}$ in a vacuum ranging from 0.2 to 4 Torr for at least 24 h. The condensation trap was operating at $-48\text{ }^{\circ}\text{C}$. The morphology of the produced materials was examined by SEM. Pore size distribution of the samples was evaluated from the SEM pictures (from different regions and at various magnifications) with the appropriate software (ImageJ 1.32j). Absorption of ethylene glycol was measured in order to check the interconnectivity of the porous structure.

Preparation of nanoporous cellulose aerogel by supercritical point drying of methanogel

A cellulose methanogel weighing 0.5 g (from 1.5% w/w solution) was placed in the high pressure cell at $40\text{ }^{\circ}\text{C}$ and 200 bar with CO_2 . At these conditions methanol and CO_2 form a supercritical mixture and the methanogel was left for 1.5 h. Then, the inlet and outlet of the cell were opened and fresh CO_2 was allowed to enter the cell to dry the gel (remove methanol). The pressure was kept constant with a back-pressure regulator and the mass flow of CO_2 was $0.42 \pm 0.09\text{ g min}^{-1}$. Continuous extraction was applied for another 3 h. Afterwards, the pressure was slowly released (more than 30 min). N_2 adsorption in the obtained aerogel was measured at 77K (BET method). The surface area was estimated by the isotherm and the pore size distribution was evaluated (assuming cylindrical pore shape) by the Kelvin equation:²²

$$r_i = 2\gamma V_L / [RT \ln(P_o/P_i)] \quad (1)$$

where r_i is the maximum pore radius filled at i th point of the isotherm, P_o/P_i the relative pressure, T the temperature (77 K), R the universal gas constant, γ (8.9 dyne cm^{-1}) the surface tension of liquid nitrogen and V_L ($34.7\text{ cm}^3\text{ mol}^{-1}$) the molar

volume of liquid nitrogen. The porosity of the material was estimated by the following equation:²³

$$P = (1 - d_p/d_b) * 100, \quad (2)$$

where d_p is the density of the porous material and d_b the density of the bulk material. The density of the bulk sample was measured using the buoyancy method (ASTM D-792) with ethylene glycol as the liquid of known density. The density of the aerogel was determined by measuring its mass and dimensions (volume). A similar experiment was also carried out but at conditions of $40\text{ }^{\circ}\text{C}$ and 80 bar, where methanol and CO_2 are in vapor-liquid equilibrium.

XRD measurements

The crystalline structure of cellulose in hydrogel and in methanogel and in the dry state was examined by XRD. All XRD measurements were carried out in the range of 2θ between 5 and 60° with a scan rate of $2^{\circ}\text{ min}^{-1}$ at room temperature. The examined materials were produced from the 1.73% solution.

Results

ScCO_2 sorption by cellulose hydrogels, and crystallinity of gels

Fig. 1a shows the mass loss of the hydrogel (after exposure in CO_2 atmosphere at $80\text{ }^{\circ}\text{C}$ and 125 bar) during CO_2 desorption as a function of time. Two distinct regions are observed, one for the simultaneous loss of CO_2 + water at the initial stage of the process (left line) and one for the continuing loss of water (right line). Also the two equations of the linear fittings corresponding to the loss of water + CO_2 and the loss of water only are shown. By subtracting the two equations, the mass loss of the hydrogel due to CO_2 desorption is estimated. These points are plotted against the square root of time in Fig. 1b. From extrapolation of this line to $t = 0$ one may obtain the sorbed amount of CO_2 by the hydrogel. The error estimations in the slope and intercept of equations shown in Fig. 1 are reported in Table 1. By a similar procedure, the sorption of CO_2 by hydrogels was measured at different pressures at $80\text{ }^{\circ}\text{C}$. The sorption isotherm is presented in Fig. 2. In the same figure the

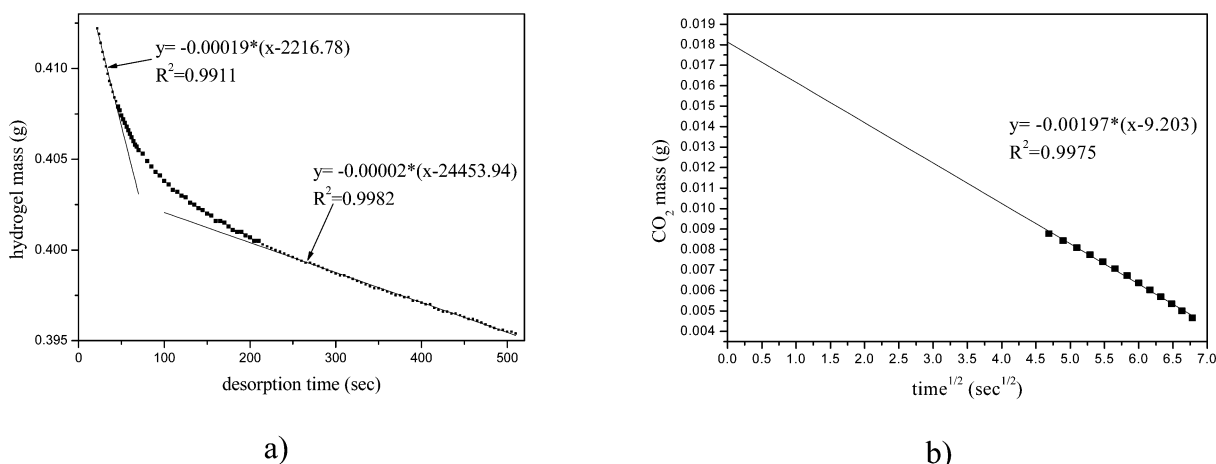
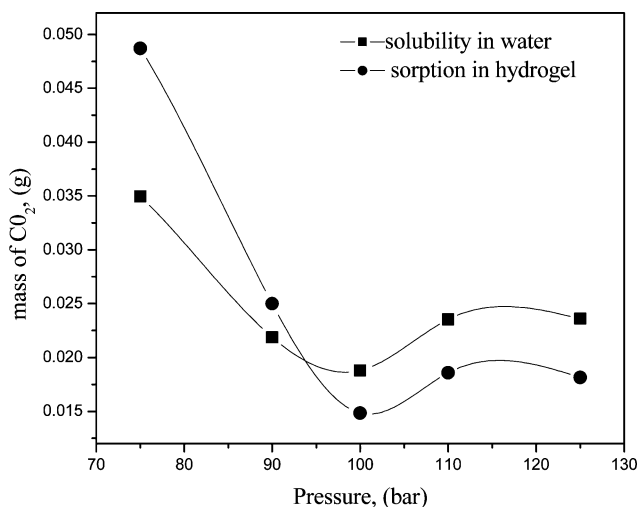


Fig. 1 (a) Representative desorption curve of hydrogel ($80\text{ }^{\circ}\text{C}$ and 125 bar), (b) calculation of CO_2 sorption (by subtracting the two equations shown in Fig. 1a).

Table 1 Error estimations in slope and intercept of equations shown in Fig. 1

	R^2	a	Absolute and relative error (%) in a	b	Absolute and relative error (%) in b
H ₂ O + CO ₂ loss	0.9911	-0.000 19	0.000 005 625 3, 2.96	2216.78	65.42, 2.95
H ₂ O loss	0.9982	-0.000 02	0.000 000 092 812 3, 0.46	24 453.94	135.44, 0.55
CO ₂ loss	0.9975	-0.001 97	0.000 03, 1.52	9.203 57	0.053 26, 0.58

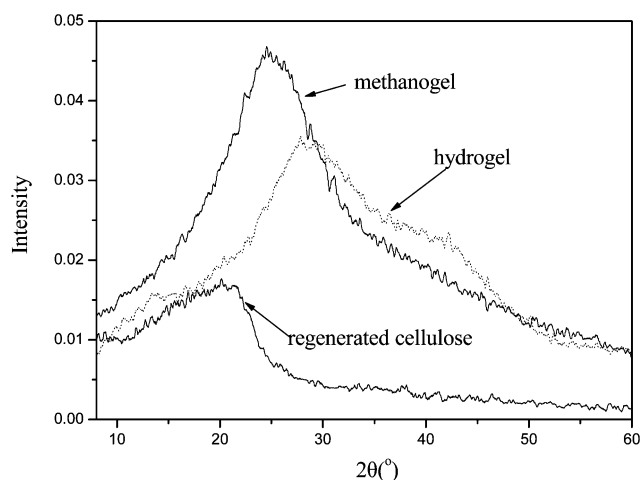
**Fig. 2** Measured sorption of CO₂ by the hydrogel (circles) and calculated solubility of CO₂ in water from water–CO₂ VLE data²⁴ (squares) at 80 °C.

solubility of CO₂ in (the same mass of) water contained in the hydrogels is shown. This solubility was calculated from vapor–liquid equilibrium data taken from the literature.²⁴ As observed, a qualitative agreement exists between the measured sorption by the hydrogel and the calculated solubility in (the water of) the hydrogel. This implies that the main mechanism of CO₂ sorption by the hydrogel is its dissolution in water. Upon pressure release (expansion), extensive foaming of the hydrogels was observed.

However, an entirely different behavior was observed in the case of methanogels. Since CO₂ is more soluble in methanol than in water, its sorption by methanogel is higher compared to sorption by hydrogel at the same external conditions. Yet, no foaming of methanogels was observed upon expansion. In some cases (higher pressures) the gel remained swollen and semi-transparent and in other cases (at lower pressures) it was extensively shrunk and no porosity could be detected. A similar result of very low porosity has been reported for chitin gels with acetone or methanol (as solvent) that were dried with CO₂.^{17,25} The swollen dry gel was a nanoporous cellulose aerogel and this deserves further discussion below, since at higher pressures methanol formed a supercritical mixture with carbon dioxide. At lower pressures (that methanol does not form a supercritical mixture with CO₂), methanol was extracted from the gel to an extent that depends on the vapor–liquid equilibrium of the CO₂–methanol system. If the methanogels are processed under vapor–liquid equilibrium conditions, shrunk materials of low or zero porosity are obtained due to surface tension of the liquid, despite the greater dissolution of CO₂ in methanol than in water.

A possible explanation of the above behavior could be the sorption of CO₂ by cellulose (besides dissolution in the

solvent). The molecule of cellulose possesses groups that could form specific interactions with CO₂, as has been reported for amorphous and semi-crystalline polymers.⁶ In order to support this explanation, we examined by XRD the structure of cellulose in the dry state (regenerated from methanol) and in hydrogels and methanogels. These XRD patterns are shown in Fig. 3. As observed, the peak of cellulose appearing in the case of hydrogel is shifted to higher angle values. From the Bragg equation it is known that higher angle values correspond to smaller lattice distances. Thus, it can be concluded that the cellulose crystallite in the hydrogel is less developed. Also, the broadness of the peak in the case of hydrogel indicates the presence of amorphous state. On the other hand, the XRD pattern of cellulose in methanogel is closer to the typical pattern of regenerated cellulose that has already been reported,²⁰ though not as intense. It is worth mentioning that, despite the fact that the methanogel sample was less thick than the hydrogel sample, the height of the peak in the methanogel is larger (usually the more thick a sample is the larger is the peak height). All these support the important conclusion that cellulose is in a rather amorphous state in the hydrogel. This can be further considered as strong evidence that CO₂ sorption by cellulose is possible in hydrogels. It is worth mentioning at this point that in the literature²⁶ a solution of chitin (similar molecule with cellulose) in an ionic liquid has been proposed as a reversible CO₂ sorbent due to the presence of amorphous chitin and the extensive CO₂–chitin interactions. Also, as reported earlier,^{27–30} a semi-crystalline derivative of cellulose (cellulose acetate) interacts with CO₂ and this suggests dissolution of CO₂ in the amorphous regions of the polymer as a possible mechanism.

**Fig. 3** XRD patterns of cellulose in gels and in the dry state.

From the information presented above, two processes can be distinguished for the production of porous cellulose materials.

An illustration of these processes can be seen in Fig. 4. Briefly, cellulose is dissolved in a room temperature ionic liquid. Regeneration with water results in hydrogels that can be foamed with high pressure (gas or supercritical) CO₂ to give porous hydrogels. The hydrogels after freeze-drying give microporous materials. If the regeneration occurs with methanol, the obtained gels must can be processed at supercritical conditions (of the CO₂ + methanol mixture) to give nanoporous aerogels. In what follows, we characterize materials produced by the two processes and examine parameters that influence pore size, focusing on the ones produced by hydrogel foaming since this is a much less studied technique.

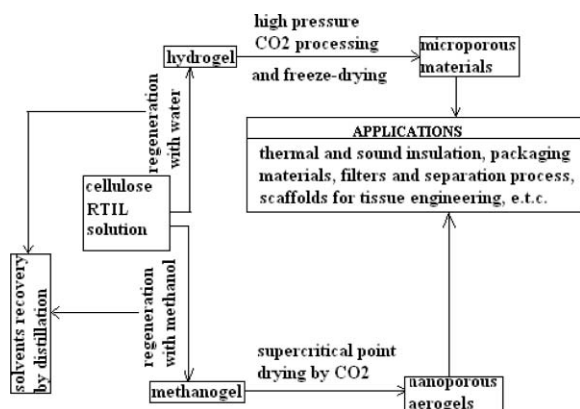


Fig. 4 Schematic representation of the two proposed processes.

Porous cellulose and composite cellulose materials produced by hydrogel foaming

Microporous cellulose materials were produced by hydrogel foaming at different conditions. In Fig. 5a and b, the influence of pressure and temperature on the pore size is presented. The effect of pressure is referred to a temperature of 80 °C and it is presented for, both, pure cellulose and cellulose–hydroxyapatite composite. The effect of temperature was examined at constant

pressure of 75 bar for hydrogels with different water content (from different solutions). Their influence on pore size is, in general, similar to the one observed in classic polymer foaming (pore size increases by increasing temperature or decreasing pressure). However, there is a noteworthy exception on the effect of pressure: At high pressures the pore size increases as the pressure increases. This can be explained by the fact that at these conditions (*e.g.* 175 bar and for the specific volume cell and sample weight) the hydrogel freezes during expansion due to the Joule–Thompson effect. The freezing results in an incomplete CO₂ desorption. This, in turn, leads to an increase in pore size, during storage of the frozen gels until freeze-drying, by merging neighbour micropores. The influence of gel content on the pore size is also shown on the same figures. In both cases (different water content or hydroxyapatite load), the pore size does not seem to be strongly influenced.

As mentioned above, at some conditions hydrogels freeze during expansion but the incomplete CO₂ desorption leads to a final porous structure. However, an alternative foaming route could be followed by immersing the frozen hydrogels in water of different temperature immediately after expansion. The pore size distribution of samples with and without second foaming is reported in Table 2. As observed, the second foaming is not enough to produce a second pore size distribution. However, the twice foamed samples exhibit much higher ethylene glycol absorption (Table 2). This is strong evidence that the second foaming leads to an increase in pore interconnection, which is often a highly desired feature. This controlling parameter (second foaming) is absent in classical polymer foaming. Representative SEM micrographs are shown in Fig. 6a–d. All samples had almost no surface porosity.

In the above process AmimCl was the ionic liquid used for the production of the hydrogels. This IL was separated from water by vacuum distillation and was recovered with a yield of 92%. Thermogravimetric analysis (TGA) thermographs, XRD patterns, and additional SEM figures of the cellulose composite materials and of regenerated cellulose are available as supplementary material.† In the supplementary material,

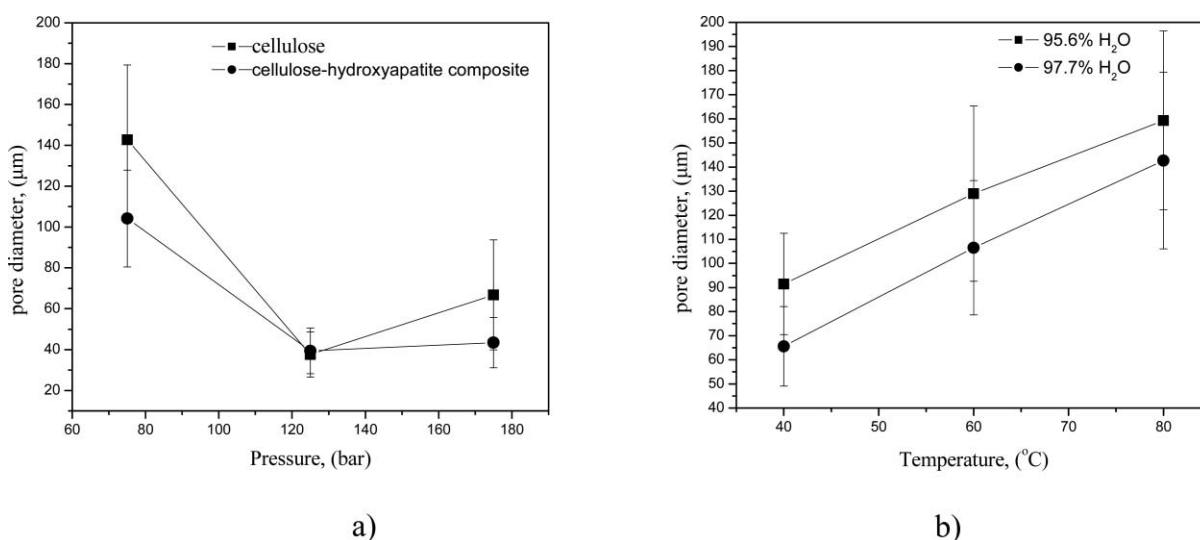


Fig. 5 Effect of different parameters on pore diameter, (a) effect of pressure and hydroxyapatite content at 80 °C, (b) effect of temperature and water content (samples produced by hydrogel foaming) at 75 bar.

Table 2 Pore size distributions and ethylene glycol absorption of samples with and without second foaming (conditions of first foaming: 125 bar, 40 °C, depressurization in less than 20 s)

Water temperature/°C	Pore size/ μm	Ethylene glycol absorption/g of ethylene glycol per 100 g of cellulose
No second foaming	54 ± 15	1350
15	48 ± 10	2150
55	57 ± 13	2930

TGA and differential scanning calorimetry thermograms of the synthesized AmimCl are also included.[†]

Characterization of the aerogel

As already mentioned, besides microporous materials, we have also produced a nanoporous cellulose aerogel by supercritical point drying of cellulose methanogel. The N_2 adsorption isotherm at 77 K of the produced aerogel is shown in Fig. 7a. The isotherm can be classified as type II or IV according to IUPAC recommendations.³¹ For relative pressures between 0.05–0.3, the surface area was calculated to be $S_{\text{BET}} = 315 \pm 35 \text{ m}^2 \text{ g}^{-1}$. In Fig. 7b the pore size distribution (calculated by the Kelvin equation) is presented. As shown, the produced material has mainly micropores (<2 nm) and mesopores (2–50 nm). The density of the material was found to

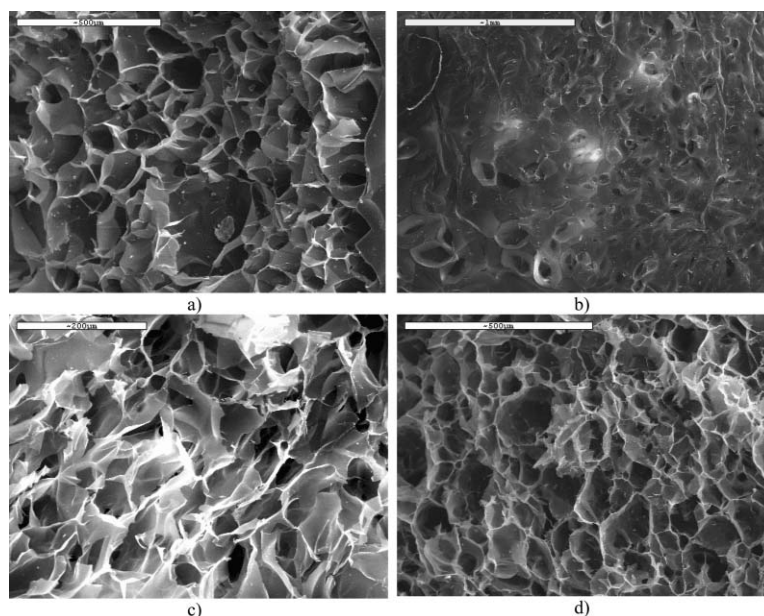


Fig. 6 Representative SEM figures (cross sections) of samples prepared at different conditions: (a) 75 bar, 40 °C, 2.86% w/w; (b) 75 bar, 40 °C, 1.73% w/w, external surface; (c) 125 bar, 40 °C, 1.73% w/w, second foaming with water at 15 °C; (d) 125 bar, 80 °C, 27.9% hydroxyapatite (2.86% and 1.73% w/w are the concentrations of the solutions of cellulose in the AmimCl).

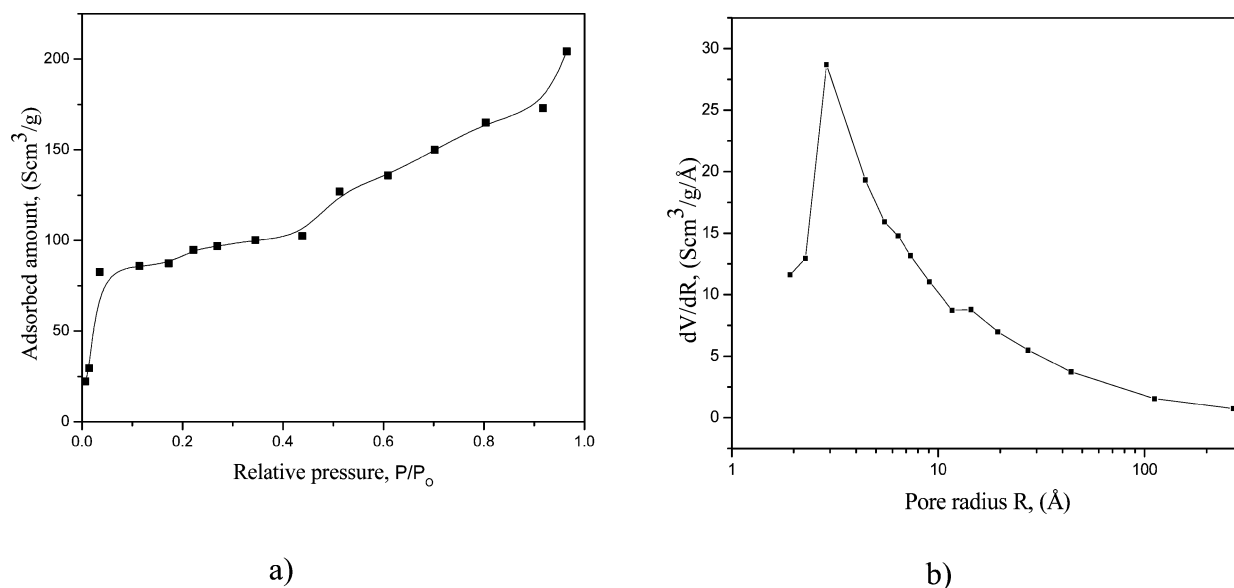


Fig. 7 (a) N_2 adsorption isotherm at 77K of cellulose aerogel, and (b) pore size distribution of the same sample calculated by the Kelvin equation.

be 0.058 g cm^{-3} which correspond to a total porosity of 94–96%.

The IL AmimCl, used for the production of the aerogel, was separated from methanol by vacuum distillation and was recovered with a yield of 90%. An atomic force microscopy (AFM) image of the cellulose aerogel is available as supplementary material.†

Conclusions

In this study, novel cellulose–composite porous materials were produced from hydrogels and alcogels. The pore size distributions obtained, varied from some nanometres to several micrometres. A RTIL was used for the dissolution process and it was recovered, to a great extent, after the regeneration process. Regeneration was applied either by water or methanol giving the corresponding type of gels. XRD examination has shown that cellulose in the hydrogels exists mainly in an amorphous state, which facilitates interactions with CO_2 . Thus, cellulose hydrogels were foamed in a procedure similar to polymer foaming. In general, pressure and temperature influence pore size distribution as in classical polymer foaming, and can be used for controlling it, except when hydrogels freeze during expansion. In the latter case, pore interconnection can be enhanced by a second foaming. This novel technique can be applied also to composite materials such as the cellulose–hydroxyapatite composites. Such a foaming technique cannot be applied to methanogels. However, the removal of methanol by CO_2 under supercritical conditions leads to the formation of nanoporous aerogels, with relatively high surface area, low density, and large porosity.

From a combined use of an abundant, renewable, biodegradable, and biocompatible biopolymer (cellulose) with two major solvent categories of green chemistry (RTILs and supercritical fluids), two promising novel green processes are proposed for the production of porous materials.

Acknowledgements

The authors acknowledge the support of this work by the Greek General Secretariat of Research and Technology in the frame of PENED 2003 (03EΔ/736).

References

- 1 K. Kurita, *Mar. Biotechnol.*, 2006, **8**, 203–226.
- 2 R. A. Quirk, R. M. France, K. M. Shakesheff and S. M. Howdle, *Curr. Opin. Solid State Mater. Sci.*, 2004, **8**, 313–321.
- 3 A. I. Cooper, *Adv. Mater.*, 2003, **15**, 1049–1059.
- 4 I. Tsvintzelis, E. Pavlidou and C. Panayiotou, *J. Supercrit. Fluids*, 2007, **40**, 317–322.
- 5 C. Kalogiannis, C. Michailof and C. Panayiotou, *Ind. Eng. Chem. Res.*, 2006, **45**, 8738–8743.
- 6 S. G. Kazarian, M. F. Vincent, F. V. Bright, C. L. Liotta and C. A. Eckert, *J. Am. Chem. Soc.*, 1996, **118**, 1729–1736.
- 7 M. Pantoula and C. Panayiotou, *J. Supercrit. Fluids*, 2006, **37**, 254–262.
- 8 C. Panayiotou and C. I. Sanchez, *J. Phys. Chem.*, 1991, **95**, 10090–10097.
- 9 C. Panayiotou, I. Tsvintzelis and I. G. Economou, *Ind. Eng. Chem. Res.*, 2007, **46**, 2628–2636.
- 10 J. G. Huddleston, A. E. Visser, W. M. Reichert, H. D. Willauer, G. A. Broker and R. D. Rogers, *Green Chem.*, 2001, **3**, 156–164.
- 11 S. Zhu, Y. Wu, Q. Chen, Z. Yu, C. Wang, S. Jin, Y. Ding and G. Wu, *Green Chem.*, 2006, **8**, 325–327.
- 12 M. Turner, S. Spear, J. Holbrey, D. Daly and R. Rogers, *Biomacromolecules*, 2005, **6**, 2497–2502.
- 13 C. Tsiptsias and C. Panayiotou, *Carbohydr. Polym.*, 2008, **74**, 99–105.
- 14 K. Y. Lee and D. J. Mooney, *Chem. Rev.*, 2001, **101**, 1869–1879.
- 15 P. Gerentes, L. Vachoud, J. Doury and A. Domard, *Biomaterials*, 2002, **23**, 1295–1302.
- 16 J. Y. Lee, B. Tan and A. I. Cooper, *Macromolecules*, 2007, **40**, 1955–196.
- 17 C. Tsiptsias and C. Panayiotou, *J. Supercrit. Fluids*, 2008, DOI: 10.1016/j.supflu.2008.07.009.
- 18 A. C. Pierre and G. M. Pajonk, *Chem. Rev.*, 2002, **102**, 4243–4265.
- 19 R. Valentin, B. Bonelli, E. Garrone, F. Di Renzo and F. Quignard, *Biomacromolecules*, 2007, **8**, 3646–3650.
- 20 H. Zhang, J. Wu, J. Zhang and J. He, *Macromolecules*, 2005, **38**, 8272–8277.
- 21 A. Kumar and R. K. Gupta, *Fundamentals of Polymers*, McGraw-Hill, New York, 1998, ch. 7.
- 22 D. Dutta, S. Chatterjee, K. T. Pillai, P. K. Pujari and B. N. Ganguly, *Chem. Phys.*, 2005, **312**, 319–324.
- 23 V. Karageorgiou and D. Kaplan, *Biomaterials*, 2005, **26**, 5474–5491.
- 24 A. Bamberger, G. Sieder and G. Maurer, *J. Supercrit. Fluids*, 2000, **17**, 97–110.
- 25 K. S. Chow, E. Khor and A. C. A. Wan, *J. Polym. Res.*, 2001, **8**, 27–35.
- 26 Haibo Xie, Suobo Zhang and Shenghai Li, *Green Chem.*, 2006, **8**, 630–633.
- 27 S. A. Stern and A. H. De Meringo, *J. Polym. Sci., Polym. Phys. Ed.*, 1978, **16**, 735–751.
- 28 E. Sada, H. Kumazawa, Y. Yoshio and S. T. Wang, *J. Polym. Sci., Part B: Polym. Phys.*, 1988, **26**, 1035–1048.
- 29 A. Y. Houde, B. Krishnakumar, G. Charati and S. A. Stern, *J. Appl. Polym. Sci.*, 1996, **62**, 2181–2192.
- 30 Z. Shen, G. S. Huvard, C. S. Warriner, M. Mc Hugh, J. L. Banyasz and M. K. Mishra, *Polymer*, 2008, **49**, 1579–1586.
- 31 J. U. Keller and R. Staudt, *Gas Adsorption Equilibria*, Springer Science + Business Media Inc, Boston, 2005.

A green protocol for synthesis of benzo-fused *N,S*-, *N,O*- and *N,N*-heterocycles in water†

Qing-Yi Zhang, Bo-Kai Liu, Wan-Qin Chen, Qi Wu and Xian-Fu Lin*

Received 24th April 2008, Accepted 24th June 2008

First published as an Advance Article on the web 8th August 2008

DOI: 10.1039/b806960c

A fast and efficient protocol which is associated with readily available starting materials, mild conditions, excellent yields, and a broad range of the products in synthetic chemistry, was established for synthesis of quinoxaline, benzoxazine, and benzothiazine derivatives in water under catalyst-free conditions.

Introduction

Heterocycles are ubiquitous among pharmaceutical compounds.¹ Benzoheterocycle is an important class of nitrogen-containing heterocycles and widely used as key building block for pharmaceutical agents. For example, benzoxazine derivatives exhibit diverse biological activities including plant resistance factors against microbial disease and insects,² potassium channel modulators,³ antirheumatic and antihypertensive activity.⁴ Benzothiazine is useful intermediates in organic synthesis,⁵ having been applied in peptide synthesis,⁶ and used as precursors to thioesters for native chemical ligation.⁷ Quinoxaline not only shows their applications as dyes⁸ and building blocks in the synthesis of organic semiconductors,⁹ but also serves as useful rigid subunits in macrocyclic receptors for molecular recognition¹⁰ and chemically controllable switches.¹¹

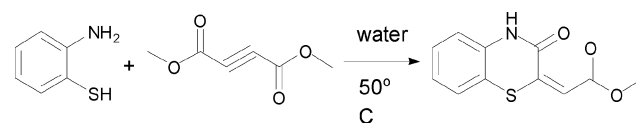
To date, much effort has been devoted to develop the nitrogen-containing heterocycles.¹² For example, various annulation methods¹³ including Pd-catalyzed,¹⁴ microwave-assisted¹⁵ or in the presence of base¹⁶ have been reported for the synthesis of benzoxazines from 2-aminophenols. Benzothiazine was synthesized with 2-aminothiophenol¹⁷ and quinoxaline was from aryl-1,2-diamine.¹⁸ However, the synthesis of these heterocycles has been predominantly carried out in organic solvent. Some limitations such as elevating temperatures, and involving catalyst and hazardous organic solvents were involved. Thus, the development of a simple and efficient method under green reaction conditions for selectively constructing these heterocycles has been advocated.

Water is considerably safe, non-toxic, environmentally friendly and cheap. It has been employed as solvent for catalyst-free formation of C–S,¹⁹ C–N²⁰ and C–C²¹ bonds by conjugate addition reaction. Recently, benzothiazoles, benzothiazolines,²² pyridine and thiazole²³ have been successfully synthesized in water under these catalyst-free conditions. This inspired us to focus on the aspect of “on water” heterocycles synthesis.

Herein, we introduced a highly selective and efficient method for constructing *N*-heterocycles in water without using any catalyst.

Results and discussion

The initial study on the cyclization between 2-aminothiophenol and dimethyl acetylenedicarboxylate (DMAD) was carried out in water at 50 °C for 30 min without any catalyst or additive (Scheme 1). A product was furnished in 97% yield after workup and simple isolation from water. The spectral and analytical data confirmed the structure as 1,4-benzothiazine-3-one. It was worthwhile to mention that the reaction process could be visually monitored. After adding 2-aminothiophenol to the DMAD in water, a turbid solution was observed. When the starting 2-aminothiophenol was completely consumed (monitored by TLC), the reaction mixture became clear and the product existed as solid in water.



Scheme 1 The reaction of 2-aminothiophenol with DMAD in water.

The reactions of 2-aminothiophenol (10 mmol) and DMAD (10 mmol) in different solvents were investigated and the results were shown in Table 1. Some polar organic solvents such as methanol, ethanol and acetonitrile proved to be the efficient media for the cyclization reaction (entries 5–7, Table 1).

Table 1 The solvent effect for synthesis of *N*-heterocycles^a

Entry	Solvent	Time/min	Yield (%) ^b
1	<i>n</i> -Hexane	30	41
2	THF	30	37
3	Toluene	30	58
4	Dioxane	30	61
5	MeOH	30	88
6	EtOH	30	82
7	MeCN	30	83
8	H ₂ O	30	97

^a 2-Aminothiophenol (10 mmol), DMAD (10 mmol), solvent (20 mL) at 50 °C. ^b Isolated yield.

Department of Chemistry, Zhejiang University, Hangzhou, 310027, People's Republic of China. E-mail: llc123@zju.edu.cn

† Electronic supplementary information (ESI) available: ¹H-NMR and ¹³C-NMR spectra for compounds 3a–5f. See DOI: 10.1039/b806960c

Table 2 The reactions of 2-aminothiophenol, 2-aminophenol and 2-aminophenylamine with DMAD or DEAD in water^a

1 + 2 $\xrightarrow[50^\circ\text{C}]{\text{water}}$ 3
X=S, O, NH R₂=CH₃, C₂H₅

Entry	Substrate	Time/ min	Product	Yield (%) ^b	Entry	Substrate	Time/ min	Product	Yield (%) ^b
1		30		97	10		35		96
2		30		96	11		40		94
3		30		96	12		40		93
4		30		96	13		60		55
5		35		95	14		30		96
6		35		94	15		30		95
7		35		95	16		30		93
8		35		95	17		30		92
9		35		93	18		35		91

^a 2-Aminophenylamine (10 mmol), DMAD (10 mmol), water (20 mL) at 50 °C. ^b Isolated yield.

However, water showed a superior advantage not only in promoting the reaction but also in isolation procedure, and excellent yield was achieved (entry 8, Table 1). When the reaction between 2-aminothiophenol and DMAD was carried out in 50 mL water, the product was formed in 95% yields after 30 min. It showed that the amount of water did not have much significant influence on the overall rate of the reaction and the product yield. So water was employed as the reaction media at 20 mL for the following reactions.

Encouraged by this result, the generality of the reaction was investigated for synthesis of *N,S*-, *N,O*- and *N,N*-heterocycles under the same conditions. Results are summarized in Table 2. Firstly, we examined the reaction of 2-aminothiophenol with DMAD or diethylacetylenedicarboxylate (DEAD) in water. The

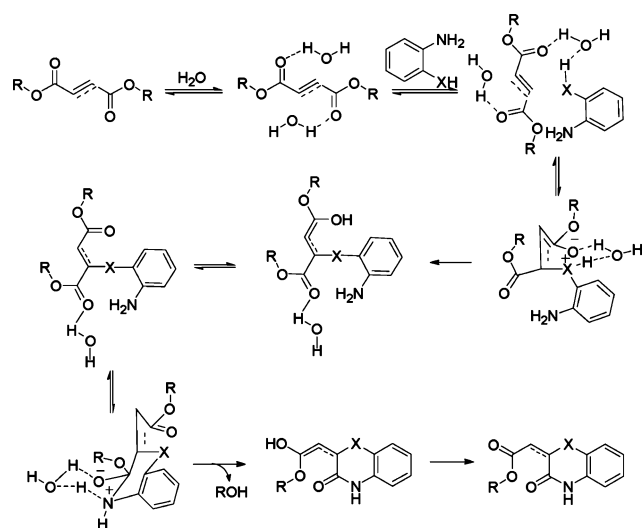
reactions proceeded smoothly and afforded the corresponding 1,4-benzothiazine-3-one with excellent yields in 30 min (entries 1–2, Table 2). 4-Chloro-2-aminothiophenol could also be used as a substrate to give the products in quantitative yields in 30 min. The reactions of diverse 2-aminophenol derivatives with DMAD in water were also investigated. For methyl, chlor, *tert*-butyl and nitro substituted 2-aminophenol derivatives, the reactions mainly generated 1,4-benzothiazine-3-one (entries 5–12, Table 2). The results showed that the substitution group played a minimal role in governing the reactivity of the substrates. The reactions of 2-aminophenylamine and 2-aminonaphthylamine with DMAD or DEAD in water were also considered. The protocol proved to be effective for all these reactions (entries 14–17, Table 2). When the aromatic ring in the substrate

was replaced by an aliphatic one, 91% product was furnished (Table 2, entry 18).

As seen from Table 2, the product of reaction was found to be influenced by the nucleophilicity of the heteroatom. The reaction of 2-aminothiophenol and 2-aminophenol with DMAD did not make products of the *N*-Michael addition. The rate of reaction of 2-aminothiophenol with DMAD was found to be faster than that of 2-aminophenol. Thus, the order of nucleophilicity of the heteroatom was $S > O > N$. On the other hand, when benzylethanamine was treated with DMAD in water, not only highly prolonged time was required, but the product was different (entry 13, Table 2).

The fumarate ester was also investigated. Only thio-Michael adduct was obtained from diethyl fumarate with 2-aminothiophenol under the identical method. Thus, the divinyl fumarate was employed, and results were summarized in Table 3. Compared with DMAD, the reaction of 2-aminothiophenol with divinyl fumarate required longer time. As seen from Table 3, 2-aminothiophenols reacted with divinyl fumarate to give the acyclic intermediates *via* thio-addition, which spontaneously underwent an intramolecular amidation reaction to furnish 3,4-dihydro-2-(vinyl acetate)-2H-1,4-benzothiazine-3-one (Table 3, entry 1). 4-Chloro-2-aminothiophenol could be also used as a substrate to give the products in 88% yield (Table 3, entry 2). 2-Aminophenol derivatives showed higher reactivity. Better yields with 71% and 70% were obtained from 2-aminophenol and 2-amino-3-hydroxypyridine, respectively (Table 3, entries 3 and 4). The *o*-phenylenediamine and 2,3-diaminonaphthalene were also considered. The reactions proceeded smoothly and afforded the corresponding products in good yields (Table 3, entries 5 and 6).

Based on these experimental observations, a tentative mechanism for the cyclization was proposed as Scheme 2. Hydrogen bond between the oxygen atom of water and the sulfhydryl hydrogen of 2-aminothiophenol (or azyl hydrogen



Scheme 2 Proposed mechanism for the annulation.

of 2-aminophenol or oxygen hydrogen of 2-aminophenylamine) increased the nucleophilicity of the sulfur atom of the 2-aminothiophenol (or oxygen atom of 2-aminophenol or nitrogen atom of 2-aminophenylamine). On the other hand, the hydrogen bond involving water and the oxygen atom in the carbonyl group increased the electrophilic character of the carbon adjacent to the carbonyl group. Thus, nucleophilic attack at the carbon atom of the unsaturated carbonyl compound by the sulfur atom (or oxygen atom or nitrogen atom) followed by intramolecular proton transfer led to the conjugate adduct. For DMAD and DEAD, regioselective heteroatom-addition took place to give the acyclic intermediates, of which the methoxy (or ethoxy) group was easily pulled off due to the conjugation between unsaturated double bonds and two carbonyl groups. Then, the intramolecular acylation took place and the corresponding

Table 3 The reactions of 2-aminothiophenol, 2-aminophenol and 2-aminophenylamine with divinyl fumarate in water^a

Entry	Substrate	Time/h	Product	Yield (%) ^b	Entry	Substrate	Time/h	Product	Yield (%) ^b
1		10		86	4		15		70
2		10		88	5		12		78
3		15		71	6		12		80

^a 2-Aminothiophenol (10 mmol), divinyl fumarate (10 mmol), water (20 mL) at 50 °C. ^b Isolated yield.

benzoheterocycles were obtained. However, the conjugation effect disappeared when the addition was carried out with fumarate. Compared with vinyl ester, the reactivity of the methyl ester or ethyl ester was very low, which hindered the cyclization.

Conclusions

In summary, a fast and efficient synthesis of quinoxalines, benzoxazines, and benzothiazines is established. The reaction showed high regioselectivity with excellent yields. This protocol is associated with readily available starting materials, mild conditions, easy operation, and a broad range of substrates. The products show potential in organic chemistry.

Experimental

Typical procedure for synthesis of *N*-heterocycles

Aromatic amine (10 mmol) was dissolved in water and the divinyl fumarate (1.68 g, 10 mmol) was added. The reaction mixture was stirred at 50 °C and monitored by TLC. Upon completion of the reaction, the solvent was removed by filtration without further purification.

2-Methoxycarbonylmethylene-3,4-dihydro-2H-1,4-benzothiazin-3-one (3a). Yellow powder. m.p. 264 °C. ¹H-NMR (500 MHz, DMSO-*d*₆, δ, ppm): 11.50 (s, 1H, NH), 7.41 (d, 1H, *J* = 7.87 Hz, benzene hydrogen), 7.14 (d, 1H, *J* = 8.05 Hz, benzene hydrogen), 7.08 (t, 1H, *J* = 7.50 Hz, *J* = 15.06 Hz, benzene hydrogen), 6.91 (s, 1H, CH), 3.73 (s, 3H, CH₃); ¹³C-NMR (125 MHz, DMSO-*d*₆, δ, ppm): 166.4 (C-12), 154.7 (C-3), 141.5 (C-2), 133.2 (C-9), 127.7 (C-10), 125.7 (C-8), 123.9 (C-7), 117.6 (C-6), 115.5 (C-5), 114.2 (C-11), 52.2 (CH₃); IR (KBr) (*v*_{max}, cm⁻¹): 3180 (NH amide), 3039 (AR-H), 2972 (RH), 1667 (C=O ester), 1667 (C=O amide), 1559 (C=C), 1500 (C=C); ESI-MS (*m/z*): 233.8 [M-1]⁻

2-Ethoxycarbonylmethylene-3,4-dihydro-2H-1,4-benzothiazin-3-one (3b). Yellow powder. m.p. 221 °C. ¹H-NMR (500 MHz, DMSO-*d*₆, δ, ppm): 11.53 (s, 1H), 7.41 (d, 1H, *J* = 7.80 Hz), 7.22 (t, 1H, *J* = 8.25 Hz), 7.13–7.08 (m, 2H), 6.89 (s, 1H), 4.19 (dd, 2H, *J* = 7.05 Hz, *J* = 7.15 Hz), 1.24 (t, 3H, *J* = 7.15 Hz); ¹³C-NMR (125 MHz, DMSO-*d*₆, δ, ppm): 166.0, 154.7, 141.4, 133.2, 127.8, 125.7, 124.0, 117.6, 115.6, 114.6, 60.9, 14.6; IR (KBr) (*v*_{max}, cm⁻¹): 3265, 2979, 1663, 1663. ESI-MS (*m/z*): 247.9 [M-1]⁻

6-Chlor-2-methoxycarbonylmethylene-3,4-dihydro-2H-1,4-benzothiazin-3-one (3c). Yellow powder. m.p. 236 °C. ¹H-NMR (500 MHz, DMSO-*d*₆, δ, ppm): 11.42 (s, 1H), 7.41 (d, 1H, *J* = 8.35 Hz), 7.16 (s, 1H), 7.09 (d, 1H, *J* = 8.10 Hz), 6.91 (s, 1H), 3.74 (s, 3H); ¹³C-NMR (125 MHz, DMSO-*d*₆, δ, ppm): 166.0, 154.5, 140.2, 134.4, 131.5, 127.1, 123.3, 116.6, 116.2, 114.9, 114.5, 52.2; IR (KBr) (*v*_{max}, cm⁻¹): 3264, 3044, 2980, 1664, 1561. ESI-MS (*m/z*): 267.8 [M-1]⁻

6-Chlor-2-ethoxycarbonylmethylene-3,4-dihydro-2H-1,4-benzothiazin-3-one (3d). Yellow powder. m.p. 201 °C. ¹H-NMR (500 MHz, DMSO-*d*₆, δ, ppm): 11.42 (s, 1H), 7.40 (d, 1H, *J* = 8.35 Hz), 7.16 (s, 1H), 7.16 (s, 1H), 7.10 (d, 1H, *J* = 8.10 Hz), 6.91 (s, 1H), 4.19 (t, 2H, *J* = 7.05 Hz), 1.25 (t, 3H, *J* = 7.15 Hz); ¹³C-NMR (125 MHz, DMSO-*d*₆, δ, ppm): 166.4, 154.6, 140.3,

134.4, 131.5, 127.1, 123.3, 116.6, 116.2, 114.9, 114.5, 61.0, 14.6; IR (KBr) (*v*_{max}, cm⁻¹): 3265, 3045, 2979, 1663, 1560. ESI-MS (*m/z*): 281.8 [M-1]⁻

2-Methoxycarbonylmethylene-3,4-dihydro-2H-1,4-benzoxazin-3-one (3e). Yellow powder. m.p. 150 °C. ¹H-NMR (500 MHz, DMSO-*d*₆, δ, ppm): 10.67 (s, 1H, NH), 7.51 (dd, 1H, *J* = 1.10 Hz, *J* = 6.80 Hz, benzene hydrogen), 7.18 (dd, 2H, *J* = 8.00 Hz, *J* = 14.85 Hz, benzene hydrogen), 7.04 (t, 1H, *J* = 1.15 Hz, benzene hydrogen), 5.61 (s, 1H, CH), 3.70 (s, 3H, CH₃); ¹³C-NMR (125 MHz, DMSO-*d*₆, δ, ppm): 169.1 (C-12), 156.4 (C-3), 140.4 (C-2), 139.3 (C-9), 125.7 (C-10), 125.1 (C-8), 123.0 (C-7), 116.8 (C-6), 116.5 (C-5), 88.8 (C-11), 51.6 (C-13); IR (KBr) (*v*_{max}, cm⁻¹): 3332 (NH amide), 3029 (AR-H), 2951 (R-H), 1766 (C=O ester), 1729, 1621 (C=O amide), 1500 (C=C), 1445 (C=C). ESI-MS (*m/z*): 217.8 [M-1]⁻

2-Methoxycarbonylmethylene-3,4-dihydro-2H-pyrido[2,3-*b*]-1,4-oxazin-3-one (3f). Brown powder. m.p. 117–118 °C (Lit. 117–119 °C). ¹H-NMR (500 MHz, DMSO-*d*₆, δ, ppm): 12.11 (s, 1H), 8.06 (dd, 1H, *J* = 1.19 Hz, *J* = 3.67 Hz), 7.57 (dd, 1H, *J* = 1.18 Hz, *J* = 6.94 Hz), 7.11 (dd, 1H, *J* = 4.86 Hz, *J* = 3.19 Hz), 6.05 (s, 1H), 3.69 (s, 1H); ¹³C-NMR (125 MHz, DMSO-*d*₆, δ, ppm): 164.3, 156.1, 151.6, 143.4, 139.70, 136.8, 123.4, 120.0, 99.1, 51.8; IR (KBr) (*v*_{max}, cm⁻¹): 3185, 1747, 1668, 1615; ESI-MS (*m/z*): 218.9 [M-H]⁻

6-Methyl-2-methoxycarbonylmethylene-3,4-dihydro-2H-1,4-benzoxazin-3-one (3g). Yellow powder. m.p. 148–149 °C. ¹H-NMR (500 MHz, DMSO-*d*₆, δ, ppm): 10.60 (s, 1H), 7.33 (d, 1H, *J* = 8.10 Hz), 7.00 (s, 1H), 6.96 (d, 1H, *J* = 8.05 Hz), 5.56 (s, 1H, CH), 3.68 (s, 3H, CH₃), 2.25 (s, 3H, CH₃); ¹³C-NMR (125 MHz, DMSO-*d*₆, δ, ppm): 169.4, 156.8, 140.4, 139.4, 133.1, 126.6, 122.7, 117.2, 116.4, 88.4, 51.8, 21.0; IR (KBr) (*v*_{max}, cm⁻¹): 3184, 1747, 1667, 1615; ESI-MS (*m/z*): 231.8 [M-1]⁻ HRMS calculated for C₁₂H₁₁NO₄, 232.0610 [M-H]⁻ found 232.0613 [M-H]⁻

7-Methyl-2-methoxycarbonylmethylene-3,4-dihydro-2H-1,4-benzoxazin-3-one (3h). Yellow powder. m.p. 147 °C. ¹H-NMR (500 MHz, DMSO-*d*₆, δ, ppm): 10.59 (s, 1H), 7.29 (s, 1H), 7.07 (d, 1H, *J* = 8.25 Hz), 6.84 (dd, 1H, *J* = 1.20 Hz, *J* = 7.00 Hz), 5.60 (s, 1H, CH), 3.70 (s, 3H), 2.26 (s, 3H); ¹³C-NMR (125 MHz, DMSO-*d*₆, δ, ppm): 169.1, 156.4, 140.4, 139.3, 125.7, 125.1, 123.0, 116.8, 116.5, 88.8, 51.6; IR (KBr) (*v*_{max}, cm⁻¹): 3331, 3029, 2951, 1766, 1729, 1621, 1500; ESI-MS (*m/z*): 231.8 [M-1]⁻; HRMS calculated for C₁₂H₁₁NO₄, 232.0610 [M-H]⁻ found 232.0611 [M-H]⁻

6-Chlor-2-methoxycarbonylmethylene-3,4-dihydro-2H-1,4-benzoxazin-3-one (3i). Yellow powder. m.p. 159 °C. ¹H-NMR (500 MHz, DMSO-*d*₆, δ, ppm): 11.66 (s, 1H), 7.69 (d, 1H, *J* = 2.25 Hz), 7.18 (d, 1H, *J* = 8.70 Hz), 7.02 (dd, 1H, *J* = 2.30 Hz, *J* = 6.35 Hz), 5.63 (s, 1H), 3.69 (s, 3H); ¹³C-NMR (125 MHz, DMSO-*d*₆, δ, ppm): 168.7, 156.2, 139.3, 138.6, 129.3, 126.5, 122.3, 118.2, 116.2, 90.1, 51.7; ESI-MS (*m/z*): 251.7 [M-1]⁻; HRMS calculated for C₁₂H₈ClNO₄, 252.0058 [M-H]⁻, found 252.0068 [M-H]⁻

6-tert-Butyl-2-methoxycarbonylmethylene-3,4-dihydro-2H-1,4-benzoxazin-3-one (3j). Yellow powder. m.p. 59–60 °C. ¹H-NMR (500 MHz, DMSO-*d*₆, δ, ppm): 10.67 (s, 1H), 7.62 (d,

1H, $J = 1.95$ Hz), 7.09 (d, 1H, $J = 8.50$ Hz), 7.05 (d, 1H, $J = 1.90$ Hz), 5.60 (s, 1H), 3.70 (s, 3H); $^{13}\text{C-NMR}$ (125 MHz, DMSO- d_6 , δ , ppm): 169.1, 156.6, 148.6, 139.3, 138.3, 124.4, 119.8, 116.1, 113.8, 88.5, 51.5, 31.6; IR (KBr) (ν_{max} , cm^{-1}): 3333, 3029, 2950, 1767, 1730, 1621. ESI-MS (m/z): 273.8 [$\text{M}-1$] $^-$; HRMS calculated for $\text{C}_{15}\text{H}_{17}\text{NO}_4$, 274.1074 [$\text{M}-\text{H}$] $^-$, found 274.1089 [$\text{M}-\text{H}$] $^-$.

5-Nitro-2-methoxycarbonylmethylene-3,4-dihydro-2H-1,4-benzoxazin-3-one (3k). Yellow powder. m.p. 243 °C. $^1\text{H-NMR}$ (500 MHz, DMSO- d_6 , δ , ppm): 10.42 (s, 1H), 8.09 (d, 1H, $J = 8.65$ Hz), 7.66 (d, 1H, $J = 7.95$ Hz), 7.45 (d, 1H, $J = 8.85$ Hz), 5.86 (s, 1H), 3.77 (s, 3H); $^{13}\text{C-NMR}$ (125 MHz, DMSO- d_6 , δ , ppm): 168.9, 155.0, 142.6, 137.7, 133.2, 131.1, 123.4, 122.2, 121.5, 93.8, 52.3; IR (KBr) (ν_{max} , cm^{-1}): 3331, 1766, 1730, 1621. ESI-MS (m/z): 262.7 [$\text{M}-1$] $^-$; HRMS calculated for $\text{C}_{11}\text{H}_8\text{N}_2\text{O}_6$, 264.0299 [$\text{M}-1$] $^-$, found 263.0307 [$\text{M}-1$] $^-$.

7-Nitro-2-methoxycarbonylmethylene-3,4-dihydro-2H-1,4-benzoxazin-3-one (3l). Yellow powder. m.p. 241–242 °C. $^1\text{H-NMR}$ (500 MHz, DMSO- d_6 , δ , ppm): 10.97 (s, 1H), 8.05–8.02 (m, 2H), 7.76 (d, 1H, $J = 8.75$ Hz), 5.77 (s, 1H), 3.74 (s, 3H); $^{13}\text{C-NMR}$ (125 MHz, DMSO- d_6 , δ , ppm): 168.3, 155.8, 141.5, 140.0, 138.1, 131.9, 121.5, 116.6, 112.54, 92.6, 51.9; IR (KBr) (ν_{max} , cm^{-1}): 3332, 1766, 1729, 1621. ESI-MS (m/z): 262.7 [$\text{M}-1$] $^-$; HRMS calculated for $\text{C}_{11}\text{H}_8\text{N}_2\text{O}_6$, 264.0299 [$\text{M}-1$] $^-$, found 263.0308 [$\text{M}-1$] $^-$.

(4-Benzyl-3-oxo-morpholin-2-ylidene)-acetic acid methyl ester (3m). $^1\text{H-NMR}$ (500 MHz, CDCl_3 , δ , ppm): 7.36–7.25 (m, 5H), 5.85 (s, 1H), 4.67 (s, 2H), 4.34 (dd, 2H, $J = 3.30$ Hz, $J = 4.95$ Hz), 3.67 (s, 3H), 3.22 (t, 2H, $J = 5.00$ Hz); $^{13}\text{C-NMR}$ (125 MHz, CDCl_3 , δ , ppm): 166.6, 163.7, 144.4, 135.8, 129.3, 129.0, 128.7, 128.2, 127.3, 95.1, 85.1, 59.0, 51.4, 46.1; IR (KBr) (ν_{max} , cm^{-1}): 3010 (=CH), 1686, 1633; ESI-MS (m/z): 262 [$\text{M}+1$] $^+$; HRMS calculated for $\text{C}_{14}\text{H}_{15}\text{NO}_4$, 261.1001, found 261.1004.

3,4-Dihydro-3-(methoxycarbonylmethylene)-quinoxalin-2(1H)-one (3n). Yellow powder. m.p. 227 °C. $^1\text{H-NMR}$ (500 MHz, DMSO- d_6 , δ , ppm): 11.73 (s, 1H, NH), 11.02 (s, 1H, NH), 7.38 (d, 1H, $J = 7.35$ Hz, benzene hydrogen), 7.067–7.00 (m, 3H, benzene hydrogen), 5.51 (s, 1H, CH), 3.67 (s, 3H, CH_3); $^{13}\text{C-NMR}$ (125 MHz, DMSO- d_6 , δ , ppm): 170.0 (C-12), 156.1 (C-3), 144.5 (C-2), 125.6 (C-9), 125.3 (C-10), 124.0 (C-8), 123.1 (C-7), 115.9 (C-6), 115.7 (C-5), 83.9 (C-11), 51.2 (C-13); IR (KBr) (ν_{max} , cm^{-1}): 3259 (NH amide), 3203 (NH), 3047 (Ar-H), 3010 (=CH), 2888 (R-H), 1688 (C=O ester), 1635 (C=O amide), 1504 (C=C), 1434 (C=C); ESI-MS (m/z): 216.7 [$\text{M}-1$] $^-$.

3,4-Dihydro-3-(ethoxycarbonylmethylene) quinoxalin-2(1H)-one (3o). Yellow powder. m.p. 218 °C. $^1\text{H-NMR}$ (500 MHz, DMSO- d_6 , δ , ppm): 11.72 (s, 1H), 11.04 (s, 1H), 7.37 (t, 1H, $J = 1.10$ Hz), 7.06–7.09 (m, 3H), 5.48 (s, 1H), 4.14 (dd, 2H, $J = 7.10$ Hz, $J = 7.05$ Hz), 1.22 (t, 3H, $J = 7.05$ Hz); $^{13}\text{C-NMR}$ (125 MHz, DMSO- d_6 , δ , ppm): 169.7, 156.2, 144.5, 125.7, 125.4, 124.0, 123.9, 115.9, 115.8, 84.3, 59.7, 14.9; IR (KBr) (ν_{max} , cm^{-1}): 3250, 3130, 3020, 2960, 1677, 1630, 1608; ESI-MS (m/z): 230.7 [$\text{M}-\text{H}$] $^-$.

3,4-Dihydro-3-(methoxycarbonylmethylene)-benzoquinoxalin-2(1H)-one (3p). Yellow powder. m.p. 239–240 °C. $^1\text{H-NMR}$

(500 MHz, DMSO- d_6 , δ , ppm): 11.94 (s, 1H), 11.07 (s, 1H), 7.79 (s, 1H), 7.75 (dd, 2H, $J = 3.70$ Hz, $J = 8.30$ Hz), 7.44 (s, 1H), 7.35 (t, 2H, $J = 7.05$ Hz), 5.60 (s, 1H), 3.70 (s, 3H); $^{13}\text{C-NMR}$ (125 MHz, DMSO- d_6 , δ , ppm): 169.9, 156.3, 143.8, 130.4, 129.6, 127.2, 126.4, 125.6, 125.3, 111.4, 111.4, 85.7, 51.4; IR (KBr) (ν_{max} , cm^{-1}): 3249, 3129, 2960, 1677, 1629; ESI-MS (m/z): 266.8 [$\text{M}-\text{H}$] $^-$.

3,4-Dihydro-3-(methoxycarbonylmethylene)-benzoquinoxalin-2(1H)-one (3q). Yellow powder. m.p. 227 °C. $^1\text{H-NMR}$ (500 MHz, DMSO- d_6 , δ , ppm): 11.95 (s, 1H), 11.13 (s, 1H), 7.83 (s, 1H), 7.76 (dd, 2H, $J = 7.65$ Hz, $J = 9.25$ Hz), 7.46 (s, 1H), 7.36 (dd, 2H, $J = 1.45$ Hz, $J = 6.15$ Hz), 5.60 (s, 1H), 4.19 (dd, 2H, $J = 7.10$ Hz, $J = 7.15$ Hz), 1.26 (t, 3H, $J = 7.05$ Hz); $^{13}\text{C-NMR}$ (125 MHz, DMSO- d_6 , δ , ppm): 169.6, 156.3, 143.8, 130.4, 129.6, 127.2, 127.1, 126.4, 125.6, 125.6, 111.4, 111.3, 86.0, 59.9, 14.8; IR (KBr) (ν_{max} , cm^{-1}): 3250, 3129, 2961, 1677, 1630; ESI-MS (m/z): 280.8 [$\text{M}-\text{H}$] $^-$.

Octahydro-3-(methoxycarbonylmethylene)-quinoxalin-2(1H)-one (3r). Yellow powder. m.p. 162 °C. $^1\text{H-NMR}$ (500 MHz, DMSO- d_6 , δ , ppm): 8.57 (s, 1H), 8.06 (s, 1H), 5.26 (s, 1H), 3.14 (d, 1H, $J = 10.28$ Hz), 3.05 (d, 1H, $J = 7.65$ Hz), 1.96 (d, 1H, $J = 9.45$ Hz), 1.86 (d, 1H, $J = 10.03$ Hz), 1.67 (m, 2H), 1.27 (m, 4H); $^{13}\text{C-NMR}$ (125 MHz, DMSO- d_6 , δ , ppm): 170.5, 160.4, 150.9, 84.2, 55.3, 55.1, 51.0, 29.7, 29.61, 24.1, 23.8; IR (KBr) (ν_{max} , cm^{-1}): 3249, 3129, 2959, 1676, 1630; ESI-MS (m/z): 222.8 [$\text{M}-\text{H}$] $^-$.

3,4-dihydro-2H-1,4-benzothiazin-2-vinyl acetates (5a). Colorless solid. 136 °C. $^1\text{H-NMR}$ (500 MHz, CDCl_3 , δ , ppm): 9.47 (s, 1H), 7.32–7.28 (m, 2H), 7.18 (t, 1H, $J = 7.37$ Hz), 7.04 (m, 1H), 6.92 (d, 1H, $J = 7.86$ Hz), 4.93 (dd, 1H, $J = 1.55$ Hz, $J = 12.44$ Hz), 4.63 (dd, 1H, $J = 1.53$ Hz, $J = 4.65$ Hz), 4.04 (dd, 1H, $J = 0.8$ Hz, $J = 6.78$ Hz), 3.15 (dd, 1H, $J = 6.45$ Hz, $J = 10.32$ Hz), 2.70 (dd, 1H, $J = 7.79$ Hz, $J = 8.96$ Hz); $^{13}\text{C-NMR}$ (125 MHz, CDCl_3 , δ , ppm): 167.7, 167.3, 141.3, 136.2, 128.3, 127.8, 124.4, 119.14, 117.7, 98.7, 37.9, 34.1; ESI-MS (m/z): 271.8 ($\text{M}+\text{Na}$) $^+$; HRMS calculated for $\text{C}_{12}\text{H}_{11}\text{NO}_3\text{S}$, 272.0352 [$\text{M}+\text{Na}$] $^+$, found 272.0351 [$\text{M}+\text{Na}$] $^+$.

6-Chlor-3,4-dihydro-2H-1,4-benzothiazin-2-vinyl acetates (5b). Colorless solid. 142 °C; $^1\text{H-NMR}$ (500 MHz, CDCl_3 , δ , ppm): 9.55 (s, 1H), 7.32–7.23 (m, 2H), 7.02 (t, 1H, $J = 1.80$ Hz, $J = 6.50$ Hz), 6.94 (s, 1H), 4.96 (dd, 1H, $J = 1.40$ Hz, $J = 12.50$ Hz), 4.65 (dd, 1H, $J = 1.40$ Hz, $J = 4.75$ Hz), 4.03 (t, 1H, $J = 7.25$ Hz), 3.16 (dd, 1H, $J = 6.60$ Hz, $J = 10.20$ Hz), 2.71 (dd, 1H, $J = 7.60$ Hz, $J = 9.15$ Hz); $^{13}\text{C-NMR}$ (125 MHz, CDCl_3 , δ , ppm): 167.5, 167.3, 141.2, 137.0, 133.5, 129.3, 117.7, 117.6, 98.9, 37.8, 33.9; HRMS calculated for $\text{C}_{12}\text{H}_{10}\text{ClNO}_3\text{S}$, 305.9965 [$\text{M}+\text{Na}$] $^+$, found 305.9964 [$\text{M}+\text{Na}$] $^+$.

3,4-dihydro-2H-1,4-benzoxazin-2-vinyl acetates (5c). Yellow solid. m.p. 145 °C; $^1\text{H-NMR}$ (500 MHz, CDCl_3 , δ , ppm): 7.96 (s, 1H), 7.38–7.29 (m, 2H), 7.05–6.92 (m, 3H), 5.01 (m, 1H), 4.95 (dd, 1H, $J = 1.56$ Hz, $J = 12.43$ Hz), 4.74 (t, 1H, $J = 1.50$ Hz), 3.25 (dd, 1H, $J = 4.19$ Hz, $J = 12.72$ Hz), 3.08 (dd, 1H, (dd, 1H, $J = 7.47$ Hz, $J = 9.43$ Hz); $^{13}\text{C-NMR}$ (125 MHz, CDCl_3 , δ , ppm): 167.3, 166.0, 141.2, 136.7, 131.6, 124.7, 123.3, 117.4, 115.9, 98.7, 73.5, 35.8; HRMS calculated for $\text{C}_{12}\text{H}_{11}\text{NO}_4$, 256.0580 [$\text{M}+\text{Na}$] $^+$, found 256.0578 [$\text{M}+\text{Na}$] $^+$.

3,4-dihydro-2H-pyrido[3,2,b]-1,4-benzoxazine-2-vinyl acetate (5d). Yellow solid. m.p. 112 °C; ¹H-NMR (500 MHz, CDCl₃, δ, ppm): 8.06–8.04 (m, 2H), 7.56 (dd, H, *J* = 1.10 Hz, *J* = 6.90 Hz), 7.11 (dd, 1H, *J* = 4.70 Hz, *J* = 3.25 Hz), 5.02 (m, 1H), 4.92 (dd, 1H, *J* = 1.60 Hz, *J* = 12.45 Hz), 4.74 (t, 1H, *J* = 1.60 Hz), 3.25 (dd, 1H, *J* = 4.20 Hz, *J* = 12.70 Hz), 3.08 (t, 1H, *J* = 7.50 Hz); ¹³C-NMR (125 MHz, CDCl₃, δ, ppm): 170.1, 167.8, 143.4, 141.3, 139.7, 136.8, 123.4, 120.0, 98.7, 73.5, 35.8; HRMS calculated for C₁₁H₁₀N₂O₄, 257.0533 [M+Na]⁺, found 257.0530 [M+Na]⁺.

3,4-Dihydro-2H-1,4-quinoxalin-3-vinyl acetates (5e). Yellow solid. m.p. 108 °C; ¹H-NMR (500 MHz, CDCl₃, δ, ppm): 8.58 (s, 1H), 7.28 (dd, 1H, *J* = 6.23 Hz, *J* = 7.67 Hz), 6.91 (m, 1H), 6.79–6.70 (m, 3H), 4.94 (dd, 1H, *J* = 1.73 Hz, *J* = 12.21 Hz), 4.66 (m, 2H), 4.39 (m, 1H), 3.24 (dd, 1H, *J* = 2.69 Hz, *J* = 14.90 Hz), 2.84 (dd, 1H, *J* = 7.25 Hz, *J* = 10.32 Hz); ¹³C-NMR (125 MHz, CDCl₃, δ, ppm): 169.4, 167.2, 141.0, 133.0, 125.2, 124.5, 120.1, 115.7, 114.8, 99.1, 52.9, 36.2; HRMS calculated for C₁₂H₁₂N₂O₃, 255.0740 [M+Na]⁺, found 255.0742 [M+Na]⁺.

3,4-Dihydro-2H-1,4-benzoquinoxaline-3-vinyl acetate (5f). Yellow solid. m.p. 91 °C; ¹H-NMR (500 MHz, CDCl₃, δ, ppm): 11.94 (s, 1H), 11.07 (s, 1H), 6.80–7.73 (m, 3H), 7.44 (s, 1H), 7.36–7.33 (m, 4H), 5.04–4.92 (m, 2H), 4.74 (t, 1H, *J* = 1.50 Hz), 3.25 (dd, 1H, *J* = 4.20 Hz, *J* = 12.70 Hz), 3.08 (dd, 1H, *J* = 7.45 Hz, *J* = 9.45 Hz); ¹³C-NMR (125 MHz, CDCl₃, δ, ppm): 169.8, 167.8, 141.9, 133.0, 129.6, 127.2, 127.1, 126.4, 125.6, 125.3, 111.4, 111.3, 99.1, 52.9, 36.4; HRMS calculated for C₁₆H₁₄N₂O₃, 305.0896 [M+Na]⁺, found 305.0898 [M+Na]⁺.

Notes and references

- 1 T. Eicher, S. Hauptmann, *The Chemistry of Heterocycles*, 2nd edn, Wiley-VCH, Weinheim, 2003.
- 2 H. M. Niemeyer, *Phytochemistry*, 1988, **27**, 3349–3358.
- 3 G. Caliendo, P. Grieco, E. Perissutti, V. Santagada, A. Santini, S. Alberizio, C. Fattorusso, A. Pinto and R. Sorrentino, *Eur. J. Med. Chem.*, 1998, **33**, 957–967; G. Caliendo, E. Perissutti, V. Santagada, F. Fiorino, B. Severino, L. Lippolis, A. Pinto and R. Sorrentino, *Bioorg. Med. Chem.*, 2002, **10**, 2663–2669, For review, see: S. Sebille, P. de Tullio, S. Boverie, M. H. Antoine, P. Lebrun and B. Pirotte, *Curr. Med. Chem.*, 2004, **11**, 1213–1222.
- 4 H. Matsuoka, N. Ohi, M. Mihara, H. Suzuki, K. Miyamoto, N. Maruyama, K. Tsuji, N. Kato, T. Akimoto, Y. Takeda, K. Yano and T. Kuroki, *J. Med. Chem.*, 1997, **40**, 105–111.
- 5 R. M. Acheson and N. F. Elmor, *Adv. Heterocycl. Chem.*, 1978, **23**, 263.
- 6 D. Yamashiro and J. Blake, *Int. J. Pept. Protein Res.*, 1981, **18**, 383–392; Y. V. Mitin and N. P. Zapevalova, *Int. J. Pept. Protein Res.*, 1990, **35**, 352–356.
- 7 P. E. Dawson, T. W. Muir, I. Clark-Lewis and S. B. H. Kent, *Science*, 1994, **266**, 776; P. E. Dawson and S. B. H. Kent, *Biochem.*, 2000, **69**, 923–960; D. S. Y. Yeo, R. Srinivasan, G. Y. J. Chen and S. Q. Yao, *Chem.–Eur. J.*, 2004, **10**, 4664–4672.
- 8 E. D. Brock, D. M. Lewis, T. I. Yousaf, H. H. Harper, (The Proctor and Gamble Company), WO 9951688, 1999; N. D. Sonawane and D. W. J. Rangnekar, *Heterocycl. Chem.*, 2002, **39**, 303–308; A. Katoh, T. Yoshida and J. Ohkando, *Heterocycles*, 2000, **52**, 911–920.
- 9 S. Dailey, J. W. Feast, R. J. Peace, I. C. Sage, S. Till and E. L. Wood, *J. Mater. Chem.*, 2001, **11**, 2238–2243; D. O'Brien, M. S. Weaver, D. G. Lidzey and D. D. C. Bradley, *Appl. Phys. Lett.*, 1996, **69**, 881–883.
- 10 T. Mizuno, W. H. Wei, L. R. Eller and J. L. Sessler, *J. Am. Chem. Soc.*, 2002, **124**, 1134–1135; A. H. M. Elwahi, *Tetrahedron*, 2000, **56**, 897–907.
- 11 J. C. Crossley and L. A. Johnston, *Chem. Commun.*, 2002, 1122.
- 12 V. Polshettiwar and R. S. Varma, *Tetrahedron Lett.*, 2008, **49**, 397–400; V. Polshettiwar and R. S. Varma, *J. Org. Chem.*, 2007, **72**, 7420–7422; Y. H. Ju and R. S. Varma, *J. Org. Chem.*, 2006, **71**, 135–141; Y. H. Ju and R. S. Varma, *Org. Lett.*, 2005, **7**, 2409–2411; Y. H. Ju and R. S. Varma, *Tetrahedron Lett.*, 2005, **46**, 6011–6014.
- 13 P. tefanič, M. Anderluh, J. Ilaš, J. Mravljak, M. Sollner-Dolenc, M. Stegnar and D. Kikelj, *J. Med. Chem.*, 2005, **48**, 3110–3113; P. Štefanič, Z. Simončič, M. Breznik, J. Plavec, M. Anderluh, E. Addicks, A. Giannis and D. Kikelj, *Org. Biomol. Chem.*, 2004, **2**, 1511–1517, For review of 1,4-benzoxazine, see: J. Llas, P. S. Anderluh, M. S. Dolenc and D. Kikelj, *Tetrahedron*, 2005, **61**, 7325–7348.
- 14 M. M. Heravi, N. Nami, H. A. Oskooie and R. Hekmatshoar, *Phosphorus, Sulfur, and Silicon, and the Related Elements*, 2005, **180**, 1873–1878; I. Yavari, M. Adib and L. Hojabri, *Tetrahedron*, 2002, **58**, 6895–6899; F. Touzeau, A. Arrault, G. Guillaumet, E. Scalbert, B. Pfeiffer, M. Rettori, P. Renard and J. Y. Mèrou, *J. Med. Chem.*, 2003, **46**, 1962–1979; A. S. Bourlot, I. Sánchez, G. Dureng, G. Guillaumet, R. Massingham, A. Monteil, E. Winslow, M. D. Pujol and J. Y. Mèrou, *J. Med. Chem.*, 1998, **41**, 3142–3158; N. G. Kundu, G. Chaudhuri and A. Upadhyay, *J. Org. Chem.*, 2001, **66**, 20–29; A. Yamazaki, I. Achiwa and K. Achiwa, *Tetrahedron: Asymmetry*, 1996, **7**, 403–406; D. Albanese, D. Landini and M. Penso, *Chem. Commun.*, 1999, 2095–2096; C. Buon, L. Chacun-Lefèvre, R. Rabot, P. Bouyssou and G. Coudert, *Tetrahedron*, 2000, **56**, 605–614; K. E. Torraca, S. I. Kuwabe and S. L. Buchwald, *J. Am. Chem. Soc.*, 2000, **122**, 12907–12908; S. Kuwabe, K. Torraca and S. L. Buchwald, *J. Am. Chem. Soc.*, 2001, **123**, 12202–12206; S. D. Cho, Y. D. Park, J. J. Kim, S. G. Lee, C. Ma, S. Y. Song, W. H. Joo, J. R. Falck, M. Shiro, D. S. Shin and Y. J. Yoon, *J. Org. Chem.*, 2003, **68**, 7918–7920.
- 15 G. Caliendo, E. Perissutti, V. Santagada, F. Fiorino, B. Severino, D. Cirillo, R. d'Emmanuele di Villa Bianca, L. Lippolis, A. Pinto and R. Sorrentino, *Eur. J. Med. Chem.*, 2004, **39**, 815–826; W. M. Dai, X. Wang and C. Ma, *Tetrahedron*, 2005, **61**, 6879–6885; G. F. Feng, J. L. Wu and W. M. Dai, *Tetrahedron*, 2006, **62**, 4635–4642.
- 16 T. Kuroita, N. Marubayashi, M. Sano, K. Kanzaki, K. Inaba and T. Kawakita, *Chem. Pharm. Bull.*, 1996, **44**, 2051–2060; G. Caliendo, P. Grieco, E. Perissutti, V. Santagada, A. Santini, S. Alberizio, C. Fattorusso, A. Pinto and R. Sorrentino, *Eur. J. Med. Chem.*, 1998, **33**, 957–967; G. Caliendo, E. Perissutti, V. Santagada, F. Fiorino, B. Severino, R. d'Emmanuele di Villa Bianca, L. Lippolis, A. Pinto and R. Sorrentino, *Bioorg. Med. Chem.*, 2002, **10**, 2663–2669; D. W. Combs, M. S. Rampulla, S. C. Bell, D. H. Klaubert, A. J. Tobia, R. Falotico, B. Haertlein, C. Lakas-Weiss and J. B. Moore, *J. Med. Chem.*, 1990, **33**, 380–386; A. Arrault, F. Touzeau, G. Guillaumet, J. M. Léger, C. Jarry and J. Y. Mèrou, *Tetrahedron*, 2002, **58**, 8145–8152.
- 17 J. Krapcho and C. F. Turk, *J. Med. Chem.*, 1973, **16**, 776–779; L. V. Saloutina, A. Y. Zapevalov, V. I. Saloutin, P. I. Slepoukin, M. I. Kodess, V. E. Kirichenko, M. G. Pervova and O. N. Chupakin, *J. Fluorine Chem.*, 2007, **128**, 769–778; V. O. Koz'minykh, V. I. Goncharov and E. N. Koz'minykh, *Russ. J. Org. Chem.*, 2006, **42**, 1715–1718.
- 18 J. Krapcho, A. Szabo and J. Williams, *J. Med. Chem.*, 1963, 214–216; J. M. Teulon, European Patent Appl. EP 1163, 1984; J. M. Teulon, *Chem. Abs.*, 1986, **104**, 109668; A. Kirchner, *J. Am. Chem. Soc.*, 1959, **81**, 1721–1726; E. N. Koz'minykh, N. M. Igidov, V. O. Koz'minykh, G. A. Shavkunova and O. A. Sof'ina, *Zh. Org. Khim.*, 2000, **36**, 1381.
- 19 G. L. Khatik, R. Kumar and A. K. Chakraborti, *Org. Lett.*, 2006, **8**, 2433–2436; B. C. Ranu and T. Mandal, *Synlett*, 2007, **6**, 925–928.
- 20 N. Azizi and M. R. Saidi, *Org. Lett.*, 2005, **7**, 3649–3651; B. C. Ranu and S. Banerjee, *Tetrahedron Lett.*, 2007, **48**, 141–143.
- 21 H. B. Zhang, L. Liu, Y. L. Chen, D. Wang and C. J. Li, *Eur. J. Org. Chem.*, 2006, **4**, 859–873; R. Breslow, *Acc. Chem. Res.*, 1991, **24**, 159–164; R. Breslow, *Acc. Chem. Res.*, 2004, **37**, 471–478.
- 22 A. K. Chakraborti, S. Rudrawar, K. B. adhav, G. Kaur and S. V. Chankeshwara, *Green Chem.*, 2007, **9**, 1335–1340.
- 23 M. Adib, M. Mahdavi, M. A. Noghani and P. Mirzaei, *Tetrahedron Lett.*, 2007, **48**, 7263–7265.

Rapid and convenient laboratory method for the preparation of *p*-*tert*-butylcalix[4]arene using microwave irradiation

Masafumi Takagaki,^a Asao Hosoda,^a Hajime Mori,^a Yasuhito Miyake,^a Keiichi Kimura,^b Hisaji Taniguchi^a and Eisaku Nomura^{*c}

Received 30th January 2008, Accepted 18th June 2008

First published as an Advance Article on the web 8th August 2008

DOI: 10.1039/b801715h

Rapid preparation of *p*-*tert*-butylcalix[4]arene using microwave irradiation was studied and *p*-*tert*-butylcalix[4]arene was obtained as a pure form in modest yield with shortening the reaction time from hours to minutes.

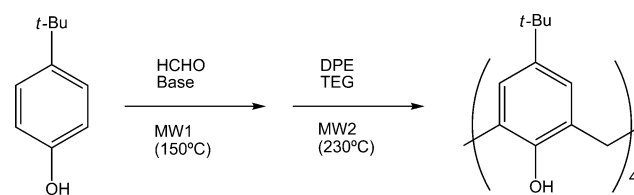
Introduction

Preparation methods of the major calixarenes, *p*-*tert*-butylcalix[*n*]arenes (*n* = 4,6,8), were established based on controlled base-catalyzed condensations of *p*-*tert*-phenol with formaldehyde.^{1–4} In these methods, the reaction mixtures were heated under reflux for several hours. In particular, high-temperature conditions for the cyclic tetramer, *p*-*tert*-butylcalix[4]arene, were required^{1,2} due to the fact that a tetramer was formed as a thermodynamically favored product from the cyclic octamer and/or linear oligomer.^{5–7} On the other hand, the cyclic octamer was considered to be the kinetically favored product. Some approaches to efficient and environmentally friendly syntheses of the calixarenes and related compounds have been continuously conducted: *e.g.* solventless procedures for calixarenes⁷ and calixresorcinarenes,⁸ and microwave-assisted syntheses for pyrogallol[4]arenes⁹ and azocalixarenes.¹⁰ However, for the major calixarenes, such as *p*-*tert*-butylcalix[4]arene, few approaches have been studied, even though yields of the isolated tetramer were around 50% or less. On the transformation of the octamer to the tetramer the pathway of fragmentation/recombination was established.⁶ It was assumed that longer heating under the high-temperature conditions caused reduction of the overall yield of the product or convergence with the tetramer as a thermodynamically product. Therefore, a microwave technique seems to be suitable for the formation of the tetramer in higher yield with shortened reaction time.

Microwave-assisted organic reactions have been of growing interest as a method for environmentally friendly processes.¹¹ The salient feature of microwave irradiation is that often a decrease in reaction time is observed. In many cases, the heating methods had possibilities for reducing by-products and/or formation of products in high yields. A modern microwave

apparatus for organic synthesis is able to control reaction conditions such as temperature, pressure, *etc.*

We report herein the rapid formation of the tetramer using microwave irradiation in an acceptable yield under fully controlled temperature conditions (Scheme 1). The influence of some reaction parameters, such as reaction temperature, solvent composition, concentration of base, and so on was examined. This microwave protocol for preparing the tetramer may be a useful laboratory method that is available only when needed.



Scheme 1

Results and discussion

In the case of microwave irradiation, it is noteworthy that polar molecules that have dipole moments are heated directly. Therefore, the use of polar solvents is an easy way to increase the temperature of the reaction mixture. In the conventional reaction system for obtaining the tetramer, diphenylether (DPE) was used to reflux at around 250 °C.² However, DPE has a low dipole moment and results in difficulties raising the temperature quickly to around 250 °C with microwave irradiation. Ethylene glycol (EG) and polyethylene glycol (PEG) are used as organic solvents for microwave-assisted high temperature reactions.¹² Therefore, the solvents consisting of an oxyethylene unit were chosen as a heating media for this reaction. The heating profiles of these solvents with microwave irradiation are shown in Fig. 1. Polyoxyethylenes having over two oxyethylene units were considered to be suitable for the formation of the tetramer. Among these solvents, the reactions using triethylene glycol (TEG) as a co-solvent (DPE/TEG = 1/2) gave the tetramer in a moderate yield (entry 10 in Table 1), which is comparable that of the conventional method. The results are summarized in Table 1. An optimized reaction procedure is described in the experimental section. While acetone was contained in the

^aIndustrial Technology Centre of Wakayama Prefecture, 60 Ogura, Wakayama, 649-6261, Japan

^bFaculty of Material Science, Wakayama University, 930 Sakaedani, Wakayama, 640-8510, Japan

^cDepartment of Material Science, Wakayama National College of Technology, 77 Noshima, Nada, Gobo Wakayama, 644-0023, Japan. E-mail: nomura@wakayama-nct.ac.jp; Fax: +81-738-29-8439; Tel: +81-738-23-8415

Table 1 Microwave-assisted calixarene-forming reaction^a

Entry	NaOH/mmol	MW1	Solvents	MW2	Yields (%)		
					Tetramer	Octamer	Hexamer
1	0.30	150 °C, 5 min	TEG (3 mL)	230 °C, 10 min	22.7	2.2	0
2	0.15	100 °C, 5 min	DPE/TEG (1/2, 3 mL)	230 °C, 10 min	20.4	0	0
3	0.15	150 °C, 5 min	DPE/TEG (1/2, 3 mL)	230 °C, 10 min	34.7	0	0
4	0.15	150 °C, 10 min	DPE/TEG (1/2, 3 mL)	230 °C, 10 min	35.9	0	0
5	0.15	150 °C, 15 min	DPE/TEG (1/2, 3 mL)	230 °C, 10 min	36.3	0	0
6	0.15	200 °C, 5 min	DPE/TEG (1/2, 3 mL)	230 °C, 10 min	25.5	0.6	0
7	0.15	150 °C, 5 min	DPE/DEG (1/2, 3 mL)	230 °C, 10 min	23.5	12.1	0
8	0.15	150 °C, 5 min	DPE/PEG200 (1/2, 3 mL)	230 °C, 10 min	34.1	0	0
9	0.15	150 °C, 5 min	DPE/Glycerol (1/2, 3 mL)	230 °C, 10 min	9.6	37.5	0
10	0.45	150 °C, 5 min	DPE/TEG (1/2, 6 mL)	230 °C, 10 min	53.7	0	0
11	0.45	150 °C, 5 min	none	230 °C, 10 min	1.7	7.8	0

^a 3.33 mmol (0.5 g) of *p*-*tert*-butylphenol, 4.04 mmol of 36% formaldehyde aq. solution and 0.15–0.45 mmol of 10 M NaOH aq. solution were placed in the flask and the microwave was irradiated at the initial stage of the reaction (MW1). After adding solvents the microwave was irradiated again (MW2).

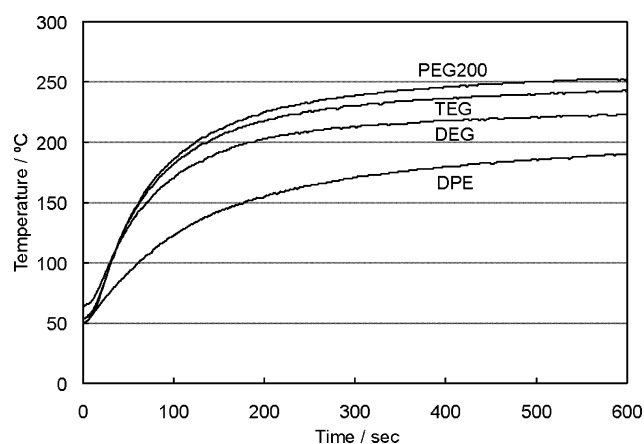


Fig. 1 Temperature profiles for DPE, DEG, TEG, and PEG200. Conditions: 2 mL of solvent was irradiated by a single-mode microwave, setting maximum temperature at 250 °C.

tetramer, obtained as a white powder after drying under reduced pressure, no other by-products in this form were detected in NMR and MS spectra. The reaction mixture after the reaction, except when forming the tetramer, contained small amounts of the pentamer, the hexamer and the heptamer, which were detected by MS spectra, as shown in Fig. 2. The purification was achieved by a simple working up process. In the general procedure, acetone and 6 M HCl were added to neutralize the mixture after the reaction. In the case of the tetramer, however, it is enough for laboratory use that only acetone was added and the resulting precipitate was filtrated, followed by washing in acetone, due to the use of a very small amount of alkali. It is noteworthy that acetone could be recovered by distillation of the discharged solvents and also DPE could be reused by distillation after extracting TEG to water.

In the preparation of the major calixarenes, temperature, nature of base, and ratio of base to phenol are known to be important factors.¹ A two-step heating process was required for the formation of the tetramer.^{1,2} In the first stage of heating the precursor was formed, consisting of the linear oligomers and/or the cyclic octamer.⁶ Upon addition of a solvent having

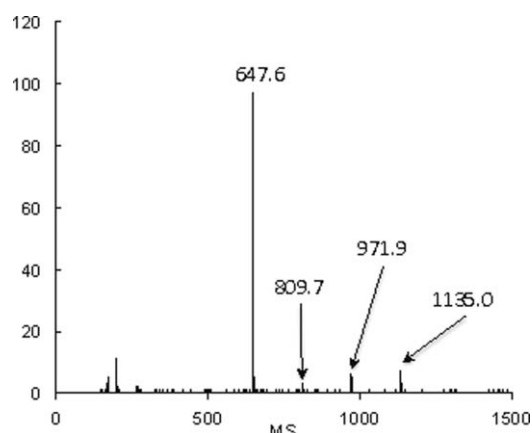


Fig. 2 ESI-TOF negative ion mass spectrum of the products in the reaction mixture: M-1 signals, the tetramer (*m/e* 647.6, calcd 647.4), the pentamer (*m/e* 809.7, calcd 809.5), the hexamer (*m/e* 971.9, calcd 971.6), the heptamer (*m/e* 1135.0, calcd 1133.7).

a high boiling point, the temperature was increased to afford the cyclic tetramer. In the reaction using a microwave, subtle temperature control was required. We examined the effect of the maximum temperature in the formation of the precursors and a temperature at 150 °C for 5 min was enough to afford the products (entry 2–6 in Table 1). The effect of a maximum temperature for the second heating after adding solvents was investigated and the results are shown in Fig. 3. Both the tetramer and the octamer were isolated in low yields with the temperature as low as 200 °C. The optimal temperature in our reaction system seemed to be around 230 °C. The yield of the tetramer did not significantly increase for longer microwave heating over 10 minutes.

The volume of the mixed-solvent consisting of DPE and TEG (1 : 2) also affected the yields of the products, as shown in Fig. 4. The octamer was produced as a major product in the absence of the solvent at the second microwave heating (entry 11 in Table 1). The optimum amount of the solvent in the reaction was around 6 mL. Larger amounts of the solvent decreased the yield of the tetramer, with the production of the octamer. It was likely to be caused by the slow rate of temperature increase.

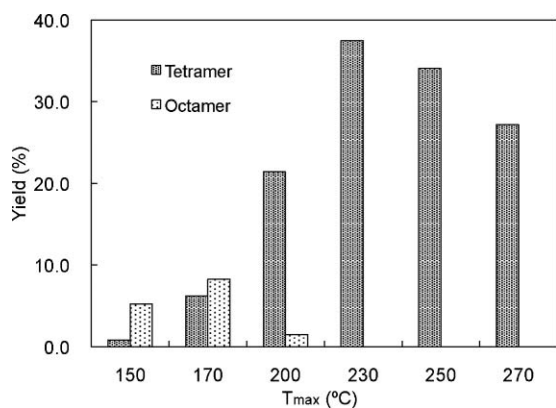


Fig. 3 Distribution of the calixarenes depending on the temperature of the second heating. Reaction conditions: 3.33 mmol (0.5 g) of *p*-*tert*-butylphenol, 4.04 mmol (0.31 mL) of formaldehyde (36% aq. solution), and 15 mM of 10 M aq. NaOH were heated with an initial microwave irradiation at max. 150 °C for 5 min in the presence of DPE/TEG(1/2, 3 mL).

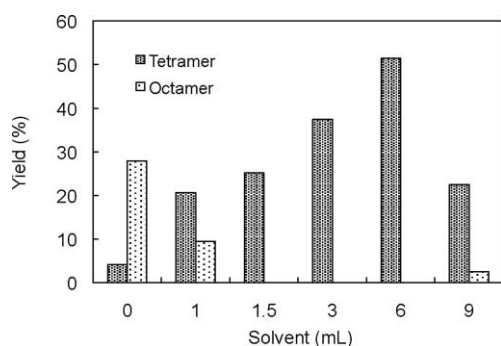


Fig. 4 Distribution of calixarenes depending on the volume of the mixed-solvent. Reaction conditions were the same as those shown in Fig. 3. Solvent composition is DPE/TEG (1/2).

The distribution of the products is usually most affected by the amount of base under the conventional conditions.¹³ The tetramer and the octamer are obtained under the condition of a low ratio of base to the phenol. On the other hand, the hexamer is produced under the higher ratio. The microwave conditions appear to yield the products in a similar fashion, as shown in Fig. 5. Although the hexamer was formed under the higher

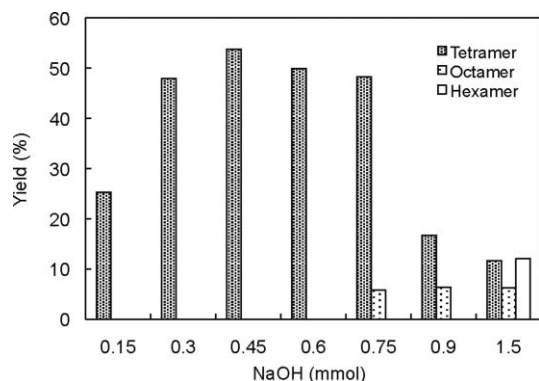


Fig. 5 Distribution of calixarenes depending on concentration of NaOH. Reaction conditions were the same as those shown in Fig. 3 except solvent composition: DPE/TEG (1/2, 6 mL).

Table 2 The yields of the calixarenes by an oil bath heating^a

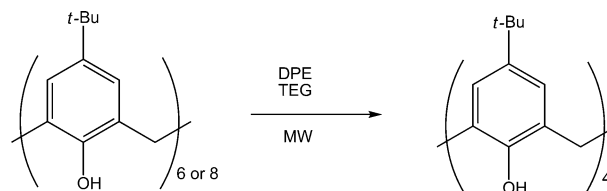
Entry	Solvents ^b	Temp/°C ^c	Yields (%)	
			Tetramer	Octamer
1	DPE/TEG (1/2, 6 mL)	230	16.9	1.8
2	DPE/TEG (1/2, 6 mL)	250	21.6	0
3	DPE/TEG (1/2, 6 mL)	260	35.1	4.2
4	DPE/TEG (1/2, 6 mL)	300	46.1	0
5	DPE (6 mL)	250	0.2	1.8
6	DPE (5 mL)	300	15.1	0
7	TEG (5 mL)	300	33.2	0

^a The reaction conditions employed were as in entry 11 in Table 1. ^b The solvent was added after the mixture was heated in an oil bath (150 °C) for 5 min. ^c After adding solvents the mixture was heated again in an oil bath keeping the temperature constant for 10 min.

ratio of the base, the total yield of the products was decreased with increasing the ratio. Unfortunately, we could not obtain the hexamer in a high yield under the microwave conditions we examined.

The microwave-assisted protocol for the formation of the tetramer was applied to the reaction using the conventional oil bath heating. The results are shown in Table 2. In any conditions we employed, the hexamer was not obtained. The yields of the tetramer were quite small compared to those achieved by microwave irradiation. The yield increased with increasing temperature, however, coming to up 46.1% yield of the tetramer even at 300 °C. The microwave irradiations thus appear to afford an efficient acceleration of the reaction.

The transformation of the octamer or the hexamer to the tetramer was investigated by using microwave irradiation (Scheme 2). If the octamer or the hexamer effectively transformed to the tetramer by microwave heating, this method could be a useful process because the octamer and the hexamer were obtained in excellent yields. Unfortunately, this was not the case, as the results that are summarized in Table 3 show. The maximum temperature for the microwave heating was higher than that of the two-step synthesis from *tert*-butylphenol. The yield of the tetramer did not increased dramatically and was equivalent to that of the two-step synthesis.



Scheme 2

Conclusions

A base-catalyzed condensation reaction to form *p*-*tert*-butylcalixarenes using microwave heating was investigated. The tetramer was obtained in moderate yield, coming along with a dramatically shortened reaction time from hours to minutes compared to the conventional heating method. The field of the calixarene chemistry has been more extensively studied during the last three decades and numerous groups have been exploring

Table 3 The transformation of the octamer and the hexamer to the tetramer using microwave heating^a

Entry	Calixarenes	NaOH/mmol	Temp/°C	Time/min	Yield (%) of the tetramer
1	The octamer	0.07	250	10	0
2	The octamer	0.07	260	20	11.8
3	The octamer	0.15	260	20	25.9
4	The octamer	0.45	260	20	46.1
5	The octamer	0.45	260	30	52.6
6	The hexamer	0.45	260	20	37.6

^a The reaction conditions: 0.5 g of the octamer or hexamer, 0.07–0.45 mmol of 10 M NaOH aq. solution and DPE/TEG (1/2, 6 mL) were placed in the flask and the microwave was irradiated.

the fundamental characteristics of calixarenes.¹⁴ Therefore, we believe the microwave process is suitable for rapid preparation of *p*-tert-butylcalix[4]arene as a laboratory method that is available when needed and that minimum starting materials and solvents should be used to reduce energy and excess product.

Experimental

The reactions with microwave heating were performed with a CEM Discover Focused Microwave Synthesis System (2.45 GHz, 300 W) equipped with a non-contact infrared temperature sensor. The reaction temperature was controlled by variable microwave irradiation (0–300 W) and cooling air. NMR spectra were recorded on a Bruker Avance400 spectrometer and residual resonance of deuterated solvent was used as internal reference. ESI-TOF MS spectra were measured using PE Biosystems Mariner spectrometer.

General procedure

To 500 mg (3.33 mmol) of *p*-tert-butylphenol and 0.31 mL (4.04 mmol) of 36% formaldehyde aq. solution in a 30 mL flask equipped with a condensed-water trap, was added 45 μ L of 10 M NaOH aq. solution, followed by heating with 300 W single mode microwave irradiation setting the maximum temperature to 150 °C for 5 minutes. After cooling, 2 mL of DPE and 4 mL of TEG were added to the mixture, followed by heating again for 10 minutes with the irradiation set at 230 °C. After cooling to room temperature, 20 mL of acetone and 6 M HCl were added to the mixture to produce precipitates. The precipitates were filtered and washed with 10 mL of acetone and water to yield 316 mg of the tetramer (53.7% based on NMR integration) as a powder form.

Acknowledgements

This work was financially supported by Ministry of Education, Culture, Sports, Science and Technology Japan.

References

- C. D. Gutsche, B. Dhawan, K. H. No and R. Muthukrishnan, *J. Am. Chem. Soc.*, 1981, **103**, 3782.
- C. D. Gutsche and M. Iqbal, *Org. Synth.*, 1990, **68**, 234.
- C. D. Gutsche, B. Dhawan, M. Leonis and D. Stewart, *Org. Synth.*, 1990, **68**, 238.
- J. H. Munch and C. D. Gutsche, *Org. Synth.*, 1990, **68**, 243.
- B. Dhawan, S. I. Chen and C. D. Gutsche, *Makromol. Chem.*, 1987, **188**, 921.
- C. D. Gutsche, D. E. Johnston, Jr. and D. R. Stewart, *J. Org. Chem.*, 1999, **64**, 3747.
- M. Makha, C. L. Raston, B. W. Skelton and A. H. White, *Green Chem.*, 2004, **6**, 158.
- M. Makha and C. L. Raston, *Chem. Commun.*, 2001, 2470.
- S. Yan, W. Chen, J. Chen, T. Jiang and Y. Yao, *Tetrahedron*, 2007, **63**, 9614.
- Y. K. Agrawal, N. C. Desai and N. D. Mehta, *Synth. Commun.*, 2007, **37**, 2243.
- (a) *Microwaves in Organic Synthesis*, ed. A. Loupy, Wiley-VCH, Weinheim, 2002; (b) M. Larhed, C. Moberg and A. Hallberg, *Acc. Chem. Res.*, 2002, **35**, 717; (c) P. Lidström, J. Tierney, B. Wathey and J. Westman, *Tetrahedron*, 2001, **57**, 9225; (d) R. S. Varma, *Green Chem.*, 1999, 43; (e) *Microwave-Enhanced Chemistry*, ed. H. M. (Skip) Kingston and S. J. Haswell, American Chemical Society, Washington, DC, 1997.
- For example: (a) E. Nomura, A. Hosoda, H. Mori and H. Taniguchi, *Green Chem.*, 2005, **7**, 863; (b) H. Koshima, M. Hamada, M. Tani, S. Iwasaki and F. Sato, *Heterocycles*, 2002, **57**, 2145.
- C. D. Gutsche, M. Iqbal and D. R. Stewart, *J. Org. Chem.*, 1986, **51**, 742.
- (a) C. D. Gutsche, *Calixarenes, Monographs in Supramolecular Chemistry*, ed. J. F. Stoddart, Royal Society of Chemistry, Cambridge, 1989; (b) C. D. Gutsche, *Calixarenes Revisited, Monographs in Supramolecular Chemistry*, ed. J. F. Stoddart, Royal Society of Chemistry, Cambridge, 1998; (c) *Calixarenes in the Nanoworld*, ed. J. Vicens and J. Harrowfield, Springer, Dordrecht, 2007.

A revision for the synthesis of β -enaminones in solvent free conditions: efficacy of different supported heteropoly acids as active and reusable catalysts

Ezzat Rafiee,^{*a,b} Mohammad Joshaghani,^{a,b} Sara Eavani^a and Solmaz Rashidzadeh^a

Received 25th February 2008, Accepted 25th June 2008

First published as an Advance Article on the web 8th August 2008

DOI: 10.1039/b803249a

Catalytic performance of different supported heteropoly acids (HPAs) in the synthesis of β -enaminones and β -enamino esters from various substituted amines and β -diketones or β -keto esters has been studied. In order to improve the yield and reaction time, the effect of various solvents, HPA loading, different amount of the catalyst and solventless conditions have been investigated. 40% (w/w) PW/SiO₂ was found to be a very efficient and reusable catalyst in comparison with others, under solvent free conditions. In this eco-friendly approach, the usage of organic solvents and hazardous reagents were minimized. Also, a high yield of products within short reaction times were obtained.

Introduction

At the beginning of the new century, interest in the development of economically simple and environmentally safe methods in synthetic organic chemistry increased. This attention is most apparent in the growth of "Green Chemistry". Green chemistry approaches not only hold out significant potential for reduction of by-products, a reduction in the waste produced and lowering of energy costs, but also in the development of new methodologies towards previously unobtainable materials, using existing technologies.¹ One particular area that has attracted considerable attention recently, involves the replacement of corrosive and toxic liquid acids such as HF and H₂SO₄ in the catalyst systems by more environmentally benign heterogeneous solid acids.²⁻⁴

Heterogeneous solid acids are advantageous over conventional homogeneous acid catalysts as they can be easily recovered from the reaction mixture thereby eliminating the need for separation through distillation or extraction. In many cases, they can be reused with only minor changes in activity and selectivity.⁵ Among them, HPAs with Keggin structures have received the most attention due to their unique structure and strong acidity.^{6,7} Flexibility in their acid strength, low toxicity and fairly high thermal stability make them an excellent and versatile catalysts for a wide variety of acid catalyzed reactions in homogeneous and heterogeneous media.⁸⁻¹¹ As it is preferable to carry out the reaction in a heterogeneous phase, it is a significantly useful target to immobilize HPAs into an insoluble, easily separable and high surface area solid.¹² For heterogeneous systems, it is possible to increase the accessibility to the acid sites and control

solid acid strength by supporting HPA on different carriers.¹³ Furthermore, wastes are not produced, helping to incorporate in clean technologies.

Synthesis of the nitrogen containing heterocyclic systems occupies an important place in the realm of natural and synthetic organic chemistry, due to their therapeutic and pharmacological properties. Enamination of β -dicarbonyl compounds forming β -enaminones is an important precursor for the synthesis of a variety of heterocycles and pharmaceutical compounds. Their basic structural units, N=C=C=O, are responsible for the synthesis of many therapeutic agents from both natural and synthetic sources including taxol, anticonvulsant, anti-inflammatory and ducarmycin classes of anti-tumor agents as well as quinoline antibacterials and quinoline antimalarials.¹⁴⁻¹⁹ They are also the intermediates for the synthesis of several amino acids, aminols, peptides and alkaloids.²⁰⁻²³ The classical method for the synthesis of these compounds is the azeotropic removal of water by refluxing an amine with 1,3-diketone in an aromatic hydrocarbon solvent.²⁴ Other improved procedures have been subsequently reported in the literature,²⁵⁻³¹ but most of them suffer from one or more of drawbacks such as drastic reaction conditions, unsatisfactory yields, the use of expensive or less easily available reagents and long reaction times. Moreover, the main disadvantage of some existing methods is that the catalysts are destroyed in the work-up procedure and cannot be recovered or reused. Therefore, despite the various methods that are available for the synthesis of β -enaminones, development of another facial method by using an eco-friendly and reusable catalyst under less hazardous conditions is of prime importance.

As a part of our program aiming at developing selective and safe methodologies for the preparation of fine chemicals³² and by comparing the performance of the heteropoly based catalysts with other solid acid catalysts, it was attempted to clarify the potential of these catalysts for enamination reactions.

^aDepartment of Chemistry, Faculty of Science, Razi University, Kermanshah, 67149, Iran. E-mail: ezzatrafiee@yahoo.com, e.rafaei@razi.ac.ir; Fax: +98 831 4274559; Tel: +98 831 4274559

^bKermanshah Oil Refining Company, Kermanshah, Iran

Results and discussion

Catalytic reaction

The catalytic activity of supported HPAs fundamentally depends on the heteroatom and peripheral atom which constitute the polyanion, the type of carrier and the HPA loading on the support. Previously, efficacy of silica supported HPAs in the synthesis of β -acetamidoketones and dihydropyridines has been studied.³² The aim of this paper is to investigate the catalytic performance of supported tungstophosphoric acid (PW), molybdophosphoric acid (PMo) and tungstosilicic acid (SiW) in the synthesis of β -enaminones, when the different carriers are used in different reaction conditions. To optimize the process conditions, the reaction of ethylacetoacetate (1 mmol) and aniline (1 mmol) was applied as the base reactants in all cases.

Initially, the model reaction was carried out in the absence of the catalyst and the yield of the product was only 5% after 30 min. Then, the same reaction was checked in the presence of only solid supports. The progress of each reaction is given in Fig. 1. KSF and K 10 montmorillonite resulted in good catalytic activity and in the presence of them, excellent yields of product were obtained in relatively short reaction times. γ -Al₂O₃ has very low activity while SiO₂ present an intermediate behavior. Nafion as a heterogeneous superacid show relatively good activity. It was observed that PW, as a homogeneous catalyst, returned an excellent yield of the product (98%) after only 1 min under this reaction condition. However, from environmental and economic considerations, it is desirable to use HPAs as heterogeneous catalysts. This encouraged us to investigate the efficiency of a PW/support as a catalyst by model system. It was found that immobilization of PW on K 10 or KSF montmorillonite has no significant effect on reactivity of these solid supports, but PW/SiO₂ and PW/ γ -Al₂O₃ show higher reactivity compared to the support only on unit weight basis (Fig. 1). Based on these observations, SiO₂ and γ -Al₂O₃ were chosen as the suitable supports for more investigations.

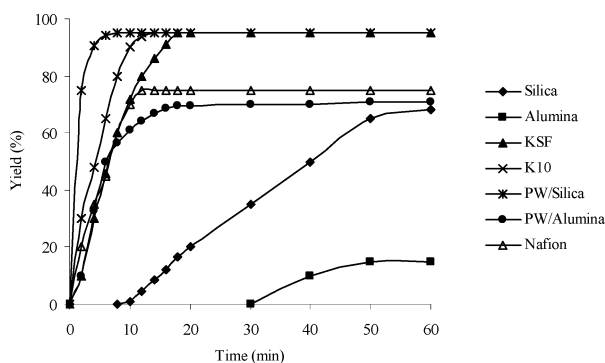


Fig. 1 Catalytic activity of various solid acids in the reaction of aniline with ethylacetoacetate.

The nature of the supporters apparently affects the acidity of supported HPAs which was probed by potentiometric titration with an organic base. This method, based on the measured potential difference, is mainly determined by the acidic environment around the electrode membrane. The measured electrode potential is an indicator of the acidic properties of the

dispersed solid particles. An aliphatic amine, as *n*-butylamine with a basic dissociation constant of approximately 10^{-6} , allows a potentiometric titration of strong acids. The titration curves obtained for different HPAs supported on SiO₂ and γ -Al₂O₃ are presented in Fig. 2. It is considered that the initial electrode potential (E_i) indicates the maximum strength of the acid sites and the value from which the plateau is reached (meq amine/mmol HPA) indicates the total number of acid sites that are present in the titrated solid. The acidic strength of the acid sites can be classified according to the following ranges: $E_i > 100$ mV (very strong sites), $0 < E_i < 100$ mV (strong sites), $-100 < E_i < 0$ mV (weak sites) and $E_i < -100$ mV (very weak sites).³³ According to the mentioned scale, all the catalysts present very strong acid sites. It was observed that γ -Al₂O₃ supported HPAs are less acidic than those supported on SiO₂. This is indicated by the initial electrode potential which is lower for HPA/ γ -Al₂O₃ than HPA/SiO₂. The observed behavior may be related to the HPA-support interaction which in turn is associated to support properties and to the nature of the species present on the catalyst.

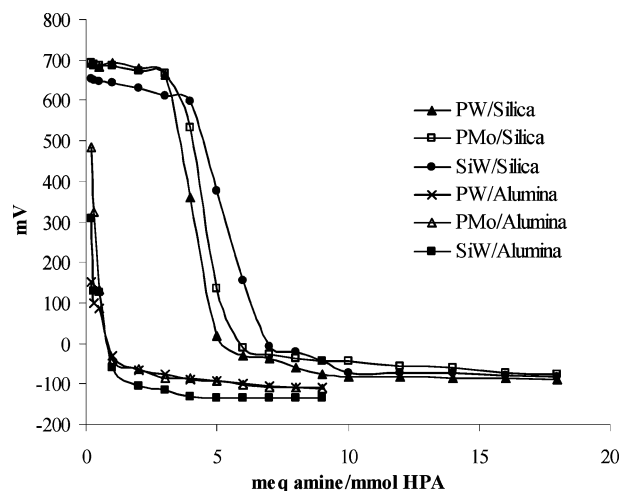
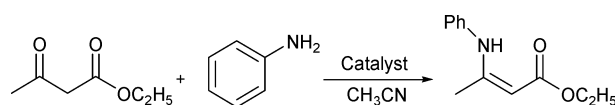


Fig. 2 Potentiometric titration curves of different HPAs supported on SiO₂ and γ -Al₂O₃.

Reactivity of different HPAs supported on SiO₂ and γ -Al₂O₃ was checked by model system. The results are summarized in Table 1. It was found that PW/SiO₂ and SiW/ γ -Al₂O₃ are more efficient catalysts in comparison with others.

The effect of different amounts of PW loading on silica as a model system was studied. The catalytic activity of 20, 40, 60 wt.% of PW on silica which represents the yield of product for the model system as a function of time, are shown in Fig. 3.

Obviously, low loading of the catalyst showed poor effect on the yield of the product. In the presence of 40 wt.% of PW/SiO₂, conversion was faster than for 60 wt.% of PW loading. Since 40 wt.% of PW/SiO₂ was the best catalyst loading, it was used to study the effect of other parameters on the activity of catalyst.

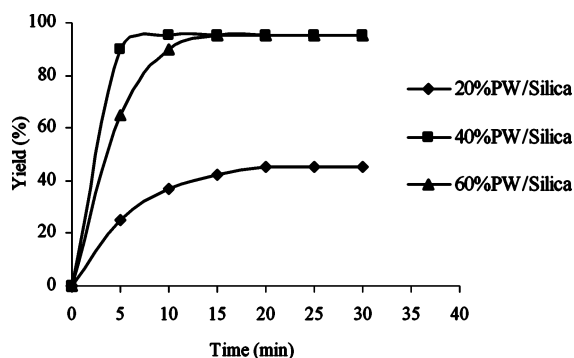


Scheme 1

Table 1 Efficacies of different HPAs in reaction of ethylacetoacetate with aniline according to Scheme 1

Entry	Catalyst ^a	Time/min	Yield (%) ^b
1	40 wt.% PW/SiO ₂	5	95
2	40 wt.% PMo/SiO ₂	7	85
3	40 wt.% SiW/SiO ₂	7	90
4	40 wt.% PW/ γ -Al ₂ O ₃	15	70
5	40 wt.% PMo/ γ -Al ₂ O ₃	5	90
6	40 wt.% SiW/ γ -Al ₂ O ₃	5	98

^a Reaction condition: ethylacetoacetate (1 mmol), aniline (1 mmol), catalyst (0.2 g). ^b Isolated yield.

**Fig. 3** Effect of PW loading on SiO₂ in the reaction of aniline with ethylacetoacetate.

It should be noted that 20, 40, 60 wt.% loadings are nominal. Elemental analysis from ICP are reported in Table 2.

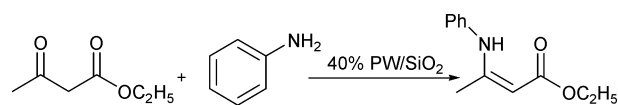
Based on the results which have been shown in Table 3, entries 1–3, using 0.2 g of catalyst in the reaction of ethylacetoacetate (1 mmol), aniline (1 mmol) was chosen as an ideal amount, while with a lesser amount (0.1 g), the reaction remains incomplete. With 0.4 g of catalyst, the reaction time decreased by only one minute in comparison with 0.2 g.

To optimize the solvent, the base reactants were stirred in the presence of an optimized amount of PW/SiO₂ under different solvents and solvent free conditions (Table 3, entries 2 and 4–8). The lowest yield of the product was obtained in water as a solvent and no improvement was observed by increasing the reaction time to 60 min. Among organic solvents, CH₃CN is the best preferred solvent for the synthesis of enaminones as the reaction time for other solvents is much greater. However, a significant improvement was observed in solvent free conditions and the yield of the product was increased to 98% after only 1 min.

Table 2 Catalyst characterisation

Catalyst	S _{BET}	Pore volume	W (wt.%) ^a
60 wt.% PW/SiO ₂	87	0.34	37.5
40 wt.% PW/SiO ₂	117	0.67	29.6
20 wt.% PW/SiO ₂	208	0.75	16.6
40 wt.% SiW/ γ -Al ₂ O ₃	200	0.18	30.2

^a W content in anhydrous catalysts from ICP. Typically, the W content from ICP was slightly lower than expected from the preparation stoichiometry.

**Scheme 2****Table 3** Efficacy of catalyst loading and solvent in reaction of ethylacetoacetate with aniline according to Scheme 2

Entry	Catalyst	Solvent	Time/min	Yield (%) ^a
1	PW/SiO ₂ (0.1 g)	CH ₃ CN	10	75
2	PW/SiO ₂ (0.2 g)	CH ₃ CN	5	95
3	PW/SiO ₂ (0.4 g)	CH ₃ CN	4	95
4	PW/SiO ₂ (0.2 g)	H ₂ O	8	50
5	PW/SiO ₂ (0.2 g)	CH ₂ Cl ₂	40	95
6	PW/SiO ₂ (0.2 g)	C ₆ H ₆	30	90
7	PW/SiO ₂ (0.2 g)	THF	38	90
8	PW/SiO ₂ (0.2 g)	Solvent free	1	98

^a Isolated yield.

Reusability of the catalyst

The stability of the active species in solution has been of concern for solid acids, especially for supported materials. Since PW/SiO₂ and SiW/ γ -Al₂O₃ showed comparable results, their reusability studies were performed by employing them in a model reaction. In the present cases, the quantities of catalysts used were too small to recollect and be reused after the first run. Hence, higher quantities of the catalysts were taken to investigate their reusability. The model reaction was carried out by using one gram of each catalyst and the experiments were properly scaled up. After each run, these catalysts were washed with suitable solvent and dried as described in the Experimental section. As shown in Table 4, in the presence of PW/SiO₂ the yield of the product was reduced to an extent of only 9% from the first run to the fourth run. When the supernatant portion of the PW/SiO₂ catalyzed reaction mixture was subjected to UV spectrum, it did not exhibit the presence of any absorption band at 265 nm assigned to Keggin type PW₁₂O₄₀³⁻.³⁴ Although this catalyst was washed after filtration to remove all the adsorbed reactants and products, it is possible that a slight amount of adsorbed species was deposited in the pore space, which might cause the blockage of active sites and loss in yield on successive runs. The reusability of SiW/ γ -Al₂O₃ was found to be unfavorable in acetonitrile as the solvent. It is due to the leaching of SiW from the support into the liquid phase. But this catalyst could be recovered and

Table 4 Reusability of catalysts in the reaction of ethylacetoacetate with aniline

Run no	Time (min)/Yield (%) ^a			
	PW/SiO ₂		SiW/ γ -Al ₂ O ₃	
	CH ₃ CN	Solvent free	CH ₃ CN	Solvent free
1	5/95	1/98	5/98	1/98
2	5/90	1/95	60/10	1/98
3	5/87	1/90	60/10	1/95
4	5/85	5/86	60/10	1/95

^a Isolated yield.

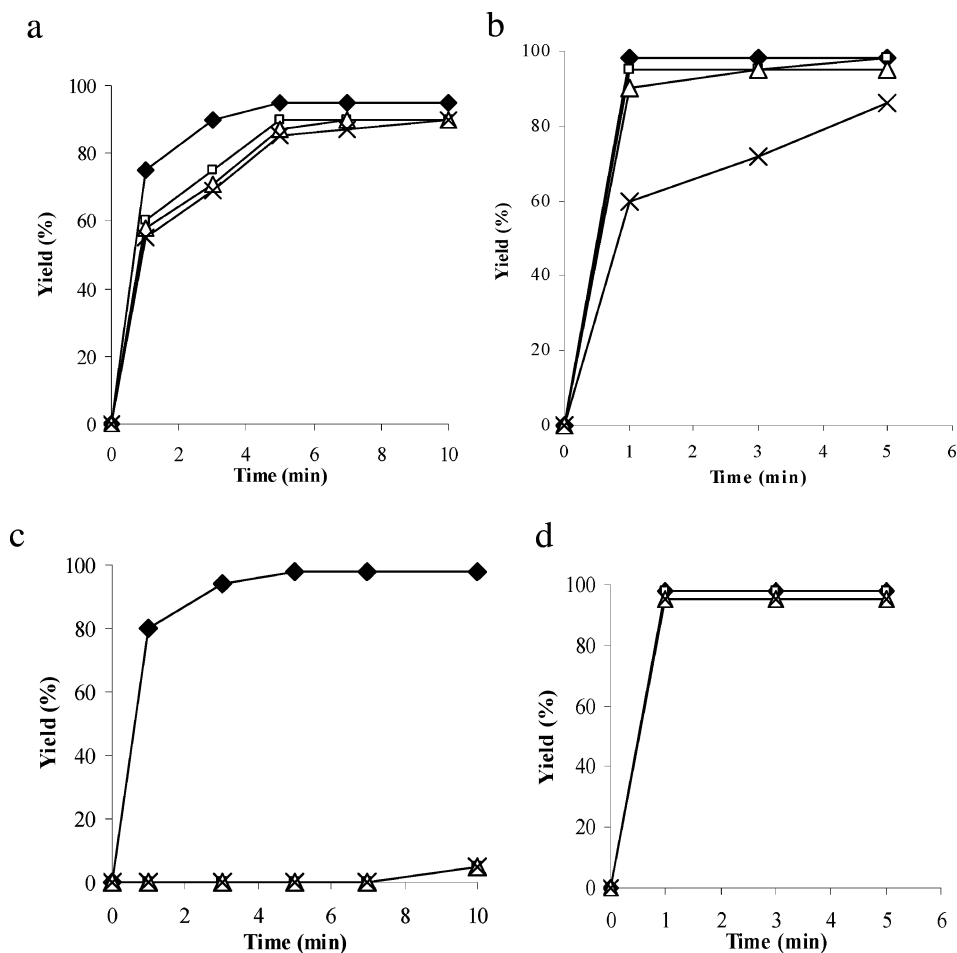


Fig. 4 Catalysts reusability: (a) PW/SiO₂ (CH₃CN), (b) PW/SiO₂ (solvent free), (c) SiW/γ-Al₂O₃ (CH₃CN), (d) SiW/γ-Al₂O₃ (solvent free); (◆) first run, (□) second run, (△) third run, (×) fourth run.

subsequently reused several times in a solventless system. It showed no significant loss of activity after four successive runs and the yield of the product remained at 95% after the fourth run under solvent free conditions. Reusability of both catalysts in two reaction conditions is shown as four different reaction profiles in Fig. 4 to assess the deactivation of the catalysts on reuse.

Synthesis of various β-enaminones

The reaction was extended to various amines and β-dicarbonyl compounds as substrates by using the catalytic amount of PW/SiO₂ and SiW/γ-Al₂O₃ as the active catalysts (Table 5). Reaction was carried out in CH₃CN as the best organic solvent and solventless system. A variety of amines including aliphatic, aromatic and benzylic amines were condensed with different β-dicarbonyl compounds including both 1,3-diketones and β-ketoesters. For each activated or weakly activated amine, the corresponding products were obtained in high to excellent yields. *p*-Nitroaniline gave poor yields in acetonitrile as solvent (entry 6). To our surprise, condensation of *p*-nitroaniline with ethylacetoacetate afforded the corresponding β-enaminone in an excellent yield under solvent free conditions, while some

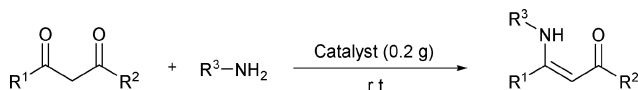
previous approaches gave negative results or very poor yields for similar reactions.^{30,31} Benzylamino enaminones as a unique class of anticonvulsant enaminones retained extensive anticonvulsant activity in the maximal electroshock seizure (MES) evaluation, while the active benzamides possess dual activity in both the electroshock and the subcutaneous pentylentetrazol (scPTZ) models.¹⁸ In this work, both of these compounds were obtained in excellent yields (entries 7, 8 and 13). Aliphatic amines effectively reacted to produce the corresponding products (entries 3, 4 and 9–12). In the reaction of 1,2-diamino ethane, 2 equivalent of β-dicarbonyl compounds were required to form the products with two enamino groups (entries 9 and 10). Additionally, the proposed procedure was successfully applied for the enamination of cyclic as well as linear β-ketoesters (entries 18 and 19). However, dimedone as a cyclic 1,3-diketone afforded low yield of the products (entries 20–22). The results clearly indicate that the solventless system is the best condition for the synthesis of various β-enaminones and under this condition, products were obtained in high to excellent yields within short reaction times. Although both of the catalysts showed rate enhancements, high yields and relatively short reaction times, PW/SiO₂ gave higher activity compared to SiW/γ-Al₂O₃ in the enamination reaction.

Experimental

Techniques

UV-Vis spectra were obtained with an Agilent (8453) UV-Vis diode-array spectrometer. IR spectra were recorded with KBr pellets using a Shimadzu 470 spectrophotometer. Surface area and porosity of HPA catalysts were measured by nitrogen

physorption on a Micromeritics ASAP 2000 instrument. The tungsten or molybdenum content in the catalysts were measured by inductively coupled plasma (ICP) atomic emission spectroscopy on a Spectro Ciros CCd spectrometer. ¹H NMR spectra were recorded on a Bruker Avance 200 MHz NMR spectrometer with CDCl₃ as the solvent and TMS as the internal standard. The potential variation was measured with a Hanna 302 pH meter and a double junction electrode.

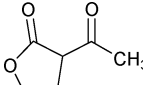
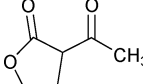
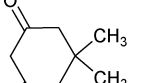
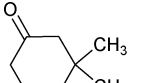
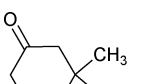


Scheme 3

Materials and catalysts

H₃PW₁₂O₄₀, H₄SiW₁₂O₄₀, and H₃PMo₁₂O₄₀ hydrate from Aldrich, Merck and Aerosil silica (*S*_{BET}, 311 m² g⁻¹) from

Table 5 Synthesis of β-enaminones at room temperature in the presence of different supported catalysts according to Scheme 3

Entry	R ¹	R ²	R ³	Product	Time (min)/Yield (%) ^a			
					PW/SiO ₂		SiW/γ-Al ₂ O ₃	
					CH ₃ CN	Solvent free	CH ₃ CN	Solvent free
1	CH ₃	OC ₂ H ₅	<i>p</i> -ClC ₆ H ₄	1a	7/96	2/98	12/94	4/96
2	CH ₃	OC ₂ H ₅	C ₆ H ₅	2b	5/95	1/98	5/98	1/98
3	CH ₃	OC ₂ H ₅	<i>n</i> -C ₄ H ₉	3c	10/98	2/95	13/98	3/98
4	CH ₃	OC ₂ H ₅	(CH ₃) ₂ CH ₂	4d	15/98	4/97	13/52	4/61
5	CH ₃	OC ₂ H ₅	<i>p</i> -CH ₃ OC ₆ H ₄	5e	10/97	1/98	9/96	1/94
6	CH ₃	OC ₂ H ₅	<i>p</i> -NO ₂ C ₆ H ₄	6f	30/10	15/92	30/5	15/90
7	CH ₃	OC ₂ H ₅	PhCH ₂	7g	3/97	2/94	7/94	5/96
8	CH ₃	OC ₂ H ₅	PhCO	8h	30/90	10/96	30/95	10/98
9 ^b	CH ₃	C ₆ H ₅	NH ₂ CH ₂ CH ₂	9i	20/94	20/96	30/95	23/90
10 ^b	CH ₃	CH ₃	NH ₂ CH ₂ CH ₂	10j	30/95	4/98	40/98	6/97
11	CH ₃	CH ₃	<i>n</i> -C ₄ H ₉	11k	30/92	10/94	13/98	3/96
12	CH ₃	CH ₃	(CH ₃) ₂ CH ₂	12l	110/93	20/90	100/50	10/57
13	CH ₃	CH ₃	PhCH ₂	13m	35/98	2/98	11/95	1/95
14	CH ₃	CH ₃	C ₆ H ₅	14n	70/92	2/61	9/70	1/76
15	CH ₃	CH ₃	<i>p</i> -CH ₃ OC ₆ H ₄	15o	15/97	1/98	4/98	1/98
16	CH ₃	CH ₃	<i>p</i> -ClC ₆ H ₄	16p	15/97	3/98	5/95	1/96
17	CH ₃	CH ₃	<i>p</i> -CH ₃ C ₆ H ₄	17q	25/95	1/98	6/90	2/93
18		CH ₃	C ₆ H ₅	18r	55/97	3/95	170/41	10/47
19			HOCH ₂ CH ₂	19s	50/97	3/95	65/95	5/94
20			C ₆ H ₅	20t	50/55	3/65	70/32	9/50
21			<i>o</i> -CH ₃ C ₆ H ₄	21u	80/52	3/60	123/42	1/53
22			PhCH ₂	22v	35/50	15/64	50/39	1/41

^a Isolated yield. ^b 1,2-diamino ethane : β-dicarbonyl compound; 1 : 2.

Degussa were used. KSF (S_{BET} , 15 m² g⁻¹) and K 10 (S_{BET} , 200 m² g⁻¹) montmorillonite clay were obtained from Fluka. γ -Alumina (S_{BET} , 250 m² g⁻¹) was obtained from Aldrich. Nafion (powder, 35–60 mesh) was purchased from Aldrich.

Preparation of the catalysts

The catalysts were prepared using solutions of PW, PMo, or SiW. The solutions were used to impregnate supports with different characteristics. The solids employed as supports were silica, KSF and K 10 montmorillonites and γ -Al₂O₃.

Silica-supported PW (PW/SiO₂) catalysts were prepared by impregnating silica (3.0 g) with an aqueous solution of PW (with concentrations depending upon the loadings, 20, 40 and 60 wt.% PW on silica). The mixture was stirred overnight at room temperature, followed by drying using a rotary evaporator, as described elsewhere.³²

For preparation of the PW/K 10, K 10 montmorillonite was dried in an oven at 120 °C for 2 h prior to its use as a support. After drying, 5.0 g of K 10 was taken. To prepare a catalyst with 40% loading of PW, 2.0 g of PW was dissolved in 4 mL of dry methanol. This solution was added dropwise to predried K 10 with constant stirring with a glass rod. Initially, with addition of PW solution, the clay was in the powdery form, but on further addition of PW solution, the clay turned to a paste form. The paste on further stirring for 10 min resulted in a free flowing powder. A similar procedure was followed for the synthesis of PW/KSF.

A catalyst based on PW supported on γ -Al₂O₃ was also prepared. The solution of PW was prepared by dissolving 2.0 g PW in 25 mL of water and 25 mL of methanol. Then 5.0 g γ -Al₂O₃ was dropped into the above solution under vigorous stirring to be impregnated for 24 h.

Acidity measurement

For the potentiometric titration, 0.05 g of solid was suspended in acetonitrile (90 mL) and stirred for 3 h. The suspension was titrated with a 0.05 N solution of *n*-butylamine in acetonitrile. The potential variation was measured with a Hanna 302 pH meter using a double junction electrode.

Typical procedure for the synthesis of β -enaminones

(A) Typical procedure for the synthesis of β -enaminones in solvent media

0.2 g of the catalyst was added to a mixture of β -dicarbonyl compound (1 mmol), amine (1 mmol) and solvent (3 mL). This solution was stirred at room temperature. Progress of the reaction was followed by GC or TLC using EtOAc/petroleum ether as eluent. After completion of the reaction, the catalyst was removed by filtration. Evaporation of the solvent followed by chromatography on a silica-gel plate or a silica-gel column gave the pure corresponding enaminone. Recovered catalyst (PW/SiO₂) was washed with CH₂Cl₂ (3 \times 10 mL), dried over MgSO₄ and calcinated at 150 °C for 1 h, before reusing (the leaching of SiW occurred in solvent media, so it can be concluded the SiW/ γ -Al₂O₃ can not be reused under this condition).

(B) Typical procedure for the synthesis of β -enaminones under solvent free conditions

A mixture of amine (1 mmol), β -dicarbonyl compound (1 mmol), and 0.2 g of catalyst was crushed at ambient temperature. After completion of the reaction as indicated by GC or TLC, the mixture was diluted with EtOAc (5 mL) and filtered. The catalyst was recovered from residue. The filtrate was concentrated and the product was purified by column chromatography on silica-gel using EtOAc/petroleum ether as eluent. Recovered catalyst was washed with CH₂Cl₂ (in the case of PW/SiO₂) or ether (in the case of SiW/ γ -Al₂O₃) (3 \times 10 mL), dried over MgSO₄ and calcinated at 150 °C for 1 h, before reusing.

Spectroscopic data for compounds 1a–22v

Compound 1a. δ_{H} (200 MHz; CDCl₃, TMS) 10.26 (1H, brs, NH), 7.11–7.33 (4H, m, Ar), 4.71 (1H, s, =CH), 4.17 (2H, q, $J_{1,2}$ 7.2, OCH₂), 1.94 (3H, s, CH₃), 1.29 (t, $J_{1,2}$ 7.2, 3H, CH₃).

Compound 2b. δ_{H} (200 MHz; CDCl₃, TMS) 10.36 (1H, brs, NH), 7.04–7.35 (5H, m, Ar), 4.68 (1H, s, =CH), 4.15 (2H, q, $J_{1,2}$ 7.2, OCH₂), 1.95 (3H, s, CH₃), 1.29 (3H, t, $J_{1,2}$ 7.2, CH₃).

Compound 3c. δ_{H} (200 MHz; CDCl₃, TMS) 8.84 (1H, brs, NH), 4.44 (1H, s, =CH), 4.08 (2H, q, $J_{1,2}$ 7.2, OCH₂), 3.17 (2H, q, $J_{1,2}$ 6.5, CH₂), 1.87 (3H, s, CH₃), 1.41–1.60 (2H, m, CH₂), 1.34–1.37 (2H, m, CH₂), 1.23 (3H, t, $J_{1,2}$ 7.2, CH₃), 0.90 (3H, t, $J_{1,2}$ 7.3 CH₃).

Compound 4d. δ_{H} (200 MHz; CDCl₃, TMS) 8.46 (1H, brs, NH), 4.30 (1H, s, =CH), 4.04 (2H, q, $J_{1,2}$ 7.2, OCH₂), 3.68 (1H, m, CH), 1.94 (3H, s, CH₃), 1.26 (3H, t, $J_{1,2}$ 7.0, CH₃), 1.20 (6H, d, $J_{1,2}$ 7.0 CH₃).

Compound 5e. δ_{H} (200 MHz; CDCl₃, TMS) 10.22 (1H, brs, NH), 7.00 (2H, d, $J_{1,2}$ 8.2, Ar), 6.82 (2H, d, $J_{1,2}$ 8.2, Ar), 4.64 (1H, s, =CH), 4.14 (2H, q, $J_{1,2}$ 7.2, OCH₂), 3.76 (s, 3H, OCH₃), 1.89 (3H, s, CH₃), 1.30 (3H, t, $J_{1,2}$ 7.2, CH₃).

Compound 6f. δ_{H} (200 MHz; CDCl₃, TMS) 6.73–7.93 (4H, m, Ar), 4.85 (1H, s, =CH), 4.21 (2H, q, $J_{1,2}$ 7.2, OCH₂), 4.01 (1H, brs, NH), 1.70 (3H, s, CH₃), 1.30 (3H, t, $J_{1,2}$ 7.2, CH₃).

Compound 7g. δ_{H} (200 MHz; CDCl₃, TMS) 8.95 (1H, brs, NH), 7.29–7.34 (2H, m, Ar), 7.16–7.30 (3H, m, Ar), 4.48 (1H, s, =CH), 4.38 (2H, d, $J_{1,2}$ 7.0, Ph-CH₂), 4.09 (2H, q, $J_{1,2}$ 7.0, OCH₂), 1.87 (3H, s, CH₃), 1.25 (3H, t, $J_{1,2}$ 7.0, CH₃).

Compound 8h. δ_{H} (200 MHz; CDCl₃, TMS) 8.02 (1H, brs, NH), 7.46–7.94 (5H, m, Ar), 5.10 (1H, s, =CH), 4.20 (2H, q, $J_{1,2}$ 8.5, OCH₂), 1.73 (3H, s, CH₃), 1.32 (3H, t, $J_{1,2}$ 8.5, CH₃).

Compound 9i. δ_{H} (200 MHz; CDCl₃, TMS) 11.57 (2H, s, NH), 7.11–8.15 (10H, m, Ar), 5.72 (2H, s, =CH), 3.29–3.83 (4H, m, CH₂-CH₂), 2.10 (6H, s, CH₃).

Compound 10j. δ_{H} (200 MHz; CDCl₃, TMS) 10.93 (2H, brs, NH), 4.97 (2H, s, =CH), 3.40–3.45 (4H, m, CH₂-CH₂), 2.01 (6H, s, CH₃), 1.93 (6H, s, CH₃CO).

Compound 11k. δ_{H} (200 MHz; CDCl₃, TMS) 10.91 (1H, brs, NH), 5.33 (1H, s, =CH), 3.13 (2H, q, $J_{1,2}$ 6.5, CH₂), 2.02 (3H, s, CH₃CO), 1.95 (3H, s, CH₃), 1.44–1.61 (2H, m, CH₂), 1.35–1.42 (2H, m, CH₂), 0.97 (3H, t, $J_{1,2}$ 7.3, CH₃).

Compound 12l. δ_{H} (200 MHz; CDCl₃, TMS) 10.82 (1H, brs, NH), 4.86 (1H, s, =CH), 3.70 (1H, m, CH), 1.96 (3H, s, CH₃CO), 1.92 (3H, s, CH₃), 1.25 (6H, d, $J_{1,2}$ 7.0, CH₃).

Compound 13m. δ_{H} (200 MHz; CDCl₃, TMS) 11.15 (1H, brs, NH), 7.22–7.36 (5H, m, Ar), 5.03 (1H, s, =CH), 4.44 (2H, d, $J_{1,2}$ 5.5, Ph-CH₂), 2.02 (3H, s, CH₃), 1.91 (3H, s, CH₃CO).

Compound 14n. δ_{H} (200 MHz; CDCl₃, TMS) 12.47 (1H, brs, NH), 7.08–7.35 (5H, m, Ar), 5.19 (1H, s, =CH), 2.10 (3H, s, CH₃), 1.96 (3H, s, OCH₃).

Compound 15o. δ_{H} (200 MHz; CDCl₃, TMS) 12.27 (1H, brs, NH), 7.04 (2H, d, $J_{1,2}$ 8, Ar), 6.81 (2H, d, $J_{1,2}$ 8, Ar), 5.16 (1H, s, =CH), 3.81 (3H, s, OCH₃), 2.09 (3H, s, CH₃), 1.91 (3H, s, CH₃CO).

Compound 16p. δ_{H} (200 MHz; CDCl₃, TMS) 12.45 (1H, brs, NH), 7.32 (2H, d, $J_{1,2}$ 8, Ar), 7.09 (2H, d, $J_{1,2}$ 8.00, Ar), 5.25 (1H, s, =CH), 2.14 (3H, s, CH₃), 2.02 (3H, s, CH₃CO).

Compound 17q. δ_{H} (200 MHz; CDCl₃, TMS) 12.40 (1H, s, NH), 6.91–7.22 (4H, m, Ar), 5.15 (1H, s, =CH), 2.31 (3H, s, Ph-CH₃), 2.10 (3H, s, CH₃), 1.91 (3H, s, CH₃CO).

Compound 18r. δ_{H} (200 MHz; CDCl₃, TMS) 10.09 (1H, brs, NH), 7.00–7.43 (5H, m, Ar), 4.30–4.44 (2H, t, $J_{1,2}$ 8.1, OCH₂), 2.89–3.01 (2H, t, $J_{1,2}$ 8.1, =C-CH₂-), 2.1 (3H, s, CH₃).

Compound 19s. δ_{H} (200 MHz; CDCl₃, TMS) 8.31 (1H, brs, NH), 4.22–4.33 (2H, t, $J_{1,2}$ 8.7, OCH₂), 3.69–3.81 (2H, t, $J_{1,2}$ 5.8, CH₂), 3.37–3.46 (2H, q, $J_{1,2}$ 5.1, 5.2, CH₂), 3.19 (1H, brs, OH), 2.80–2.91 (2H, t, $J_{1,2}$ 7.3, =C-CH₂-), 2.1 (3H, s, CH₃).

Compound 20t. δ_{H} (200 MHz; CDCl₃, TMS) 6.46–7.01 (5H, m, Ar), 5.54 (1H, s, =CH), 4.00 (1H, brs, NH), 2.86 (2H, s, CH₂CO), 1.88 (2H, s, CH₂C), 1.11 (6H, s, CH₃).

Compound 21u. δ_{H} (200 MHz; CDCl₃, TMS) 7.03–7.25 (4H, m, Ar), 6.69 (1H, brs, NH), 4.95 (1H, s, =CH), 2.32 (2H, s, CH₂CO), 2.23 (2H, s, CH₂C), 2.17 (3H, s, Ph-CH₃), 1.10 (6H, s, CH₃).

Compound 22v. δ_{H} (200 MHz; CDCl₃, TMS) 43–7.58 (5H, m, Ar), 5.49 (1H, brs, NH), 5.21 (1H, s, =CH), 4.44 (2H, d, $J_{1,2}$ 7.0, Ph-CH₂), 2.41 (2H, s, CH₂CO), 2.23 (2H, s, CH₂C), 1.18 (6H, s).

Conclusions

Supported HPAs have become popular because of their super acidic properties. The results presented in this work demonstrated a novel, very mild and efficient method for the conversion of β -ketoesters and β -diketones to β -enaminones in the presence of aromatic and aliphatic amines using a catalytic amount of PW/SiO₂ and SiW/ γ -Al₂O₃ at room temperature. These catalysts can be prepared easily with available and inexpensive reagents which are reusable and non-hazardous. A simple procedure combined with low toxicity and reusability of the catalysts, make this method an economic and waste-free chemical process for the synthesis of β -enaminones.

Acknowledgements

The authors thank the Razi University Research Council and Kermanshah Oil Refining Company for support of this work.

Notes and references

- G. W. V. Cave, C. L. Raston and J. L. Scott, *Chem. Commun.*, 2001, 2159.
- J. M. Thomas, *Sci. Am.*, 1992, **266**, 112.
- M. Misono and T. Okuhara, *CHEMTECH*, 1993, **11**, 23.
- A. Corma and A. Mart'inez, *Catal. Rev. Sci. Eng.*, 1993, **35**, 483.
- S. E. Sen, S. M. Smith and K. A. Sullivan, *Tetrahedron*, 1999, **55**, 12657.
- M. Misono, *Catal. Rev. Sci. Eng.*, 1987, **29**, 269.
- I. V. Kozhevnikov, *Catal. Rev. Sci. Eng.*, 1995, **37**, 311.
- L. C. W. Baker and D. C. Glick, *Chem. Rev.*, 1998, **98**, 3.
- R. Neumann, *Prog. Inorg. Chem.*, 1998, **47**, 317.
- T. Okuhara, *Chem. Rev.*, 2002, **102**, 3641.
- Y. Izumi, K. Urabe and M. Onaka, *Microporous Mesoporous Mater.*, 1998, **21**, 629.
- Y. Izumi, K. Hisano and T. Hida, *Appl. Catal., A*, 1999, **181**, 277.
- J. B. Moffat, in *Metal-Oxygen Clusters-The Surface and Catalytic Properties of Heteropoly Oxometalates*, Kluwer, New York, 2001.
- J. E. Foster, J. M. Nicholson, R. Butcher, J. P. Stables, I. O. Edafiogho, A. M. Goodwin, M. C. Henson, C. A. Smith and K. R. Scott, *Bioorg. Med. Chem.*, 1999, **7**, 2415; I. O. Edafiogho, J. A. Moore, M. S. Alexander and K. R. Scott, *J. Pharm. Sci.*, 1994, **83**, 1155.
- J. P. Michael, C. B. Koning, G. D. Hosken and T. V. Stanbury, *Tetrahedron*, 2001, **57**, 9635; C. J. Valduga, H. S. Braibante and E. F. J. Braibante, *J. Heterocycl. Chem.*, 1998, **35**, 189; H. M. C. Ferraz, E. O. Oliveira, M. E. Payret-Arrua and C. A. Brandt, *J. Org. Chem.*, 1995, **60**, 7357.
- G. Dannhardt, A. Bauer and U. Nowe, *J. Prakt. Chem.*, 1998, **340**, 256.
- F. C. Appelbaum and P. A. Hunter, *Int. J. Antimicrob. Agents*, 2000, **16**, 5; D. L. Boger, T. Ishizaki, J. R. J. Wysocki, S. A. Munk, P. A. Kitos and O. Suntornwat, *J. Am. Chem. Soc.*, 1989, **111**, 6461; Y. F. Wang, T. Izawa, S. Kobayashi and M. Ohno, *J. Am. Chem. Soc.*, 1982, **104**, 6465.
- I. O. Edafiogho, K. V. V. Ananthalakshmi and S. B. Kombian, *Bioorg. Med. Chem.*, 2006, **14**, 5266; N. D. Eddington, D. S. Cox, R. R. Roberts, R. J. Butcher, I. O. Edafiogho, J. P. Stables, N. Cooke, A. M. Goodwin, C. A. Smith and K. R. Scott, *Eur. J. Med. Chem.*, 2002, **37**, 635; K. V. V. Ananthalakshmi, I. O. Edafiogho and S. B. Kombian, *Neuroscience (Oxford)*, 2006, **141**, 345.
- N. D. Eddington, D. S. Cox, R. R. Roberts, J. P. Stables, C. B. Powell and K. R. Scott, *Curr. Med. Chem.*, 2000, **7**, 417; N. N. Salama, N. D. Eddington, D. Payne, T. L. Wilson and K. R. Scott, *Curr. Med. Chem.*, 2004, **11**, 2093.
- D. Potin, F. Dumas and J. Angelo, *J. Am. Chem. Soc.*, 1990, **112**, 3483; G. Bartoli, C. Cimarelli, E. Marcantoni, G. Palmieri and M. Petrini, *J. Org. Chem.*, 1994, **59**, 5328; G. Palmieri and C. Cimmerelli, *J. Org. Chem.*, 1996, **61**, 5557; L. G. Beholz, R. Benovsky, D. L. Ward, N. S. Bata and J. R. Stille, *J. Org. Chem.*, 1997, **62**, 1033.
- C. Alan, A. C. Spivey, R. Srikanan, C. M. Diaper, J. David and D. Turner, *Org. Biomol. Chem.*, 2003, 1638; H. M. Hassneen and T. A. Abdallah, *Molecules*, 2003, **8**, 333; J. P. Michael, C. B. Koning, D. Gravestock, G. D. Hosken, A. S. Howard, C. M. Jungmann, R. W. M. Krause, A. S. Parsons, S. C. Pelly and T. V. Stanbury, *Pure Appl. Chem.*, 1999, **71**, 979.
- Y. C. Shi, H. M. Yang, W. B. Shen, C. G. Yan and X. Y. Hu, *Polyhedron*, 2004, **23**, 15; G. J. Reddy, D. Latha, C. Thirupathiah and K. S. Rao, *Tetrahedron Lett.*, 2005, **46**, 301; S. Cunha, F. Damasceno and J. Ferrari, *Tetrahedron Lett.*, 2007, **48**, 5795.
- J. M. Rodriguez and A. D. Hamilton, *Tetrahedron Lett.*, 2006, **47**, 7443; F. Tanaka and R. Fuller, *Bioorg. Med. Chem. Lett.*, 2006, **16**, 4059.
- G. Baraldi, D. Simoni and S. Manfredini, *Synthesis*, 1983, 902; D. F. Martin, G. A. Janusonis and B. B. Martin, *J. Am. Chem. Soc.*, 1961, **83**, 73.
- B. Rechsteimer, F. Texier-Boullet and J. Hamelin, *Tetrahedron Lett.*, 1993, **34**, 5071.

- 26 M. E. F. Braibante, H. T. S. Braibante and S. J. S. Salvatore, *Quim. Nova*, 1990, **13**, 67; P. G. Baraldi, D. Simoni and S. Manfredini, *Synthesis*, 1983, **11**; M. E. F. Braibante, H. T. S. Braibante, L. Missio and A. Andricopulo, *Synthesis*, 1994, 898; A. H. Stefani, M. I. Costa and D. D. O Silva, *Synthesis*, 2000, **11**.
- 27 A. Arcadi, G. Bianchi, S. D. Giuseppe and F. Marinelli, *Green Chem.*, 2003, 64.
- 28 G. Bartoli, M. Bosco, M. Locatelli, E. Marcantoni, P. Melchiorre and L. Sambri, *Synlett*, 2004, 239.
- 29 C. A. Brandt, A. C. M. P. Da Silvar, C. G. Pancote, C. L. Brito and M. A. B. Da Silveira, *Synthesis*, 2004, 1557; B. J. Turunen and G. I. Georg, *Synfacts*, 2006, 10; R. Dalpozzo, A. De Nino, M. Nardi, B. Russo and A. Procopio, *Synthesis*, 2006, 7.
- 30 M. M. Khodaei, A. P. Khosropour and M. Kookhazadeh, *Synlett*, 2004, 1980; A. R. Khosropour, M. M. Khodaei and M. Kookhazadeh, *Tetrahedron Lett.*, 2004, **45**, 1725; M. M. Khodaei, A. R. Khosropour and M. Kookhazadeh, *Russ. J. Org. Chem.*, 2005, **41**.
- 31 B. Das, K. Venkateswarlu, A. Majhi, M. R. Reddy, K. N. Reddy, Y. K. Rao, K. Ravikumar and B. Sridhar, *J. Mol. Catal. A: Chem.*, 2006, **246**, 276.
- 32 E. F. Kozhevnikova, E. Rafiee and I. V. Kozhevnikov, *Appl. Catal., A*, 2004, **260**, 25; E. Rafiee, F. Shahbazi, M. Joshaghani and F. Tork, *J. Mol. Catal. A: Chem.*, 2005, **242**, 129; E. Rafiee and F. Shahbazi, *J. Mol. Catal. A: Chem.*, 2006, **250**, 57; E. Rafiee, F. Tork and M. Joshaghani, *Bioorg. Med. Chem. Lett.*, 2006, **16**, 1221.
- 33 R. Cid and G. Pecci, *Appl. Catal.*, 1985, **14**, 15.
- 34 M. Kimura, T. Nakato and T. Okuhara, *Appl. Catal., A*, 1997, **165**, 227.

Potential green fungicide: 16-oxo-1-oxa-4-azoniacyclohexadecan-4-ium tetrafluoroborate

Yanhong Dong,^a Xiaomei Liang,^a Huizhu Yuan,^b Shuhua Qi,^b Fuheng Chen^a and Daoquan Wang^{*a}

Received 7th April 2008, Accepted 17th June 2008

First published as an Advance Article on the web 11th August 2008

DOI: 10.1039/b805797d

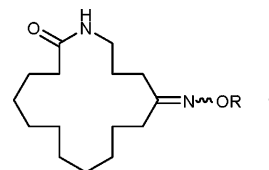
16-Oxo-1-oxa-4-azoniacyclohexadecan-4-ium tetrafluoroborate (**2a**) and its sulfonyl derivatives (**2b–2i**) were synthesized, their structures were confirmed by ¹H NMR and elemental analysis and their fungicidal activities were investigated. Among them, compound **2a** was not only more effective than compounds **2b–2i** against the *Rhizoctonia solani* Kühn *in vitro* bioassay, but also better than the commercial fungicide Carbendazim both in pot culture experiments and field efficacy trial. These results once again proved the correctness of our original proposal that macrocyclic compounds with two polarizable groups (one hydrogen-bonding donor and one hydrogen-bonding acceptor) on the ring may have certain good bioactivity. Furthermore, **2a** has low toxicity, is safe for human beings, and its synthesis is a green and most economical process, because the atoms of the starting materials are almost fully utilized.

1. Introduction

With the growing concern about the environment and human health, matters such as pesticide pollution, negative impacts on our environment and the poisoning of non-targeted species have been paid wide attention. Green and sustainable chemistry concerns the development of processes and technologies that results in little waste and fewer environmental emissions in more efficient chemical reactions than in “traditional” chemical reactions. The green pesticides have great potential in promoting the development of agriculture. The characteristics of green pesticides include (1) extremely high activity with low dosage and rapid efficacy, (2) high selectivity with effects only on harmful organisms, and (3) non-polluting, either being nontoxic or only having low toxicity with rapid degradation.¹ The design of new, selective and highly effective green pesticides that cause no harm to human health and the environment is quite an important task in agrochemical science and in the industrial sector.² So, the development of novel compounds and technologies of green pesticides is the main goal of pesticide research in the future.

Our strategy for discovering new fungicides was to imitate the chemistry of biologically active natural products. In a previous paper,³ we reported the design and synthesis of macrolactam and macrolactone derivatives with an oxime ether side chain to improve fungicidal activity of general macrocyclic compounds. A bioassay showed that they have good fungicidal activity against *Rhizoctonia solani* Kühn. Among them, those with a hydrogen-bonding acceptor (=N–O–) and a hydrogen-bonding donor (–CONH–) on the ring and having a three methylenes’

distance between two polarizable groups have the best fungicidal activity. Namely, 12-alkoxyimino-1,15-pentadecanlactams (**1**) have the best fungicidal activity.



Based on these facts, we synthesized a novel macrocyclic compound **2a** with a hydrogen-bonding donor (NH) and a hydrogen-bonding acceptor (C=O) on the ring and two methylene groups between these two polarizable groups. And for further verifying this judgment, we designed and synthesized some sulfonyl derivatives (compounds **2b–2i**) of **2a** with only one polarizable group (C=O), studied and compared the relationship between their structures and bioactivity.

The synthetic route of compounds **2a** and **2b–2i** is shown in Scheme 1. An intramolecular Schmidt reaction of cyclododecanone with 2-azidoethanol gave **2a**, which was sulfonylated to afford compounds **2b–2i**.

The syntheses, fungicidal activities *in vivo* and *in vitro*, toxicology, and structure–activity relationships of **2a** and **2b–2i** are reported herein.

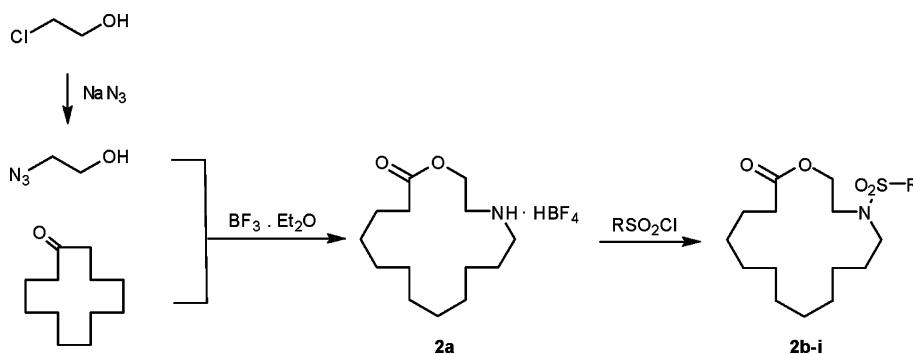
2. Experimental

2.1 General

Infrared spectra were recorded in potassium bromide disks on a Shimadzu IR-435 spectrophotometer; the ¹H NMR and ¹³C NMR spectra were recorded on a Bruker DPX 300 MHz NMR spectrometer; chemical shift values are given in ppm relative to TMS in CDCl₃; TLC was performed on precoated silica gel GF₂₅₄ sheets and detected by employing a mixture of 10%

^aKey Laboratory of Pesticide Chemistry and Application Technology, Department of Applied Chemistry, China Agricultural University, Beijing, 100094, People's Republic of China. E-mail: wangdq@cau.edu.cn; Fax: 86-10-62732219; Tel: 86-10-62732219

^bInstitute of Plant Protection, Chinese Academy of Agriculture Science, Beijing, 100094, People's Republic of China



Scheme 1

methanol (v/v) in methylene chloride; column chromatography was performed on silica gel (Merck, 230–400 mesh) and eluted by methylene chloride; MS was performed on a ThermoFinnigan LCQ; elemental analysis was performed by the analytical center at the Institute of Chemistry (Beijing), Chinese Academy of Science; melting points were measured on a Yanagimoto melting-point apparatus and are uncorrected. The solvents and reagents were used as received or were dried prior to use as needed.

2.2 Chemical synthesis

2.2.1 Preparation of 2-azidoethanol (1)⁴. 2-Chloroethanol (165 g, 2.05 mol) was added rapidly to a solution of sodium azide (157 g, 2.42 mol) in 500 mL of water at room temperature. The reaction mixture was stirred at 30 °C for 1 h and then at 70 °C for 72 h. The resulting solution was cooled to room temperature, saturated with sodium sulfate, and extracted with 4 × 400 mL of methylene chloride. The combined organic layers were dried over anhydrous sodium sulfate and concentrated on a rotary evaporator to give 166 g (1.91 mol, 93%) of crude 2-azidoethanol. Although this substance can be purified by reduced pressure distillation (47–48 °C, 1 mm), but ¹H NMR showed that the undistilled material was of adequate purity for use in the next reaction. ¹H NMR (δ (ppm); CDCl₃): 3.39(t, J = 4.2 Hz, 2H), 3.71(t, J = 5.2 Hz, 2H). IR, ν_{\max} (KBr disc)/cm⁻¹: 3320, 2920, 2860, 2070, 1430, 1340, 1060.

2.2.2 Synthesis of 16-oxo-1-oxa-4-azoniacyclohexadecan-4-ium tetrafluoroborate (2a)⁵. 2-Azidoethanol (5.22 g, 0.06 mol) was added dropwise to a solution of boron trifluoride etherate (35 g, 0.11 mol, 47%) and cyclododecanone (9.1 g, 0.05 mol) in a 500 mL three-necked flask under stirring at 35 °C for 1 h. The mixture solution was warmed up to 65 °C in 1 h and stirred for 12 h. TLC indicated the absence of cyclododecanone. After cooling, saturated aqueous sodium bicarbonate (100 mL) was added under 35 °C over 1 h, and the resulting mixture was stirred overnight. The mixture was then extracted with 5 × 150 mL of methylene chloride. The organic extracts were combined, dried over anhydrous sodium sulfate, and filtered. The filtrate was concentrated on a rotary evaporator to give red dope. The latter was frozen at -20 °C for 48 h to give a light gray solid. After filtering, the solid was washed with anhydrous diethyl ether (50 mL × 2), and then dried under vacuum to give 15.5 g of 16-oxo-1-oxa-4-azoniacyclohexadecan-4-ium tetrafluoro-borate. Yield: 94%. mp 51–53 °C. ¹H NMR

(δ (ppm); CDCl₃): 1.35–1.48(m, 14H), 1.63–1.83(m, 4H), 2.44(t, 2H, J = 7.3 Hz), 3.20(t, 2H, J = 7.6 Hz), 3.44–3.47(m, 2H), 4.39–4.42(m, 2H), 6.84–6.97(b, 2H). ¹³C NMR (δ (ppm); CDCl₃): 23.97, 24.00, 24.38, 25.59, 25.62, 25.83, 25.86, 26.03, 26.97, 33.41, 46.68, 47.60, 59.21, 173.74. IR, ν_{\max} (KBr disc)/cm⁻¹: 2930, 2857, 1744, 1575, 1466, 1159. Anal. calcd for C₁₄H₂₈BF₄NO₂: C, 51.08; H, 8.57; N, 4.25%. Found: C, 51.16; H, 8.97; N, 4.25%. MS (negative mode): m/z = 87 (BF₄⁻).

2.2.3 General procedure for the synthesis of 4-arylsulfonyl-1-oxa-4-azacyclohexadecan-16-one (2b-i). To a solution of 16-oxo-1-oxa-4-azoniacyclohexadecan-4-ium tetrafluoroborate (1.01 g, 3 mmol) and pyridine (0.95 g, 12 mmol) in 30 mL anhydrous acetonitrile was added dropwise arylsulfonyl chloride (4 mmol). After stirring and refluxing for 15 h, the mixture was concentrated by evaporation and the residue was washed with water (30 mL). The aqueous solution was extracted by methylene chloride (10 mL × 3), the combined organic layer was washed with water (10 mL × 3) and then dried over anhydrous sodium sulfate. After removal of the solvent, the residue was separated by column chromatography on silica gel (200–300 mesh) with methylene chloride as eluant to give arylsulfonyl-1-oxa-4-azacyclohexadecan-16-one (2b-i).

4-(Phenylsulfonyl)-1-oxa-4-azacyclohexadecan-16-one (2b). Yield: 60%, mp 49–51 °C. ¹H NMR (δ (ppm); CDCl₃): 1.26–1.37(m, 14H), 1.53–1.70(m, 4H), 2.32(t, J = 7.2 Hz, 2H), 3.17(t, J = 7.6 Hz, 2H), 3.38(t, J = 5.3 Hz, 2H), 4.25(t, J = 4.5 Hz, 2H), 7.49–7.62(m, 3H), 7.80–7.83(m, 2H). ¹³C NMR (δ (ppm); CDCl₃): 23.69, 24.80, 25.70, 25.71, 25.85, 25.98, 26.68, 26.77, 27.81, 33.77, 47.44, 49.65, 63.57, 127.05, 129.04, 132.49, 139.35, 173.44. IR, ν_{\max} (KBr disc)/cm⁻¹: 2939, 2856, 1732, 1453, 1335, 1151, 1090, 988, 744. Anal. calcd for C₂₀H₃₁NO₄S: C, 62.96; H, 8.19; N, 3.67%. Found: C, 62.90; H, 8.22; N, 3.93%.

4-Tosyl-1-oxa-4-azacyclohexadecan-16-one (2c). Yield: 49%, mp 40–41 °C. ¹H NMR (δ (ppm); CDCl₃): 1.26–1.37(m, 14H), 1.57–1.68(m, 4H), 2.32(t, J = 7.2 Hz, 2H), 2.43(s, 3H), 3.15(t, J = 7.6 Hz, 2H), 3.36(t, J = 5.3 Hz, 2H), 4.24(t, J = 5.2 Hz, 2H), 7.30(d, J = 8.0 Hz, 2H), 7.67–7.71(m, 2H). ¹³C NMR (δ (ppm); CDCl₃): 21.42, 23.72, 24.83, 25.73, 25.87, 26.01, 26.72, 26.79, 27.85, 33.81, 47.46, 49.66, 63.65, 127.15, 129.66, 136.37, 143.28, 173.52. IR, ν_{\max} (KBr disc)/cm⁻¹: 2942, 2855, 1729, 1598, 1456, 1376, 1330, 1287, 1154, 1090, 987, 731. Anal. calcd for C₂₁H₃₃NO₄S: C, 63.76; H, 8.41; N, 3.54%. Found: C, 63.63; H, 8.53; N, 3.54%.

4-(2-Chlorophenylsulfonyl)-1-oxa-4-azacyclohexadecan-16-one (2d). Yield: 49%, liquid. $^1\text{H NMR}$ (δ (ppm); CDCl_3): 1.22–1.38(m, 14H), 1.50–1.60(m, 2H), 1.63–1.72(m, 2H), 2.33(t, $J = 7.2$ Hz, 2H), 3.34(t, $J = 7.8$ Hz, 2H), 3.62(t, $J = 5.4$ Hz, 2H), 4.22(t, $J = 5.3$ Hz, 2H), 7.37–7.42(m, 1H), 7.46–7.54(m, 2H), 8.09–8.12(m, 1H). $^{13}\text{C NMR}$ (δ (ppm); CDCl_3): 23.80, 24.63, 25.60, 25.68, 25.92, 25.94, 26.47, 26.81, 27.01, 33.93, 46.49, 48.64, 63.69, 126.96, 131.98, 132.01, 132.02, 133.52, 137.67, 173.43. IR, ν_{max} (KBr disc)/ cm^{-1} : 2936, 2857, 1736, 1575, 1458, 1340, 1247, 1161, 1043, 980, 763. Anal. calcd for $\text{C}_{20}\text{H}_{30}\text{ClNO}_4\text{S}$: C, 57.75; H, 7.27; N, 3.37%. Found: C, 58.24; H, 7.50; N, 3.42%.

4-(4-Chlorophenylsulfonyl)-1-oxa-4-azacyclohexadecan-16-one (2e). Yield: 49%, mp 66–69 °C. $^1\text{H NMR}$ (δ (ppm); CDCl_3): 1.26–1.37(m, 14H), 1.52–1.70(m, 4H), 2.32(t, $J = 7.2$ Hz, 2H), 3.17(t, $J = 7.6$ Hz, 2H), 3.38(t, $J = 5.3$ Hz, 2H), 4.25(t, $J = 5.2$ Hz, 2H), 7.47–7.51(m, 2H), 7.73–7.77(m, 2H). $^{13}\text{C NMR}$ (δ (ppm); CDCl_3): 23.75, 24.86, 25.76, 25.77, 25.92, 26.05, 26.72, 26.84, 27.84, 33.83, 47.52, 49.72, 63.53, 128.57, 129.42, 138.06, 139.10, 173.51. IR, ν_{max} (KBr disc)/ cm^{-1} : 3096, 2933, 2857, 1728, 1580, 1467, 1367, 1337, 1243, 1158, 1090, 984, 764. Anal. calcd for $\text{C}_{20}\text{H}_{30}\text{ClNO}_4\text{S}$: C, 57.75; H, 7.27; N, 3.37%. Found: C, 57.88; H, 7.40; N, 3.20%.

4-(2-Nitrophenylsulfonyl)-1-oxa-4-azacyclohexadecan-16-one (2f). Yield: 48%, liquid. $^1\text{H NMR}$ (δ (ppm); CDCl_3): 1.26–1.38(m, 14H), 1.54–1.72(m, 4H), 2.33(t, $J = 7.3$ Hz, 2H), 3.36(t, $J = 7.8$ Hz, 2H), 3.60(t, $J = 5.3$ Hz, 2H), 4.25(t, $J = 5.2$ Hz, 2H), 7.64–7.74(m, 3H), 8.01–8.04(m, 1H). $^{13}\text{C NMR}$ (δ (ppm); CDCl_3): 23.75, 24.63, 25.58, 25.63, 25.88, 25.91, 26.48, 26.79, 27.19, 33.90, 46.60, 48.96, 63.59, 124.19, 130.71, 131.64, 133.24, 133.56, 148.07, 173.40. IR, ν_{max} (KBr disc)/ cm^{-1} : 3095, 2940, 2857, 1735, 1545, 1458, 1371, 1345, 1168, 1056, 981, 743. Anal. calcd for $\text{C}_{20}\text{H}_{30}\text{N}_2\text{O}_6\text{S}$: C, 56.32; H, 7.09; N, 6.57%. Found: C, 56.65; H, 7.27; N, 6.62%.

4-(3-Nitrophenylsulfonyl)-1-oxa-4-azacyclohexadecan-16-one (2g). Yield: 48%, mp 64–66 °C. $^1\text{H NMR}$ (δ (ppm); CDCl_3): 1.26–1.37(m, 14H), 1.55–1.68(m, 4H), 2.32(t, $J = 7.1$ Hz, 2H), 3.25(t, $J = 7.7$ Hz, 2H), 3.46(t, $J = 5.3$ Hz, 2H), 4.27(t, $J = 5.2$ Hz, 2H), 7.73–7.78(m, 1H), 8.13–8.17(m, 1H), 8.42–8.46(m, 1H), 8.64–8.66(m, 1H). $^{13}\text{C NMR}$ (δ (ppm); CDCl_3): 23.70, 24.81, 25.70, 25.72, 25.86, 26.00, 26.62, 26.81, 27.84, 33.74, 47.60, 49.84, 63.32, 122.16, 126.98, 130.52, 132.55, 141.98,

148.40, 173.41. IR, ν_{max} (KBr disc)/ cm^{-1} : 3092, 2934, 2856, 1729, 1524, 1463, 1356, 1163, 767. Anal. calcd for $\text{C}_{20}\text{H}_{30}\text{N}_2\text{O}_6\text{S}$: C, 56.32; H, 7.09; N, 6.57%. Found: C, 56.16; H, 7.13; N, 6.51%.

4-(4-Bromophenylsulfonyl)-1-oxa-4-azacyclohexadecan-16-one (2h). Yield: 30%, mp 67–70 °C. $^1\text{H NMR}$ (δ (ppm); CDCl_3): 1.26–1.37(m, 14H), 1.55–1.68(m, 4H), 2.32(t, $J = 7.1$ Hz, 2H), 3.17(t, $J = 7.6$ Hz, 2H), 3.38(t, $J = 5.3$ Hz, 2H), 4.25(t, $J = 5.2$ Hz, 2H), 7.63–7.70(m, 4H). $^{13}\text{C NMR}$ (δ (ppm); CDCl_3): 23.74, 24.84, 25.74, 25.75, 25.90, 26.03, 26.70, 26.82, 27.84, 33.82, 47.52, 49.72, 63.51, 127.52, 128.66, 132.39, 138.55, 173.50. IR, ν_{max} (KBr disc)/ cm^{-1} : 2931, 2857, 1728, 1574, 1463, 1391, 1338, 1242, 1158, 1076, 966, 756. Anal. calcd for $\text{C}_{20}\text{H}_{30}\text{BrNO}_4\text{S}$: C, 52.17; H, 6.57; N, 3.04%. Found: C, 51.88; H, 6.59; N, 3.06%.

4-(4-Acetaminophenylsulfonyl)-1-oxa-4-azacyclohexadecan-16-one (2i). Yield: 55%, mp 126–128 °C. $^1\text{H NMR}$ (δ (ppm); CDCl_3): 1.27–1.37(m, 14H), 1.55–1.70(m, 4H), 2.21(s, 3H), 2.32(t, $J = 7.2$ Hz, 2H), 3.14(t, $J = 7.6$ Hz, 2H), 3.35(t, $J = 5.3$ Hz, 2H), 4.24(t, $J = 5.2$ Hz, 2H), 7.65–7.77(m, 5H). $^{13}\text{C NMR}$ (δ (ppm); CDCl_3): 23.73, 24.57, 24.85, 25.73, 25.74, 25.88, 26.02, 26.72, 26.80, 27.88, 33.86, 47.52, 49.79, 63.66, 119.43, 128.29, 133.70, 142.14, 168.91, 173.50. IR, ν_{max} (KBr disc)/ cm^{-1} : 3330, 2931, 2856, 1709, 1599, 1456, 1335, 1263, 1155, 1092, 980, 742. Anal. calcd for $\text{C}_{22}\text{H}_{34}\text{N}_2\text{O}_6\text{S}$: C, 60.25; H, 7.81; N, 6.39%. Found: C, 59.98; H, 7.85; N, 6.47%.

2.3 Bioassay of fungicidal activity

2.3.1 Bioassay of fungicidal activity of compounds 2a–2i in vitro. The fungicidal activity of all the synthesized compounds against *Rhizoctonia solani* Kühn, *Fulvia fulva* (Cooke) Ciferri, *Colletotrichum orbiculare* (Berk. et Mont.) Arx, *Verticillium dahliae* Kleb., *Sclerotinia sclerotiorum* (Lib.) de Bary and *Alternaria kikuchiarna* Tanaka *in vitro* was evaluated using the mycelium growth rate test⁶ and commercial fungicide Chlorothalonil was used as a control. The results were given in Table 1.

2.3.2 Bioassay of fungicidal activity of compound 2a in vivo.

2.3.2.1 Pot culture experiments of 2a. Soil drenching. Thirty tomato seeds grown in soil contaminated with *Rhizoctonia solani* Kühn in each plastic pot were soil-drenched with 50 ml of **2a** and commercial Carbendazim solution at a concentration of

Table 1 Inhibition rate of the compounds **2a–2i** against six fungus species

Compd	Inhibition rate (%)					
	<i>Rhizoctonia solani</i> Kühn	<i>Fulvia fulva</i> (Cooke) Ciferri	<i>Colletotrichum orbiculare</i> (Berk. et Mont.) Arx	<i>Verticillium dahliae</i> Kleb.	<i>Sclerotinia sclerotiorum</i> (Lib.) de Bary	<i>Alternaria kikuchiarna</i> Tanaka
2a	96.0	89.3	73.2	86.9	85.7	85.7
2b	0.0	63.6	56.3	61.9	61.3	66.6
2c	0.0	50.1	46.4	50.7	39.5	52.5
2d	0.0	59.3	43.8	50.7	49.3	55.6
2e	0.0	45.0	0.0	44.5	39.5	55.6
2f	0.0	45.0	43.8	34.6	36.0	52.5
2g	0.0	45.0	35.4	50.7	46.2	46.2
2h	7.5	45.0	29.6	44.5	39.5	55.6
2i	27.1	39.8	32.5	41.3	32.4	32.4
Chlorothalonil	96.6	88.1	90.8	91.1	91.7	76.1

Table 2 The potted test effect of **2a** against *Rhizoctonia solani* Kühn (tomato† or cotton‡)

Compd	Mode of action	Effect (%)
2a	Soil drenching†	61.9
	Foliar spraying†	94.1
	Seed dressing‡	87.2
Carbendazim	Soil drenching†	17.5
	Foliar spraying†	42.7
	Seed dressing‡	79.2

0.1% separately. The seeds were allowed to grow in a greenhouse. One week after planting, an investigation was carried out to determine whether diseases had occurred on their seedlings. The results of preliminary soil drenching bioassay of **2a** compared with commercial fungicide Carbendazim are listed in Table 2.

Foliar spraying. Thirty tomato seeds grown in sterilized soil in each plastic pot were planted in greenhouse. **2a** and commercial Carbendazim were dissolved in water to be 0.05% solutions separately, and the solutions were applied to seedlings (cotyledon stage) as foliar sprays with a hand sprayer. When the plants were just dry, the solutions containing *Rhizoctonia solani* Kühn mycelia were sprayed into each pot. After growing in greenhouse for one week, an investigation was carried out to determine whether diseases had occurred on their seedlings. The results of preliminary foliar spraying bioassay of **2a** compared with commercial agricultural fungicide Carbendazim are listed in Table 2.

Seed dressing. Ten cotton seeds dressed with **2a** and commercial Carbendazim (**2a** or Carbendazim/seeds: 0.3%), grown in soil inoculated with *Rhizoctonia solani* Kühn mycelium (0.1% weight of pot soil), were planted in greenhouse. After growing for one week, an investigation was carried out to determine whether diseases had occurred on their seedlings. The results of a seed dressing bioassay of **2a** compared with commercial fungicide Carbendazim are listed in Table 2.

2.3.2.2 Field efficacy trials of 2a. Field efficacy trials were conducted in 2006–2007 on the Research Farm of Institute of Cotton, Shanxi Province Academy of Agriculture Science, based on standard procedure of People's Republic of China.⁷ **2a** was formulated as 25% (w/w) wettable powder and commercial fungicide Carbendazim was used as a control. The results are summarized in Table 3.

2.4 Toxicological test of 2a

The toxicological test was performed based on the standard procedure of the People's Republic of China.⁸ The results are summarized in Table 4.

Table 3 The field efficacy trials effect of **2a** against *Rhizoctonia solani* Kühn (cotton)

Compd.	Mode of action	Dosage (2a /seeds (%), w/w)	Effect (%)	
			2006	2007
2a	Seed dressing	0.10	55.8	48.9
		0.15	61.9	63.6
Carbendazim	Seed dressing	0.15	49.6	53.4

Table 4 The toxicological test results of **2a**

Subject	Results
Rat acute oral (LD ₅₀ , mg kg ⁻¹)	3160 (male) 3160 (female)
Rat acute dermal (LD ₅₀ , mg kg ⁻¹)	>2000 (male) >2000 (female)
Eye irritation	Medium
Skin irritation	Not irritation
Ames test	Negative

3. Results and discussion

3.1 Chemical synthesis and economical utilization of chemical atoms

A significant goal of green chemistry must be to maximize the efficiency of use of the raw materials and to minimize the creation of waste.⁹ In this paper, we chose the reaction of 2-azidoethanol with cyclododecanone in the presence of borotrifluoride to synthesize the title compounds **2a** as in ref. 5, but there were some improvements made, *i.e.* the reaction was carried out without solvent and the time for the enlargement of the ring was much shorter (12 h) than in the reference (24–72 h). Besides that, based on the data of elemental analysis and MS (negative mode), the final product was identified as 16-oxo-1-xoa-4-azoniacylhexadecan-4-ium tetrafluoroborate (**2a**) rather than free 1-oxa-4-aza- cyclohexadecan-16-one, as reported in the reference.

From the synthesis of compound **2a** we can see that all of the atoms of the raw materials including boron trifluoride were almost fully utilized, except one nitrogen molecule and part of the boron atoms being lost. In addition, the hazard to the environment caused by the solvent (methylene chloride was used in the reference) was eliminated. Therefore it is a green technology with high atom economy.

3.2. Toxicological test

The results of the toxicological test indicated that **2a** was a low toxicity compound based on the classification standard procedure of the People's Republic of China⁸ and safe to human beings.

3.3. Biological assay

The preliminary bioassay *in vitro* (Table 1) indicated that all the synthesized compounds exhibited some fungicidal activity against *Rhizoctonia solani* Kühn, *Fulvia fulva* (Cooke) Ciferri, *Colletotrichum orbiculare* (Berk. et Mont.) Arx, *Verticillium dahliae* Kleb., *Sclerotinia sclerotiorum* (Lib.) de Bary and *Alternaria kikuchiarna* Tanaka. Among them, compound **2a** is the best one, its bioactivity against *Fulvia fulva* (Cooke) Ciferri and *Alternaria kikuchiarna* Tanaka was better than that of the control fungicide Chlorothalonil, and its bioactivity against *Rhizoctonia solani* Kühn was almost similar to that of Chlorothalonil and **2b–2i** exhibited less fungicidal activity. *Rhizoctonia solani* Kühn is an important agricultural fungus species which always seriously damages cotton production in China,¹⁰ therefore the efficacy of **2a** against *Rhizoctonia solani* Kühn was further evaluated. The results of potted test (whichever the mode of action, soil

drenching, foliar spraying or seed dressing) and field trial showed that **2a** against *Rhizoctonia solani* Kühn was more active than commercial fungicide Carbendazim as well (Tables 2 and 3).

3.4. The structure–activity relationship

In our previous paper, we postulated that macrocyclic compounds with two polarizable groups (one hydrogen-bonding donor and one hydrogen-bonding acceptor) and two–three methylene groups' distance between these two polarizable groups would exhibit certain good bioactivity. In this paper, the fact that compound **2a** with one hydrogen-bonding donor (NH) and one hydrogen-bonding acceptor (C=O) and with two methylenes' distance between these two polarizable groups has a good fungicidal activity proved the correctness of this postulation. Consistent with this, compounds **2b–2i**, although they are sulfonyl compounds, but with only one hydrogen-bonding acceptor (C=O) and without a hydrogen-bonding donor in the macrocyclic ring, do have fungicidal activities, but they are less than that of compound **2a**. This further supports our initial proposal.

Conclusions

A potential green agricultural fungicide 16-oxo-1-oxa-4-azoniacyclohexadecan-4-ium tetrafluoroborate (**2a**) was synthesized. The effect data of pot culture experiments and field efficacy trials showed that it has excellent fungicidal activity against *Rhizoctonia solani* Kühn compared to commercial fungicide Carbendazim. In addition, low toxicity, and green synthetic technology with high atom economy indicate that **2a** may be expected to further develop as a useful fungicide.

Acknowledgements

We acknowledge financial support of this investigation by the National Basic Research Program of China (2003CB114407). We also thank Dr Zhang Li-Ping, Shanxi Academy of Agricultural Science for the help of field test and Dr Wang Jing, Tianjin Center of Disease Prevent and Control for the accomplishment of the toxicological test.

References

- 1 J. C. Liu, H. W. He and X. M. Feng, *Chin. J. Pestic.*, 2005, **44**, 1–4.
- 2 O. Lopez, J. G. Fernandez-Bolanos and M. V. Gil, *Green Chem.*, 2005, **7**, 431–442.
- 3 J.-X. Huang, Y.-M. Jia, X.-M. Liang, W.-J. Zhu, J.-J. Zhang, Y.-H. Dong, H.-Z. Yuan, S.-H. Qi, J.-P. Wu, F.-H. Chen and D.-Q. Wang, *J. Agric. Food Chem.*, 2007, **55**, 10857–10863.
- 4 R. H. Smith, Jr, A. F. Mehl, D. L. Shantz, Jr, G. N. Chmurny and C. J. Michejda, *J. Org. Chem.*, 1988, **53**, 1467–1471.
- 5 J. E. A. Forsee, J., *J. Org. Chem.*, 1999, **64**, 4381–4385.
- 6 X.-H. Li, X.-L. Yang, Y. Ling, Z.-J. Fan, X.-M. Liang, D.-Q. Wang, F.-H. Chen and Z.-M. Li, *J. Agric. Food Chem.*, 2005, **53**, 2202–2206.
- 7 Standardization Administration of the People's Republic of China, Standard No. GB/T 17980.93-2004, *Pesticide-guidelines for the field efficacy trials (II)—Part 93: Fungicides seed treatment against seedling diseases of cotton*, Beijing, 2004.
- 8 Standardization Administration of the People's Republic of China, Standard No. GB 15670-1995, *Toxicological test methods of pesticides for registration*, Beijing, 1995.
- 9 B. M. Trost, *Acc. Chem. Res.*, 2002, **35**, 695–705.
- 10 (a) S. Q. Chen, B. Wu, Z. Qin, G. Z. Lin, L. Den and X. M. Den, *Southwest China J. Agric. Sci.*, 1998, **12**(1), 56–60; (b) S. J. Gong, G. Y. Li and G. C. Ling, *J. Shihezi Univ. (Nat. Sci.)*, 2004, **22**(suppl.), 55–56; (c) Z. S. Deng, B. C. Zhang, Z. H. Sun and M. L. Zhou, *Plant Prot.*, 2006, **32**(4), 36–39.

A simple and eco-friendly approach for the synthesis of 2-imino and 2-oxo-2*H*-chromene-3-carboxamides†

Fernanda Proença* and Marta Costa

Received 8th May 2008, Accepted 27th June 2008

First published as an Advance Article on the web 11th August 2008

DOI: 10.1039/b807892k

A series of new 2-imino-2*H*-chromene-3-carboxamides **5** were synthesized in excellent yield and high atom economy by the Knoevenagel condensation of salicylaldehyde derivatives **4** and *N*-substituted cyanoacetamides **3** using aqueous sodium carbonate or hydrogen carbonate solution, at room temperature. Treatment of compounds **5** with aqueous HCl led to the formation of the corresponding 2-oxochromenes **6**.

Introduction

In recent years, the pharmaceutical industry has actively promoted the development of greener alternatives for the preparation of drugs and drug candidates, in an effort to replace their poor atom economy reactions and polluting procedures.¹ Amide bond formation was identified as one of the most common transformations utilized in the synthesis of new products.² Several chemical approaches generate great quantities of waste and/or involve non-aqueous conditions. The development of new, environmentally benign methods for amide formation was considered one of the major challenges in the near future.

Chromene derivatives have attracted considerable interest due to their diverse biological properties and therapeutical applications, namely as anti-HIV, anti-tuberculosis, anti-inflammatory and anti-fungal agents.³ Naturally occurring chromenes were found in plants⁴ and have been used as valuable leads for the design and synthesis of new pharmacophores for medicinal chemistry and drug development.

A brief analysis of previous synthetic approaches for the preparation of 2*H*-chromene-3-carboxamides showed that the reaction of substituted salicylaldehydes and *N*-aryl cyanoacetamide was one of the methods used to generate these compounds, by refluxing the reagents in ethanol and piperidine.⁵ The heterocyclization of benzaldimines and carbon suboxide in diethyl ether was also reported to lead to 2-oxo-2*H*-chromene-3-carboxamides.⁶ A recent approach started with the reaction of substituted salicylaldehydes with diethylmalonate to generate the ethyl 2-oxo-2*H*-chromene-3-carboxylate. Hydrolysis of the ester function and activation of the carboxylic acid as an acyl chloride, allowed the preparation of the amide substituent upon reaction with primary amines using diethyl ether, THF or chloroform as solvents.^{3b,7}

Results and discussion

An important research area recently explored by our research group is the synthesis of new chromene-based structures as potential drug candidates.⁸ As part of this work, we now report a simple and eco-friendly synthesis of substituted 2-imino- and 2-oxo-2*H*-chromene-3-carboxamides **5** and **6** from substituted salicylaldehydes **4** and cyanoacetamides **3**.

A wide variety of cyanoacetamides was prepared by direct combination of methylcyanoacetate and primary or secondary alkyl amines, inspired by a procedure previously described by Gazit *et al.*⁹ Most of the products were formed at room temperature and in the absence of solvent. The solid was isolated by filtration, after the addition of a few drops of diethyl ether (Table 1). Analytically pure samples were isolated in most cases (**3a–u**) with the exception of compounds **3e** and **f**. In these cases, the product was a viscous oil, used directly in the next synthetic step. The 2-cyanoacetamides were prepared with an atom economy of 75–87%, as only a molecule of methanol was released in the process. The ultimate goal was to prepare 2*H*-chromenes bearing a substituted amide in the 3-position of the chromene ring. Alkyl chains with biologically interesting nitrogen-containing moieties were selected as substituents on the amide nitrogen.

The synthesis of 2-imino-2*H*-chromene-3-carboxamides **5** occurred when the cyanoacetamides **3a–u** were combined with salicylaldehydes **4**, using aqueous sodium carbonate or hydrogen carbonate solution at room temperature (Scheme 1).

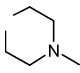
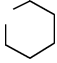
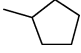
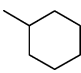
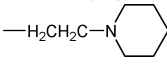
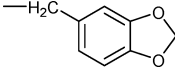
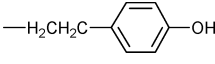
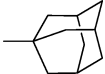
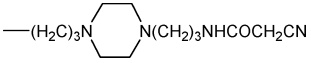
The product of the Knoevenagel cyclocondensation precipitated from the reaction mixture and was isolated in almost quantitative yield and a very high atom economy, since only a molecule of water was wasted (Table 2). When this reaction was performed using di-cyanoacetamides **3s–u**, the analogous dimeric chromenes **5** were isolated. *N,N*-Disubstituted cyanoacetamides **3a** and **b** did not react with 3-methoxysalicylaldehyde after 2 h to 5 days at room temperature. This absence of reactivity was attributed to stereochemical hindrance caused by the disubstituted amide unit.

The 2-oxochromenes **6** were easily prepared either from the corresponding 2-iminochromenes **5** or upon combination of the reagents **1** and **2** in aqueous base followed by addition of

Centro de Química, Universidade do Minho, Campos de Gualtar, 4710-057, Braga, Portugal. E-mail: fproenca@quimica.uminho.pt, martacosta@quimica.uminho.pt; Fax: +351 253 604382; Tel: +351 253 604379

† Electronic supplementary information (ESI) available: Analytical data for compounds **3**, **5** and **6**. See DOI: 10.1039/b807892k

Table 1 Uncatalyzed synthesis of 2-cyanoacetamides **3**

Compound 3	R ₁	R ₂	Yield [atom economy] (%)
3a			84 [84]
3b			84 [83] ^a
3c	H	-CH ₂ CH ₂ OCH ₃	96 [82]
3d	H	-CH ₂ CH ₂ OH	81 [80]
3e	H	-CH ₂ (CH ₂) ₂ OH	100 [84]
3f	H	-CH ₂ (CH ₂) ₄ OH	100 [84]
3g	H	-CH(CH ₂ CH ₃)CH ₂ OH	91 [83]
3h	H		84 [82]
3i	H		83 [84]
3j	H	-CH ₂ CH(OH)CH ₂ OH	100 [83]
3k	H	-C(CH ₂ OH) ₃	66 [85]
3l	H	-CH ₂ CH(Ph)OH	96 [86]
3m	H		60 [80]
3n	H		84 [87]
3o	H		78 [86] ^b
3p	H	-CH ₂ CH(OCH ₂ CH ₃) ₂	78 [86] ^c
3q	H		75 [87] ^b
3r	H	-(CH ₂) ₂ NHCOCH ₂ CN	99 [75] ^d
3s	H	-(CH ₂) ₃ NHCOCH ₂ CN	100 [76] ^d
3t	H		100 [84]
3u	H	-(CH ₂) ₃ O(CH ₂) ₄ O(CH ₂) ₃ NHCOCH ₂ CN	93 [84]

^a Commercially available. ^b Synthesized with EtOH and heating (70–80 °C). ^c Synthesized with heating (80 °C). ^d Reported in ref. 9.

concentrated hydrochloric acid and heating at 80–90 °C for 1 to 2 h. The products were again isolated in excellent yield and good atom economy.

Conclusions

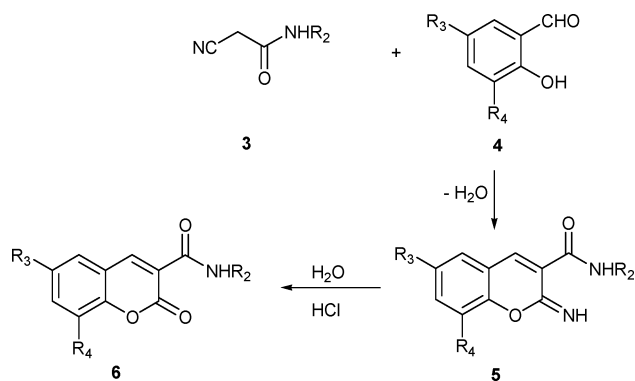
A convenient, clean and efficient method was developed for the synthesis of 2*H*-chromene-3-carboxamides, an important class of potentially bioactive compounds. The 2-imino and 2-oxo-2*H*-chromene-3-carboxamides were prepared in water, an excellent solvent in terms of environmental impact and with reduced waste

production. The compounds were isolated by simple filtration in a high purity form.

Experimental

Materials and methods

All compounds were fully characterized by elemental analysis and spectroscopic data. The NMR spectra were recorded on a Varian Unity Plus (¹H: 300 MHz, ¹³C: 75 MHz), including the ¹H–¹³C correlation spectra (HMQC and HMBC) and deuterated DMSO was used as solvent. IR spectra were recorded on a



Scheme 1

FT-IR Bomem MB 104 using Nujol mulls and NaCl cells. The reactions were monitored by thin layer chromatography (TLC) using silica gel 60 F₂₅₄ (Merck). The melting points were determined on a Stuart SMP3 melting point apparatus and are uncorrected. Elemental analyses were performed on a LECO CHNS-932 instrument.

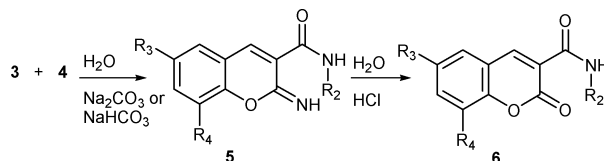
Typical procedure for the synthesis of 2-cyanoacetamides 3

In a round bottomed flask cyclopentanamine **1h** (0.26 g, 302 μ l, 3.03 mmol) was added to methyl cyanoacetate **2** (0.30 g, 270 μ l, 3.03 mmol) and the mixture was stirred at room temperature for 2 h. A yellow solid started to precipitate from the reaction mixture, which was kept at room temperature for a further 10 min. The yellow solid was filtered and washed with diethyl ether leading to the pure product **3h** (0.38 g, 2.54 mmol, 94%).

Typical procedure for the synthesis of 2-imino-2H-chromene-3-carboxamides 5

2-Cyano-*N*-[1,3-dihydroxy-2-(hydroxymethyl)propan-2-yl]acetamide **3k** (0.11 g, 0.59 mmol) was added to a suspension of 3-methoxysalicylaldehyde **4** (0.08 g, 0.60 mmol) in aqueous NaHCO₃ (0.05 M, 2.00 ml) and the reaction mixture was stirred in an ice bath for 30 min. The yellow suspension was stirred at room temperature for a further 22 h. The yellow solid was filtered and washed with water and a few drops of diethyl ether leading to the pure product **5k** (0.17 g, 0.54 mmol, 93%).

Table 2 Aqueous synthesis of 2-imino-2H-chromene-3-carboxamides **5** and 2-oxo-2H-chromene-3-carboxamides **6**



Compound 4		Compound 3	Product 5	Product 6
R ₃	R ₄		Yield [atom economy] (%)	Yield [atom economy] (%)
H	OCH ₃	3c	100 [94]	—
H	OCH ₃	3d	84 [94]	—
H	OCH ₃	3e	77 [94]	—
H	OCH ₃	3f	67 [94]	—
H	OCH ₃	3g	87 [94]	—
H	OCH ₃	3h	38 [94]	—
H	OCH ₃	3i	69 [94]	—
H	OCH ₃	3j	74 [94]	80 [95]
H	OCH ₃	3k	93 [95]	—
H	OCH ₃	3l	81 [95]	—
H	OCH ₃	3n	12 [95] ^a	—
H	OCH ₃	3o	60 [95]	—
H	OCH ₃	3p	100 [95]	21 [95]
H	OCH ₃	3s	88 [93]	—
H	OCH ₃	3t	100 [94]	—
H	OCH ₃	3u	45 [94]	—
H	OH	3j	—	40 [94]
H	H	3c	93 [93]	71 [94]
H	H	3g	91 [94]	62 [94]
H	H	3j	—	53 [94]
H	H	3t	—	50 [94]
Cl	H	3c	83 [94]	—
Cl	H	3j	—	100 [95]
Cl	H	3g	84 [94]	—
Br	H	3c	99 [94]	89 [95]
Br	H	3j	—	100 [95]
Br	H	3l	—	80 [96]
Br	H	3p	99 [95]	—

^a Synthesized with aqueous NaOH (0.5 M) for 36 h at room temperature and then neutralized with 1 equivalent of TFA.

Typical procedure for the synthesis of 2-oxo-2H-chromene-3-carboxamides **6**

2-Cyano-*N*-(2,3-dihydroxypropyl)acetamide **3j** (0.11 g, 0.70 mmol) was added to a suspension of 5-chlorosalicylaldehyde **4** (0.11 g, 0.72 mmol) in aqueous Na₂CO₃ (0.05 M, 3.60 ml) and the yellow suspension was stirred at room temperature for 24 h. Concentrated HCl (0.10 g, 220 μl, 2.66 mmol) was added to the suspension and the reaction mixture was heated at 80 °C for 1 h 30 min. The suspension was cooled to room temperature in an ice bath and the white solid was filtered and washed with water leading to the pure product **6j** (0.21 g, 0.70 mmol, 100%).

Acknowledgements

The authors gratefully acknowledge the financial support by the University of Minho and Fundação para a Ciência e Tecnologia (project POCI/QUI/59356/2004) and the PhD grant awarded to Marta Costa (SFRH/BD/31531/2006).

Notes and references

- D. J. C. Constable, P. J. Dunn, J. D. Hayler, G. R. Humphrey, J. L. Leazer, Jr., R. J. Linderman, K. Lorenz, J. Manley, B. A. Pearlman, A. Wells, A. Zaks and T. Y. Zhang, *Green Chem.*, 2007, **9**, 411–420.
- (a) J. S. Carey, D. Laffan, C. Thomson and M. T. Williams, *Org. Biomol. Chem.*, 2006, **4**, 2337–2347; (b) R. W. Dugger, J. A. Ragan and D. H. B. Ripin, *Org. Process Res. Dev.*, 2005, **9**, 253–258.
- (a) L. Abrunhosa, M. Costa, F. Areias, A. Venâncio and F. Proença, *J. Ind. Microbiol. Biotechnol.*, 2007, **34**, 787–792; (b) F. Chimenti, B. Bizzarri, A. Bolasco, D. Secci, P. Chimenti, S. Carradori, A. Granese, D. Rivanera, D. Lilli, A. Zicari, M. M. Scaltrito and F. Sisto, *Bioorg. Med. Chem. Lett.*, 2007, **17**, 3065–3071; (c) I. Kostova, *Mini-Rev. Med. Chem.*, 2006, **6**, 365–374; (d) A. Nayyar and R. Jain, *Curr. Med. Chem.*, 2005, **12**, 1873–1886; (e) K. Fylaktakidou, D. Hadjipavlou-Litina, K. Litinas and D. Nicolaidis, *Curr. Pharm. Des.*, 2004, **10**, 3813–3833; (f) K. Asres, A. Seyoum, C. Veeresham, F. Bucar and S. Gibbons, *Phytother. Res.*, 2005, **19**, 557–58.
- M. Curini, G. Cravotto, F. Epifano and G. Giannone, *Curr. Med. Chem.*, 2006, **13**, 199–222.
- C. Huang, F. Wu and Y. Ai, *Bioorg. Med. Chem. Lett.*, 1995, **5**, 2423–2428.
- F. Chimenti, B. Bizzarri, A. Bolasco, D. Secci, P. Chimenti, S. Carradori, A. Granese, D. Rivanera, D. Lilli, M. M. Scaltrito and M. I. Brenciaglia, *Eur. J. Med. Chem.*, 2006, **41**, 208–212.
- S. Robert, C. Bertolla, B. Masereel, J.-M. Dogné and L. Pochet, *J. Med. Chem.*, 2008, DOI: 10.1021/jm8002697.
- L. Abrunhosa, M. Costa, F. Areias, A. Venâncio and F. Proença, *J. Org. Chem.*, 2008, **73**, 1954–1962.
- A. Gazit, N. Osherov, C. Gilon and A. Levitzki, *J. Med. Chem.*, 1996, **39**, 4905–4911.

Hydroxyapatite-supported palladium (0) as a highly efficient catalyst for the Suzuki coupling and aerobic oxidation of benzyl alcohols in water

Navjot Jamwal, Monika Gupta and Satya Paul*

Received 6th February 2008, Accepted 1st July 2008

First published as an Advance Article on the web 11th August 2008

DOI: 10.1039/b802135j

A hydroxyapatite-supported palladium (0) catalyst was prepared and employed for the Suzuki coupling and aerobic oxidation of benzyl alcohols in water. This green procedure provides biaryls, heteroaryls and polyaryls in excellent yields with very high turnover numbers. The catalyst was equally efficient for the selective aerobic oxidation of benzyl alcohols under an air atmosphere. In both the cases, the catalyst can be recycled up to five times without significant loss of activity.

Introduction

The unavoidable choice of a specific solvent for a desired chemical reaction can have profound economical, environmental, and societal implications. The pressing need to develop alternative solvents to some extent originates from these implications and constitutes an essential strategy under the emerging field of green chemistry.¹ In this context, various non-conventional media² have been developed. Among these, water can undoubtedly be considered the cleanest solvent available, and the use and release of clean water clearly will have the least impact on the environment.³

In recent times, the development of heterogeneous catalysts⁴ has taken the lead over their homogeneous counterparts because of simplified recovery, recyclability and potential for incorporation in continuous reactors and microreactors. Among various solid supports commonly used for the preparation of heterogeneous catalysts, hydroxyapatite has received much attention.⁵ Recently, hydroxyapatite-supported palladium catalysts have been used as highly efficient catalysts in organic syntheses.⁶

The Suzuki reaction is one of the most versatile and utilized reactions for the selective construction of carbon–carbon bonds,^{4a} in particular for the construction of biaryls,^{4a,7} since these have a diverse spectrum of applications,⁸ ranging from pharmaceuticals to material science. Therefore, the development of easily available or prepared, inexpensive catalysts, and environmentally benign solvents and methodology avoiding the use of expensive and toxic ligands remains a highly desirable goal. Recently, various catalytic systems have been reported for the Suzuki coupling in water.⁹

The controlled oxidation of primary alcohols to aldehydes without forming over-oxidised products is a challenging task for the chemists. There are number of methodologies^{4d,10} available for alcohol oxidation, however, oxidations using molecular oxygen are highly attractive alternatives,^{10,11} since they are atom efficient and produce water as the only by-product.¹² However, oxidations which could be accomplished under atmospheric air

in the aqueous phase are highly preferred. In the context of green chemistry, aqueous phase alcohol oxidations have been reported.¹³

In this paper, we report the simple preparation of hydroxyapatite-supported palladium (0) and its application for the synthesis of biaryls, polyaryls and heteroaryls *via* Suzuki coupling between aryl bromides, including bromophenol, bromoaniline, and benzenboronic acid, heteroarylboronic acids, using inexpensive K_2CO_3 as base, tetrabutylammonium bromide (TBAB) as phase transfer catalyst and water as solvent; and selective oxidation of benzyl alcohols to corresponding aldehydes using water as solvent under atmospheric air.

Results and discussion

Catalyst preparation and characterization

Hydroxyapatite used for the preparation of hydroxyapatite-supported Pd (0) catalyst (HAP-Pd⁰) was prepared according to the literature procedure with slight modification.^{5b} HAP-Pd⁰ was prepared by stirring a mixture of hydroxyapatite and Pd(OAc)₂ in ethanol for 3 h, followed by dropwise addition of hydrazine hydrate (80%) and the stirring was again continued for 5 h. The colour of the catalyst changed to dark grey, which indicated reduction from Pd(II) to Pd(0). In order to make the reaction medium completely heterogeneous, the catalyst was conditioned by refluxing for 6 h in ethanol, toluene and acetonitrile, respectively, each for 2 h, to remove any physisorbed palladium acetate. The conditioned catalyst was quite stable and could be used for several days.

The characterization of HAP-Pd⁰ was done by XRD, atomic absorption spectrophotometer (AAS) analysis, SEM and TEM.

Powder XRD diffraction patterns of HAP-Pd⁰ (Fig. 1) exhibited a broad reflection corresponding to the hydroxyapatite support. Three additional reflections were found in the XRD pattern ($2\theta = 39^\circ$, 46° and 65°) which could be attributed to Pd(0) (ref. JCPDS file: 46–1043).

The amount of the palladium supported on hydroxyapatite was determined by AAS analysis and found to be 1.1 mmol g⁻¹.

HAP-Pd⁰ was also investigated using transmission electron microscopy (TEM) and scanning electron microscopy (SEM).

Department of Chemistry, University of Jammu, Jammu, 180 006, India.
E-mail: paul7@rediffmail.com; Fax: +91-191-2505086;
Tel: +91-191-2453841

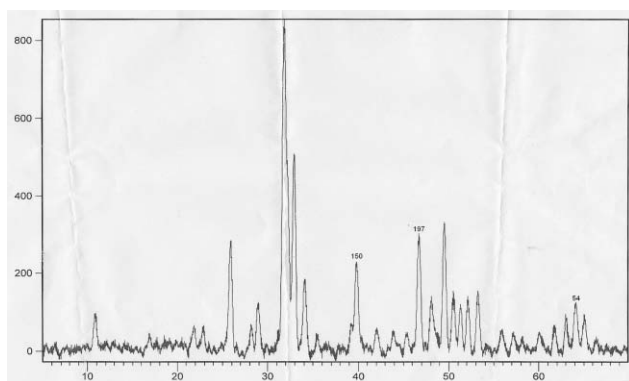


Fig. 1 XRD diffraction patterns of HAP-Pd⁰.

The TEM micrograph (Fig. 2) shows the distribution of palladium onto hydroxyapatite and the average particle diameter was found to be about 20 nm. The physical form of the catalyst was characterized using an SEM micrograph (Fig. 3). The catalyst is a fine homogeneous powder with porous structure.

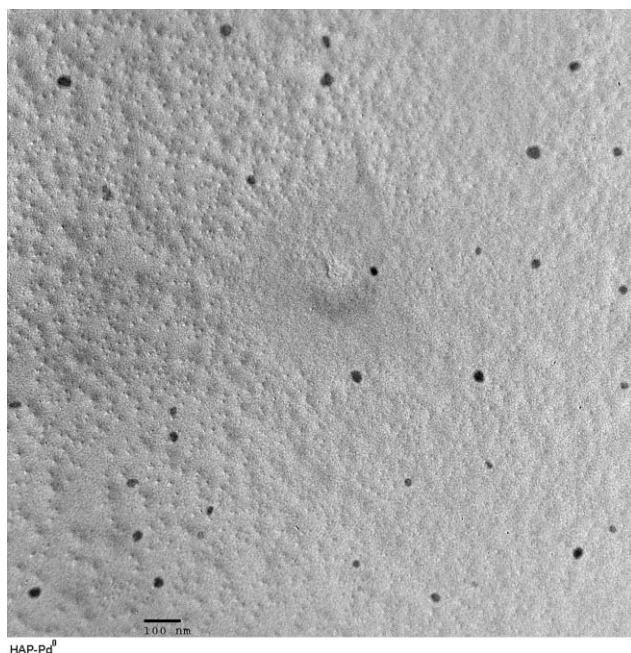
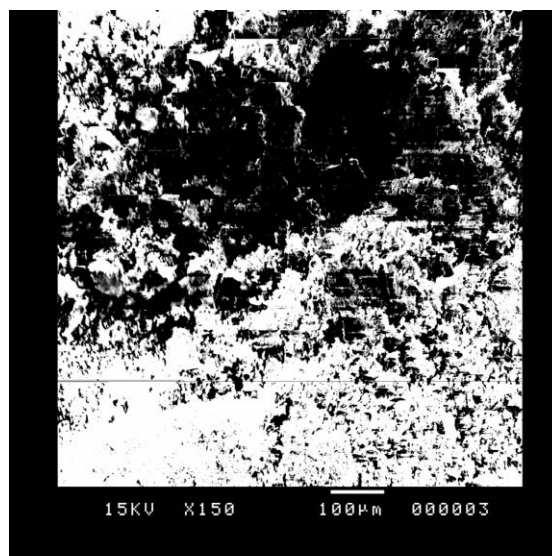


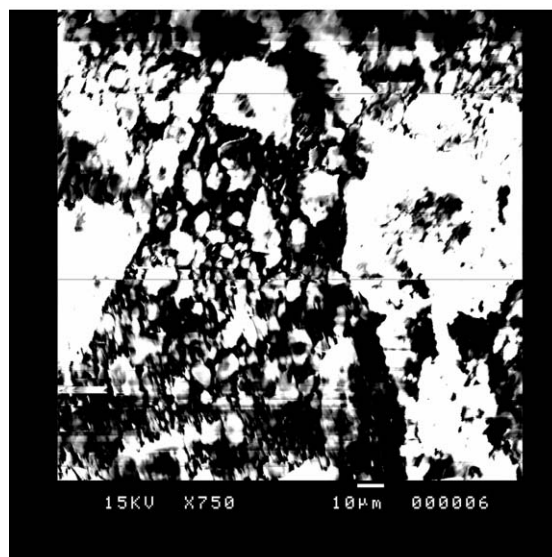
Fig. 2 TEM micrographs of HAP-Pd⁰.

Catalyst testing for the Suzuki reaction

To test the activity of HAP-Pd⁰ for the Suzuki reaction, 4-bromoacetophenone and benzenboronic acid were selected as the test substrates. The Suzuki coupling between 4-bromoacetophenone (1 mmol) and benzenboronic acid (1.5 mmol) was attempted in the presence of HAP-Pd⁰ catalyst (0.3 g), equivalent to 0.33 mol% of Pd, in water (6 mL) at 100 °C using K₂CO₃ (3 mmol) as base in the absence as well as presence of tetrabutylammonium bromide (TBAB) as phase transfer catalyst. It was found that in the absence of TBAB, 4-acetylbiphenyl was obtained in 87% isolated yield in 5.5 h, whereas in the presence of TBAB, 4-acetylbiphenyl was obtained



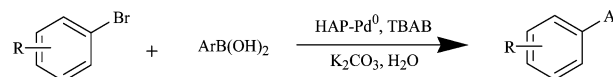
(a)



(b)

Fig. 3 SEM of HAP-Pd⁰ at (a) 15 kV × 150 and (b) 15 kV × 750.

in 94% isolated yield in 4 h. Thus, TBAB enhances the rate of the reaction by transferring haloarene to the aqueous phase and hence reaction with benzenboronic acid faster. Such a rate enhancement in the presence of TBAB has already been reported earlier.¹⁴



Scheme 1

To demonstrate the versatility of the catalytic system, bromoarenes substituted with electron-withdrawing and electron-donating groups gave excellent results (Table 1). Bromophenol, which is considered as a poor substrate for the Suzuki coupling, also undergoes reaction efficiently (entry 9, Table 1). Further, similar conditions were also successful for bromoaniline (entry 10, Table 1). Heteroarylboronic acids are generally

Table 1 Suzuki coupling between aryl bromides and boronic acids in the presence of HAP-Pd⁰ using water as solvent^a

Entry	Aryl bromide	Boronic acid	Time/h	Yield ^b (%)
1	Bromobenzene	Benzene boronic acid	5	90
2	4-Bromoanisole	Benzene boronic acid	6	84
3	4-bromobenzonitrile	Benzene boronic acid	4	95
4	4-Bromoacetophenone	Benzene boronic acid	4	94
5	4-Bromoacetophenone	Benzene boronic acid	7.5	92 ^c
6	4-Bromobenzophenone	Benzene boronic acid	4	92
7	4'-Bromobiphenyl	Benzene boronic acid	5	90
8	4-Bromotoluidine	Benzene boronic acid	6	87
9	4-Bromophenol	Benzene boronic acid	12	82 ^d
10	4-Bromoaniline	Benzene boronic acid	11	78 ^d
11	1,4-Dibromobenzene	Benzene boronic acid	24	93 ^e
12	1,2-Dibromobenzene	Benzene boronic acid	22	93 ^f
13	4-Bromoacetophenone	3-Thiopheneboronic acid	15	84 ^g
14	4-Bromoacetophenone	2-Thiopheneboronic acid	25	60 ^{g, h}
15	4-Bromoacetophenone	4-Pyridineboronic acid	15	76 ^g
16	4-Bromoacetophenone	3-Pyridineboronic acid	16	78 ^g

^a The molar ratios of aryl bromide : boronic acid : K₂CO₃ : TBAB : HAP-Pd⁰ are 1 : 1.5 : 3 : 1 : 0.3. ^b Yield of isolated products. ^c The reaction was carried out with 4-bromoacetophenone (50 mmol), benzene boronic acid (75 mmol), K₂CO₃ (150 mmol), HAP-Pd⁰ (12 g) and water (250 mL) for 7.5 h at 100 °C. ^d The products were obtained after passing through column of silica gel and elution with EtOAc : pet. ether (0.2 : 9.8). ^e The product of the Suzuki coupling is 4-(phenyl)biphenyl. ^f The product of the Suzuki coupling is 2-(phenyl)biphenyl. ^g HAP-Pd⁰ (0.5 g, 0.55 mol% Pd) was used. ^h Rest being the starting materials.

considered as poor substrates for the Suzuki reaction. Recently, Suzuki–Miyaura coupling of *N*-heteroaryl halides and *N*-heteroarylboronic acids has been reported in water.¹⁵ However, very few heterogeneous catalytic systems have been reported.¹⁶ Our methodology, making use of HAP-Pd⁰, was found to be highly efficient for the Suzuki coupling of *N*- and *S*-heteroarylboronic acids in water (entries 13–16, Table 1). It can therefore be suggested that *N* or *S*-atoms prefer to engage in hydrogen bonding with water rather than to co-ordinate to the soft Pd, leading to much higher catalytic activities.

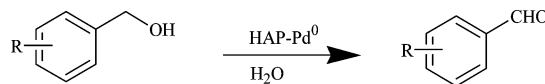
Multinuclear aromatics develop the concept of aromaticity and supramolecular benzene chemistry, and lead to wide applications in material and biological sciences.¹⁷ Recently, the synthesis of polyaryls has been reported using palladium acetate in a domestic microwave oven.¹⁸ Although the authors have reported good yields of polyaryls, this process is commercially unacceptable as it leads to non-recoverable palladium acetate. Recently, we have reported¹⁹ the synthesis of polyaryls using silica supported palladium catalyst using *o*-xylene as solvent, K₂CO₃ as base and 120 °C as the reaction temperature. Here we extend the use of HAP-Pd⁰ to consecutive Suzuki reactions leading to the synthesis of polyaryls in a single step in high yields using water as solvent (entries 11–12, Table 1).

In industry, scaling up of reaction conditions is highly desirable. To scale-up the reaction conditions, the reaction in case of entry 4 (Table 1) was carried out by stirring a mixture of 4-bromoacetophenone (50 mmol), benzeneboronic acid (75 mmol), K₂CO₃ (150 mmol), TBAB (50 mmol) and 12 g of HAP-Pd⁰ in distilled water (250 mL) for 7.5 h. After a similar work-up, 4-acetylbiphenyl was obtained in 92% isolated yield (entry 5, Table 1).

Catalyst testing for the oxidation of benzyl alcohols

The activity of HAP-Pd⁰ was also tested for the selective oxidation of benzyl alcohols using water as solvent and atmospheric

air as the source of molecular oxygen. Benzyl alcohol was selected as the test substrate. The reaction was carried out using benzyl alcohol (1 mmol), HAP-Pd⁰ (0.1 g, 0.11 mol% Pd), water (5 mL) and atmospheric air as the source of oxygen under stirring at 100 °C for 7 h. It was found that benzaldehyde was obtained in 95% isolated yield with 100% selectivity.

**Scheme 2**

To demonstrate the versatility of the catalytic system for the oxidation, benzyl alcohols substituted with various electron-withdrawing and electron-donating groups were chosen, and excellent results were obtained (Table 2).

Table 2 Oxidation of benzyl alcohols to the corresponding aldehydes in the presence of HAP-Pd⁰ under air atmosphere using water as solvent^a

Entry	Alcohol	Time/h	Yield ^b (%)
1	Benzyl alcohol	7	95
2	Benzyl alcohol	9	92 ^c
3	4-(MeO)C ₆ H ₄ CH ₂ OH	7	96
4	4-MeC ₆ H ₄ CH ₂ OH	7	92
5	4-(Cl)C ₆ H ₄ CH ₂ OH	7.5	91
6	4-(F)C ₆ H ₄ CH ₂ OH	7.5	93
7	4-(NO ₂)C ₆ H ₄ CH ₂ OH	8	90
8	3-(NO ₂)C ₆ H ₄ CH ₂ OH	7.5	87
9	1-Pentanol	10	45 ^d
10	1-Pentanol	48	72 ^d
11	1-Pentanol	8	80 ^e

^a The molar ratio of alcohol : HAP-Pd⁰ is 1 : 0.1. ^b Yield of isolated products. ^c The reaction was carried out with benzyl alcohol (50 mmol), HAP-Pd⁰ (4 g) and distilled water (200 mL) at 100 °C for 9 h. ^d Rest being the starting materials. ^e The reaction was carried out under molecular oxygen.

Once we were able to carry out the oxidation of benzyl alcohols efficiently under atmospheric air with HAP-Pd⁰, then attempts were made to perform the oxidation of other aliphatic alcohols. 1-Pentanol was selected as the test substrate. Unfortunately, under the reaction conditions lower conversion was observed, though selectivity was quite high (entry 9, Table 2). Further, if the reaction time was increased to 48 h, 1-pentanol was obtained in 72% isolated yield (entry 10, Table 2). However, with molecular oxygen, the catalyst was quite effective and selective (entry 11, Table 2).

To scale-up the reaction conditions, oxidation of benzyl alcohol (50 mmol) was carried by stirring with HAP-Pd⁰ (4 g) in distilled water (200 mL) at 100 °C for 9 h. After the usual work-up, benzaldehyde was obtained in 92% isolated yield (entry 2, Table 2).

Recyclability

When using a supported metal catalyst, one important point is the deactivation and recyclability of the catalyst. To test this, a series of 5 consecutive runs of the coupling between 4-bromoacetophenone and benzenboronic acid in the presence of HAP-Pd⁰ was carried out (1st use: 94% isolated yield after 4 h; 3rd use: 93% after 4 h; 5th use: 92% after 4 h). These results demonstrate that almost there is no change in the activity of HAP-Pd⁰ up to the 5th use.

The deactivation and recyclability becomes more important in the case of oxidation reactions. To test this, a series of 5 consecutive runs of the oxidation of benzyl alcohol using HAP-Pd⁰ under air atmosphere was carried out (1st use: 95% isolated yield after 7 h; 3rd use: 90% after 7 h; 5th use: 86% after 7 h). Thus, there is little change in the activity of the catalyst for the oxidation of benzyl alcohol under air using water as solvent.

Experimental

General

The chemicals used were either prepared in our laboratories or purchased from Aldrich Chemical Company and Merck. The products were characterized by comparison of their physical data with those of known samples or by their spectral data. The ¹H NMR data were recorded in CDCl₃ on a Bruker DPX 200 (200 MHz) spectrometer using TMS as an internal standard. The IR spectra were recorded on a Perkin–Elmer FTIR spectrophotometer using KBr windows, and mass spectra were recorded using a Bruker Esquires 3000 (ESI). XRD spectra were recorded on a Bruker AXSD8 X-ray diffraction spectrometer and SEM using a Jeol T-300 scanning electron microscope. Transmission electron micrographs (TEM) were recorded on a H7500 Hitachi. The amount of the palladium supported on HAP was determined by stirring the sample in dilute HNO₃ and subjecting to AAS analysis on GBC Avanta-M atomic absorption spectrometer manufactured by GBC Scientific agencies.

Preparation of hydroxyapatite

Diammonium hydrogen phosphate (7.92 g) was added in double distilled water (250 mL) in a borosil beaker (400 mL) and

maintained at a pH greater than 12, by addition of ammonium hydroxide (Merck) (70–75 mL). This solution was then transferred into 150 mL of a solution containing 24 g of calcium nitrate [Ca(NO₃)₂·4H₂O] with constant stirring (10 min). The suspension was then refluxed for 5 h and the solid was filtered off, washed with double distilled water (500 mL) and dried in the oven at 90 °C. The HAP was calcined in air at 700 °C for 30 min before use.

Preparation of hydroxyapatite-supported Pd(0) [HAP-Pd⁰]

To hydroxyapatite (3 g) in ethanol (25 mL) in a round-bottom flask (50 mL), Pd(OAc)₂ (0.05 g) was added and the reaction mixture was stirred at room temperature for 3 h. Hydrazine hydrate (80%, 2 mL) was added dropwise over a period of 15 min and the reaction mixture was again stirred at room temperature for 5 h. The colour of the reaction mixture changed to dark grey. HAP-Pd⁰ was filtered off and washed with ethanol (10 mL) and acetone (3 × 20 mL). In order to remove any physisorbed Pd(OAc)₂, the catalyst was conditioned by refluxing for 6 h in ethanol, toluene and acetonitrile, respectively, each for 2 h. Finally, the HAP-Pd⁰ was dried in oven for 5 h and stored in a desiccator.

General procedure for the Suzuki coupling between aryl bromides and boronic acids in the presence of HAP-Pd⁰ using water as solvent

To a mixture of aryl halide (1 mmol), aryl/heteroaryl boronic acid (1.5 mmol), TBAB (1 mmol), K₂CO₃ (3 mmol), HAP-Pd⁰ (0.3 g, 0.33 mol% Pd) in a round-bottom flask (25 mL), double distilled water (6 mL) was added. The reaction mixture was stirred at 100 °C for an appropriate time until complete conversion of aryl halide took place (monitored by TLC). After completion, the reaction mixture was cooled to room temperature and filtered. The residue was washed with hot ethyl acetate (approx. 70 °C, 3 × 10 mL) followed by double distilled water (3 × 50 mL). The organic layer was washed with water and dried over anhydrous Na₂SO₄. Finally, the product was obtained after removal of the solvent under reduced pressure followed either by crystallization or passing through a column of silica gel. The catalyst was dried at 100 °C for 1 h and can be reused.

The structures of the products were confirmed by IR, ¹H NMR, mass spectral data and comparison with authentic samples available commercially or prepared according to literature methods.

General procedure for the oxidation of benzyl alcohols in the presence of HAP-Pd⁰ under air atmosphere

To a mixture of benzyl alcohol (1 mmol) and HAP-Pd⁰ (0.1 g, 0.11 mol% Pd) in a round-bottom flask (25 mL), double distilled water (5 mL) was added. The reaction mixture was stirred at 100 °C for an appropriate time (monitored by TLC). On completion, the reaction mixture was cooled to room temperature and filtered. The residue was washed with hot ethyl acetate (approx. 70 °C, 3 × 5 mL) followed by double distilled water (3 × 50 mL). The organic layer was washed with water and dried over anhydrous Na₂SO₄. Finally, the product was obtained after removal of the solvent under reduced pressure followed by

passing through a column of silica gel and elution with EtOAc : pet. ether. The catalyst was dried at 100 °C for 1 h and can be reused.

The structures of the products were confirmed by IR, ¹H NMR, mass spectral data and comparison with authentic samples available commercially or prepared according to literature methods.

Conclusions

In conclusion, we have reported the simple preparation of hydroxyapatite-supported palladium (0) and its successful application for the Suzuki coupling and oxidation of benzyl alcohols under air atmosphere using water as solvent. The catalyst was found to be highly efficient and recyclable for both Suzuki coupling and oxidation of benzyl alcohols under an air atmosphere.

Acknowledgements

We thank the Head, Institute Instrumentation Centre, Indian Institute of Technology (IIT) Roorkee for AAS analysis and XRD; Head, SAIF, Punjab University Chandigarh for TEM and Dr A. K. Sahni for recording SEM.

Notes and references

- (a) P. T. Anastas, and J. C. Warner, *Green Chemistry: Theory and Practice*, Oxford University Press, New York, 1988; (b) A. S. Matlack, *Introduction to Green Chemistry*, Marcel Dekker, Inc., New York, 2001; (c) M. Lancaster, *Green Chemistry: An Introductory Text*, Royal Society of Chemistry, Cambridge, 2002; (d) J. H. Clark, and D. J. Macquarrie, *Handbook of Green Chemistry & Technology*, Blackwell Publishers, Oxford, 2002; (e) J. H. Clark, *Green Chem.*, 2006, **8**, 17.
- (a) *Solvent-free Organic Synthesis*, ed. K. Tanaka, Wiley-VCH, Weinheim, 2003; (b) *Supercritical Carbon Dioxide in Polymer Reaction Engineering*, ed. M. F. Kemmere and T. Meyer, Wiley-VCH, Weinheim, 2005; (c) V. I. Parvulescu and C. Hardacre, *Chem. Rev.*, 2007, **107**, 2615; (d) *Handbook of Fluorous Chemistry*, ed. J. A. Gladysz, D. P. Curran, and I. T. Horvath, Wiley-VCH, Weinheim, 2004; (e) C.-J. Li, *Chem. Rev.*, 1993, **93**, 2023; C.-J. Li, *Chem. Rev.*, 2005, **105**, 3095; (f) C.-J. Li and L. Chen, *Chem. Soc. Rev.*, 2006, **35**, 68; (g) *Organic Reactions in Water*, ed. U. Lindstorm, Blackwell Publishing, Oxford, 2007.
- The release of contaminated waste water resulting from a chemical or manufacturing process, however, is a serious environmental problem, and there is typically a high cost associated with the recycling/purification of contaminated water, see: W. Wei, C. C. K. Keh, C.-J. Li and R. S. Varma, *Clean Technol. Environ. Policy*, 2004, **6**, 250 and references cited therein.
- (a) L. Yin and J. Liebscher, *Chem. Rev.*, 2007, **107**, 133 and references cited therein; (b) H. Li, L. Wang and P. Li, *Synthesis*, 2007, 1635; (c) V. Budarin, J. H. Clark, J. J. E. Hardy, R. Luque, K. Milkowski, S. J. Tavener and A. J. Wilson, *Angew. Chem., Int. Ed.*, 2006, **45**, 3782; (d) D. Choudhary, S. Paul, R. Gupta and J. H. Clark, *Green Chem.*, 2006, **8**, 479 and references cited therein.
- (a) W. Chen, Z. Huang, Y. Liu and Q. He, *Catal. Commun.*, 2008, **9**, 516; (b) A. Solhy, J. H. Clark, R. Tahir, S. Sebti and M. Larzek, *Green Chem.*, 2006, **8**, 871; (c) D. Mahajan, B. A. Ganai, R. L. Sharma and K. K. Kapoor, *Tetrahedron Lett.*, 2006, **47**, 7919.
- (a) K. Mori, K. Yamaguchi, T. Hara, T. Mizugaki, K. Ebitani and K. Kaneda, *J. Am. Chem. Soc.*, 2002, **124**, 11572; (b) T. Hara, K. Mori, M. Oshiba, T. Mizugaki, K. Ebitani and K. Kaneda, *Green Chem.*, 2004, **6**, 507; (c) K. Mori, T. Hara, M. Oshiba, T. Mizugaki, K. Ebitani and K. Kaneda, *New J. Chem.*, 2005, **29**, 1174.
- (a) A. Suzuki and N. Miyaura, *Chem. Rev.*, 1995, **95**, 2457; (b) A. Suzuki, *J. Organomet. Chem.*, 1999, **576**, 147; (c) A. Suzuki, *J. Organomet. Chem.*, 2002, **653**, 83; (d) S. P. Stanforth, *Tetrahedron*, 1998, **54**, 263.
- (a) D. A. Horton, G. T. Bourne and M. L. Smythe, *Chem. Rev.*, 2003, **103**, 893; (b) P. J. Hajduk, M. Bures, J. Praestgaard and S. W. Fesik, *J. Med. Chem.*, 2000, **43**, 3443; (c) K. F. Croom and G. M. Keating, *Am. J. Cardiovasc. Drugs*, 2004, **4**, 395.
- (a) C. Fleckenstein, S. Roy, S. Leuthaußer and H. Plenio, *Chem. Commun.*, 2007, 2870; (b) F. Churruca, R. SanMartin, B. Inés, I. Tellitu and E. Dominguez, *Adv. Synth. Catal.*, 2006, **348**, 1836; (c) Q. Yang, S. Ma, J. Li, F. Xiao and H. Xiang, *Chem. Commun.*, 2006, 2495.
- (a) R. A. Sheldon, I. W. C. E. Arends and A. Dijkstra, *Catal. Today*, 2000, **57**, 157; (b) B. Karmi, S. Abedi, J. H. Clark and V. Budarin, *Angew. Chem., Int. Ed.*, 2006, **45**, 4776 and references cited therein.
- (a) B. Z. Zhan and A. Thompson, *Tetrahedron*, 2004, **60**, 2917; (b) T. Mallat and A. Baiker, *Chem. Rev.*, 2004, **104**, 3037.
- (a) For a general discussion of atom economy in organic synthesis see: B. M. Trost, *Science*, 1991, **254**, 1471; (b) B. M. Trost, *Angew. Chem., Int. Ed. Engl.*, 1995, **34**, 259.
- (a) N. Komiya, T. Nakae, H. Sato and T. Naota, *Chem. Commun.*, 2006, 4829; (b) H. G. Manyar, G. S. Chaure and A. Kumar, *Green Chem.*, 2006, **8**, 344; (c) P. Gogoi and D. Konwar, *Org. Biomol. Chem.*, 2005, **3**, 3473.
- (a) W. Solodenko, U. Schon, J. Messinger, A. Glinschert and A. Kirschning, *Synlett*, 2004, 1699; (b) S.-S. Yi, D.-H. Lee, E. Sin and Y.-S. Lee, *Tetrahedron Lett.*, 2007, **48**, 6771 and references cited therein.
- C. A. Fleckenstein and H. Plenio, *Green Chem.*, 2007, **9**, 1287.
- (a) J. J. E. Hardy, S. Hubert, D. J. Macquarrie and A. J. Wilson, *Green Chem.*, 2004, **6**, 53; (b) S. Alesi, F. D. Maria, M. Melucci, D. J. Macquarrie, R. Luque and G. Barbarella, *Green Chem.*, 2008, **10**, 517.
- (a) G. W. Gary and P. A. Winsor, *Liquid Crystals and Plastic Crystals*, John Wiley and Sons, New York, 1974, vol. 1; (b) D. J. Schneider, D. A. Landis, P. A. Fleitz, C. J. Seliskar, J. M. Kaufman and R. N. Steppel, *Laser Chem.*, 1991, **11**, 49; (c) S.-M. Yang, J.-J. Shie, J.-M. Fang, S. K. Nandy, H.-Y. Chang, S.-H. Lu and G. Wang, *J. Org. Chem.*, 2002, **67**, 5208 and references cited therein.
- B. Basu, P. Das, Md. M. H. Bhuiyan and S. Jha, *Tetrahedron Lett.*, 2003, **44**, 3817.
- S. Paul and J. H. Clark, *Green Chem.*, 2003, **5**, 635.

Improved chemoselective, ecofriendly conditions for the conversion of primary alkyl halides into nitroalkanes under PEG400

Roberto Ballini,* Luciano Barboni and Alessandro Palmieri

Received 8th April 2008, Accepted 18th June 2008

First published as an Advance Article on the web 11th August 2008

DOI: 10.1039/b805985c

Treatment of primary alkyl bromides or iodides with 1.5–3 equivalents of sodium nitrite, at room temperature, in PEG400 as solvent, allows the chemoselective formation of primary nitroalkanes in satisfactory to good yields, under ecofriendly reaction conditions.

It is widely acknowledged that there is a growing need for more environmentally acceptable processes in the chemical industry. This trend towards what has become known as “sustainable technology” necessitates a paradigm shift from traditional concepts of processes efficiency, that focus largely on chemical yield, to one that assigns economic value to eliminating waste at source and avoiding the use of toxic and/or hazardous substances.

In this context, an important aspect which is receiving increasing attention is the use of alternative reaction media that circumvent the problems associated with many of the traditional volatile organic solvents (VOCs). It has been estimated that *ca.* 85% of the total mass of chemicals involved in pharmaceutical manufacture comprises solvents,¹ and from the green chemistry point of view there are several issues which influence the choice of solvent. It should be relatively nontoxic and relatively nonhazardous, not inflammable (such as volatile solvents, *e.g.* pentane or diethyl ether) or corrosive.

A number of companies have published solvent selection guides,^{2,3} and more recently other authors^{4,5} published a detailed and comprehensive approach to the environmental selection of solvents.

Removal of residual solvent from products is usually achieved by evaporation or distillation and most popular solvents are, therefore, highly volatile. Spillage and evaporation inevitably leads to atmospheric pollution. Moreover, worker exposure to volatile organic compounds is a serious health issue.⁶ Another class of solvents which presents environmental problems comprises the polar aprotic solvents, such as dimethylformamide and dimethyl sulfoxide, that are the solvent of choice for many nucleophilic substitutions. They have high boiling points and not easily removed by distillation, in addition, they are also water-miscible which enables their separation by washing with water. Unfortunately, this inevitably leads to contaminated aqueous effluent.

Nitroalkanes are one of the main classes of compounds in organic chemistry due to their high chemical versatility⁷ and their importance as key building blocks for the synthesis of a variety of fine chemicals.⁸ Thus, the availability of nitroalkanes appears

crucial and the development of new ecofriendly procedures for their preparation remains an important goal.

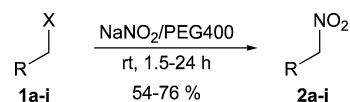
Nitroalkanes can be obtained from many sources, however, the conversion of alkyl halides into nitro compounds, by using metal nitrite, is one of the most used strategies.^{7,9} For these procedures silver nitrite in diethyl ether, potassium nitrite or sodium nitrite in *N,N*-dimethylformamide (DMF) or in dimethyl sulfoxide (DMSO) have been proposed.^{9,10}

In order to improve the ecofriendly reaction conditions for the above method, recently we reported¹¹ the first conversion of primary alkyl halides into nitroalkanes under aqueous medium. The method has been realized by reaction of primary alkyl halides with 4 equivalents of silver nitrite; however, the drawbacks of this procedure consist of the need of a large excess of expensive reagents, such as silver nitrite, and the formation, as side products, of the corresponding alcohol due to the competitive nucleophilic action of water *vs.* nitrite.

With the aim of improving the ecosustainability of this fundamental method for the preparation of nitroalkanes, we wish here to propose the conversion of alkyl halides into nitro compounds by using sodium nitrite in polyethylene glycol (PEG400) as green reaction media.

In fact, recently PEG has attracted great interest as novel solvent for catalytic processes since it is relatively inexpensive, essentially nontoxic, readily available and biodegradable material (PEG is approved for use in beverages).^{5,12}

Thus, treatment of primary alkyl halides **1** with 1.5–3 equivalents of sodium nitrite, at room temperature, in PEG400 as solvent, allows the chemoselective formation of primary nitroalkanes in satisfactory to good yields (Scheme 1).

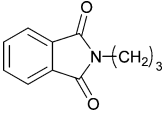


Scheme 1 Conversion of primary alkyl halides into nitroalkanes.

In order to verify the potential of the procedure, we tested a variety of primary alkyl halides and only alkyl iodides and bromides were converted into the corresponding nitro derivatives, while chloro derivatives were inactive. However, this result can be considered as a chemoselective procedure for the survival of the chloro atom during the nitration of

Dipartimento di Scienze Chimiche dell'Università di Camerino, Via S. Agostino 1, 62032, Camerino, Italy. E-mail: roberto.ballini@unicam.it; Fax: +39 0737 402297; Tel: +39 0737 402270

Table 1 Nitroalkanes **2** prepared and reaction conditions

	R	X	equivalents of NaNO ₂	Reaction times/h	Yield (%) ^a of 2
a	<i>n</i> -C ₇ H ₁₅	I	1.5	2.5	70
b	<i>n</i> -C ₁₁ H ₂₃	I	1.5	4	76
c	<i>n</i> -C ₁₀ H ₂₁	Br	3	24	54
d	CH ₂ =CH(CH ₂) ₈	Br	3	20	72
e	HO(CH ₂) ₈	Br	3	5	73 ^b
f	Ph(CH ₂) ₂	Br	1.5	4.5	71
f	Ph(CH ₂) ₂	I	1.5	1.5	74
g	AcO(CH ₂) ₃	I	1.5	2	68
h	Cl(CH ₂) ₃	I	1.5	3	70
i		Br	3	22	63
j	CH ₂ =CHCH ₂ OCO(CH ₂) ₇	Br	3	20	71

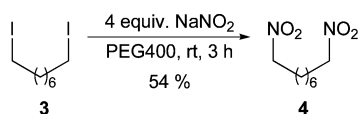
^a Yield of pure isolated product. ^b With this nitroalkane, a better yield is obtained by extraction with Et₂O due to its low solubility in cyclohexane.

iodides or bromides (**1h** to **2h**, Table 1). Moreover, due to the mildness of the procedure other functionalities such as esters, hydroxyl, carbon-carbon double bonds, ethers, aromatics and amides can be preserved (Table 1). It should be noted that only traces of alkylnitrite could be observed (2–6%, detected as the corresponding alcohol¹³ by GC-MS).

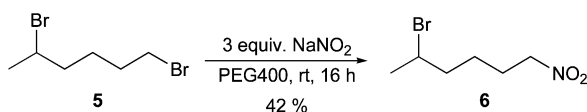
Although the procedure works well with both alkyl iodides and bromides, the latter need a larger amount of sodium nitrite (3 equiv. vs 1.5) and a longer reaction time.

It is important to note that PEG400, after the extraction with cyclohexane, can be recycled at least twice for the same reaction before its disposal as waste. In addition, cyclohexane can be recovered by distillation and reused for further extractions.

Moreover, the procedure offers the opportunity to convert, in a one-pot process, α,ω -diiodo structures, such as **3** into the corresponding 1,8-dinitrooctane **4** in 54% overall yield (Scheme 2).

**Scheme 2** Conversion of 1,8-diiodooctane into 1,8-dinitrooctane.

The conversion of secondary halo derivatives fails by our method, and this result can be applied for the chemoselective nitration of primary iodides or bromides in the presence of a secondary one. In fact treatment of 1,5-dibromohexane **5** with four equivalents of sodium nitrite, in PEG400, produces 1-nitro-4-bromohexane **6** as the exclusive nitroderivative (42% yield, Scheme 3).

**Scheme 3** Chemoselective nitration of 1,5-dibromohexane.

Thus, the reported method represents an improved, chemoselective, ecosustainable procedure for the synthesis of primary

nitroalkanes from the corresponding halo derivatives since it can be realized avoiding both volatile and toxic organic solvents during the process. In addition, PEG400 can be reused twice for the same reaction (with comparable yields) before its disposal as waste. In fact, the conversion of **1a** into **2a**, gives the following results: (i) 1st recycle 70%, 2nd recycle 67%, 3rd recycle 41%.

Experimental

Typical procedure

A mixture of PEG400 (2 mL) and NaNO₂ (1.5–3 mmol, Table 1) was stirred for 3 h at room temperature, then the halide **1** (1 mmol) was added and the reaction was stirred for the appropriate time (Table 1). Finally, the solution was treated with 2 mL of cyclohexane and stirred for additional 5 min, then the stirring was stopped and the upper layer was transferred into another flask; the same procedure was repeated another 3 times (4 × 2 mL). Most of the cyclohexane is, then, removed by distillation (and reused), while the residue is directly charged on a chromatographic column (EtOAc/cyclohexane) giving the pure product **2**.†

PEG400, after the extraction with cyclohexane, can be reused at least twice for the same reaction, simply by adding one more mmol of NaNO₂.

9-Nitrononan-1-ol (2e). Waxy white solid, IR (nujol) ν : 1376, 1560, 3401 cm⁻¹. ¹H NMR (CDCl₃, 400 MHz) δ (ppm) 1.20–1.66 (m, 13H), 1.89–2.10 (m, 2H), 3.63 (t, 2H, $J = 6.6$ Hz), 4.38 (t, 2H, $J = 7.1$ Hz). ¹³C NMR (CDCl₃, 100 MHz) δ (ppm) 25.9, 26.4, 27.6, 29.0, 29.4, 32.9, 63.2, 75.9. GC-MS (m/z): 124, 95, 81, 69, 55 (100), 41, 30. Elemental analysis for C₉H₁₉NO₃: Calcd: C, 57.12; H, 10.12, N, 7.40. Found: C, 57.69; H, 10.88; N, 7.19.

5-Bromo-1-nitrohexane (6). Oil, IR (neat) ν : 1378, 1552, 2926 cm⁻¹. ¹H NMR (CDCl₃, 400 MHz) δ (ppm) 1.46–1.56 (m, 1H), 1.57–1.68 (m, 1H), 1.70 (d, 3H, $J = 6.9$ Hz), 1.77–1.88 (m, 2H),

† The syntheses of the nitrocompounds **2**, except for **2e** and **6**, have already been reported in the literature and all our spectral data are in agreement with those published.^{11,14–17}

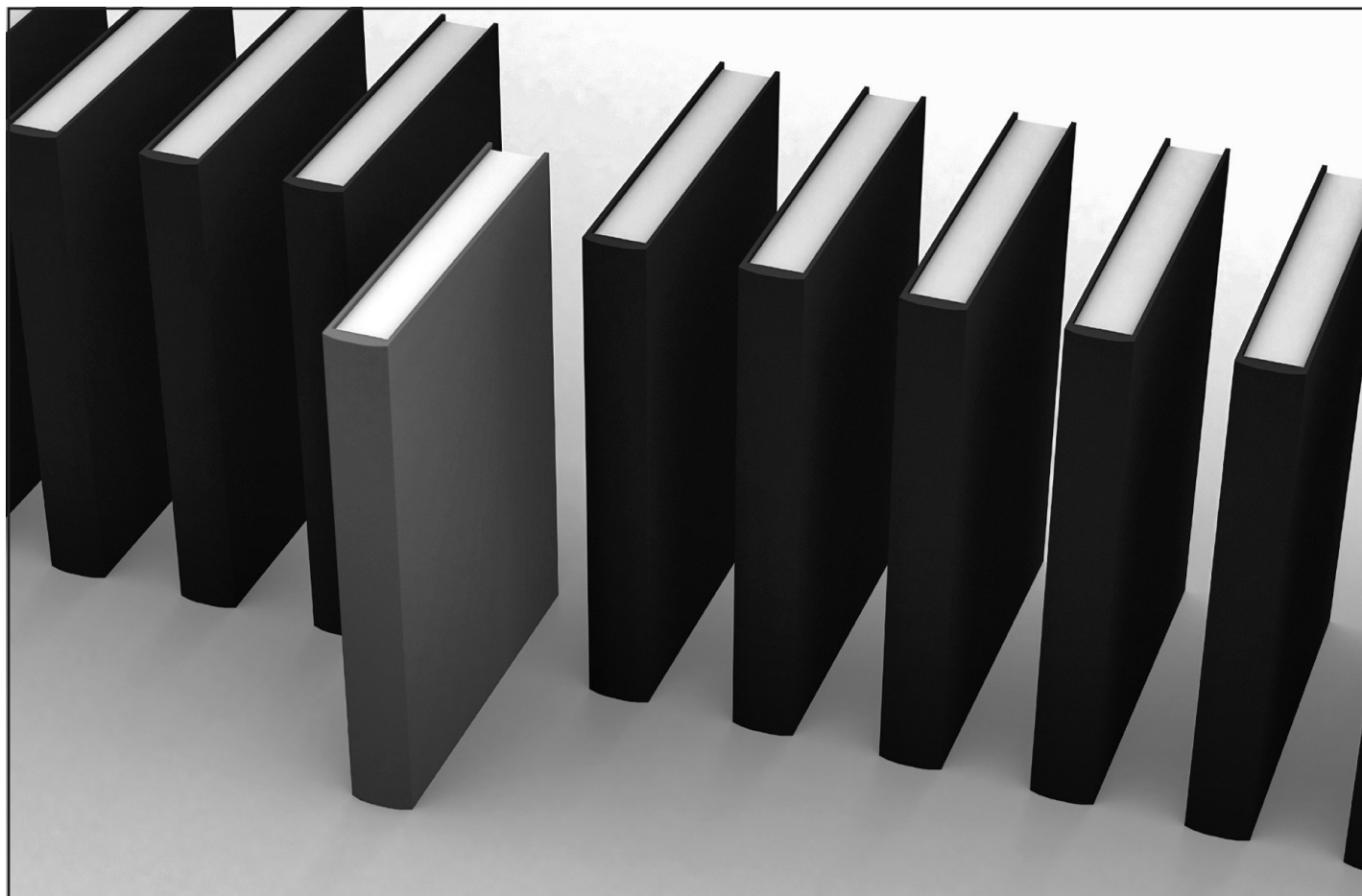
1.94–2.11 (m, 2H), 4.05–4.16 (m, 1H), 4.40 (t, 2H, $J = 7.0$ Hz). ^{13}C NMR (CDCl_3 , 100 MHz) δ (ppm) 24.7, 26.6, 26.8, 40.3, 50.8, 75.5. GC-MS (m/z): 130, 83, 55 (100), 41, 29. Elemental analysis for $\text{C}_6\text{H}_{12}\text{BrNO}_2$. Calcd: C, 34.31; H, 5.76, N, 6.67. Found: C, 34.75; H, 5.98; N, 6.38.

Acknowledgements

Financial support from the University of Camerino and MUR-Italy (National Project ‘‘Sintesi organiche ecosostenibili mediate da nuovi sistemi catalitici’’) is gratefully acknowledged.

Notes and references

- D. J. C. Constable, A. D. Curzons and V. L. Cunningham, *Green Chem.*, 2002, **4**, 521.
- A. D. Curzons, D. C. Constable and V. L. Cunningham, *Clean Prod. Process.*, 1999, **1**, 82.
- C. Jimenez-Gonzales, A. D. Curzons, D. J. C. Constable and V. L. Cunningham, *Clean Technol. Environ. Pollut.*, 2005, **7**, 42.
- C. Capello, U. Fisher and K. Hungerbuhler, *Green Chem.*, 2007, **9**, 917.
- R. A. Sheldon, *Green Chem.*, 2005, **7**, 267.
- K. Alfonsi, J. Colberg, P. J. Dunn, T. Fevig, S. Jennings, T. A. Johnson, H. P. Kleine, C. Knight, M. A. Nagy, D. A. Perry and M. Stefaniak, *Green Chem.*, 2008, **10**, 31.
- G. Rosini and R. Ballini, *Synthesis*, 1988, 833; R. Ballini, G. Bosica, D. Fiorini, A. Palmieri and M. Petrini, *Chem. Rev.*, 2005, **105**, 933; R. Ballini and M. Petrini, *Tetrahedron*, 2004, **60**, 1017; R. Ballini, G. Bosica, D. Fiorini and A. Palmieri, *Tetrahedron*, 2005, **61**, 8971; R. Ballini, L. Barboni, F. Fringuelli, A. Palmieri, F. Pizzo and L. Vaccaro, *Green Chem.*, 2007, **9**, 823.
- R. Ballini, in *Studies in Natural Products Chemistry*, ed. Atta-ur-Rahman, Elsevier, Amsterdam, 1997, vol. 19, p. 117; R. Ballini, A. Palmieri and P. Righi, *Tetrahedron*, 2007, **63**, 12099.
- N. Ono, *The Nitro Group in Organic Synthesis*, Wiley-VCH, New York, 2001; D. Seebach, E. W. Colvin, F. Lehr and T. Weller, *Chimia*, 1979, **33**, 1.
- N. Kornblum, *Org. React.*, 1962, **12**, 101; H. Feuer and G. Leston, *Organic Synthesis*, Wiley, New York, 1963; N. Kornblum, H. O. Larson, R. K. Blackwood, D. D. Mooberry, E. P. Oliveto and G. E. Graham, *J. Am. Chem. Soc.*, 1956, **78**, 1497; T. A. Ainscow, M. R. Belmont, J. L. Henshall, R. M. Hooper and D. J. Simmons, *Tetrahedron Lett.*, 1987, **43**, 115; J. K. Addo, P. Teesdale-Spittle and J. O. Hoberg, *Synthesis*, 2005, 1923; C. J. Easton, L. Xia, M. J. Pitt, A. Ferrante, A. Poulos and D. A. Rathjen, *Synthesis*, 2001, 451.
- R. Ballini, L. Barboni and G. Giarlo, *J. Org. Chem.*, 2004, **69**, 6907.
- J. Chen, S. K. Spear, J. G. Huddleston and R. D. Rogers, *Green Chem.*, 2005, **7**, 64.
- N. Kornblum, R. K. Blackwood and D. D. Mooberry, *J. Am. Chem. Soc.*, 1956, **78**, 1501; M. P. Doyle, J. W. Terpstra, R. A. Pickering and D. M. LePoire, *J. Org. Chem.*, 1983, **48**, 3379.
- J. Mc Nulty, J. J. Nair, S. Cheekoori, V. Larichev, A. Capretta and Al. J. Robertson, *Chem.–Eur. J.*, 2006, **12**, 9314.
- V. Gil and A. J. MacLeod, *Tetrahedron*, 1980, **36**, 779.
- A. Goti, A. Brandi, G. Danza, A. Guarna, D. Donati and F. De Sarlo, *J. Chem. Soc., Perkin Trans. 1*, 1989, 1253.
- S. R. Woodcock, A. J. V. Marwitz, P. Bruno and B. P. Branchand, *Org. Lett.*, 2006, **8**, 3931.



'Green Chemistry book of choice'



Why not take advantage of free book chapters from the RSC? Through our 'Green Chemistry book of choice' scheme *Green Chemistry* will regularly highlight a book from the RSC eBook Collection relevant to your research interests. Read the latest chapter today by visiting the *Green Chemistry* website.

The RSC eBook Collection offers:

- Over 900 new and existing books
- Fully searchable
- Unlimited access

Why not take a look today? Go online to find out more!

RSC Publishing

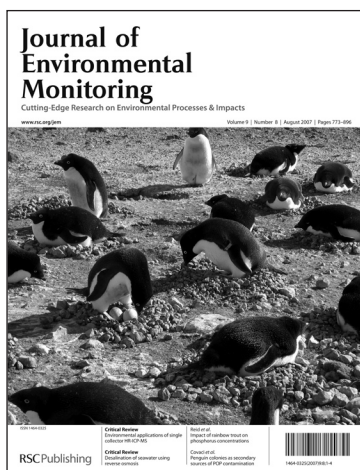
www.rsc.org/greenchem

Registered Charity Number 207890



The must-have primary research journal for environmental issues

Comprehensive and high quality coverage of multidisciplinary, international research relating to the measurement, pathways, impact and management of contaminants in all environments.



- Highly visible and cited in MEDLINE
- Accelerated publication rates, typically around 80 days
- Dedicated to the measurement of natural and anthropogenic sources of pollution with a view to assessing environmental and human health effects

Submit your work to JEM today

RSCPublishing

www.rsc.org/jem

Registered Charity Number 207890

25 years

of stimulating
progress in all
areas of natural
products research

Downloaded on 09 November 2010
Published on 01 September 2008 on <http://pubs.rsc.org> | doi:10.1039/B813953A



Join the celebrations...

Natural Product Reports is celebrating 25 years of publishing reviews in key areas including: bioorganic chemistry, chemical biology, chemical ecology and carbohydrates

- Impact factor 7.66*
- High visibility – indexed in MEDLINE
- “Hot off the Press” literature highlights published in each issue

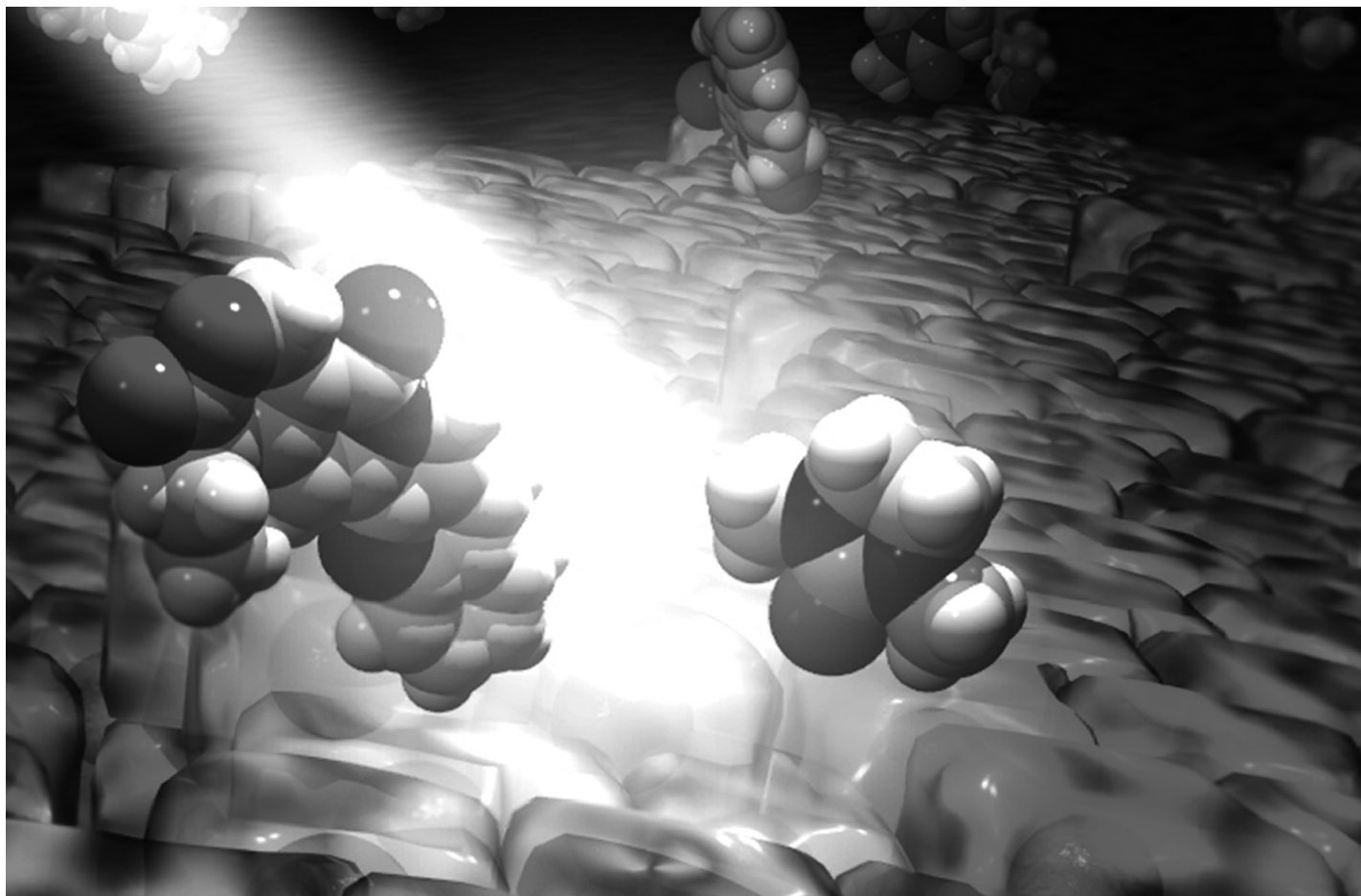
...go online to find out more

* 2007 Thomson Scientific (ISI) Journal Citation Reports ®

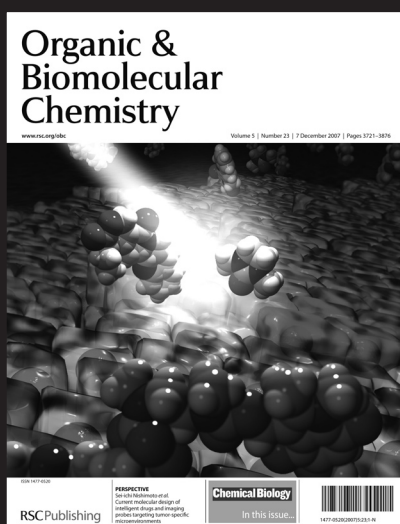
RSC Publishing

www.rsc.org/npr

Registered Charity Number 207890



Organic & Biomolecular Chemistry...



OBC has achieved tremendous success since the first issue was published in January 2003. Can any other 'young' journal boast such highly cited papers, published quickly after independent peer review to such exacting standards?

- Now one of the leading journals in the field, impact factor 2.874*
- Short publication times – average 21 days from acceptance for papers, and 13 days for communications
- Enhanced HTML articles – hyperlinked compound information, ontology terms linked to definitions and related articles, links to IUPAC Gold Book terms, and more . . .

* 2006 Thomson Scientific (ISI) Journal Citation Reports®

... *high quality - high impact!*

RSC Publishing

www.rsc.org/obc

Registered Charity Number 207890

RSC eBook Collection

Access and download existing and new books from the RSC

- **Comprehensive:** covering all areas of the chemical sciences
- **Fully searchable:** advance search and filter options
- **Wide ranging:** from research level monograph to popular science book



See for yourself –
go online to search
the collection and
read selected
chapters
for free!

'I wish the others were as easy to use.'



'ReSource is the best online submission system of any publisher.'

'It leads the way for online submission and refereeing.'



ReSource



A selection of comments received from just a few of the thousands of satisfied RSC authors and referees who have used ReSource to submit and referee manuscripts. The online portal provides a host of services, to help you through every step of the publication process.

authors benefit from a user-friendly electronic submission process, manuscript tracking facilities, online proof collection, free pdf reprints, and can review all aspects of their publishing history

referees can download articles, submit reports, monitor the outcome of reviewed manuscripts, and check and update their personal profile

NEW!! We have added a number of enhancements to ReSource, to improve your publishing experience even further. New features include:

- the facility for authors to save manuscript submissions at key stages in the process (handy for those juggling a hectic research schedule)
- checklists and support notes (with useful hints, tips and reminders)
- and a fresh new look (so that you can more easily see what you have done and need to do next)

A class-leading submission and refereeing service, top quality high impact journals, all from a not-for-profit society publisher ... is it any wonder that more and more researchers are supporting RSC Publishing? Go online today and find out more.

Registered Charity No. 207890

RSC Publishing

www.rsc.org/resource